REPUBLIC OF TÜRKİYE
YILDIZ TECHNICAL UNIVERSITY
GRADUATE SCHOOL OF SCIENCE AND ENGINEERING

A METHOD TO DESIGN OF PERFORATED SOLAR SCREENS IN TERMS OF THERMAL AND VISUAL COMFORT

Fatma ZOROĞLU

DOCTOR OF PHILOSOPHY THESIS

Department of Architecture

Program of Building Physics

Supervisor

Prof. Dr. Gülay ZORER GEDİK

Co-Supervisor

Prof. Dr. Fatma Rengin ÜNVER

September, 2025

REPUBLIC OF TÜRKİYE

YILDIZ TECHNICAL UNIVERSITY

GRADUATE SCHOOL OF SCIENCE AND ENGINEERING

A METHOD TO DESIGN OF PERFORATED SOLAR SCREENS IN TERMS OF THERMAL AND VISUAL COMFORT

A thesis submitted by Fatma ZOROĞLU in partial fulfillment of the requirements for the degree of **DOCTOR OF PHILOSOPHY** is approved by the committee on 01.09.2025 in Department of Architecture, Program of Building Physics.

Prof. Dr. Gülay ZORER GEDİK Yildiz Technical University Supervisor	Prof. Dr. Fatma Rengin ÜNVER Yildiz Technical University Co- supervisor

Approved By the Examining Committee

Prof. Dr. Gülay ZORER GEDİK, Supervisor
Yildiz Technical University _____

Assoc. Prof. Dr. Suzi Dilara MANGAN, Member
Yildiz Technical University _____

Prof. Dr. Gülten MANİOĞLU, Member
Istanbul Technical University _____

Assoc. Prof. Dr. Şensin AYDIN YAĞMUR, Üye
Yildiz Technical University _____

Assist. Prof. Dr. Ferhan KORKMAZ HASMADEN, Üye
Özyeğin University _____

I hereby declare that I have obtained the required legal permissions during data collection and exploitation procedures, that I have made the in-text citations and cited the references properly, that I haven't falsified and/or fabricated research data and results of the study and that I have abided by the principles of the scientific research and ethics during my Thesis Study under the title of "A METHOD TO DESIGN OF PERFORATED SOLAR SCREENS IN TERMS OF THERMAL AND VISUAL COMFORT" supervised by my supervisor, Prof. Dr. Gülay ZORER GEDİK. In the case of a discovery of false statement, I am to acknowledge any legal consequence.

Fatma ZOROĞLU

Signature

This work was supported by the project no “ 4165 - FDK-2021-4165 - of YTU Coordinatorship of Scientific Research Projects” and “1059B142000644 – TUBITAK - 2214-A International Research Fellowship Programme for PhD Students”.

Dedicated to my family

Dad, Mom and Sisters

ACKNOWLEDGEMENTS

I am writing this acknowledgment with profound gratitude as I completed my doctoral thesis at the Department of Architecture, Yıldız Technical University. First and foremost, I extend my deepest appreciation to myself. I have made significant progress in my academic career and continue to pursue further advancement.

As I bring my doctoral thesis to a close, I would like to express my sincere and deepest appreciation to all those who have supported, guided, and inspired me throughout this meaningful and challenging academic endeavor.

With the utmost respect and gratitude, I would like to acknowledge the invaluable mentorship of my supervisor, Prof. Dr. Gülay Zorer Gedik. Her unwavering support, insightful guidance, and scholarly expertise have played a pivotal role in shaping the direction and quality of this research. Her mentorship has left a lasting impact on my academic journey. Dear Mrs. Zorer Gedik, thank you for your unwavering encouragement, patience, and consistent support throughout this journey.

I also wish to express my sincere appreciation to my co-supervisor Prof. Dr. Fatma Rengin Ünver for her generous assistance. I am deeply appreciative of the time, dedication, and thoughtful guidance she has invested in my development as a researcher. I am equally grateful to my thesis committee members, Prof. Dr. Gülten Manioğlu, Assoc. Prof. Dr. Suzi Dilara Mangan for their generous assistance, insightful suggestions and contributions.

I extend my deepest gratitude to my dearest family. I am especially indebted to my father, MSc. Economist Kürşat Zoroğlu and my mother Nurgül Zoroğlu for their unconditional love, unwavering encouragement, and immeasurable sacrifices. My sisters, MD Urology Surgery Specialist Hatice Zoroğlu and architecture student Ceren Zoroğlu always supported me and their beliefs on me has been the foundation of my resilience. They were always there when I needed them. I know that your

support and love will always be by my side, guiding and strengthening me throughout my life. My family are secret heroes behind my every success.

I would like to acknowledge all members of the Building Physics research group, YTU for all their support and help. I also would like to thank my friends and colleagues, especially, Res. Asst. Ahmet Bircan Atmaca and Res. Asst. Arca Gizem İpekçi for their collaborative spirit and shared enthusiasm. Their companionship and constructive discussions have enriched this academic experience and made it both intellectually fulfilling and personally rewarding.

During my doctoral research, I was fortunate to be awarded a TÜBİTAK 2214-A International Research Fellowship by The Scientific and Technological Research Council of Turkey, which enabled me to conduct part of my studies at the Technical University of Denmark (DTU). My time in Denmark was not only academically enriching but also personally rewarding. I would like to express my sincere thanks to my host supervisor, Prof. Dr. Bjarne Wilkens Olesen, for his invaluable mentorship. I am also grateful to Assoc. Prof. Dr. Ongun Berk Kazancı and Assist. Prof. Dr. Mandana Khanie for their generous support and collaboration. Their expertise and guidance significantly contributed to the experimental aspects of my research.

I would also like to extend my appreciation to Çuhadaroğlu Aluminum Industry and Trade Inc., whose material and technical support were integral to the successful implementation of my field studies.

Fatma ZOROĞLU

TABLE OF CONTENTS

LIST OF SYMBOLS ix
LIST OF ABBREVIATIONS x
LIST OF FIGURES xi
LIST OF TABLES xv
ABSTRACT xvii
ÖZET xix
1 INTRODUCTION 1
1.1. Background 1
1.2. Problem statement 2
1.3. The objectives and hypothesis of the study 3
1.4. Lıterature Revıew 5
2 SHADING DEVICES AND THEIR PERFORMANCES 25
2.1. Shading Devices 25
2.1.1 Perforated Solar Screens (PSS) 27
2.2. Indoor Comfort Conditions 29
2.2.1. Thermal Comfort 30
2.2.2. Visual Comfort 35
3 A METHOD TO DESIGN OF PERFORATED SOLAR SCREENS IN TERMS OF THERMAL AND VISUAL COMFORT 39
3.1. Data collection and analysis methods 42
3.1.1. Observations 42
3.1.2. Field Studies 45
3.1.3. Verifications for Measurements and Simulations 56
3.2. Analysis and Evaluation of Field Study and Verification Results 58
3.3. Designing of Perforated Solar Screens (PSS) 60
3.4. Simulations and Optimizations of Perforated Solar Screens (PSS) 63
3.4.1. Key Performance Indicators (KPI) In Terms Of Thermal and Visual Comfort 63
3.4.2. Design parameters 66

3.4.3. Parametric Modelling and Simulation Setting 68
3.5. Analysis and Evaluation of Simulation and Optimization Results 77
4 APPLICATION OF THE DEVELOPED METHOD 81
4.1. Data collection and analysis to test developed method 81
4.1.1. Observations of classrooms 81
4.1.2. Conducting of Field Studies on Current Classrooms 83
4.1.3. Conducting Verifications for Measurements and Simulations 98
4.2. Field Study and Verification Results 98
4.2.1. Verifications for Measurements 98
4.2.2. Thermal comfort Measurement and Survey Results 102
4.2.3. Visual comfort Measurement and Survey Results 113
4.2.4. Verification Results for Simulations 120
4.3. Designing of Perforated Solar Screens (PSS) for classrooms 122
4.4. Conducting Simulations and Optimizations for Designed Perforated Solar Screens (PSS) 128
4.4.1. Simulation settings for KPI 132
5 RESULTS 136
5.1. Analysis of Simulation and Optimization Results to Determine Optimum Perforated Solar Screens (PSS) 136
5.1.1. Evaluation of Optimization Results in terms of KPI 136
5.1.2. Application of TOPSIS Analysis and Evaluation of Optimization Results in terms of KPI 156
5.1.3. Evaluation of Optimization Results in terms of Design Parameters 159
5.1.4. Evaluation of Optimization Results in terms of PMV 164
6 DISCUSSION 167
7 CONCLUSION 171
REFERENCES 178
A APPENDIX 186
PUBLICATIONS FROM THE THESIS 198

LIST OF SYMBOLS

Tg	Mean Radiant Temperature
Ta	Air Temperature
RH	Relative Humidity
Va	Air Velocity

LIST OF ABBREVIATIONS

AMV	Actual Mean Vote
APD	Actual Percentage Dissatisfied
ASHRAE	American Society of Heating, Refrigerating and Air-Conditioning Engineers
CIE	International Commission on Illumination
DA	Daylight Autonomy
DAv	Daylight Availability
EN	European Standards
HVAC	Heating, Ventilating and Air Conditioning
IESNA	Illuminating Engineering Society of North America
ISO	International Organization for Standartizasyon
KPI	Key performance indicators
MRT	Mean Radiant Temperature
PMV	Predicted Mean Vote
PPD	Predicted Percentage Dissatisfied
PSS	Perforated Solar Screen
sDA	Spatial Daylight Autonomy
SPSS	Statistical Package for the Social Sciences
TOPSIS	Technique for Order Preference by Similarity to Ideal Solution (İdeal Çözüme Benzerliğe Göre Tercih Sıralama Tekniği)
TSI	Turkish Standard Institute (Türk Standartları Enstitüsü)

LIST OF FIGURES

Figure 1.1 Hole and depth ratio 14

Figure 1.2 Shading device parameters 15

Figure 1.3 PSS design variables 16

Figure 1.4 PSS combinations determined for the study. The orientation changes towards the main points 17

Figure 1.5 Forms of the two-storey PSS (a) with coincident holes open, (b) shifted to the right, (c) shifted to the left, (d) shifted up, (e) shifted down and (f) with coincident holes closed 18

Figure 1.6 Horizontal and vertical shading device models 19

Figure 2.1 Distribution and Dimensioning of PSSs 28

Figure 2.2 Cherokee Lofts (System:Perforated metal panel/ Direction: East / Function : Shading and Natural Ventilation 28

Figure 2.3 (a) Raif Dinçkök Cultural Center, Perforated WS panels and (b) Administrative Center Jesenice 29

Figure 2.4 Acceptable indoor temperatures depending on outdoor temperature .. 33

Figure 2.5 Adaptive model graph with acceptable operative temperature limits for naturally ventilated spaces 34

Figure 3.1 Method of the study 41

Figure 3.2 Data collection with references and measurements 29

Figure 3.3 Observation method 29

Figure 3.4. Method of field studies 29

Figure 3.5. Method of Verifications for Measurements and Simulations 57

Figure 4.1. Camera Positions and Fields of View (Red-shaded areas indicate non-visible zones) 82

Figure 4.2 Photograph Captured from Classroom Cameras on 15.06.2021 at 10:00 AM 82

Figure 4.3 Photograph Captured from Classroom Cameras on 30.05.2021 and 15.06.2021 at 10:00, 12:00, 14:00, 16:00 and 18:00 83

Figure 4.4 Field study location 84

Figure 4.5 Exterior and interior visuals of classrooms 84

Figure 4.6 Furnished plan of classrooms B- 501- B-502 and B- 503 85

Figure 4.7 Sections of classroom B-501 85

Figure 4.8 TESTO 635 - Humidity and Temperature Measurement Device, capable of measuring pressure 87

Figure 4.9 Thermal Comfort Measurement Points in Classrooms (Points 1, 2, and 3 for short-term measurements, and Point 4 for fixed measurements, Point 5 for outdoor weather conditions measurement) 92

Figure 4.10 TESTO 480 and Delta Ohm HD 32.3A PMV-PPD measurement devices 93

Figure 4.11 Protective enclosures for thermal comfort measurement devices 95

Figure 4.12 Measurement Points for Illuminance Levels in Classrooms and on chalkboard 97

Figure 4.13 (a) Konica Minolta illuminance meter and (b) Konica Minolta Cm 2600d Spectrophotometer 97

Figure 4.14 Thermal and visual comfort surveys 98

Figure 4.15 Verification of measurement devices (MBE results for PMV, air temperature and globe temperature) 83

Figure 4.16 Comparison of classrooms 102

Figure 4.17 Measurement Schedule 102

Figure 4.18 Short-term Measurement Results on October 26, 2021 (Mean Radiant Temperature, Air Temperature, Relative Humidity, Air velocity, and PMV) 104

Figure 4.19 Short-term Measurement Results on November 17, 2021 (Mean Radiant Temperature, Air Temperature, Relative Humidity, Air velocity, and PMV) 105

Figure 4.20 Long-term Measurement Results for Classroom B-503 on November 17, 2021 (Mean Radiant Temperature, Air Temperature, Relative Humidity, Air velocity, and PMV) 106

Figure 4.21 Occupancy of Classroom B-503 from 8:00 AM to 5:00 PM on November 17, 2021 106

Figure 4.22 Occupancy of All Classrooms from 8:00 AM to 5:00 PM on November 17, 2021 107

Figure 4.23 Long-term Measurement Results for Classroom B-503 from November 15–19, 2021 (Mean Radiant Temperature, Air Temperature, Relative Humidity, Air velocity, and PMV 107

Figure 4.24 Long-term Measurement Results for Classroom B-501 from November 3–19, 2021 (Mean Radiant Temperature, Air Temperature, Relative Humidity, Air velocity, and PMV) 108

Figure 4.25 Occupancy of Classroom B-501 from 8:00 AM to 5:00 PM between November 3–19, 2021 108

Figure 4.26 Long-term Measurement Results for Classroom B-502 from November 3–19, 2021 (Mean Radiant Temperature, Air Temperature, Relative Humidity, Air velocity, and PMV) 109

Figure 4.27 Occupancy of Classroom B-502 from 8:00 AM to 5:00 PM between November 3–19, 2021 109

Figure 4.28 Long-term Measurement Results for Classroom B-503 from November 3–19, 2021 (Mean Radiant Temperature, Air Temperature, Relative Humidity, Air velocity, and PMV) 110

Figure 4.29 Occupancy of Classroom B-503 from 8:00 AM to 5:00 PM between November 3–19, 2021 110

Figure4.30 Linear Regression Graph of Thermal Sensation Based on Location 112

Figure 4.31 Linear Regression Graph Assessing the Impact of Solar Radiation from the Window Based on Location 113

Figure 4.32 Results of the illuminance level measurement conducted on August 3, 2021 (external horizontal illuminance: 94,500 lux). 113

Figure 4.33 Results of the illuminance level measurement conducted on September 21, 2021 (external horizontal illuminance: 60,000 lux) 114

Figure 4.34 Results of the illuminance level measurement conducted on October 26, 2021 (external horizontal illuminance: 26,000 lux) 114

Figure 4.35 Results of the illuminance level measurement conducted on November 17, 2021 (external horizontal illuminance: 15,000 lux) 115

Figure 4.36 Illuminance level measurements in classrooms with curtains open on the specified dates. 116

Figure 4.37 Illuminance level measurements in classrooms with curtains closed on the specified dates. 117

Figure 4.38 Linear regression graph illustrating the relationship between glare on the desks and student location 118

Figure 4.39 Linear regression graph of illuminance distribution uniformity on desks based on student location 119

Figure 4.40 Linear regression graph illustrating shadow formation on desks based on student location 119

Figure 4.41 Linear regression graph of the effect of sunlight on glare on the board based on student location 120

Figure 4.42 Measurements and Simulation results for air temperature and PMV 104

Figure 4.43 Regression for air temperature (Date/Period: 24.02.2021 / 14.30-17.00 - (for each classroom for three points (total 9 points)) 104

Figure 4.44 Regression for PMV (Date/Period: 24.02.2021 / 14.30-17.00 - (for each classroom each three points (total 9 points)) 122

Figure 4.45 Regression for illuminance level (Date/Period: 24.02.2021 / 12.20-15.40 - (for each classroom for 12 points (total 36 points)) 122

Figure 4.46 Example of the designed PSS based on solar angles 123

Figure 4.47 3D model of the designed PSS and its variable design parameters. 123

Figure 4.48 Representation of the basic design principle of the designed PSS according to solar radiation (a) and design parameters (b) 124

Figure 4.49 3D Model of rooms and parametric PSS 129

Figure 4.50 Calculation and generation time of KPIs (sDA,ASE,Solar Radiation and PMV) 130

Figure 4.51 Thermal Comfort calculation adjustments 134

Figure 4.52 Example graph of optimization results performed with the Octopus plugin 135

Figure 5.1 The best scenarios determined for classroom B-501 is shown in the Octopus Pareto scatter plot coordinate graph 138

Figure 5.2 The best scenarios determined for classroom B-502 is shown in the Octopus Pareto scatter plot coordinate graph 143

Figure 5.3 The best scenarios determined for classroom B-503 is shown in the Octopus Pareto scatter plot coordinate graph 147

Figure 5.4 Designs of Opt-4, Opt-5, and Opt-9 Scenarios for the B-501 Classroom 160

Figure 5.5 Designs of Opt-2, Opt-6, and Opt-9 Scenarios for the B-502 Classroom 162

Figure 5.6 Designs of Opt-2 Scenarios for the B-503 Classroom 163

LIST OF TABLES

Table 1.1 Studies related shading devices.....6

Table 1.2 Studies related perforated solar screens (PSS).....11

Table 2.1 Classification of shading devices.....14

Table 2.2 Classification of comfort status according to standards.....33

Table2.3 Recommended daylight provision by daylight openings in vertical and.....36

Table 2.4 Recommended daily sunlight exposure 36

Table 3.1 Radiance parameters (Website of Radiance, 2020) 76

Table 4.1 Physical characteristics of classrooms 86

Table 4.2 Current transparency ratios of rooms.....86

Table 4.3 Building envelope section layers according to architectural drawings and U values from measurements.....87

Table 4.4 Building envelope section layers and U values determined in TS825 2013 according to architectural drawing section layers.....88

Table 4.5 Reflection coefficients of the classroom interior surfaces and furnishings 90

Table 4.6 Classroom Device Specifications, Visual Representations, and Spatial Configurations (The luminaire is equipped with two fluorescent lamps) 90

Table 4.7 Field study measurement Parameters.....92

Table 4.8 Delta Ohm thermal comfort measurement device probes.....94

Table 4.9 The mean values and standard deviations of the measurement results obtained under both protected and unprotected conditions for the devices.....100

Table 4.10 Results of the Thermal Comfort Survey Conducted in Classrooms on November 17, 2021 (Results are presented as percentage values (%)) 111

Table 4.11 Visual comfort survey results conducted on November 17, 2021 (expressed as percentages (%)).....118

Table 4.12 Solar radiation angles reaching the southern side according to latitude for the Northern Hemisphere 123

Table 4.13 The colorimetric measurements and reflection coefficient of the samples 125

Table 4.14 Perforated solar screen (PSS) design variables 126

Table 4.15 3D Model examples of the designed PSSs..... 127

Table 4.16 Examples of design versions dependent on the angle variable (with other variables held constant)..... 128

Table 4.17 Influence of geometrical resolution on simulation time 130

Table 4.18 Definitions of KPI and simulation settings used in optimization 132

Table 5.1 Calculation results of the best scenarios for classroom B-501 140

Table 5.2 Values of annual solar radiation incident on the window plane for classroom B-501 expressed in terms of heat gain..... 141

Table 5.3 Calculation results of the best scenarios for classroom B-502 145

Table 5.4 Annual solar radiation incident on the window plane for classroom B-502 expressed in terms of heat gain..... 146

Table 5.5 Calculation results of the best scenarios for classroom B-503 149

Table 5.6 Annual solar radiation incident on the window plane for classroom B-503 expressed in terms of heat gain..... 150

Table 5.7 Mean and standard deviation values of the best scenario calculation results for the classrooms..... 154

Table 5.8 TOPSIS results for classroom B-501 (southeast orientation) 156

Table 5.9 TOPSIS results for classroom B-502 (south orientation) 157

Table 5.10 TOPSIS results for classroom B-503 (southwest orientation)..... 157

Table 5.11 Design feature of the optimal scenarios for classroom B-501 (Southeast orientation)..... 159

Table 5.12 Design feature of the optimal scenarios for classroom B-502 (South orientation)..... 160

Table 5.13 Design feature of the optimal scenarios for classroom B-503 (Southwest orientation)..... 162

Table 5.14 PMV results of the optimal scenarios for three classrooms..... 165

ABSTRACT

A Method to Design of Perforated Solar Screens in terms of Thermal And Visual Comfort

Fatma ZOROĞLU

Department of Architecture

Program of Building Physics

Doctor of Philosophy Thesis

Supervisor: Prof. Dr. Gülay ZORER GEDİK

Co- supervisor: Assoc. Prof. Dr. Fatma Rengin ÜNVER

Spaces with high Window-to-Wall Ratios (WWR), particularly those exposed to intense solar radiation during the afternoon hours, are prone to visual and thermal discomfort. External shading devices are recognized as effective passive strategies to mitigate these issues. While numerous simulation-based studies have investigated the impact of shading devices on indoor environmental conditions, there remains a need for approaches that simultaneously address thermal and visual comfort within a single framework. Traditional shading solutions such as horizontal, vertical, and combined configurations have been extensively utilized; however, perforated solar screens (PSS) have recently emerged as innovative alternatives. Despite their growing application, particularly due to aesthetic preferences, the functional evaluation of PSSs is still underexplored. In this thesis, angled PSSs are introduced as an original design approach that passively modulates solar gains through geometric selectivity, distinguishing them from conventional flat systems.

The primary aim of this study is to present a method for evaluating shading devices with the objective of ensuring thermal and visual comfort in indoors. A parametric optimization framework was developed to identify suitable designs by varying parameters such as angle, perforation ratio, reflection coefficient, and façade distance, and then applied to real rooms to test its feasibility.

The methodological process consisted of data collection, definition of design parameters, parametric simulations, multi-objective optimization, and identification of optimal PSS designs. Within this framework, field studies (measurements and surveys), observation-based studies, validation of both measurements and simulations, and statistical analyses were conducted. As part of testing the methodology, a novel angled PSS was designed to minimize direct solar radiation while enhancing diffuse daylight. To identify the most effective PSS for classrooms with south-facing façades, key design parameters were defined. Parametric analyses were conducted within the developed optimization framework, and the optimizations were carried out by considering solar radiation, Annual Sunlight Exposure (ASE), and Spatial Daylight Autonomy (sDA) as well as simulation-based evaluation of Predicted Mean Vote (PMV), used as key performance indicators (KPI).

Through the implementation of the proposed method, the study also contributes to the literature by performing orientation-specific optimizations for three classrooms (south, southwest, and southeast) with similar characteristics, thereby examining how orientation and adjacent façade transparency influence performance outcomes. The method developed in this thesis is applicable not only to façades with different orientations and transparency levels but also to diverse building types and climate conditions, extending its relevance beyond PSSs to shading devices of varied forms.

Keywords: Perforated solar screens, thermal comfort, visual comfort, optimization, parametric design, shading devices

ÖZET

Delikli Gölgeleme Elemanlarının Isıl ve Görsel Konfor Açısından Tasarımına Yönelik Bir Yöntem

Fatma ZOROĞLU

Mimarlık Anabilim Dalı

Yapı Fiziği Programı

Doktora Tezi

Danışman: Prof. Dr. Gülay Zorer GEDİK

Eş-Danışman: Prof. Dr. Fatma Rengin ÜNVER

Saydamlık oranı yüksek olan, özellikle öğleden sonraki saatlerde yoğun güneş ışınımına maruz kalan mekânlarda, görsel ve ısıl konfor bakımından olumsuz koşullar oluşabilmektedir. Aşırı günışığı nedeni ile oluşabilecek sorunları hafifletmek amacıyla dış gölgeleme elemanları, etkili pasif stratejiler olarak yaygın şekilde kullanılmaktadır. Gölgeleme elemanlarının iç mekân koşulları üzerindeki etkilerini inceleyen çok sayıda simülasyon temelli çalışma bulunmasına rağmen, ısıl ve görsel konforun birlikte ele alındığı bütüncül çalışmalara halen ihtiyaç duyulmaktadır. Yatay, düşey ve kafes sistemler gibi farklı biçimlerde geleneksel gölgeleme elemanları yaygın biçimde kullanılmaktadır; ancak delikli gölgeleme elemanları, bir diğer adıyla mesh sistemler, son yıllarda yeni alternatif tasarımlar olarak ortaya çıkmıştır. Estetik tercihlere bağlı olarak artan kullanımlarına karşın, bu elemanların işlevsel performansına yönelik değerlendirmeler sınırlı kalmıştır. Bu tez kapsamında, açılı delikli gölgeleme elemanları (PSS) özgün bir tasarım yaklaşımı olarak sunulmakta, geometrik seçicilik yoluyla güneş kazançlarını pasif biçimde düzenleyerek konvansiyonel düz sistemlerden ayrışmaktadır.

Çalışmanın amacı gölgeleme elemanı tasarımında çevresel faktörleri değerlendirerek, iç mekânlarda ısıl ve görsel konforu sağlamayı hedefleyen bir yöntem geliştirmektir. Bu kapsamda parametrik optimizasyon yaklaşımı ile açı, delik oranı, yansıtma katsayısı ve cephe mesafesi gibi değişkenler üzerinden en uygun tasarım belirlenmiş ve geliştirilen yöntem gerçek mekânlarda uygulanarak uygulanabilirliği test edilmiştir. Çalışmada geliştirilen yöntem adımları temelde; veri toplanması, tasarımın yapılması, simülasyonlar ve optimizasyonların yapılması ve en uygun PSS tasarımının belirlenmesi süreçlerinden oluşmaktadır. Bu kapsamda alan çalışmaları (ölçme ve anket), gözleme dayalı incelmeler, ölçmeler ve simülasyonlar için doğrulama çalışmaları ve istatistiksel analizler yapılmıştır.

Tez kapsamında tasarlanan açılı PSS, doğrudan güneş ışınımını azaltırken dağınık gün ışığının katkısını artırmayı hedeflemiştir. Güney cephesi bulunan derslikler için en uygun delikli gölgeleme elemanı tasarımını belirlemek üzere temel tasarım değişkenleri belirlenmiştir. Geliştirilen optimizasyon yöntemi çerçevesinde ise, parametrik analizler gerçekleştirilmiş ve optimizasyonlar, güneş ışınımı, yıllık güneş ışığına maruz kalma (ASE) ve gün ışığı erişilebilirliği (sDA) dikkate alınarak yapılmış ve simülasyonlar PMV hesabı ile yapılmıştır.

Önerilen yöntem, benzer özelliklere sahip üç derslikte (güney, güneybatı, güneydoğu) uygulanarak, yönelime bağlı performans farklılıkları da ortaya konmuştur. Tezde geliştirilen yaklaşım yalnızca bu dersliklerle sınırlı olmayıp, farklı cephe yönelimleri, şeffaflık oranları, bina tipleri ve iklim koşulları için de uygulanabilir olup; delikli gölgeleme elemanlarının yanı sıra farklı biçimlerdeki gölgeleme sistemlerinin tasarımında da kullanılabilir.

Anahtar Kelimeler: Delikli gölgeleme elemaları, ısıl konfor, görsel konfor, optimizasyon, parametric tasarım

1
INTRODUCTION

1.1. Background

Buildings serve a fundamental role in protecting individuals from adverse environmental conditions. In developed countries, individuals spend approximately 90% of their time indoors (Working Group for Sustainable Construction, 2004). Consequently, ensuring that indoor environments adhere to thermal comfort standards is crucial for both health and productivity. This is particularly significant in educational buildings, where compliance with thermal comfort conditions has a direct impact on students' attention, focus, perception, and learning outcomes. The lack of appropriate visual comfort in classrooms and other educational spaces can lead to physiological and psychological challenges, including perceptual distortions, reduced concentration, fatigue, headaches, and frequent illnesses (R. Ünver, 2015). Therefore, ensuring thermal and visual comfort in spaces where educational activities take place is of paramount importance.

Globally, the building sector is responsible for a significant proportion of energy consumption. In 2010, energy use in this sector was distributed as follows: 20% in China, 19% in the United States, 15% in OECD countries, 6% in Russia, and 40% in other nations (US Department of Energy [DOE], 2012). In Turkey, approximately 26% of the total energy consumption originates from the residential and services sectors. Of this, 65% is attributed to heating, cooling, hot water, and ventilation systems; 20% to lighting; and 15% to household appliances and electronic devices (Acuner, E., 2013). Thus, while achieving optimal comfort conditions, energy efficiency must also be prioritized.

Studies have demonstrated that passive design strategies—such as self-shading facades, shading devices, optimized window-to-wall ratios, and building orientation—are effective in reducing solar heat gain, offering potential energy savings between 4.64% and 76.57% (LG Valladares-Rendón et al., 2017). Excessive solar heat gain increases cooling demands, leading to an estimated 28% rise in energy consumption for air conditioning systems (A. J., D. Arastech, 2006).

The design of transparent building components, including their transparency ratios, daylight transmittance coefficients, and the integration of solar control devices, is critical for managing solar heat gains. Solar radiation transmitted through glazing primarily enters as shortwave radiation; upon being absorbed by interior surfaces, it is re-emitted as longwave radiation. This process traps heat indoors, contributing to a greenhouse effect. Additionally, direct solar radiation can cause excessive daylight illumination, resulting in visual discomfort, thermal discomfort, and glare. To prevent these adverse effects, solar radiation must be controlled before it reaches transparent surfaces, which can be effectively achieved through the passive use of shading devices.

1.2. Problem statement

Shading devices are essential components in building design, implemented in various configurations and systems to address functional and environmental requirements. Horizontal, vertical, and combined horizontal-vertical (cage) shading systems are among the earliest and most commonly utilized solutions. In recent years, perforated solar screens (PSS), often referred to as mesh systems, have emerged as innovative design features. However, their integration into architectural projects is largely driven by aesthetic considerations rather than a comprehensive understanding of their functional performance. Consequently, research on PSSs remains limited.

When properly designed, PSSs can effectively regulate solar radiation. These systems have the potential to prevent excessive heat gain during cooling periods while facilitating the utilization of solar energy during heating periods. Additionally, they contribute to visual comfort by ensuring adequate daylight levels and reducing glare, thereby enhancing indoor environmental quality. In this thesis,

an angled PSS design was specifically developed as an original solution, introducing a geometry-based approach that passively modulates solar gains and admits diffuse daylight, setting it apart from conventional flat or uniformly perforated systems.

A literature review by Kırımtat et al. revealed that experimental studies on shading devices account for only 20% of the research, while investigations focused on educational buildings, such as schools and universities, constitute merely 9%. This underscores a significant gap in the evaluation of PSSs, particularly in terms of their impact on thermal comfort, visual comfort, and energy efficiency in educational settings.

To address this research gap, a comprehensive approach that integrates simulation and experimental studies is essential. Such a methodology not only enhances the reliability of findings but also enables comparative analyses, facilitating the identification of the most effective PSSs for specific applications.

1.3. The objectives and hypothesis of the study

Ensuring that indoor spaces where individuals spend extended periods comply with comfort standards is fundamental for promoting user well-being and health. Within the framework of sustainable architectural design, passive systems, including solar control devices, play a pivotal role in achieving energy-efficient buildings.

In this thesis, a systematic method is developed and tested for the design of angled perforated solar screens (PSSs), introduced as an original approach that regulates both thermal and visual comfort through geometric selectivity. The hypothesis is that optimally designed angled PSSs significantly enhance thermal and visual comfort in indoor environments compared to unshaded façades or conventional flat systems, thereby contributing to reduced energy demand and improved indoor environmental quality. The primary objective is to identify the most effective shading configurations that balance these requirements, with key performance indicators (KPIs) defined as summer and winter solar radiation on windows, Spatial Daylight Autonomy (sDA), Annual Sunlight Exposure (ASE), and Predicted Mean Vote (PMV). The foresight is that variations in design parameters—such as angle,

perforation ratio, reflection coefficient, and façade distance—directly influence indoor thermal and visual comfort conditions. By following the method proposed in this thesis, it becomes possible to achieve optimum comfort conditions through parametric optimization of angled shading systems. The optimal designs are also expected to vary depending on orientation and other spatial features, underscoring the necessity of orientation-specific evaluations. It is expected that application of the suggested methodology will demonstrate differences between optimal solutions in terms of KPIs, design parameters, and room properties.

By employing a combination of simulation and experimental methodologies, the study seeks to generate reliable data for evaluating the performance of shading systems. Ultimately, the findings aim to support the selection of angled PSSs that align with maintaining optimal comfort conditions, contributing to sustainable architectural practices and improved indoor environmental quality.

Thesis Highlights;

Building upon the background, identified research gap, and the defined objectives and hypotheses, this thesis makes the following original contributions:

- **Proposes and applies a systematic methodology** that integrates field studies, user surveys, simulation-based validation, and multi-objective parametric optimization, ensuring both technical rigor and user-centered evaluation.
- **Introduces angled perforated solar screens (PSSs) as an innovative shading design,** moving beyond conventional flat or uniformly perforated solar screen designs by incorporating geometric selectivity to passively modulate solar gains.
- **Defines and employs key performance indicators (KPI)—**including solar radiation, Annual Sun Exposure (ASE), Spatial Daylight Autonomy (sDA), and Predicted Mean Vote (PMV)(with simulations)—to provide a holistic framework for assessing both thermal and visual comfort.
- **Demonstrates orientation-specific optimization** by applying the methodology to three classrooms (south, southeast, and southwest), showing how orientation influence optimal shading strategies.

- **Verify simulation outcomes against empirical data,** strengthening the reliability of the optimization process and ensuring context-specific accuracy.
- **Establishes a replicable framework** that can be extended beyond the tested classrooms to various building types, orientations, and climatic conditions, highlighting its adaptability for diverse architectural contexts.

1.4. Lıterature Revıew

Many studies on shading devices have primarily focused on energy consumption and/or daylight levels. Most research has concentrated on the impact of reducing heat gains on energy consumption, but there is a lack of studies that simultaneously address daylight and thermal comfort in the context of shading devices. Furthermore, most of the studies have relied on simulation programs, with only a few incorporating both simulations and measurements. However, experimental studies, including both measurements and surveys aimed at understanding user satisfaction, are essential to comprehensively evaluate these three factors in relation to shading devices.

Research on perforated solar screens (PSS, mesh systems) is relatively limited. This study aims to fill this gap by developing a method to thoroughly assess the effects of PSSs within an enclosed space and to evaluate the optimal hole ratios of these devices in terms of both thermal and visual comfort.

Studies in the literature on shading devices (Table 1.1) and PSSs (Table 1.2) are summarized in the tables below.

Table 1.1 Studies related shading devices

Author(s)	Year	Method	Study Focus (Shading Devices and …)	Climate & Location	Building Type	Shading Device Type & Characteristics
Peter, G. et al.	2007	Simulation (EnergyPlus, DOE-2.1E), Field Study	Energy consumption and daylighting, visual comfort	Humid continental	School / University	Motorized mini blinds, fixed shading screen, fixed mini blinds, fixed vertical fins
Manzan, M. et al.	2009	Simulation	Energy consumption and daylighting, visual comfort	Humid continental	School / University, Office	Fixed flat panel positioned parallel to the window
Hammad, & Abu-Hijleh	2010	Simulation	Energy consumption	Abu Dhabi, UAE (hot desert)	Office	Vertical and horizontal dynamic louvers
Ahmed, A.Y. et al.	2011	Field Study	Thermal comfort	Subtropical	Office	Fixed vertical fins, diagonal fins, egg-crate
Nedhal, A. et al.	2011	Simulation	Thermal comfort	Equatorial	Residential	Vertical, horizontal, and egg-crate
Omidfar, A.	2011	Simulation (DesignBuilder, EnergyPlus)	Energy consumption, daylighting, visual comfort	Continental	Office	Fixed shading screen
Ahmed, H. et al.	2012	Simulation	Daylighting and visual comfort	Arid	Residential	Fixed solar screen
Kim, Y.-S. et al.	2013	Field Study	Daylighting and visual comfort	Laboratory conditions	Office	Movable perforated panels and movable fabric blinds

Table 1.1 Studies related shading devices (continued…)

Yao, J.	2014	Simulation (EnergyPlus), Field Study	Energy consumption, visual and thermal comfort	Ningbo, China (humid subtropical)	Residential	Movable solar shading
Atzeri et al.	2014	Simulation (EnergyPlus)	Energy consumption, visual and thermal comfort	Rome, Mediterranean	Office	Indoor and outdoor shading devices
Stazi et al.	2014	Simulation (EnergyPlus), Field Study	Energy, visual and thermal comfort, lifecycle environmental impact	Mediterranean	School / University	Movable aluminum horizontal louvers, movable aluminum sliding perforated panels, movable traditional aluminum and wooden persiana
Jinia, M.A. et al.	2015	Field Study	Daylight penetration with fixed shading	Dhaka, tropical	Residential	Fixed external shading devices
Shahdan et al.	2018	Simulation	Effectiveness of external shading on energy use	Tropical / Subtropical	Case study building	Configurations of external shading devices
Jayaweera et al.	2021	Simulation + Field study	Daylight and energy in high-rise residential with shading	Dense urban tropics	Residential (high-rise)	External shading devices
Koç, & Kalfa	2021	Simulation (DesignBuilder)	Office energy performance with shading	Mediterranean	Office	Overhangs, horizontal/vertical louvers, egg-crate
Daneshi et al.	2022	Hybrid machine learning + Optimization	Performance-based shading design tool	Tehran, Semi-arid	Office	External fixed shading devices
Kirimtat, & Manioğlu	2024	Simulation + multi-objective optimization (MOO)	Dynamic shading device evaluation	İzmir, Hot and Humid	Office	New-generation dynamic shading devices

The effectiveness of shading devices in mitigating solar heat gain and improving building performance has been a central topic in architectural and engineering research. Table 1.1 summarizes key findings from several studies focusing on the impact of various shading strategies on daylighting, energy consumption, and thermal comfort across different climatic zones and building types.

A field study conducted by Jinia et al. (2020) in Dhaka, a tropical region, investigated the effect of fixed external shading devices on daylight penetration. The study highlights that fixed shading is an effective strategy for managing daylight in tropical climates, where high sun angles and intense solar radiation are prevalent (Jinia et al., 2020). However, the study's focus on fixed devices is a limitation, as it does not address the potential benefits of dynamic or adaptive shading systems, which could offer greater flexibility and performance optimization throughout the day and across different seasons.

Moving beyond a single climatic zone, Shahdan et al. (2018) used simulation to evaluate the effectiveness of external shading on energy use within a case study building. Their research explored different configurations of external shading devices and demonstrated their significant role in reducing a building's cooling load (Shahdan et al., 2018). As well as the limitations of shading configurations and calculation cooling loads, a key limitation of this work is its reliance solely on simulation, which may not fully capture the real-world complexities and variations of building performance.

The study by Jayaweera et al. (2020) combined both simulation and field study to examine the relationship between daylight and energy use in high-rise residential buildings in dense urban tropical areas (Jayaweera et al., 2020). This hybrid approach provides a more robust analysis by validating simulation models with real-world data. The research concluded that external shading devices are crucial for balancing daylight and energy efficiency in high-density urban environments. Despite its strengths, this study assesses the daylight and energy performance excluding thermal comfort, and the study's specific focus on high-rise residential

buildings in a dense urban context limits the generalizability of its findings to other building types or less-dense environments.

Koç and Kalfa (2020) utilized DesignBuilder simulation software to analyze the energy performance of an office building in a Mediterranean climate. Their research systematically evaluated various shading types, including overhangs, horizontal and vertical louvers, and egg-crate systems. The study found that the optimal shading configuration significantly depends on the building's orientation and local climate conditions (Koç and Kalfa, 2020). This study focuses only on energy consumption, not daylight and thermal performance, and investigates limited shading configurations.

Recent research has also explored advanced design and optimization methods. Daneshi et al. (2020) developed a hybrid machine learning (ML) and optimization tool to create a performance-based shading design tool using parametric solar shading models (Daneshi et al., 2020). This approach represents a significant advancement by enabling architects and designers to generate and evaluate complex shading geometries for optimal performance. While innovative, the study's primary focus on developing a tool and its theoretical application leaves a gap in real-world validation. The lack of a specific case study or field data makes it difficult to assess the tool's practical effectiveness and reliability. Also, this study has not investigated thermal comfort performance.

Similarly, Kirimtat and Manioğlu (2020) presents a simulation-based performance evaluation of new-generation dynamic shading devices for a glass-covered office building in a hot and humid climate. The study employs a multi-objective optimization (MOO) method to simultaneously minimize cooling energy consumption and maximize thermal comfort. The authors propose a unique parametric design using software like Rhinoceros 3D and Grasshopper 3D to find optimal cell sizes and blade angles for different building orientations (Kirimtat and Manioğlu, 2020). Their research demonstrated the better performance of dynamic systems over traditional fixed devices, particularly in adapting to changing solar conditions. The study's main contribution is the optimization of conflicting performance goals in the design of dynamic shading systems. However, the research has several limitations, including its focus on energy consumption and

thermal comfort performance, excluding daylight performance and visual comfort, and its purely simulation-based methodology without real-world validation.

Despite a substantial body of research on shading devices, a notable gap persists in studies that holistically assess their combined impact on energy consumption, daylighting, and thermal comfort. Most of the existing literature is also heavily reliant on simulation-based methodologies, often lacking empirical validation through real-world measurements and user feedback. This holistic gap is also evident in the literature on specific, advanced systems such as perforated shading devices.

Table 1.2 Studies related perforated solar screens (PSS)

Author(s)	Year	Method	Study Focus (Shading Devices and …)	Climate & Location	Building Type	Shading Device Type & Characteristics
Hien & Istiadji	2003	Simulation and field measurements	Daylighting and natural ventilation	Tropical – Singapore	Residential (high-rise)	Perforated panels; six scenario
Omidfar, A. et al.	2011	Simulation	Energy consumption, daylighting and visibility	—	Office	Shading screen (form)
Sherif, A.H.; Saber, E.;	2012	Simulation	Daylight and visual comfort	Arid	Residential	Fixed solar screen
Sherif, A.H.; Sabry, H.;	2012	Simulation	Daylighting and glare	Desert (arid)	Residential	Solar screens; rotation angle and opening aspect ratio
Kim & Kim	2013	Field measurements	Daylight and visual comfort	Laboratory/testbed	Office (test room)	Movable perforated panels and fabric blinds
Sabry, H. et al.	2014	Simulation	Energy consumption; daylighting; visual comfort	Desert (arid)	Residential	Effect of screen depth and perforation ratio, **Solar screens** (The effect of axial rotation and aspect ratio change of their apertures)
Keleş, N.S.	2016	Simulation (Ecotect, EnergyPlus)	Energy consumption and Daylight level	Temperate – Germany	Office / University	Vertical and horizontal shading devices
Blanco, J.M. et al.	2016	Simulation (EnergyPlus via DesignBuilder) and	Energy consumption and Thermal behavior	Spain (temperate)	Office (case study)	Perforated metal sheet DSF; (color, material, perforation ratio and air chamber width, location and wind inflow)

Table 1.2 Studies related perforated solar screens (PSS) (continued…)

Author(s)	Year	Method	Study Focus (Shading Devices and …)	Climate & Location	Building Type	Shading Device Type & Characteristics
Lavin & Fiorito	2017	Simulation and field study	Energy consumption and UDI, DGP	Australia (hot-humid/subtropical)	Office	Perforated screens (size and distribution)
Chi, D.A. et al.	2017	Simulation	Energy consumption and Daylighting	Mediterranean – Seville, Spain	Office	Perforated solar screens(PSS) (perforation ratio, shape, matrix and orientation)
Chi, D.A. et al.	2018	Simulation	Energy consumption and Daylight availability	Mediterranean – Seville, Spain	Office	Perforated solar screens(PSS) (perforation ratio, shape, matrix and orientation)
Alawadhi, E.M.	2018	Simulation and field study /Experimental	Illuminance; heat flow reduction	Hot arid – Kuwait	Residential/test room	Double solar screens (perforated; misalignment patterns)
Blanco, J.M. et al.	2019	Simulation and field monitoring	Energy consumption, Thermal behaviour; visual constraints	Spain (temperate)	Office (service building)	Double-skin perforated façades (orientation, location)
**Srisamranungrung & **	**2020**	Simulation	Balance of natural ventilation, daylighting & thermal effects in DSPF	Temperate – Japan	Office (generic model)	Double-skin perforated façade with ventilation ports
**Srisamranungrung & **	**2021**	Simulation	Correlations between performance and DSPF design parameters	Japan (—)	Office (generic model)	Double-skin façade utilizing perforated screen
Chi, D.A. et al.	**2021**	Simulation	Daylight availability & low energy use in offices	Mediterranean – Seville, Spain	Office	Perforated solar screens (ratio, shape, matrix, orientation)

Table 1.2 Studies related perforated solar screens (PSS) (continued…)

Author(s)	Year	Method	Study Focus (Shading Devices and …)	Climate & Location	Building Type	Shading Device Type & Characteristics
Abdelhamid, F.M. et al.	**2023**	Simulation	Daylighting & glare in hot-dry climate with patterned perforations	Hot-dry – Egypt	Classroom/office (modeled	Parametric patterned perforated façade
Naik & Kachhwaha	2023	Review + meta-analysis	Dynamic vs static solar screens for performance	Various	—	**Dynamic/perforated screens** (performance synthesis)
Huang, L. et al.	**2024**	Simulation	Daylighting & visual comfort with **non-uniform** PSS	—	Office (modeled)	Non-uniform perforated solar screens
Elsiana, F. et al.	**2024**	Simulation	Daylighting evaluation in the tropics	Tropical – Indonesia	Office/Classroom	Perforated screen façade with light shelf
Gaber, S. et al.	**2025**	Simulation + Machine Learning	Optimizing PSS for daylight & energy	Hot arid – multi-city (UAE context)	Office (modeled	Perforated solar screens; ANN-based optimization
El-Bahrawy, A. M. F.	2025	Simulation	**Balancing PSS parameters** for glare & daylight optimisation	Hot-dry – Egypt	Office (modeled)	**Perforation % / matrix / thickness / separation**

Among the studies on perforated solar screens (PSS), A. Sherif et al. investigated the performance of perforated wooden solar screens in a typical residential building located in a hot, dry desert climate zone. The study, conducted using the EnergyPlus simulation program, examined the effects of varying hole ratios and depths of the solar screens on annual energy loads. The results indicated that energy savings of up to 30% were achieved for east and west-facing orientations. The study recommended a design with a hole ratio of 80-90% and a depth/opening width ratio of 1:1 as optimal (A. Sherif et al., 2012).

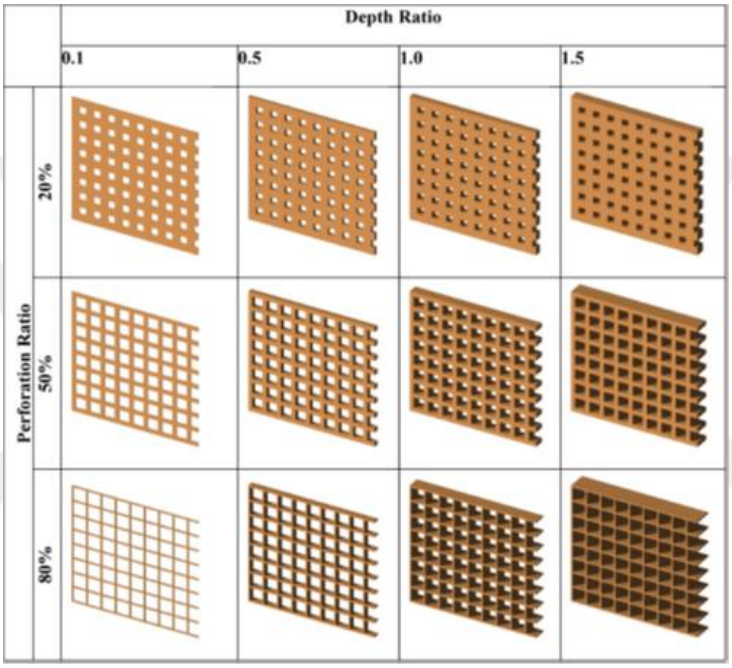

Figure 1.1 Hole and depth ratio (A. Sherif et al., 2012).

H. Sabry et al. conducted a study on the design of solar screens aimed at providing visual comfort and minimizing energy consumption in a residence located in the desert region of Saudi Arabia. The study focused on the effects of axial rotation of solar screens and changes in the aspect ratio of their apertures. Dynamic Daylight Performance Metrics (DDPM) and EnergyPlus simulation software were used to evaluate the performance of the systems.

The study's findings indicated that non-rotated solar screens with large horizontal apertures (aspect ratio 18:1) performed better for north and south orientations. In contrast, solar screens that rotated along their vertical axis with smaller apertures (aspect ratio 1:1) were more effective for east and west orientations. These

configurations improved daylighting performance while minimizing energy consumption. The combination of these factors resulted in a daylight area coverage of 66-97% in the tested spaces. Additionally, the use of solar screens led to a 25% reduction in energy consumption compared to the scenario without solar screens (H. Sabry et al., 2014).

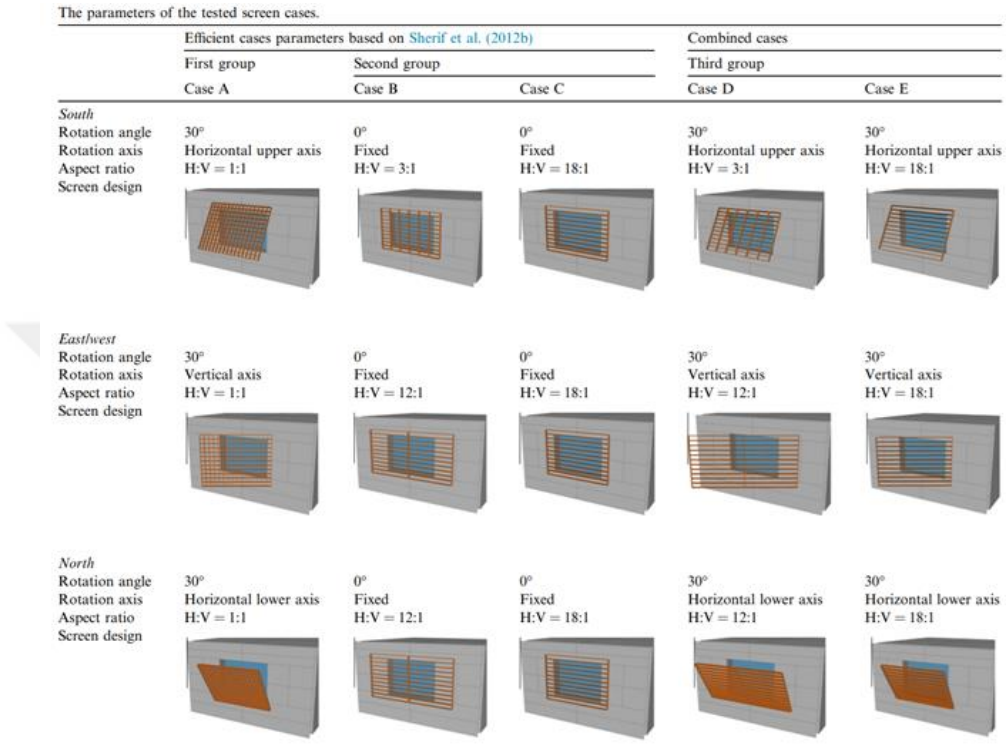

The parameters of the tested screen cases.

	Efficient cases parameters based on Sherif et al. (2012b)			Combined cases	
	First group	Second group		Third group	
	Case A	Case B	Case C	Case D	Case E
South					
Rotation angle	30°	0°	0°	30°	30°
Rotation axis	Horizontal upper axis	Fixed	Fixed	Horizontal upper axis	Horizontal upper axis
Aspect ratio	H:V = 1:1	H:V = 3:1	H:V = 18:1	H:V = 3:1	H:V = 18:1
Screen design					
East/west					
Rotation angle	30°	0°	0°	30°	30°
Rotation axis	Vertical axis	Fixed	Fixed	Vertical axis	Vertical axis
Aspect ratio	H:V = 1:1	H:V = 12:1	H:V = 18:1	H:V = 12:1	H:V = 18:1
Screen design					
North					
Rotation angle	30°	0°	0°	30°	30°
Rotation axis	Horizontal lower axis	Fixed	Fixed	Horizontal lower axis	Horizontal lower axis
Aspect ratio	H:V = 1:1	H:V = 12:1	H:V = 18:1	H:V = 12:1	H:V = 18:1
Screen design					

Figure 1.2 Shading device parameters (H. Sabry et al. 2014).

Perforated shading panels (PSS, or perforated solar screens) are designed to control solar radiation while maintaining adequate daylight levels. In one study, the daylight performance and energy consumption of PSS facades were analyzed in an integrated manner. The study considered variables such as hole ratio, shape, and matrix of the PSS, with 16 combinations optimized using the DOA (Orthogonal Arrays) method. These combinations were simulated on the south facade of a building in Seville, Spain.

When comparing the non-optimized facade with the optimized PSS, the results revealed a 50% increase in the actual daylight area and a 55% reduction in total energy demand. The DOA analysis evaluated daylight performance by examining non-daylit, partially daylit, actual daylit, and overlit areas, while energy

consumption was assessed based on TSRE (annual transmitted solar radiation energy), lighting energy, cooling energy, and heating energy.

The DOA study determined that the optimal PSS configuration was a 37.5% hole ratio, a 3x7 matrix, and a hexagonal shape. While all PSS configurations reduced solar gains through radiation, none provided sufficient daylight levels on their own. However, the optimized PSS increased the actual daylit area by 50% and reduced TSRE by 63%. Although lighting energy consumption increased by 62%, cooling and heating loads decreased by 58% and 86%, respectively. As a result, a total annual reduction of 55% in energy consumption was achieved. The study recommended further evaluation of factors such as thickness, material, slope, visual comfort, and external views for future research (DA Chi et al., 2017).

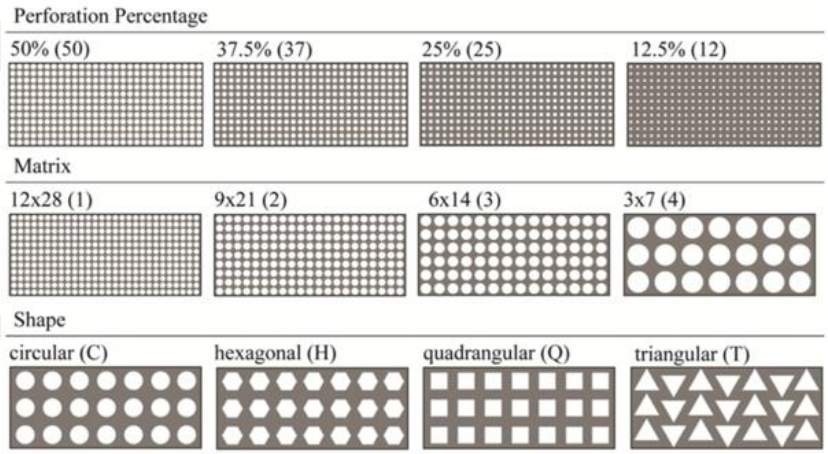

Figure 1.3 PSS design variables (DA Chi et al. 2017).

A similar study on PSSs was conducted by DA Chi et al. to investigate the relationship between Daylight Availability (DAv) and annual energy consumption (including artificial lighting, heating, and cooling systems) in an open-plan office located in Seville, Spain. The primary objective of this study was to determine whether the DAv areas projected onto the work plane would impact the total building energy consumption.

The study revealed a strong linear relationship between the overlit area and cooling energy consumption. It was found that reducing the overlit area to below 40% for the south-facing facade and below 50% for the north, east, and west facades resulted

in a total energy consumption of less than 120 kWh/m² per year. The DAv areas were categorized as 'fully daylit,' 'partially daylit,' 'non-daylit,' and 'overlit.'

The study suggests that future research could further explore issues related to sunlight accessibility, glare, and uniform daylight distribution, particularly in varying climatic conditions (DA Chi et al., 2018).

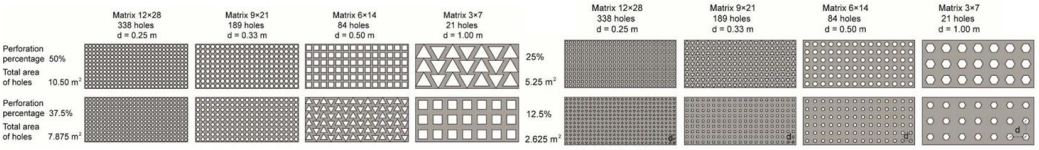

Figure 1.4 PSS combinations determined for the study. The orientation changes towards the main points (DA Chi et al., 2018).

In their study, EM Alawadhi et al. experimentally investigated the performance of a ‘double solar screen (DSS)’ positioned outside a window facing west. The purpose of the DSS was to control the amount of daylight entering the window and mitigate the negative effects of solar radiation. For the examined DSS, two identical square perforated panels, each with a hole ratio of 25%, were used. Panels without a solar screen and those with a single solar screen were also considered for comparison.

The best performance in terms of illumination was achieved when the holes were oriented downward. Daylight data were obtained using the Ecotect program. The highest reduction in heat flow from the window was observed when the panels were oriented correctly. Heat flow calculations were performed, and measurements were taken using a Heat Flux Sensor. The optimal performance in terms of both illumination and heat reduction was achieved with the downward orientation of the panels (EM Alawadhi et al., 2018).

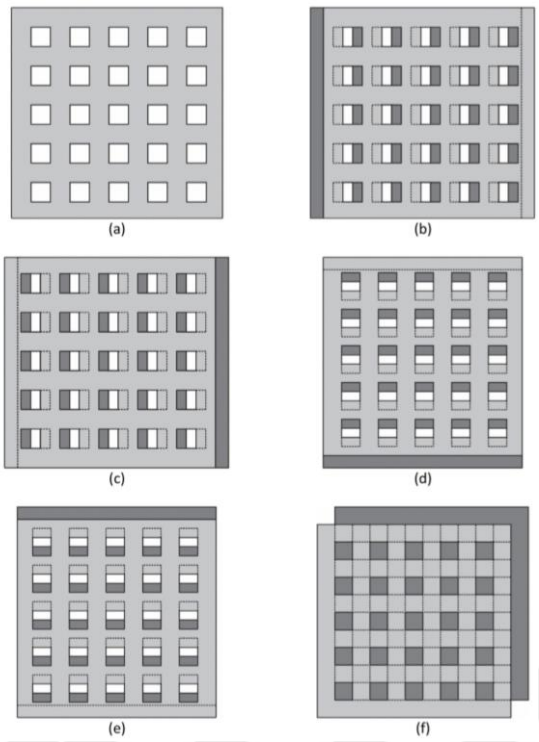

Figure 1.5 Forms of the two-storey PSS (a) with coincident holes open, (b) shifted to the right, (c) shifted to the left, (d) shifted up, (e) shifted down and (f) with coincident holes closed (EM Alawadhi et al., 2018).

In another study, shading devices were proposed for a southwest-facing office building located on the HfT Stuttgart campus in Germany, using the Ecotect program. Energy analyses were conducted for the proposed shading devices, and illuminance levels were compared using the EnergyPlus program. The study defined the cooling period as 5 months (May-September) and the heating period as 7 months (October-April).

The analysis revealed that the configuration using vertical and multiple horizontal shading devices (5) resulted in the lowest cooling energy consumption. This configuration achieved a 60.43% reduction in cooling energy consumption but caused a 25.94% increase in heating energy consumption. The study concluded that the shading device configuration that provided the highest reduction in annual energy consumption was the horizontal and vertical broken shading device model (4), which resulted in an 11.23% reduction in annual energy consumption (Keleş, 2016).

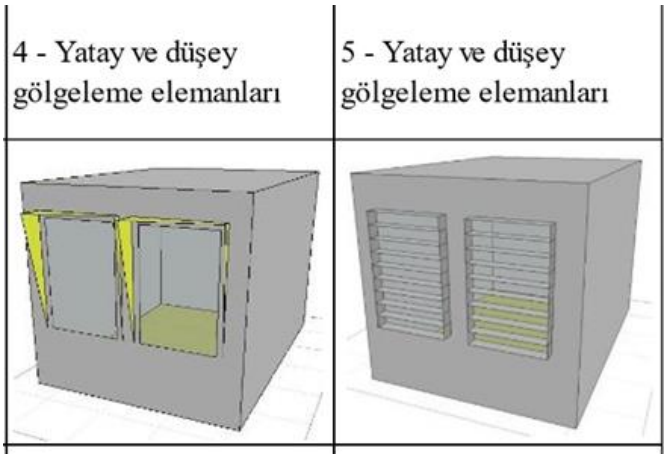

Figure 1.6 Horizontal and vertical shading device models (Keleş, 2016)

The application of solar shading systems in building design has been widely investigated in recent decades, primarily focusing on their contribution to reducing cooling loads and enhancing indoor daylighting. Early studies predominantly relied on simulation-based evaluations, emphasizing energy consumption or daylight availability as the key performance metrics (Peter G. et al., 2007; Manzan et al., 2009). However, these studies often treated thermal comfort and visual comfort as independent variables and rarely adopted a comprehensive, integrative approach. Moreover, limited effort has been made to validate simulation outputs with in-situ measurements or user-based evaluations, resulting in a gap between theoretical modeling and practical applicability.

Within the literature focused on perforated solar screens (PSS)—also referred to as perforated façades or mesh systems—researchers have examined variables such as hole ratio, depth, aperture shape, and material properties (Sherif et al., 2012; Chi et al., 2017, 2018). These studies have shown that PSS can effectively reduce solar heat gains and modulate indoor lighting conditions.

At the conclusion of their 2017 study, Doris A. Chi and colleagues recommended that further research should evaluate factors such as thickness, material, slope, visual comfort, and external view considerations (Doris A. Chi et al., 2017). In their 2018 study, Doris A. Chi and her team suggested that future studies could focus on issues such as daylight accessibility, glare, and uniform daylight distribution across different climates (Doris A. Chi et al., 2018).

Yet, most of these investigations were carried out through static simulations, typically conducted under specific climatic conditions (e.g., hot-arid or Mediterranean), and applied primarily to residential or office buildings. Only a few studies integrated user feedback, glare analysis, or real-time illuminance data, which are essential for a holistic assessment of comfort and usability (Kim et al., 2013; Alawadhi, 2018). Furthermore, experimental studies incorporating dynamic behavior, seasonal variations, or adaptive responses to changing environmental conditions remain scarce.

Traditional methods used geometrical calculations to find optimal design of external shading devices for thermal and visual comfort. This study suggested that their method may be used in computer programs (Gedik, 2002). A concise and practical method for designing external shading devices—moving beyond traditional rule-of-thumb and geometric approaches—has been proposed, aiming to optimize both thermal and visual comfort while paving the way for future implementation as a computerized design tool. While PSSs are increasingly used for their aesthetic appeal and ability to diffuse light, their performance has not been adequately explored in a multi-objective context that simultaneously balances thermal comfort and daylight, nor have they been sufficiently validated with empirical data as well as investigation with simulations. Therefore, this study aims to address these limitations by providing a comprehensive analysis of PSSs.

Studies on PSSs primarily focus on visual comfort and thermal comfort separately (Table 1.2). However, these factors should be considered in an integrated manner, with optimization carried out by accounting for shading design parameters. The aim of this study is to develop a method for designing optimal perforated solar screens that effectively provide both thermal and visual comfort.

Studies by Srisamranrungruang & Hiyama (2020, 2021) provide a foundational understanding of double-skin perforated façades (DSPF). Their 2020 study, focused on a temperate climate in Japan, explores the intricate balance between natural ventilation, daylight, and thermal effects. This work highlights the multifaceted nature of DSPF performance, demonstrating that these façades are not merely static sun-shading devices but active components in a building's environmental control system (Srisamranrungruang & Hiyama, 2020). A subsequent study by the same

authors (Srisamranrungruang & Hiyama, 2021) further investigates the correlations between design parameters and overall building performance, offering valuable insights into how perforation geometry and other variables influence outcomes. However, a notable limitation of these studies is their reliance on generic office models and a single climate context. While their findings are valuable for understanding fundamental principles, they may not be directly transferable to different building types or climates without further validation. Crucially, while these studies address individual performance metrics, they do not provide a comprehensive, multi-objective evaluation of visual and thermal comfort performance simultaneously within a single integrated framework.

Chi et al. (2021) investigated the impact of PSSs on daylight availability and energy use in a Mediterranean climate. This research is significant as it analyzes the effect of various parameters like perforation ratio, shape, and matrix on building performance (Chi et al., 2021). The study provides a clear link between design choices and tangible energy savings, a critical contribution to the field. Nevertheless, the study's focus on a specific climate and office type might limit the generalizability of its findings to other contexts. Similar to the previous studies, this research focuses on specific performance aspects without a holistic evaluation that integrates visual comfort and thermal comfort performance. Additionally, the study's reliance on simulation without any mention of empirical validation or measurement of an existing building raises questions about the accuracy and reliability of its results.

Abdelhamid et al. (2024) explore the impact of parametric patterned façades on daylight quality and visual comfort, highlighting the importance of visual aesthetics and occupant well-being in addition to energy performance (Abdelhamid et al., 2024). El-Bahrawy et al. (2025) delve into the specific balancing act required to optimize both daylight and glare performance by adjusting perforation percentage, matrix, and thickness (El-Bahrawy et al., 2025). These studies evaluate daylight and visual comfort but do not fully integrate their findings with thermal and energy performance.

The trend towards more complex and optimized systems is also evident in recent literature. Huang et al. (2024) investigate non-uniform PSSs, moving beyond the

traditional uniform perforation patterns. Their work on daylighting and visual comfort suggests that non-uniform designs can achieve superior performance by adapting to specific solar conditions (Huang et al., 2024). This study pushes the boundaries of façade design by introducing a new level of complexity. A significant limitation is that the research focuses on visual comfort and daylighting, neglecting to evaluate thermal and energy impacts simultaneously. The absence of on-site measurements and simulation validation is another key deficiency in this work.

Gaber et al. (2025) utilize a hybrid approach combining simulation with machine learning (specifically, an ANN-based optimization) to enhance daylight and energy efficiency (Gaber et al., 2025). This represents a significant leap forward, as it moves beyond simple parametric studies to a data-driven optimization process that can handle the complexity of multiple design variables. While this approach is highly promising, the practical implementation of such a complex optimization process and the validation of its results in a real-world setting remain a challenge. Despite its advanced approach, this study's primary focus is on daylight and energy efficiency, and it does not explicitly integrate the assessment of thermal comfort. The paper mentions multi-city contexts, but it does not detail any pre-existing measurements of these locations for model calibration or validation.

In contrast, the human-centric experimental work by Naik & Kachhwaha (2023) makes a different contribution by focusing on occupant perception and thermal pleasure (Naik & Kachhwaha, 2023), yet even this study lacks a holistic analysis that integrates its findings with building energy performance. Their study demonstrates that dynamic screens can enhance occupant thermal pleasure through visual variability, a phenomenon known as "thermal alliesthesia." This finding highlights that the value of façade design extends beyond simple energy performance to include occupant well-being and comfort. Another limitation of this work is its lack of a holistic assessment that integrates visual comfort and thermal comfort performance into a single, comprehensive analysis.

Current research on perforated façades predominantly relies on simulation-based studies that fail to provide a holistic, multi-objective assessment of visual and thermal comfort simultaneously. A significant and recurring deficiency is the lack of empirical validation, as few studies validate their models with real-world

measurements. In light of the above, several critical gaps persist in the current literature. Future studies should pursue a holistic approach that integrates thermal comfort and visual comfort into a unified evaluation framework. There is a pressing need for experimental research that tests optimized PSS configurations under diverse climatic conditions and building types, incorporating both quantitative metrics and qualitative user feedback. Addressing these research gaps will contribute to the development of comprehensive, climate-responsive, and user-oriented shading design strategies.

Building on these gaps, this study introduces a novel PSS design with angled perforations, which differs from conventional uniform or non-uniform systems (Huang et al., 2024; El-Bahrawy et al., 2025). Unlike prior research that largely examined visual and thermal comfort separately (Srisamranrungruang & Hiyama, 2020, 2021; Chi et al., 2021), the proposed angled PSS design explicitly integrates both aspects within a single optimization framework. Moreover, while recent studies explored aesthetics and occupant perception (Abdelhamid et al., 2024; Naik & Kachhwaha, 2023) or advanced optimization methods (Gaber et al., 2025), they remain limited either by scope or lack of empirical validation. The angled PSS concept presented here addresses these shortcomings by enabling dynamic modulation of solar radiation and daylight, thereby enhancing both visual and thermal comfort. Thus, this angled system represents a distinct façade device typology that expands the design vocabulary of perforated shading systems.

This study aims to address these gaps by proposing a methodologically integrated framework that evaluates thermal comfort and visual comfort of PSSs using both simulation and field studies. Unlike prior studies that predominantly focused on energy-related parameters, this research investigates thermal and visual parameters defining key performance indicators (KPI) and design parameters. The methodology suggest that conducting optimizations to determine best PSS design in terms of KPI. Thus, the interdependent effects of PSS design parameters were also investigated—such as slat angle, dimensions, hole ratio, reflection factor, and distance from the building—on both environmental and perceptual comfort. Moreover, the suggested methodology tested in three classrooms that have different orientation. Therefore, by focusing on an enclosed space context with variable

façade orientations, the study expands the applicability of developed methodology and designed PSS to a broader range of building types and climatic contexts.

2
SHADING DEVICES AND THEIR PERFORMANCES

2.1. Shading Devices

Among passive cooling systems, solar control devices, defined as heat mitigation systems (NB Geetha & R. Velraj, 2012), are classified into two main categories: fixed and movable. Additionally, based on their placement, these devices are categorized as internal, external, or intermediate systems (L. Bellia et al., 2014).

When shading devices are positioned externally, they effectively block solar radiation before it reaches the building's glass surfaces. In contrast, internal shading devices allow solar radiation to penetrate the interior, where it contributes to the greenhouse effect. Specifically, long-wavelength radiation, which cannot pass back through the glass, becomes trapped inside, leading to increased interior temperatures and higher cooling loads (G. Kim et al., 2012). Studies have consistently demonstrated the superior effectiveness of external shading devices in reducing solar heat gain (Atzeri et al., 2014), while fixed shading devices have been identified as an economical and practical solution (AAY Freewan, 2014; NA Al-Tamimi & SFS Fadzil, 2011).

External fixed shading devices are widely utilized to regulate solar radiation and enhance energy efficiency. However, these devices may inadvertently reduce natural daylight availability, increasing reliance on artificial lighting systems. Additionally, they may obstruct beneficial winter sunlight, thereby impacting overall thermal comfort. For this reason, the precise selection of shading device

types and their optimal placement is crucial to achieving a balance between daylight access, visual comfort, and thermal comfort.

The operation of shading devices can be classified as fixed, mechanically operated, or computer-controlled systems. When shading devices are installed on the building's exterior, they integrate seamlessly with the architectural facade, functioning as an integral component of the building envelope (Sönmez et al., 2018). However, positioning shading devices too close to the building envelope can lead to overheating due to limited ventilation. To prevent such issues, it is recommended to create a buffer zone between the shading device and the building envelope, allowing for improved thermal performance and air circulation.

Table 2.1 Classification of shading devices (Bellia et al., 2014)

Classification of shading devices in buildings	**Exterior**	**Middle**	**İnterior**
Fixed Shading Devices	√	-	√
Movable (manual or automatic) shading devices	√	√	√

In the design of shading devices, material selection is as crucial as factors such as shape, hole ratio, and placement. Among the key considerations in material selection and design are wind resistance and the provision of adequate tolerance margins to account for the expansion of materials due to thermal effects (Eşsiz & Ekinci, 2004). Commonly used materials for shading devices include glass, aluminum, and wood (Sönmez et al., 2018). The advantages of metal facade systems include ease of assembly, low maintenance requirements, and flexibility in design.

When using metal as a material, thermal expansion can lead to friction between the connected metal surfaces. A common solution to this issue is the use of plastic washers to separate the surfaces. The number of fixings required depends on vertical and wind loads, and the connections can be either visible or concealed. Various connection techniques are available, depending on the type of metal used, such as point connections (e.g., bolts, screws, clips) and flat metal connections (e.g., soldering, welding, and bonding). Materials like aluminum, stainless steel, zinc, tin, copper, and titanium are resistant to natural corrosion under typical weather

conditions and generally do not require additional protection. Other materials commonly used in metal facades include steel, stainless steel, aluminum, zinc, titanium, copper, lead, and tin, with metal thicknesses ranging from 0.5 mm to 6 mm. For perforated sheets thicker than 6 mm, softer materials are recommended (Eşsiz & Ekinci, 2004).

For shading devices located externally, attention must be paid to the formation of the rust-patina layer. A well-formed patina layer is achieved when the wetting-drying cycles occur regularly. Surfaces facing west and south receive more sunlight, resulting in a more uniform oxide layer, while those facing north and east remain wet for longer periods, causing slower patina formation, especially on the northern facade. To prevent moisture retention, it is essential to avoid details that could trap water, and joints should be tightly sealed and leak-proof. It is recommended that facade panels have thicknesses in the range of $1.6 \leq t \leq 76$ mm. The use of perforated panels accelerates the drying process. A common practice is to connect metals resistant to atmospheric corrosion to the main structure using nuts and bolts. In this context, stainless steel or galvanized steel fasteners are recommended. In regions such as Istanbul, it has been observed that reducing the surface area facilitates the completion of the wetting-drying cycle. Thin sheets, including perforated sheets, can be used to optimize this process (Es & Girgin, 2018).

2.1.1 Perforated Solar Screens (PSS)

Perforated solar screens are effective in reducing cooling loads and thermal discomfort. These devices can be defined as external perforated panels (Harris, 2006) placed outside windows or as solar control panels (solar screens). Based on a review of the literature, the most widely used term was identified as "perforated solar screens," and the most suitable Turkish equivalent was determined to be "delikli gölgeleme elemanları".

To achieve optimal energy performance and prevent overheating, it is essential to control the solar radiation passing through the window during periods of excessive heat. PSSs have been utilized for centuries in Middle Eastern countries. Increasing the hole depth of these devices blocks a portion of the incoming solar radiation, thereby reducing the amount that passes through. However, this also diminishes the

external visual connection. A reduction in the hole ratio further limits the passage of solar radiation from all directions (A. Sherif et al., 2012).

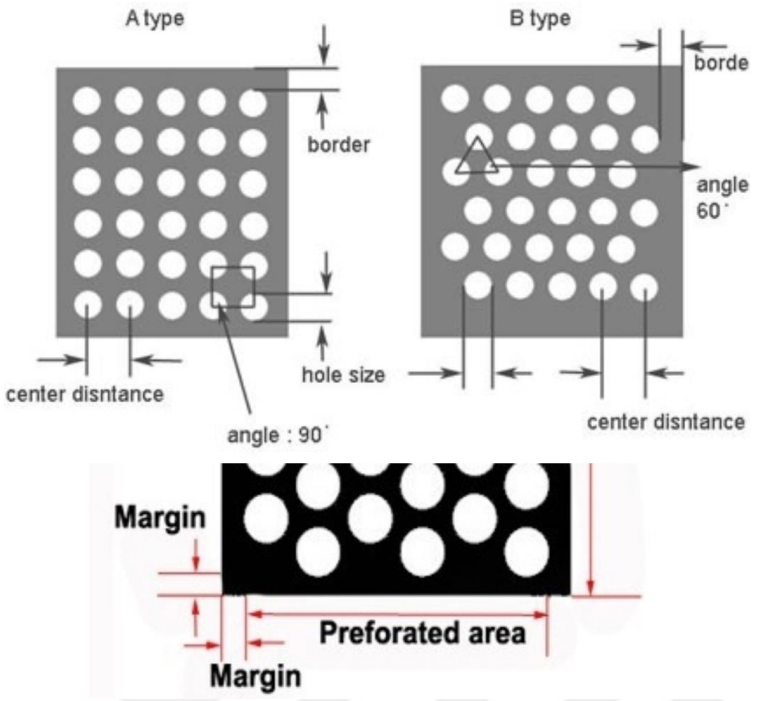

Figure 2.1 Distribution and Dimensioning of PSSs

Examples of the Use of PSSs on Exterior Facades:



Figure 2.2 Cherokee Lofts (System:Perforated metal panel/ Direction: East / Function : Shading and Natural Ventilation (Şenyurt, Altın, 2014))



Figure 2.3 (a) Raif Dinçkök Cultural Center, Perforated WS panels and (b) Administrative Center Jesenice

2.2. Indoor Comfort Conditions

From the past to the present, humans have taken various measures to meet their shelter needs, protecting themselves from external environmental conditions. Over time, they have developed building structures and their envelopes to minimize the impact of these external climatic factors. The building envelope acts as a barrier, separating internal conditions from the outside environment. In developed countries, people spend up to 90% of their time indoors (Working Group For Sustainable Construction, 2004). As a result, the spaces where we spend most of our time must meet comfort standards to support healthy and productive living.

Until the 1990s, building planning focused primarily on ensuring user comfort, often prioritizing the provision of air conditioning systems to improve indoor quality, while energy efficiency was considered secondary. Today, however, building design balances user comfort with the need to reduce energy consumption, increase energy efficiency, and protect the environment. Modern regulations emphasize sustainable building practices, aiming to reduce energy consumption and improve energy efficiency. A significant portion of a building's energy is consumed

to maintain indoor quality, which directly impacts users' health, productivity, and comfort.

Providing interior quality refers to creating an environment that satisfies the user's comfort requirements. While user satisfaction is achieved by maintaining proper comfort conditions, energy consumption can be minimized by improving building efficiency during use. For individuals to lead healthy and productive lives, buildings must adhere to specific comfort standards. Comfort conditions are typically categorized into thermal comfort, auditory comfort, visual comfort, and indoor air quality. This study investigates thermal comfort and visual comfort together through the use of PSSs.

2.2.1. Thermal Comfort

Thermal comfort refers to the satisfaction of individuals with the thermal conditions of their environment (ASHRAE 55, 2020). It varies from person to person and depends on both personal factors (e.g., clothing insulation level, activity level) and environmental factors (e.g., air temperature, radiant temperature, relative humidity, air velocity). These factors can be controlled within a building to achieve thermal comfort. International standards such as ASHRAE 55 and EN ISO 7730 provide guidelines to assess users' satisfaction with the thermal conditions of their environment. Thermal comfort in indoor environments is determined by both subjective and objective factors. Subjective parameters include age, gender, subcutaneous fat, and health status, which vary from person to person. Objective parameters include indoor temperature, Mean Radiant Temperature, relative humidity, air velocity, activity level, and clothing insulation level.

To achieve thermal comfort, the heat balance equation must be satisfied. In the human body, heat inputs include metabolic rate (M), conduction (I), convection (T), and radiation (I), while heat outputs include conduction (I), convection (T), radiation (I), latent heat outputs such as evaporation (B) and respiration (S).

Comfort ranges in standards are determined in terms of operative temperature, which represents both air temperature and Mean Radiant Temperature. The Mean Radiant Temperature is the inhomogeneous temperature formed by radiation and convection, which may cause regional discomfort. While subjective parameters

vary from person to person, thermal comfort can be achieved by controlling objective parameters. Since thermal comfort is a relative psychological concept, it is impossible to ensure 100% satisfaction for all individuals in an environment. According to ASHRAE 55 standards, if 80% of the users are satisfied with the thermal conditions, the environment is considered thermally comfortable. Building types and functions influence indoor temperature values, as different spaces have specific requirements for thermal comfort. Care must be taken not to cause regional discomfort while achieving the desired temperature.

Studies on thermal comfort began in 1774 (Taleghani et al., 2013), and significant research has been conducted since the 1970s on the development of models to improve thermal comfort (Zhao et al., 2020). In 1970, P.O. Fanger introduced the steady-state model based on the heat balance of the human body for air-conditioned spaces. Fanger's analytical model developed a scale consisting of seven different sensations, expressing individuals' thermal perceptions based on psychological perception and statistical data. The first classical thermal comfort model, based on the thermal balance equation, is the PMV (Predicted Mean Vote) and PPD (Predicted Percentage Dissatisfied) scale. This model translates people's sense of comfort into numerical data, taking into account factors such as air temperature, radiation temperature, relative humidity, air velocity, clothing insulation, and activity level (Fanger, 1970). The PMV-PPD thermal comfort indices are included in standards such as ASHRAE 55 (American Society of Heating, Refrigerating, and Air-Conditioning Engineers) and ISO 7730 (International Organization for Standardization) (ASHRAE 55, 2020; EN ISO 7730, 2005).

However, since the PMV-PPD model was developed with a limited number of subjects in air-conditioned laboratory environments, it may not accurately determine thermal comfort in different geographical locations, climate types, or buildings with natural ventilation (Nicol, 2004; Yao et al., 2010; Pereira et al., 2014). As a result, PMV is not suitable for dynamic environmental conditions (Zhao et al., 2020). In response, various models such as ePMV (Fanger et al., 2002), eSET and aSET (Gao et al., 2015), aPMV (Yao et al., 2009), and ATHB (Schweiker et al., 2015) were developed to address the discrepancies between predicted comfort temperatures and those observed in field studies. However, these models have been

criticized for not being comprehensive or sufficient for adaptive comfort models (de Dear et al., 2020).

The adaptive comfort model, proposed by De Dear and Brager in 1998 based on field studies, reflects more realistic thermal requirements. It was incorporated into the ASHRAE 55 standard in 2004 and has been included in several other standards (EN 15251, 2007; prEN 16798–1, 2015; GB/T 50785, 2012; ISSO 74, 2006). The adaptive comfort model, derived from 21,000 measurements taken in 160 buildings (mostly offices), links indoor temperatures or acceptable temperature ranges to outdoor meteorological conditions. It is used to define acceptable thermal conditions in spaces with user-controlled natural ventilation (ASHRAE 55, 2020).

Among the thermal comfort models, Fanger's PMV-PPD model is widely used and included in standards for mechanically air-conditioned buildings, while the adaptive model, developed by De Dear and Brager, is applied to naturally ventilated buildings (de Dear et al., 2020; ASHRAE 55, 2020).

For this thesis, the PMV-PPD model, along with the AMV-APD indices derived from survey results, are employed to assess thermal comfort. The Actual Mean Vote (AMV) is used to measure users' satisfaction with the thermal conditions and is determined using a 7-point thermal sensation scale. The Predicted Mean Vote (PMV) is calculated by converting the scale into numerical data. When calculating PMV, six variables are considered: clothing insulation level, activity level, indoor air temperature, Mean Radiant Temperature, air velocity, and relative humidity.

The comfort status is determined based on the limit values provided in ISO 7730 and ASHRAE 55 standards (ASHRAE 55, 2020; BS EN ISO 7730, 2005) (Table 2.2). According to these standards, PMV values between -0.5 and +0.5 and AMV values between -1 and +1 are considered comfortable. The closer PMV and AMV are to zero, the more comfortable the environment. AMV is determined by responses to the seven-stage thermal sensation scale. The AMV range indicates that the PPD value is within 10%. The Predicted Percentage Dissatisfied (PPD) is derived from PMV values to estimate the percentage of people dissatisfied with the thermal environment. According to ASHRAE 55, if at least 80% of the users are

satisfied with the thermal sensation, the environment is considered thermally comfortable (ASHRAE 55, 2020).

Table 2.2 Classification of comfort status according to standards (ASHRAE 55, 2020; BS EN ISO 7730, 2005)

Category	ISO 7730		ASHRAE 55	
	PPD	**PMV**	**PPD**	**PMV**
A (I)	6%	±0.2	10%	±0.5
B (II)	10%	±0.5	20%	±0.85
C (III)	15%	±0.7	-	-

The BS EN 15251:2007 standard specifies the temperature values required to achieve the range of -0.5 < PMV < +0.5, depending on function, activity level (met), and clothing insulation (clo) values. For offices and similar buildings without mechanical cooling (activity levels between 1.0 and 1.3 met), acceptable indoor temperatures during the summer months are defined based on outdoor temperatures (Figure 2.4).

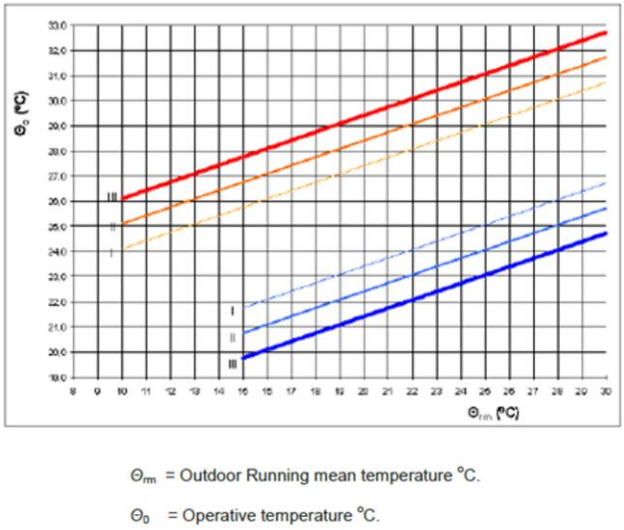

Figure 2.4 Acceptable indoor temperatures depending on outdoor temperature (BS EN 15251:2007)

The values shown in the graph are derived using calculation methods. For Category 2, the calculation equations are as follows;

Upper limit: Θi max = 0.33 Θrm + 18.8 + 3

Lower limit: Θi min = 0.33 Θrm + 18.8 – 3

is given as.

Θi= internal operative temperature limit value, °C

Θrm = mean outdoor temperature, with an upper limit of 10 < Θrm < 30 °C, and a lower limit of 15 < Θrm < 30 °C.

The standards also categorizes heating and cooling temperature ranges for energy calculations into three categories based on function, activity level, and clothing insulation. For classrooms (approximately 1.2 met) the cooling temperature is given in the range of 23 °C - 26.0 °C for a clothing insulation level of 0.5 clo in the summer months. In winter months the heating temperature is given in the range of 20 °C - 24 °C for a clothing insulation level of 1 clo. In mechanically controlled environments, for classrooms (approximately 1.2 met), the minimum heating temperature for Category 2 is recommended as 20 °C for a clothing insulation level of approximately 1 clo in winter months.

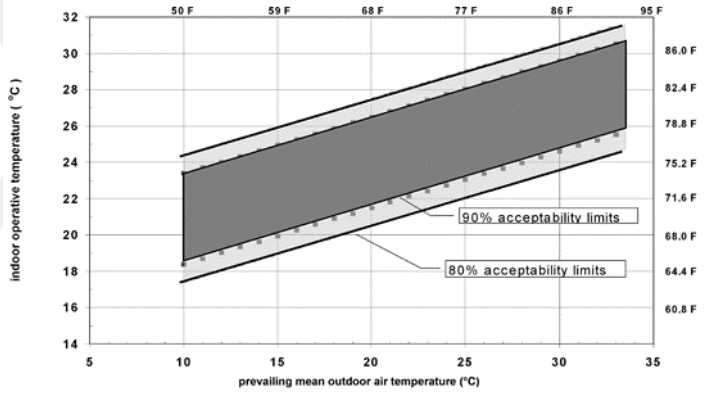

Figure 2.5 Adaptive model graph with acceptable operative temperature limits for naturally ventilated spaces (ASHRAE 55, 2020)

The comfort range for the adaptive comfort model is defined between 10°C and 33.5°C for outdoor temperatures, as shown in Figure 2.5. For naturally ventilated spaces without mechanical cooling, acceptable comfort ranges are determined based on activity level (1-1.3 met) and clothing insulation levels (0.5-1 clo). Acceptable comfort limits are defined as 80% (operative temperature: 22.1 - 29.1°C) and 90% (operative temperature: 23.1 - 28.1°C).

In addition to PMV analysis, this thesis explicitly incorporated solar radiation incident on the south façade as a Key Performance Indicator (KPI) for thermal comfort. Since solar radiation directly affect Mean Radiant Temperature their

inclusion ensures that thermal comfort evaluations extend beyond indoor parameters to capture façade-specific effects. Morover, solar radiation significantly influences indoor operative temperature and is directly related to heating and cooling loads (Arens et al., 2015; Tzempelikos, 2010). For instance, in Istanbul's mixed climate, excessive summer solar radiation increases cooling loads, while insufficient winter radiation raises heating demand. Shading devices therefore play a decisive role in maintaining seasonal balance. By integrating solar radiation as a KPI, the optimization of PSSs are able to balance seasonal heat gains, thereby supporting both thermal comfort and energy efficiency.

2.2.2. Visual Comfort

Visual comfort is achieved when the illumination level is adequate to enhance visual performance, enabling efficient work and meeting both the physiological and psychological needs of users (Yılmaz & Yener). International organizations such as the CIE (International Commission on Illumination), IESNA (Illuminating Engineering Society of North America), CIBSE (The Chartered Institution of Building Services Engineers), and EN (European Standards) have established comprehensive criteria to define and evaluate visual comfort conditions.

Transparent areas play a key role in establishing a visual connection between the interior and exterior environments. As the transparent area increases, it creates a positive psychological effect by providing a sense of openness (Chandra, 2003). Daylight can enhance user satisfaction and productivity and has a positive impact on health. However, uncontrolled daylight exposure may also cause glare, overheating, and thermal discomfort (Chi et al., 2018), and excessive glare can reduce performance and increase reliance on artificial lighting, thereby raising energy consumption (Velds, 1999).

The TS EN 17037:2023 Daylight in Buildings standard provides a framework for optimizing daylight performance in indoor spaces. It defines four main criteria: **sufficient daylight illuminance, visual connection with the exterior, adequate sun exposure, and glare protection.** The standard recommends a minimum daylight illuminance of 300 lux for at least 50% of daylight hours across 50% of the working plane, while also requiring 100 lux for 95% of the working plane. In

addition, it specifies a minimum of 1.5 hours of direct sunlight exposure per day and sets threshold values for glare protection.

Table 2.3 Recommended daylight provision by daylight openings in vertical and inclined surface

Level of recommendation for vertical and inclined daylight opening	Target illuminance E_T lx	Fraction of space for target level $F_{plane,\%}$	Minimum target illuminance E_{TM} lx	Fraction of space for minimum target level $F_{plane,\%}$	Fraction of daylight hours $F_{time,\%}$
Minimum	300	50 %	100	95 %	50 %
Medium	500	50 %	300	95 %	50 %
High	750	50 %	500	95 %	50 %
NOTE Table A.3 gives target daylight factor (D_T) and minimum target daylight factor (D_{TM}) corresponding to target illuminance level and minimum target illuminance, respectively, for the CEN capital cities.					

Table 2.4 Recommended daily sunlight exposure

Level of recommendation for exposure to sunlight	Sunlight exposure
Minimum	**1,5 h**
Medium	**3,0 h**
High	**4,0 h**

For illuminance analysis, the standard defines calculation grids based on the geometry of the space, with the reference plane positioned 0.85 m above the floor and calculation points distributed to meet spatial ratios between length and width. The TS EN 17037:2023 Daylight in Buildings standard provides the formula:

$$p = 0.5 \times 5 \log_{10}(d) \tag{2.1}$$

In this formula, d represents the long side of the calculation area in meters, and p is the maximum distance between points in meters. The standard specifies that the ratio between the length and width of the grid distance should fall between 0.5 and 2. It is recommended that the grid be placed 0.5 m inside the walls, with the reference plane set 0.85 m above the ground. After applying this formula, the number of calculation points is determined approximately, and the distance between the calculation points is calculated. This formula is used to create the calculation grids for daylight analysis.

The standard also includes methods for calculating the Daylight Factor (DF) as a static metric, while acknowledging that dynamic metrics such as Daylight Autonomy (DA) and Spatial Daylight Autonomy (sDA) provide a more realistic assessment under changing sky conditions. The DF is determined based on the average external illumination, considering more than half of the daylight hours and for 50% and 95% of the room.

The equations used to calculate the daylight factor are as follows: (Here, the specific equations would be provided for calculating the daylight factor, as indicated in the original standard).;

$$D_T = \frac{\text{illuminance level}}{E_{v,d,med}} = \frac{300\ \text{lx}}{E_{v,d,med}} \times 100\left[\%\right] \tag{2.2}$$

$$D_{TM} = \frac{\text{illuminance level}}{E_{v,d,med}} = \frac{100\ \text{lx}}{E_{v,d,med}} \times 100\left[\%\right] \tag{2.3}$$

The calculation results based on the average external illuminance of 19,000 lux, as specified for Ankara in the TS EN 17037:2023 standard, are as follows:

The daylight factor for 50% of the room (providing 300 lux) is 1.58%.

The daylight factor for 100% of the room (providing 100 lux) is 0.5%.

These results reflect the daylight availability within the building, based on the external illuminance conditions and the required daylight levels as per the standard.

Annual Sun Exposure (ASE) is a daylight metric that quantifies the percentage of floor area receiving more than 1000 lux of direct sunlight for more than 250 hours annually, serving as an indicator of potential glare and thermal discomfort (IES, 2012). While ASE was originally developed within the LEED v4 daylight credit framework (USGBC, 2013), it can be conceptually related to the TS EN 17037:2023 standard, which establishes requirements for daylight provision, sunlight exposure, and glare control (CEN, 2021). In this context, ASE is particularly relevant for the design and optimization of shading devices, as these systems are widely recognized for their ability to regulate solar gains, prevent

excessive sunlight exposure, and enhance both visual and thermal comfort (Tzempelikos & Athienitis, 2007; Reinhart & Andersen, 2006). ASE highlights the risk of overexposure that can compromise both visual and thermal conditions, thereby supporting a balanced evaluation of daylight performance in buildings. Thus, combining ASE with daylight provision provides a comprehensive framework for evaluating shading device performance, ensuring a balance between daylight sufficiency and the mitigation of overexposure in indoor environments.

Within the scope of this thesis, visual comfort was evaluated in line with TS EN 17037:2023, with a particular focus on dynamic metrics. Spatial Daylight Autonomy (sDA) are selected as a primary KPI to quantify the percentage of floor area achieving 300 lux for at least 50% of occupied hours, while Annual Sun Exposure (ASE) are used to assess excessive sun exposure by calculating the percentage of the area receiving more than 1000 lux for over 250 hours per year. These two indicators were prioritized because they capture both the beneficial and adverse effects of daylight, offering a balanced framework for assessing visual comfort. In addition, summer and winter solar radiation values incident on the south façade were integrated as complementary KPIs to link visual comfort with thermal performance, given the direct influence of solar radiation on indoor comfort.

Considering Istanbul's mixed climate, characterized by high summer solar gains and moderate winter daylight availability, the use of both sDA and ASE proved essential. While sDA ensured sufficient daylight access in classrooms, ASE helped to identify conditions of potential glare and overheating. Furthermore, the amphitheater-style classroom layout studied in this thesis required adapting the interpretation of TS EN 17037 criteria: in this context, establishing a visual connection with the exterior was less relevant for most occupants, while horizontal illuminance on the working plane became the primary metric for assessing visual comfort.

In summary, the evaluation framework developed in this study integrates TS EN 17037 requirements with Istanbul-specific climatic and spatial conditions, ensuring that optimization of PSSs addresses both international standards and local performance needs.

3
A METHOD TO DESIGN OF PERFORATED SOLAR SCREENS IN TERMS OF THERMAL AND VISUAL COMFORT

The primary aim of this study is to introduce and demonstrate a methodological framework that evaluates environmental factors in the design of shading devices with the objective of ensuring thermal and visual comfort conditions in indoor environments. In this context, a systematic method has been developed to identify the most suitable shading configuration with respect to thermal and visual comfort through the parametric optimization of shading devices. This methodological approach allows researchers to test multiple design parameters while maintaining a clear focus on performance outcomes.

The methodological steps of the study are structured as follows: data collection, determination of the design, conducting simulations and optimizations, and identifying the optimal design. Within this framework, field studies (including measurements and surveys), observation-based studies, validation procedures for both measurements and simulations, and statistical analyses are carried out. It is suggested that the integration of both objective and subjective data sources enhances the reliability of the results, and therefore this approach is also adopted here.

Within the scope of this thesis, a parametric perforated solar screen (PSS) was designed with a focus on thermal and visual comfort conditions in the interior environment. Additionally, an optimization method is implemented to identify the optimum PSS by integrating design parameters with comfort-related performance

(thermal and visual comfort) criteria. The integration of design development and optimization ensures both conceptual clarity and performance-based refinement.

The specified method essentially incorporates two interrelated approaches. It comprises two principal stages: first, proposing a design for a parametric PSS that addresses thermal and visual comfort conditions; and second, performing optimization of this proposal based on the key performance indicators associated with these conditions.

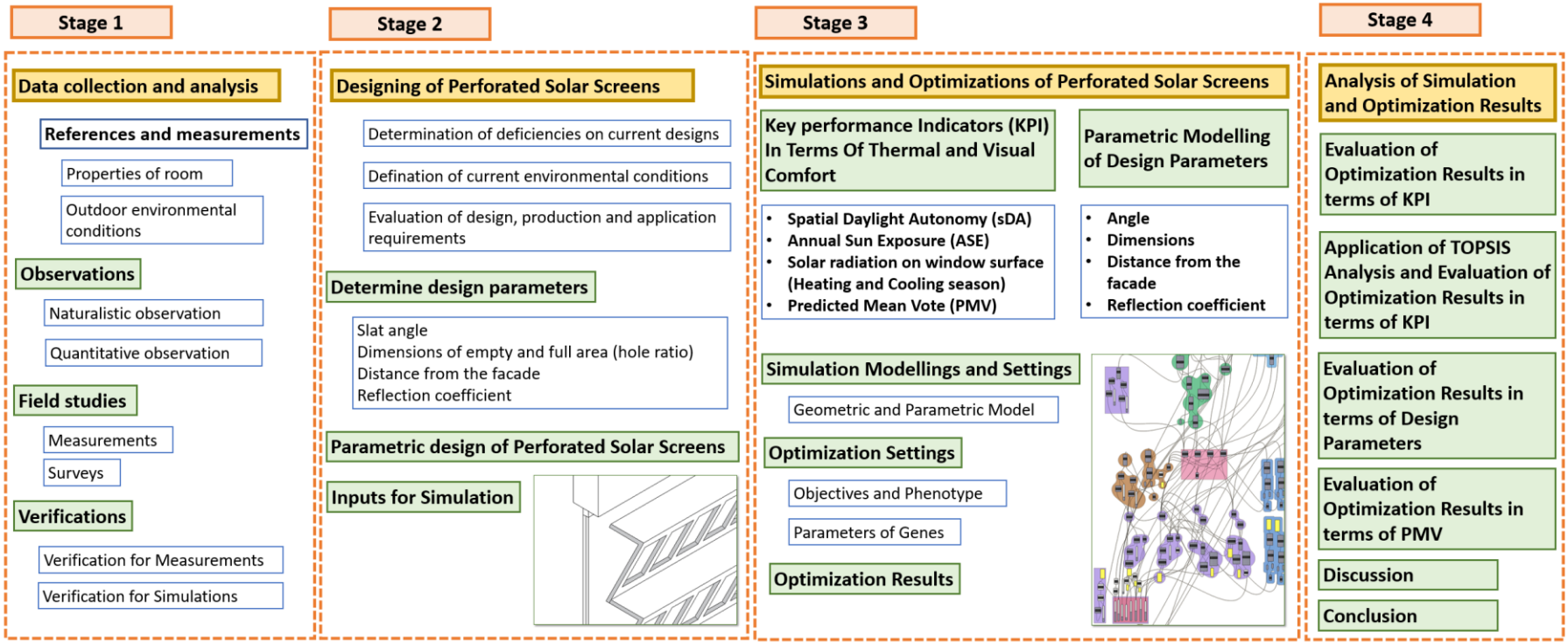

Figure 3.1. Method of the study

3.1. Data collection and analysis methods

The designed perforated solar screens are intended to be suitable for practical application; thus, simulations and optimizations are applied for the existing rooms. To achieve this, the current conditions of the selected rooms are identified and analyzed through objective methods (measurements) and subjective methods(survey) to evaluate thermal and visual comfort criteria. The simulations are validated using data obtained from the measurements related to thermal and visual comfort. Attention should be given to the accuracy of the validation process, as it forms the basis for trustworthy simulation-based evaluations.

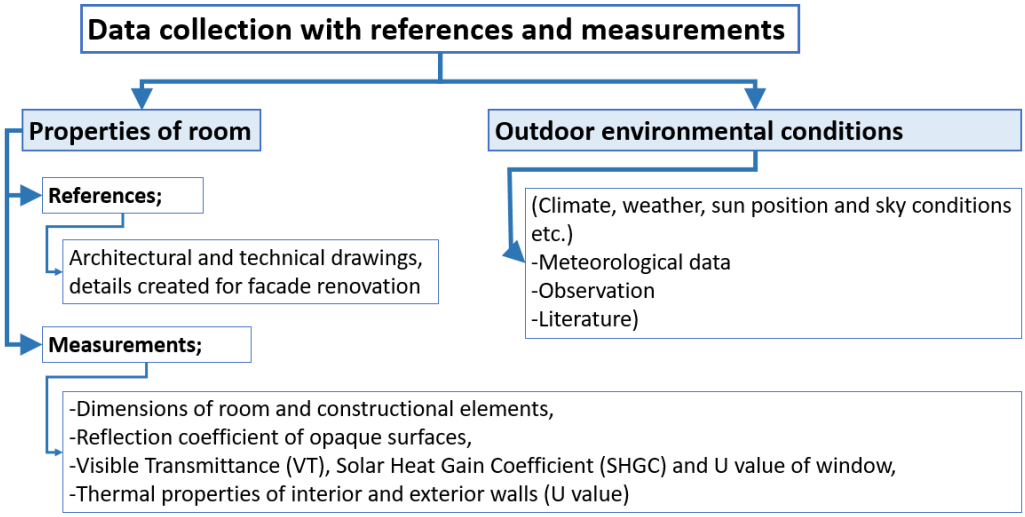

Figure 3.2 Data collection with references and measurements

In determining the study rooms within the scope of the thesis, several factors should be considered, including the orientation of the room altitude above sea level, room dimensions, seating arrangement, number of simultaneous users, building envelope properties, construction materials, transparency ratio, interior material characteristics, HVAC system specifications, and lighting device attributes. These factors should be systematically documented because they directly influence thermal and visual comfort assessments.

3.1.1. Observations

Determining user behavior within rooms is crucial for identifying the need for shading devices. Observations are carried out by documenting existing conditions and taking systematic notes. In this thesis, a camera system is installed for

observations. And the recordings are analyzed to assess factors such as window and curtain opening frequencies, user locations, and related behaviors. Data including the academic calendar, usage periods, observations, camera records, number of users, clothing insulation levels, and activity levels are collected. Organizing these datasets systematically allows them to be effectively transformed into input parameters for the simulation program.

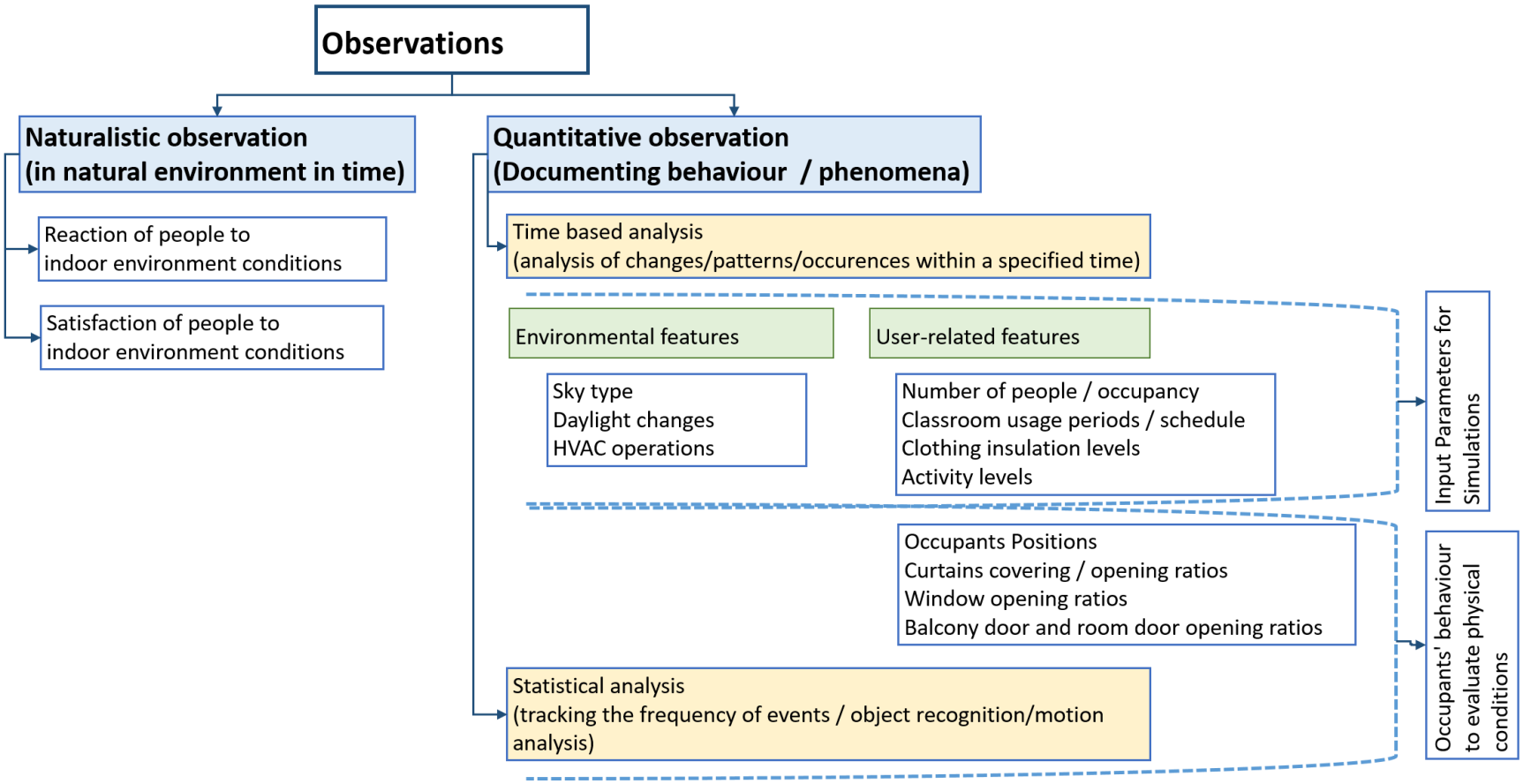

Figure 3.3. Observation method

3.1.2. Field Studies

The field studies may involve different methodologies and are generally based on measurement and survey methods. The field studies are undertaken for the definition and assessment of environmental conditions.

The methodology of this thesis is developed to determine best design of perforated solar screens in terms of thermal and visual confort. Therefore, to design shading devices is necessary to identify current environmental conditions of rooms. This process allows an understanding of existing deficiencies, the current comfort levels, and the specific needs of the rooms. In addition, the physical and functional features of the rooms must be defined to ensure a correct evaluation of the results. The collected data also serve as input datasets for the simulations.

Two approaches are selected for field studies: one based on measurements and the other on surveys. Measurements are divided into two steps: the definition of building properties and the identification of current conditions. The purpose of the surveys is to evaluate user perception in terms of current thermal and visual comfort. By analyzing these field study results separately and in combination, it becomes possible to design and determine the most effective shading devices.

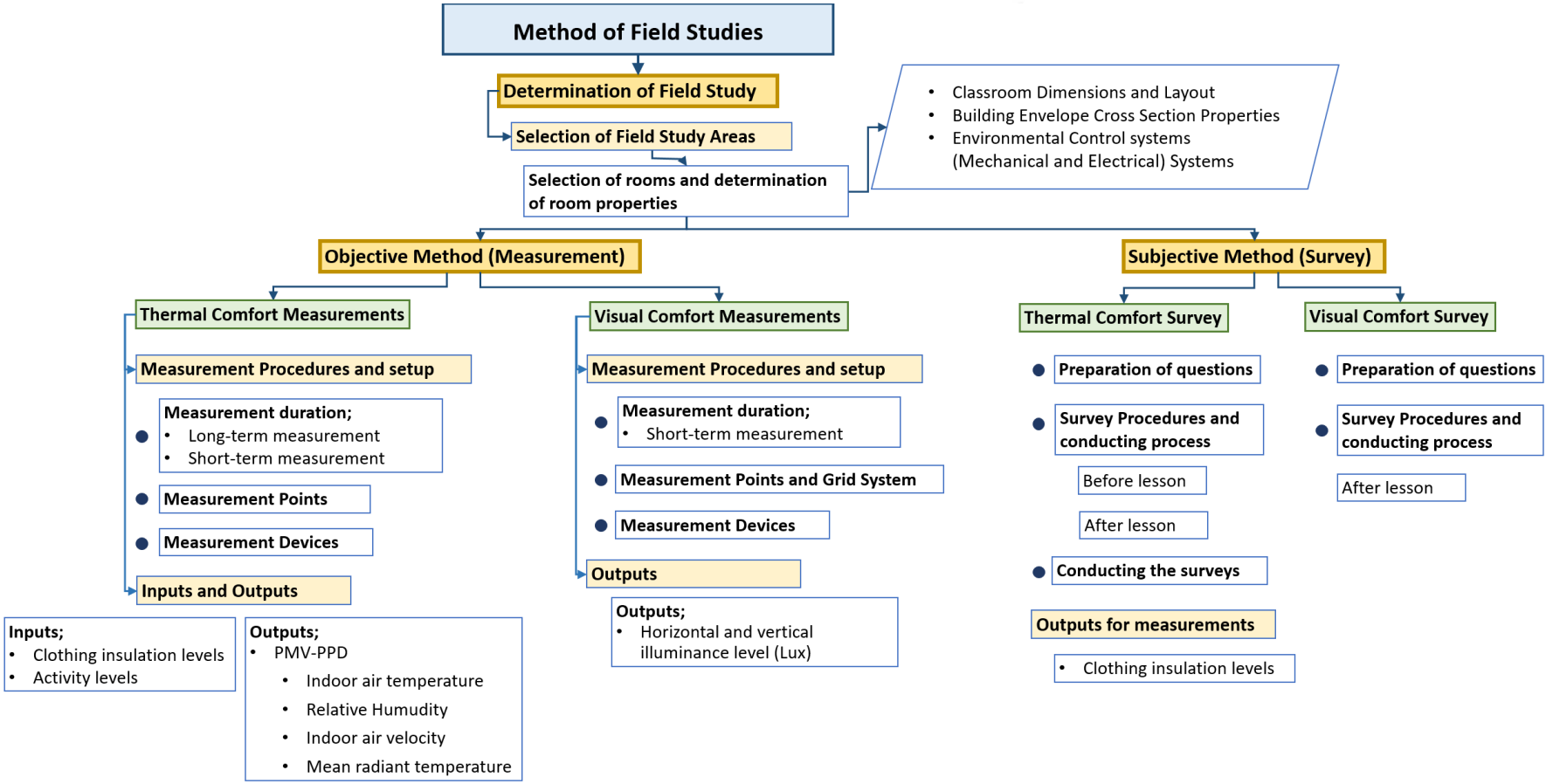

Figure 3.4. Method of field studies

The proposed methodology is applicable to different building types. For example, educational buildings consist of diverse units, including classrooms, laboratories, conference halls, and administrative spaces, with classrooms serving as the fundamental units. The quality of the teaching-learning interaction in classrooms heavily depends on the comfort of the indoor environment. Therefore, achieving optimal environmental conditions in educational buildings is considered essential, given that thermal and visual discomfort can negatively affect the performance and well-being of both students and instructors. Providing healthy and supportive educational environments ensures the protection of student and teacher health as well as productivity (Daisey, Angell, & Apte, 2003; Bakó-Biró, Clements-Croome, Kochhar, Awbi, & Williams, 2012).

Creating suitable environmental conditions in university classrooms is particularly important. However, classrooms with large glass facades often experience unavoidable thermal and visual discomfort. These spaces tend to have elevated cooling loads due to high transparency and excessive heating loads during colder periods. To mitigate these issues, external shading devices are recommended for installation in front of transparent surfaces in existing buildings. Such devices must also be carefully designed to meet visual comfort requirements. The proper design of PSSs, a modern architectural solution, can contribute significantly to improving both thermal and visual comfort.

A review on shading device simulations in buildings by Kırımtat et al. revealed that only 20% of the studies employed experimental approaches, with research conducted in school or university settings comprising just 9%. Furthermore, studies on PSSs have primarily focused on residential and office buildings (Table 1.2).

3.1.2.1. Determination of Field Study

Thermal comfort and visual comfort are assessed using various methods in field studies. The most widely applied approaches include the objective method, which relies on measurements, and the subjective method, which involves surveys. Within the scope of this research, both methods are utilized to be utilized for determining the thermal comfort and visual comfort conditions. In this stage of the study, the

conditions of the case application, the determinations, and the measurement procedures are explained below.

The field studies are designed to implement continuous measurements using fixed devices, complemented by surveys administered at one-month intervals over the course of one year (or more). These assessments are carried out for the existing conditions. For experimental studies, specially designed adiabatic rooms are considered ideal. However, this research is planned to implement surveys and measurements during peak user occupancy periods. Since adiabatic rooms have limited user capacity, it is deemed more appropriate to conduct the study in classrooms with high user density and frequent use.

Selection of Field Study Areas;

The selection of study areas within the scope of this research is based on various factors, including the orientation of the room, elevation above sea level, room dimensions, seating arrangements, occupant density, building envelope characteristics, construction materials, transparency ratios, interior material properties, HVAC systems, and lighting device specifications. Given that most school buildings lack mechanical cooling systems in classrooms, this is defined as a key consideration in selecting air-conditioning systems for the study areas. In this thesis, to apply the proposed method, classrooms with mechanical heating and natural ventilation were chosen to allow for diverse evaluations of thermal comfort.

Selection of Classrooms;

For assessing the effect of PSSs, it is recommended that the selection of rooms be based on the presence of transparent surfaces on the facades and transparency ratios. To apply the proposed method and assess the effect of designed PSSs, classrooms are selected based on the presence of transparent surfaces on the south-facing façade and high transparency ratios. In this thesis, to apply the proposed method and design PSS for real conditions, three classrooms with south, southeast, and southwest orientations were selected as study area. Thermal and visual comfort field studies are conducted to determine the suitability of these classrooms for the study.

University classrooms are predominantly designed as lecture halls, including the selected classrooms, which feature a lecture hall seating arrangement with a north-facing viewing direction (Figure 4.5, 4.6 and 4.7). As expected, discomfort in areas near the windows can occur due to the high transparency ratio of the south-facing façades. Due to the volumetric shape of the classrooms and thermophysical principles—where heated air rises and is replaced by cooler air—hot air accumulated near the windows. This phenomenon intensified discomfort in these areas, especially during occupancy. Similarly, it is expected that excessive illumination on the working planes near the windows reaches levels that could cause discomfort. These expectations support that the selected classrooms are suitable for the implementation of PSSs to improve thermal and visual comfort conditions.

Classroom Dimensions and Layout;

In building performance studies, establishing a precise geometrical model of the studied spaces is a fundamental prerequisite for accurate analysis. For this purpose, the dimensions of the selected classrooms were initially ascertained using existing architectural drawings. To ensure the reliability of the data and account for any potential discrepancies between the original plans and the as-built conditions, these dimensions were subsequently verified through detailed on-site measurements.

To facilitate a comparative analysis of the impact of PSSs on comfort conditions, it is essential to standardize all physical attributes of the classrooms. If there are any differences on features of rooms the evaluations should be done considering these situations. This study suggest that to find best design, the evaluation and optimizations should be made for each room in its own right.

Determination of Building Envelope Cross Section Properties;

Indoor thermal comfort is closely linked to the properties of the building envelope. To accurately assess thermal comfort, it is essential to determine the U-value of the building envelope components. To obtain reliable results, the building envelope section layers and U-values is determined through both measurements and architectural project drawings. In this thesis, tThe TESTO 635 Humidity and Temperature Measurement Device was employed to measure the U-value of both

opaque and transparent building envelope components. To ensure accurate determination of the building envelope cross section properties, architectural project drawings were used in conjunction with the U-value measurements.

After determining the building envelope section layers and U-values, these are compared against the values specified in TS825 2013. To ensure accurate data input into the simulation program, approximate values for the section layers and U-values are derived, and suggested section layers are established. The final building envelope characteristics are determined based on the requirements outlined in the ASHRAE 90.1-2010 standards. These characteristics are then incorporated into the simulation program, where the corresponding building envelopes are created.

Subsequently, the reflection coefficients of surfaces and the features of lighting devices are specified based on the room characteristics and the properties of the materials used.

3.1.2.2. Objective Method (Measurement)

Thermal Comfort Measurements;

Thermal comfort is influenced by both objective and subjective parameters. Subjective parameters, which pertain to the individual characteristics of the human body, therefore vary from person to person. Consequently, thermal comfort assessments are typically based on objective parameters, which can be categorized into personal and environmental factors. While personal factors have standardized values established through research and international standards, environmental factors vary depending on the specific conditions of the environment.

Among personal factors, clothing insulation level significantly affects thermal comfort. This parameter, determined by the insulating properties of clothing, is under individual control, allowing people to adjust their thermal comfort by altering their clothing. Clothing insulation levels vary with outdoor temperature changes and are standardized as 0.5 clo for cooling periods and 1 clo for heating periods according to BS EN ISO 7730 (2005).

However, studies, such as Zoroğlu and Gedik (2017), showed that utilizing the standard clo values does not substantially affect the results. Instead, determining

instantaneous clothing insulation levels prior to measurements and entering them into the measurement device produces more accurate assessments.

To evaluate thermal comfort conditions, a combination of both long-term and short-term measurement methods can be carried out. In this study, this dual approach was employed. As a key input for these measurements, clothing insulation (clo) values were calculated for specific periods. Additionally, clothing insulation levels obtained from survey data were used in the calculations and compared with results from surveys conducted at one-month intervals.

Activity level, another personal factor, influences thermal comfort through the metabolic heat generated by physical activity. For individuals engaged in various activities within the same environment, their thermal comfort conditions will differ. The standards (ISO 7730 and ASHRAE) categorize activity levels such as "sedentary activity" for sitting, listening, reading, and writing and specify the activity level as 1.2 met (70 W/m^2). It is suggested that, activity levels are determined by observing general student behaviors and aligning them with these standards-based values (Zhang et al., 2020).

Thermal Comfort Measurement Standards and Setup;

When measuring thermal comfort, it is essential to follow international standards like ISO 7730, ISO 7726, and ASHRAE 55. In the context of this study, clear definitions of measurement durations, intervals, and device configurations are crucial to ensure consistency. As noted in similar research, long-term measurements are typically implemented with permanently installed devices, while short-term measurements are conducted to capture real-time variations. This combined approach allows for both continuous monitoring and detailed spot evaluations. Building on this methodology, when designing the procedure, attention should be paid to the representativeness of the selected periods, ensuring that both peak and off-peak usage conditions are covered. It is also recommended that measurements be repeated under comparable conditions to verify reliability, a common practice to enhance the robustness of findings.

In line with established protocols, measurement points are determined based on classroom layouts and research objectives. To effectively capture variations in

thermal conditions, devices should be positioned both near transparent façades and in zones farther away from them. To ensure consistency with ASHRAE guidelines, air temperature and air velocity are measured at 0.1 m, 0.6 m, and 1.1 m heights, while humidity and Mean Radiant Temperature are assessed at 0.6 m. For the purposes of this study, the reference height of 0.6 m is adopted as the standard for seated occupants. Drawing from similar studies on thermal comfort, it is advised that measurement points be selected to represent both critical discomfort zones and areas of stable environmental performance. Placing sensors in contrasting locations ensures a more comprehensive evaluation of the shading device's effect across the classroom.

In order to accurately assess thermal conditions, thermal comfort parameters are measured using devices capable of calculating Predicted Mean Vote (PMV) and Predicted Percentage of Dissatisfied (PPD). Consistent with similar experimental setups, the Delta Ohm HD 32.3A Microclimate Analyzer and the Testo 480 Digital Temperature and Humidity Meter are employed for indoor measurements of air temperature, humidity, air velocity, and Mean Radiant Temperature. Personal factors, such as clothing insulation and activity level, are input into the devices to compute PMV and PPD values. To ensure uninterrupted data collection, which is a key requirement for reliable long-term studies, protective enclosures and uninterruptible power supply (UPS) units are installed with the measurement devices. Furthermore, as a prerequisite for data accuracy and a standard procedure in this field, it is recommended that devices be calibrated prior to installation to minimize potential measurement errors. Protective measures, such as enclosures and UPS systems, should always be integrated into long-term monitoring strategies to safeguard the accuracy and continuity of the data.

Visual Comfort Measurements;

Numerous studies highlight the significant role that visual conditions play in user (student) activity and performance in classrooms. This section provides a guide on the methodology used to assess visual comfort in classrooms. Evaluating the appropriateness of visual conditions requires comparing parameters such as illuminance level, average illuminance level, and uniformity of illuminance distribution with the standards.

Visual comfort assessments are undertaken by determining illuminance levels and verifying them against ranges specified in the standards. Depending on the light sources, interior lighting is classified into three categories; natural lighting, artificial lighting, and integrated lighting (natural + artificial).

The standards that define illuminance levels and other related criteria include:

-TS EN 17037:2023 (Daylight in Buildings) for daylight illuminance and similar parameters,

-TS EN 12464-1:2021 (Light and Lighting - Lighting of Workplaces - Part 1: Indoor Workplaces) for artificial lighting.

Key visual comfort criteria outlined in these standards include; provision of daylight illumination, establishment of a visual connection with the external environment, consideration of exposure to sunlight, minimization of glare, maintenance of adequate illuminance levels, uniformity in the distribution of illuminance, and appropriate light color (e.g., color rendering index).

Visual Comfort Measurement Standards and Setup;

For visual comfort assessments, it is essential to measure illuminance levels on representative working surfaces. Measurements are performed on work planes, with horizontal illuminance measured on desks and vertical illuminance on chalkboards.

To calculate daylight illuminance levels, the formula specified in the TS EN 17037:2023 Daylight in Buildings standard for creating calculation grids is employed. The formula for determining point spacing is:

p=0.5×5log10(d) $$p = 0.5 \times 5 \log_{10}(d)$$

where: p: Maximum distance between points (m),

d: Long side dimension of the calculation area (m).

It is recommended that the grid system maintain a 0.5 m distance from the walls.

Due to practical constraints, simultaneous measurements at all grid points are not feasible. However, minimizing the time interval between successive measurements is necessary for ensuring accuracy. It should be noted that the grid calculation

method in TS EN 17037:2023 is primarily intended for computational analysis rather than direct field measurements. Therefore, a reduced number of grid points may be applied to optimize the measurement process while still preserving data reliability.

Furthermore, sky conditions significantly impact visual comfort assessments and must be determined for each measurement session.

The Konica Minolta Illuminance Meter is employed to measure illuminance level and to calculate average illuminance level, and uniformity of illuminance distribution. For the measurements related visual comfort The Konica Minolta CM 2600d Spectrophotometer and Konica Minolta illuminance meter were utilized.

3.1.2.3. Subjective Method (Survey)

A critical consideration for any survey is establishing a clear participant profile and determining the number of users. Ensuring that survey participants comprehend the questions and articulate their responses clearly is essential to the reliability of the survey results. In this study, the participant profile consisted of university students.

The surveys are designed and categorized into two main groups: thermal comfort and visual comfort. They include demographic questions (e.g., gender, age, height, weight, employment status, education level) to facilitate classification of the results. For instance, numerous studies have identified gender-based differences in thermal comfort. The survey questions aimed at assessing thermal comfort and visual comfort are developed in accordance with the BS EN ISO 10551:2019 standard. Organizing questions under internationally recognized standards not only enhances comparability across studies but also provides a consistent framework for interpreting subjective responses.

Thermal Comfort Survey;

This thesis's primary focus on thermal comfort, this section of the survey is comprehensively designed to enable a detailed evaluation. Since indoor thermal comfort varies based on the number of users and the duration of their stay, the thermal comfort questions are divided into two phases: "before the lesson" and "after the lesson." This two-phase approach is considered important to capture

temporal variations in user perception, which may otherwise be overlooked in single-point surveys.

The survey questions are developed to capture both subjective and objective parameters influencing thermal comfort. Demographic factors such as gender, age, weight, and height were considered subjective parameters. For objective parameters, a table is developed to determine clothing insulation levels, and Question 4 addressed activity levels before and after the lesson. The clothing insulation questions are prepared using ASHRAE 55 and ISO 7730 standards.

Ji et al. (2018) found that new metabolic rates stabilize after 3–5 minutes of walking and return to baseline within 4–5 minutes of rest. Similarly, Zhang et al. (2020) observed stabilization within 5–6 minutes post-exercise, with baseline achieved after 7–9 minutes. Based on these findings, students are asked about their activities at 5-minute intervals before the lesson to account for differing activity levels. After the lesson, they are questioned about their activities in the preceding 15 minutes, when activities are expected to converge.

Questions 1, 3 (before the lesson), and 3 (after the lesson) are formulated to address thermal sensation changes relative to environmental conditions and time spent indoors. Responses to these questions are designed with consideration of adaptation studies and metabolic rate changes (Ji et al., 2018; Zhang et al., 2020). As temperature, radiant temperature, air velocity, and humidity vary by location, Question 2 in the post-lesson survey requires users to indicate the point closest to their position.

To assess thermal comfort before and after the lesson, a 7-point thermal sensation scale is utilized. Responses to this question facilitate the calculation of AMV and APD values, which can then be compared with PMV and PPD values from measurement results. Questions 6, 7, and 8 (before the lesson) and Questions 7, 8, and 9 (after the lesson) are formulated following ISO 10551 standards. Post-lesson Question 5 assesses the importance users attribute to thermal comfort, while Question 10 examines their reactions to the thermal conditions of the environment.

Questions 11 and 12 are included post-lesson to evaluate the effects of transparency ratio. Question 11 focuses on regional discomfort and perceptions of radiation

asymmetry, while Question 12 identifies factors causing discomfort, offering predefined options. Ensuring optimal thermal comfort in classrooms is critical for effective learning. Accordingly, Question 13 evaluetes the impact of thermal comfort on students' understanding and comprehension of the lesson.

Visual Comfort Survey;

The visual comfort survey is administered in a single stage, post-lesson, to ensure accurate evaluation of the environment. Allowing users sufficient time to observe and assess their surroundings enhances the reliability of responses. During survey administration, the lighting conditions (e.g., integrated lighting or daylight) are recorded. Sky conditions are also documented, as they play a crucial role in visual comfort assessments. Recording contextual factors alongside user responses is considered essential for aligning subjective evaluations with objective measurements.

Demographic questions from the thermal comfort survey, along with Question 2 (location, post-lesson) and Question 3 (duration, pre- and post-lesson), are incorporated in evaluating visual comfort. Questions 1-4 are formulated in accordance with ISO 10551 to assess subjective perceptions of environmental illuminance. In classrooms with high transparency ratios, such structured questioning ensures that potential issues such as glare and uneven illuminance distribution are systematically captured. High transparency ratios in classrooms are anticipated, with shading devices incorporated to mitigate negative effects.

Question 5 addresses issues related to transparency, such as glare and light contrast. Maintaining visual comfort is regarded as essential for effective learning; therefore, Question 6, administered post-lesson, investigates the influence of visual comfort on students' comprehension and understanding of the lesson. This final stage of the survey highlights the direct connection between environmental quality and educational effectiveness, reinforcing the broader purpose of comfort assessments.

3.1.3. Verifications for Measurements and Simulations

Verification processes are undertaken for both measurement studies and simulations. The thermal comfort measurement verifications encompass the following steps and field study conditions are examined with these steps:

(1) comparison of measurement devices with each other,

(2) evaluation of the status of measurement devices within protective enclosures,

(3) comparison of thermal conditions across classrooms.

Comparative analyses are carried out on the results obtained from different measurement devices, and the influence of the protective cages designed to safeguard these devices was assessed through fixed on-site measurements. Conducting such multi-step verification ensures that device performance, environmental influences, and inter-room variations are consistently accounted for in the measurement process.

Subsequently, the simulations are verified with thermal and visual comfort measurement results. To optimize PSSs designed for existing rooms in accordance with thermal and visual comfort requirements, initially simulations are validated against on-site measurements. This step is considered essential for ensuring that computational models accurately replicate real-world conditions, thereby providing a reliable foundation for subsequent optimization studies.

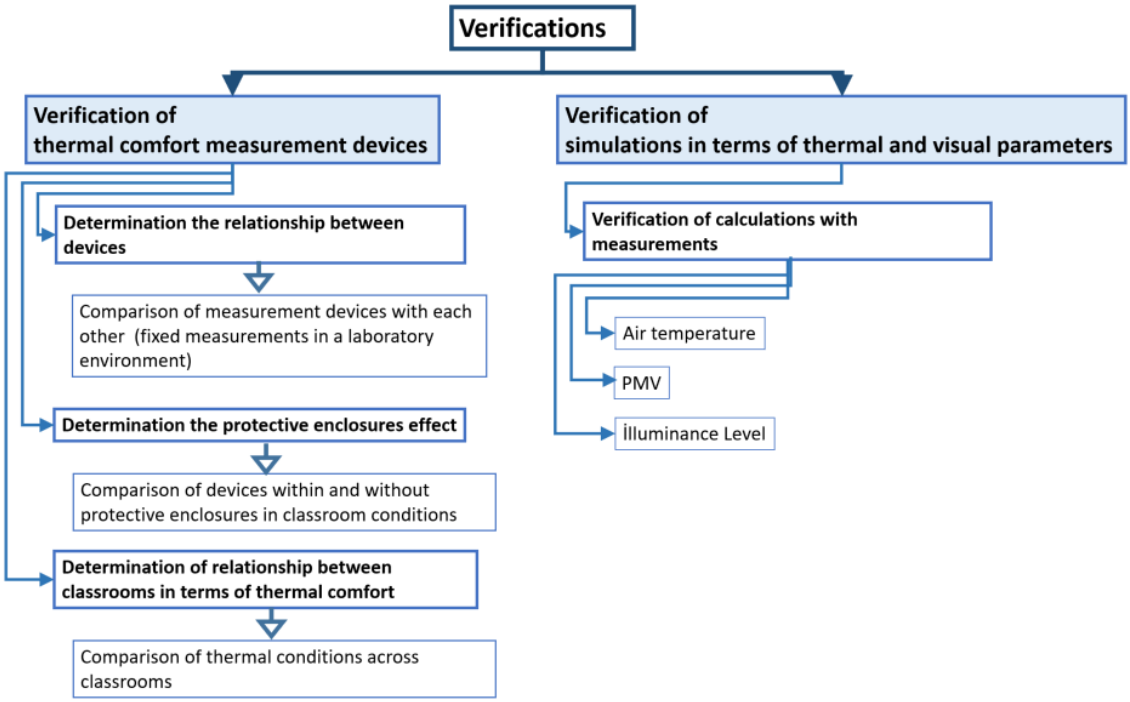

Figure 3.5 Method of Verifications for Measurements and Simulations

3.2. Analysis and Evaluation of Field Study and Verification Results

In thermal and visual comfort research, reliable outcomes depend on the systematic integration of field measurements, surveys, and verification procedures. In this thesis, field study results (including measurement and survey outcomes) together with verification procedures are systematically analyzed to ensure reliability, accuracy, and comparability. This process is structured into four complementary stages, each of which has been applied in this research to provide methodological rigor and context-specific reliability.

- **Verification for measurements**

Before comfort evaluations are conducted, the reliability of measurement devices must be verified. This is achieved by applying statistical comparisons, such as Mean Bias Error (MBE) and coefficient of determination (R^2), to test calibration consistency and to examine whether protective enclosures affect device performance. In this thesis, both laboratory and field-based verification steps were conducted, confirming consistency among devices and demonstrating that protective enclosures had a negligible effect on the results.

- **Thermal and visual comfort measurement analysis**

Thermal comfort analysis requires both objective and comparative evaluation. Parameters such as Predicted Mean Vote (PMV) and Predicted Percentage Dissatisfied (PPD) are interpreted against the comfort thresholds defined in ASHRAE 55 and ISO 7730. For comparability across classrooms, MBE and R^2 were additionally employed, following ASHRAE Standard 14 guidelines, to test statistical reliability. Such analyses can be applied to identify potential spatial variations in thermal comfort, especially near windows with high transparency ratios, and to emphasize the influence of orientation on performance. In this thesis, these methods were implemented as a guideline to demonstrate the importance of integrating both spatial and orientation-related factors into the evaluation process.

For visual comfort analysis, illuminance levels should be measured on the working plane under different façade and sky conditions. The analysis needs to assess

whether measured values comply with the ranges recommended in TS EN 17037, with particular emphasis on identifying excessive illuminance levels that may cause discomfort. To ensure reliability, measurements should be conducted under both open- and closed-curtain conditions. In this thesis, this procedure was applied to systematically assess visual comfort performance and to establish a replicable framework for evaluating the necessity of implementing perforated solar screens (PSSs).

By combining thermal and visual datasets, the analysis not only quantifies the extent of discomfort but also identifies critical areas and time periods where shading interventions are most effective. In this thesis, both short-term (instantaneous) and long-term (continuous) measurement campaigns were carried out to capture daily and seasonal variations, providing a robust dataset for comfort evaluation.

- **Thermal and visual comfort survey analysis**

Objective data alone may not fully capture users' comfort experience; therefore, surveys are recommended to complement field measurements. Survey responses are typically analyzed using frequency analysis to determine response distributions and regression analysis to explore correlations between user-reported comfort and environmental parameters. In this thesis, it is suggested that to analyse the survey results, frequency and regression analyses should be applied to explore patterns between user perceptions and physical variables such as location or façade exposure. For example, in this thesis, survey data collected concurrently with measurements confirmed the field results to determine whether users seated closer to windows reported warmer sensations and higher glare perception.

- **Verification for simulations**

To ensure that optimization results are robust, simulation outputs should be validated against field measurements. This is typically done through regression analysis between measured and simulated values (e.g., air temperature, illuminance), thereby confirming the accuracy of the simulation framework. In this thesis, such validation steps confirmed the reliability of simulation-based comfort assessments, ensuring that the optimization of perforated solar screens is grounded in accurate, context-specific input data.

Overall, the combination of device verification, field measurements, surveys, and simulation validation provides a replicable methodological framework for thermal and visual comfort research. In this thesis, this integrated approach ensured that both technical precision and user-centered perspectives were systematically incorporated into the design and optimization of shading systems.

3.3. Designing of Perforated Solar Screens (PSS)

Previous research on the single-hole plate shading systems (uniform/flat), an exterior building component, has explored design variables including hole ratio, shape, matrix, depth, axial rotation, and the aspect ratio of its openings. Some studies further suggested that additional evaluations regarding thickness, material, and slope should be considered for future studies (Doris A. Chi et al., 2017).

In this thesis, the proposed design module explicitly adopts an angled-perforation configuration, developed by analyzing existing and literature-based perforated solar screens and the design principles of horizontal, vertical, and lattice shading devices. The screen is conceived as a lattice-like perforated solar device with the horizontal shading function realized by the geometry of the angled perforations rather than by relying on panel thickness; this preserves a lightweight assembly while delivering effective solar control and daylight modulation.

Given the angled configuration, manufacturability constraints (e.g., feasible bending/angling limits, joinery, and tolerances) inform the admissible design space from the outset and motivate a staged optimization workflow.

Regarding both fixed and kinetic shading devices, the planned design is conceived as manually adjustable. The device is designed to be foldable and features adjustable openings, allowing it to be either fully open or closed, depending on the desired conditions. This low-complexity actuation strategy targets robustness and cost-effectiveness while enabling seasonal and diurnal adaptation of solar access and daylight distribution.

The variable design parameters used in the modeling of the PSSs mounted on the building’s exterior include hole ratio, depth (thickness), the angle between

horizontal and vertical devices, distance from the building, and the reflection coefficient.

The design parameters of the PSSs, intended for use on the building's exterior, are determined according to criteria that ensure thermal and visual comfort within the interior. These design parameters—such as hole ratio, angle, reflection factor, and distance from the building—can be adjusted based on the climate, orientation, and function of the room in which they are applied. The dimensions of these design parameters are specifically chosen to optimize interior thermal and visual comfort conditions. It is recommended that parameter ranges be carefully selected to balance solar control with sufficient daylight penetration. Accordingly, they should be re-optimized for each room or zone to maintain target thermal and visual comfort metrics under local boundary conditions. Following the first optimization pass, parameter bounds are updated using the observed extrema of high-performing solutions, and a second pass is executed over the contracted ranges to improve numerical efficiency and solution fidelity; comfort metrics (e.g., PMV) are subsequently evaluated for the shortlisted designs.

The primary goal of the design is to minimize direct solar radiation while enhancing indirect solar radiation during the cooling period, thereby improving both thermal and visual comfort. To achieve this, the design parameters should be re-optimized for each room to ensure the best possible comfort conditions. Design variations can be generated by modifying any combination of length, angle, and multiplier values for the design parameters.

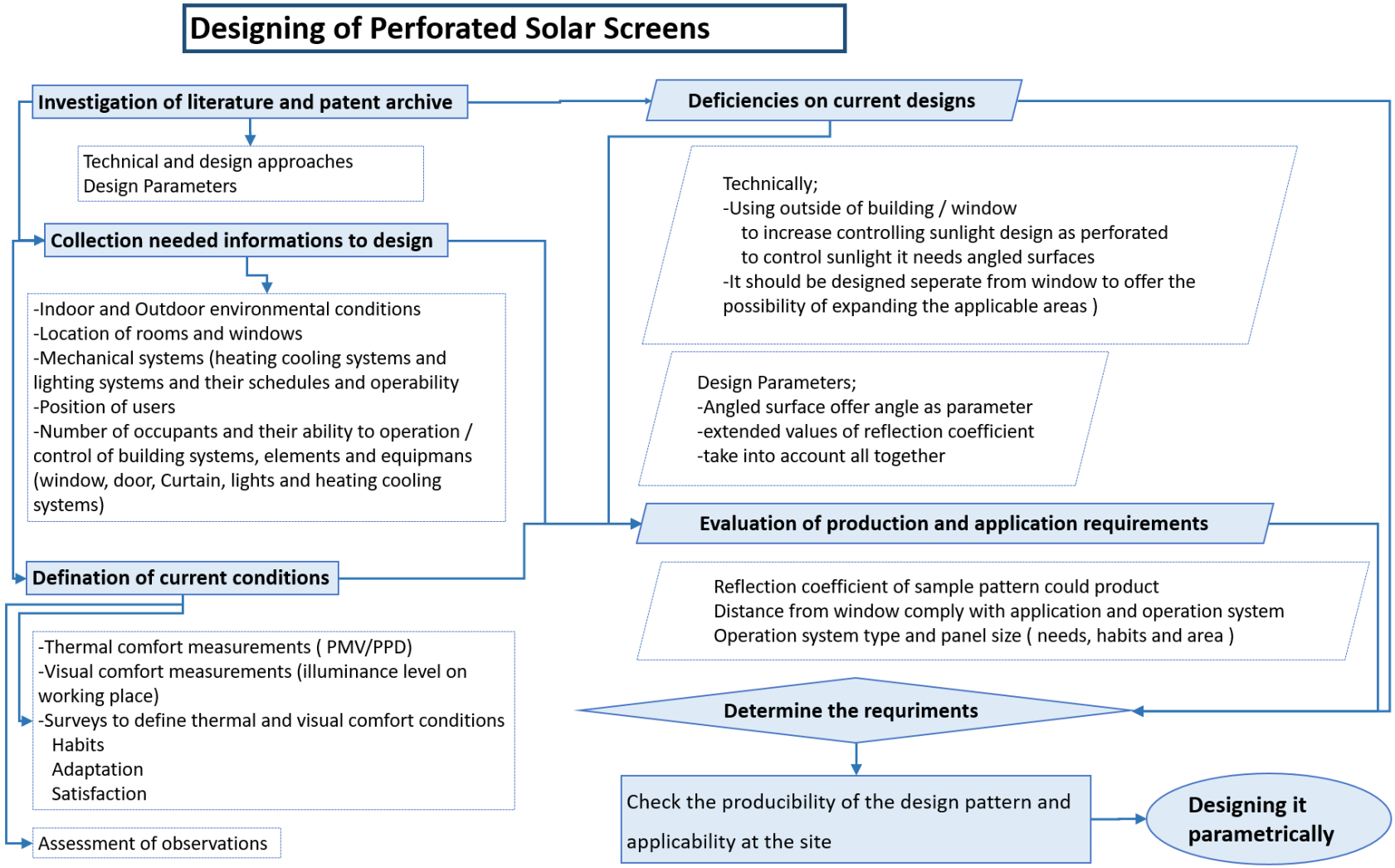

Figure 3.6. Design method and process of perforated solar screens

3.4. Simulations and Optimizations of Perforated Solar Screens (PSS)

Simulation and optimization processes are employed to evaluate the performance of perforated solar screens and to identify the most suitable configurations for maintaining indoor thermal and visual comfort. This section establishes a structured framework, beginning with the identification of comfort-related Key Performance Indicators (KPIs), design parameters, followed by optimization procedures and detailed simulations.

3.4.1. Key Performance Indicators (KPI) In Terms Of Thermal and Visual Comfort

The optimizations for the visual and thermal comfort conditions of the interior space are performed based on the design parameters established for the shading device. The relevant Key Performance Indicators (KPIs) in terms of visual and thermal comfort are defined by reference to standards such as ASHRAE 55, ISO 7730, TS EN 12464-1, and TS EN 17037, as well as prior research. Integrating both standard-based and context-specific KPIs ensures that the evaluation framework is comprehensive and comparable to international benchmarks.

The optimization is carried out by incorporating KPIs and design parameters. Subsequently, simulations are executed to identify optimal solutions, including the calculation of Predicted Mean Vote (PMV). In optimizations, KPIs are aligned with thermal and visual comfort evaluation criteria from standards, with additional consideration of tested classroom-specific usage conditions. This alignment ensures that comfort evaluations are not only theoretically grounded but also practically relevant.

During the first stage, optimization covers the entire range of design parameter values. After identifying preliminary optimal solutions, parameter ranges are refined for the second stage. However, since the calculation time remains considerable, the second stage focuses on detailed simulations of the previously optimized solutions rather than repeating the optimization. This two-step strategy is recommended in simulation-based studies, as it reduces computational load while preserving analytical depth.

In the first stage, optimizations encompassed all design parameter value ranges, focusing on criteria used to determine thermal and visual comfort assessment parameters.

First stage, optimization, was performed for;

- Spatial Daylight Autonomy (sDA),
- Summer and winter solar radiation on windows
- Annual Sun Exposure (ASE)

The criteria for evaluating visual comfort conditions, as specified in the TS EN 17037 Daylight standard, include sufficient daylight illuminance, visual connection with the exterior, daylight exposure, and protection from glare. Calculations are conducted for selected criteria according to the physical features of the study classrooms. For instance, in amphitheater-style classrooms, establishing a visual connection with the exterior may not always be feasible; thus, horizontal illuminance on the working plane becomes a more critical metric for visual comfort assessment. The room in question is a classroom with an amphitheater layout, where the seating arrangement faces away from the high-transparency facade. Only the individual in the narrator's position faces the high-transparency facade. Under these conditions, establishing a visual connection with the external environment and addressing glare for students are not feasible. However, the illuminance level on the working plane remains an important criterion for visual comfort.

To evaluate daylight illuminance and daylight accessibility, calculation methods and metrics developed in line with the criteria provided in the TS EN 17037 standard are utilized. Daylight metrics are divided into dynamic and static categories. The Daylight Factor (DF), as defined in TS EN 17037, is a static metric that does not account for changing sky conditions. However, dynamic metrics such as DA, sDA, and UDI take changing sky conditions into account (Cho, Yoo, and Kim 2014; Chi, Moreno, and Navarro 2018), providing results that are more reflective of real-world conditions.

In this thesis, sDA is included as KPI in the optimization process. DA and sDA are indices calculated based on the criteria for daylight illuminance as specified in the EN 17037 standard. DA represents the percentage of time when the target

illuminance level is met or exceeded in more than 50% of the area (DA 300/50). sDA indicates the percentage of the area where the target illuminance level is met or exceeded for at least 50% of the time (sDA300/50). The IES LM-83 standard recommends using sDA, which defines the point that will be "daylit" if the DA exceeds 50% for at least 50% of the usage hours at a illuminance level of 300 lux. These sDA targets are also specified in LEED v4.

Daylight exposure can improve occupant satisfaction, productivity, and health, and it supports circadian rhythm stimulation (Boyce et al., 2003). However, excessive daylight exposure can cause glare, overheating, and thermal discomfort (Xue et al., 2014). The TS EN 17037 standard, along with IES-LM-83-12 and similar studies, suggests calculating the Annual Sun Exposure (ASE) index to assess daylight exposure. ASE measures potential visual discomfort caused by direct sunlight and calculates the percentage of area that exceeds a specified direct sunlight illuminance level (1,000 lux) for a certain number of hours (250 hours) annually. This percentage should not exceed 10%, although up to 20% is acceptable in rooms with solar control devices (31-33). This index is also included in the calculations within the scope of optimization method proposed in this thesis.

Thermal comfort depends on environmental parameters such as air temperature, air currents, relative humidity, and radiation temperature, in addition to personal parameters. Among these, radiation temperature is influenced by solar radiation, which significantly affects thermal comfort (Arens et al., 2015; Marino, Nucara, & Pietrafesa, 2017; Tzempelikos, 2010). Given that a substantial amount of energy is consumed to maintain comfort conditions in buildings (Zani et al., 2018), solar radiation plays a crucial role in energy-efficient design (Huang & Zhai, 2020). A study that calculated the solar radiation received by the exterior facade of a window indicated that the use of shading devices reduced cooling loads by 17%-20% (Cho et al., 2014).

By controlling the solar radiation reaching the exterior facade, both thermal comfort can be achieved and energy consumption reduced. Solar radiation passing through transparent areas causes indoor heating, leading to increased cooling demand. The PSSs proposed in this thesis are designed to control the solar radiation reaching the window surface, thus ensuring indoor thermal comfort conditions. The calculation

of amount of solar radiation reaching the window area on south facade is included as a KPI in the first stage of optimization to support thermal comfort conditions.

To better understand the effect of the PSS to thermal comfort conditions, in the second stage simulations are conducted.

Second stage, simulations, are performed for;

- Predicted Mean Vote (PMV)

In the first optimization, KPI affecting thermal comfort and providing information about thermal comfort conditions are addressed. In the second stage, the aim of simulations is to deeply investigate the performance of PSSs on thermal comfort. Among the thermal comfort models, Fanger's PMV-PPD model for mechanically air-conditioned buildings and the adaptive model developed by Dear and Brager for naturally ventilated buildings are the most widely used and included in standards (ASHRAE, 2017; de Dear et al., 2020). In the second optimization, the PMV index is employed to evaluate thermal comfort. PMV-PPD (Predicted Mean Vote - Predicted Percentage of Dissatisfied) thermal comfort indices are included in standards such as ASHRAE 55 and ISO 7730 (ASHRAE, 2020; ISO 7730, 2005). These standards are used to calculate thermal comfort conditions in the optimization and other analyses. Comfort status is determined based on the limit values provided for PMV in these standards.

The impact of optimized PSSs on indoor comfort is further analyzed through parameters such as Mean Radiant Temperature, inner window surface temperature, and glare. Including these supplementary parameters ensures that the evaluation does not rely solely on aggregated indices, but instead provides a comprehensive understanding of environmental performance under real operational conditions.

3.4.2. Design parameters

The optimizations are performed based on the design parameters of angled perforated solar screens (PSS) designed in this thesis. Prior work on PSS largely examines flat, uniform plates, varying matrix/openness, thickness, and separation distance to balance daylight and heat gains. By introducing intentional angular selectivity, the present PSS is designed to intercept direct solar radiation while

preferentially admitting diffuse light. This strategy improved visual and thermal comfort when direct sun is suppressed but diffuse illuminance is maintained.

The device is conceived from the outset as angled, and therefore its admissible design space is bounded by production feasibility (bending/angling limits, joinery, tolerances) and by measured optical properties of realizable finishes. The angled configuration, its distinction from prior designs, and the two-stage optimization approach are documented in the project file; manufacturability and parameter limits were reviewed with an industry partner, and reflectance factors were measured on supplied samples to anchor simulations in real products.

Parameter ranges are first explored broadly and then contracted using the extrema of high-performing solutions, improving numerical efficiency without losing relevant design diversity. In this thesis, for optimizations, thickness parameter was excluded because it would increase runtime; thickness is therefore tested only on simulations. An additional, depending on manufacturing allowance, the design should be adopted on production feasibility. For example, the designed PSS designed with angle so, to supply the angled design the manufacturing process need to an additional area (it is presented in figure 4.48 and table 4.14 (g)) as fixed based on production feasibility.

The angle domain and screening logic are referenced to the solar angles on a south-facing façade at the project latitude (Northern Hemisphere) to ensure seasonal/diurnal relevance. Tilting the perforations imparts a directional transmittance: rays within defined altitude/azimuth bands are geometrically occluded, while higher-order sky components (diffuse skylight) are admitted and redistributed into the space.

In this thesis, optimizations were conducted with following design variables and fixed inputs. It is suggested that if the simulation time takes a long time, conduct a second optimization by contracting the value ranges of design parameters.

Design Parameters of PSS;

- **Perforation angle** (a) [°]: 0–180° (5°); contracted values: 20–35° (5°)
- **Perforation pitch/openness:**
    - full+empty (c): 0.02–0.10 / contracted values: 0.06–0.10 m;

    - empty (d): 0.01–0.09 / contracted values: 0.04–0.09 m;
    - full (e): 0.02–0.10 / contracted values: 0.07–0.10 m;
    - empty length (f): 0.02–0.10 / contracted values: 0.07–0.10 m.
- **Façade distance (h) [m]:** 0.02–0.15 / contracted values: 0.04–0.10
- **Surface reflectance coefficient (ρ):** 0.47, 0.67, 0.77.
- **Fixed/derived parameters (held constant during search);**
    - Thickness (b) [m] = 0.001–0.003. (Excluded from the optimization loop due to disproportionate daylight-simulation cost (≈80 s → ≈12,000 s when varied)).
    - Manufacturing allowance (g) [m] = 0.015.

The overarching objective is to minimize direct solar radiation while increasing indirect (diffuse) contribution during the cooling period, thereby improving thermal and visual comfort. The primary goal is to attenuate direct solar gains while enhancing diffuse/indirect contribution during cooling seasons, thereby improving both thermal and visual comfort. Within this objective, design parameters can be generated by systematically modifying length, angle, recflection coefficient and others, ensuring a balanced interplay between solar control and daylight availability as the design progresses from concept to fabrication.

Given the orientation- and program-dependence, the design parameters defined in this thesis should be re-optimized for each room/zone using the contracted ranges. Then, comfort outcomes (e.g., ASE, sDA, PMV, solar radiation) are calculated before final selection. This approach offers an opportunities because angled perforated shadings that suppress direct beam yet preserve diffuse daylight outperform flat, uniformly perforated shadings tuned on openness alone.

3.4.3. Parametric Modelling and Simulation Setting

Following a literature review focused on optimizing results, Rhinoceros - Grasshopper is selected as the software for parametric modeling of variable criteria for PSSs. Additionally, EnergyPlus, Ladybug, Honeybee and Radiance are employed to simulate the thermal and visual comfort results of the models. Octopus is utilized to perform multi-objective optimizations. The design is modeled using Rhinoceros 6.0, a visual programming software, in conjunction with Grasshopper, a computational and algorithmic parametric modeling program. Grasshopper enables algorithmic modeling and translates parametric

codes into architectural design components. This framework supports iterative exploration of design options and provides a robust foundation for linking environmental simulations (thermal and visual comfort) with parametric variations of shading designs.

Radiance, a daylighting and energy modeling plugin optimized for Rhinoceros, provides an enhanced user interface for Grasshopper. The Grasshopper components enable daylight analysis using Radiance/DAYSIM and thermal performance analysis using EnergyPlus. This integrated environment allows for the simultaneous evaluation of daylighting and energy performance, which is considered essential in multi-criteria design processes.

Previous studies have employed EnergyPlus (Sherif, Sabry, and Rakha, 2012; Blanco et al., 2019), Grasshopper (Diva, Chi et al., 2017; Gadelhak, 2013), and Ladybug, as well as Daysim (Lavin and Fiorito, 2017), in the design of PSSs. The interface through Ladybug and Honeybee plugins facilitates the integration of the Daysim and EnergyPlus engines for daylighting and thermal comfort simulations within Grasshopper. Furthermore, real-time weather data can be imported via Ladybug, ensuring that the models reflect actual climatic conditions rather than relying solely on static data inputs.

For multi-objective optimization, the Octopus plugin, which processes embedded multi-objective genetic algorithms within Grasshopper, is utilized. The Octopus plugin is widely employed in optimization studies (Ohki et al., 2019; Konis et al., 2016; Bakmohammadi et al., 2020; Zhang et al., 2017; Shahbazi et al., 2019; Touloupaki and Theodosiou, 2017; Mahdavinejad and Mohammadi, 2016). In comparison with other optimization tools available in Grasshopper, Octopus is capable of simultaneously evaluating multiple objectives, providing Pareto-optimal solutions, and identifying trade-offs among conflicting criteria. Octopus modifies the solution population using principles such as selection, crossover, and mutation, evolving toward the optimal solution by selecting the best solutions from these populations and improving subsequent generations. The initial generation consists of 200 populations, with following generations comprising 100 populations. This optimization method is widely used for rapid multi-objective optimization using the HypE reduction method. This evolutionary approach enables the exploration of large solution spaces and the progressive elimination of less suitable design alternatives. Through several iterations and the removal of non-optimal alternatives, Octopus generates a pool of feasible solutions that align with the defined objective functions, such as maximizing spatial daylight autonomy (sDA) and minimizing annual sunlight exposure (ASE).

In this developed optimization methodology, Rhinoceros - Grasshopper program plugins are employed for simulations and optimizations. By modifying the specified design parameters of the angled PSS, visual comfort and thermal comfort parameters are calculated for existing classrooms through simulations. The data obtained from these analyses are optimized using the Octopus plugin, resulting in the identification of the PSSs screens that demonstrate optimal performance across multiple criteria.

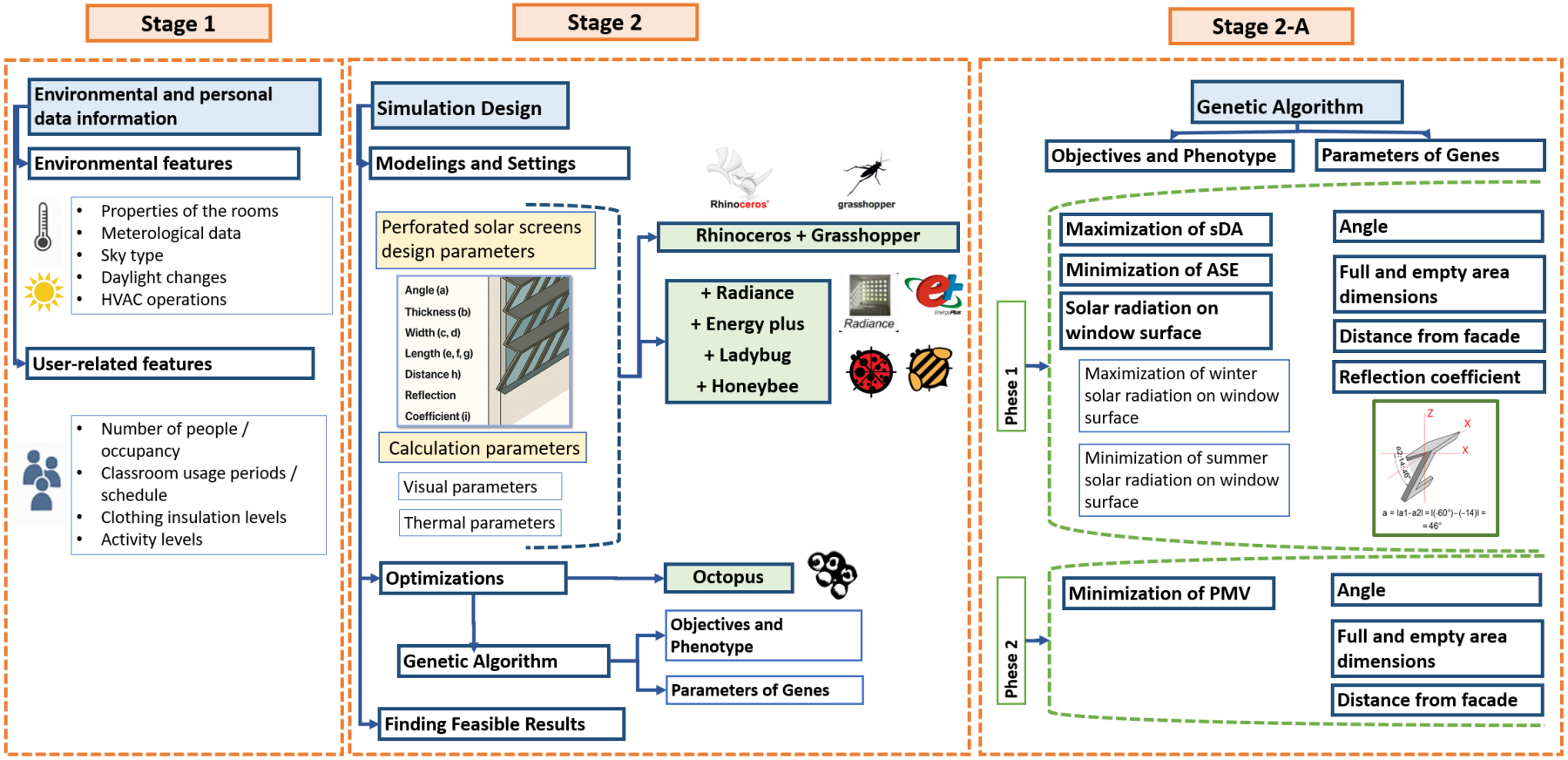

Figure 3.7. Optimization Modellings and Settings

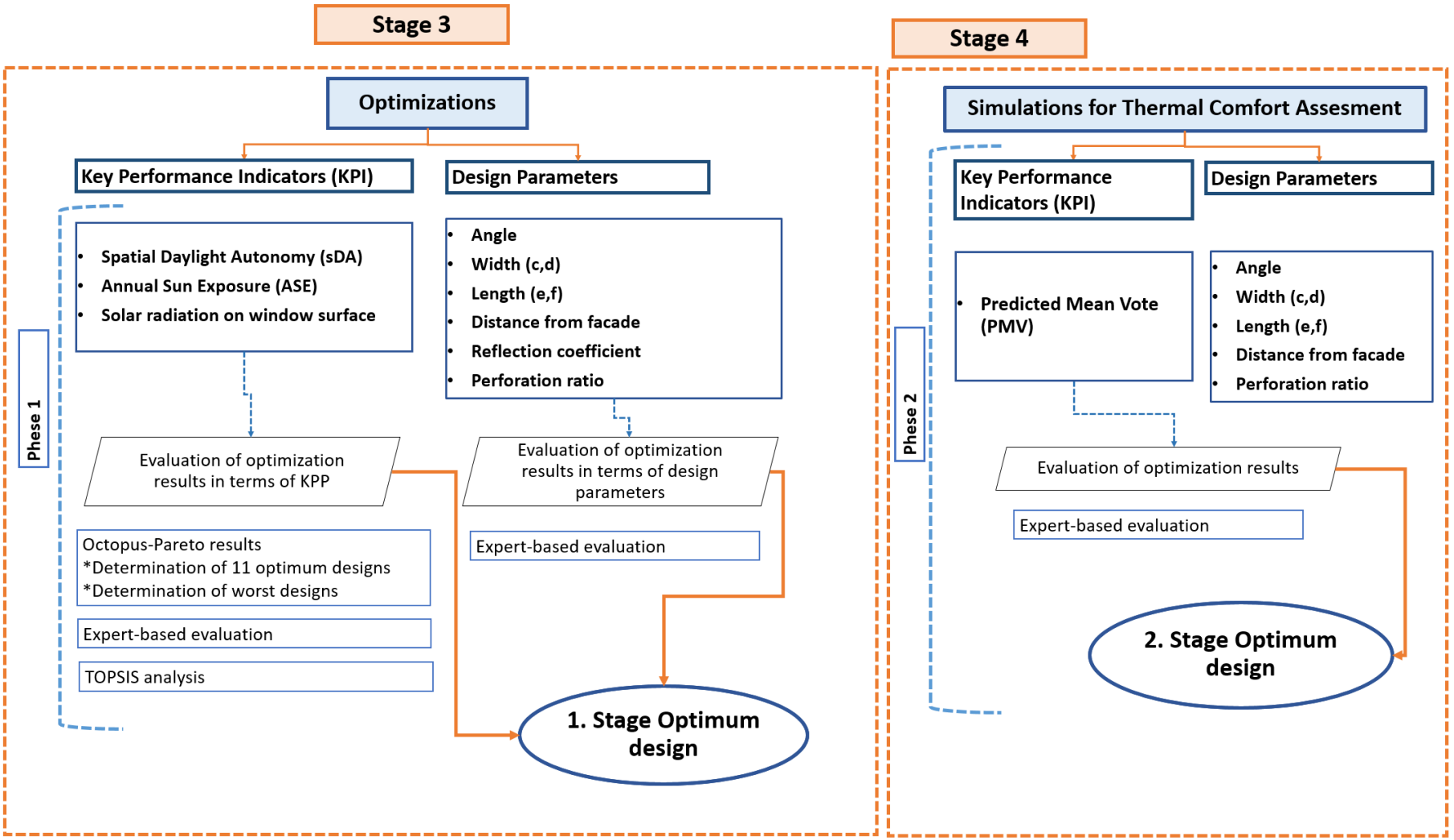

Figure 3.8. Optimization Methods

The proposed methodology suggest that the evaluation of daylight illuminance levels and daylight accessibility is conducted using calculation methods and metrics aligned with the criteria established in the TS EN 17037 standard. Daylight metrics are categorized into static and dynamic metrics. The Daylight Factor, as outlined in TS EN 17037, is a static metric that does not account for varying sky conditions. In contrast, widely used dynamic metrics, such as Daylight Autonomy (DA), Spatial Daylight Autonomy (sDA), and Useful Daylight Illuminance (UDI), incorporate changing sky conditions, providing results that more accurately reflect real-world scenarios (Cho, Yoo, and Kim, 2014; Chi, Moreno, and Navarro, 2018).

DA and sDA are indices calculated following the methods provided in EN 17037 to evaluate daylight illuminance levels. In this optimization methodology, sDA values are incorporated as a KPI in the optimization process. The sDA metric indicates the percentage of a space that meets or exceeds a specified illuminance threshold for at least 50% of operational hours (e.g., sDA 300/50). This metric represents the percentage of the area where the DA value for a target illuminance level (e.g., 300 lux) is achieved for at least 50% of the operational hours within the analyzed workspace.

Daylight plays a critical role in enhancing occupant satisfaction and productivity, supporting health, and providing circadian stimulus (Boyce et al., 2003). However, excessive exposure to daylight, including solar radiation, can lead to visual discomfort, overheating, and thermal discomfort (Xue et al., 2014). The TS EN 17037 standard provides guidelines for assessing daylight exposure, while the IES-LM-83-12 standard and similar studies in the literature recommend the Annual Sun Exposure (ASE) index for evaluating potential discomfort caused by direct sunlight.

The ASE index measures the percentage of a space where direct sunlight exceeds a specified illuminance threshold (1,000 lux) for more than 250 hours annually. The recommended threshold is below 10%; however, in spaces equipped with sun control systems, this limit may be extended up to 20% (31–33). By including ASE in the analysis, the methodology ensures a balanced evaluation between sufficient daylight access and the prevention of excessive sun exposure.

Solar radiation significantly impacts thermal comfort (Arens et al., 2015; Marino, Nucara, & Pietrafesa, 2017; Tzempelikos et al., 2010) and is a critical factor in energy-efficient building design (Huang & Zhai, 2020). Shading devices have been shown to reduce cooling loads by approximately 17–20% (Cho et al., 2014). Controlling solar radiation on building façades not only enhances thermal comfort but also reduces energy consumption.

Within the scope of this thesis, the amount of solar radiation incident on the window surfaces is calculated. Solar radiation passing through transparent surfaces contributes to indoor heating via the greenhouse effect. To address this, PSSs are proposed for external application. These screens aim to regulate the amount of solar radiation reaching the window surfaces, thereby improving indoor thermal comfort. The calculation of solar radiation entering highly transparent south-facing rooms aims to ensure optimal thermal comfort.

The initial optimization considered KPI that influence visual and comfort while the second simulation incorporated the Predicted Mean Vote (PMV) index to comprehensively evaluate thermal comfort conditions. PMV-PPD (Predicted Mean Vote - Predicted Percentage of Dissatisfied) indices, defined in thermal comfort standards such as ASHRAE Standard 55 (ASHRAE, 2020) and ISO 7730 (ISO 7730, 2005), are employed in the optimization and subsequent analyses. These standards establish comfort boundaries based on PMV values. The second-stage optimization assessed the influence of optimally designed PSSs on various indoor conditions, including Mean Radiant Temperature, window surface temperature, and visual discomfort due to glare and etc. which affect indoor comfort conditions for the optimum PSSs.

Computation times are also considered a critical factor during optimization. In the first stage, shorter computation times allow for broader value ranges for design parameters.

In the second stage, the inclusion of PMV calculations significantly increases computation times. To manage these computational demands, the range of design parameter value ranges are reduced during the second stage. This staged adjustment between broad exploration and targeted evaluation is commonly recommended to ensure both accuracy and computational feasibility. Although we narrowed the range of variables, computational efficiency remained significantly high. Therefore, after the first stage optimization, simulations are done to calculate the PMV values of optimal solutions.

By systematically refining the parameters and incorporating advanced metrics, this study achieves a comprehensive analysis of thermal comfort and daylight conditions, ensuring the effectiveness of the proposed PSSs in improving indoor environmental quality. The methodology presented here can therefore serve as a replicable framework for evaluating shading systems that can be adapted to other building typologies, shading device designs and environmental contexts.

3.4.3.1. Simulation and Optimization Settings

For the simulation process, the model is initially constructed to closely represent real-world conditions. To ensure reliability, the simulation results are validated through on-site measurements. Proximate environmental influences—for instance, devices or structures with the potential to generate shading—are systematically identified to ensure that external conditions are appropriately considered within the simulation framework. The design parameters of the PSS are defined, and value ranges for these parameters are determined. The design is then developed with parametric flexibility, enabling dynamic adjustments to the defined parameters. This approach allows iterative testing of design alternatives while maintaining consistency with measured environmental conditions.

In the calculation of daylight illuminance levels, depending on location, the Perez clearness index method is employed, utilizing a sky condition classification system. The Honeybee Program categorizes CIE sky types as sunny clear, clear, partly sunny, average, cloudy, and uniform skies. For the simulations, the sky type is selected. Daylight illuminance levels are evaluated using target illuminance levels specified in the TS EN 17037:2023 standard. Adjustments are made to align the simulations with the calculation surfaces described in the standard.

For the simulations, the Radiance parameter settings for daylight calculations are adopted as the default values provided by the Ladybug/Honeybee version 0.065 (2020) Radiance plugin. The specific Radiance parameter settings and their recommended values, which influence both calculation accuracy and computation time, are presented in Table 3.1 (Radiance website, 2020).

Adjustments to these Radiance settings significantly increase the computation time for daylight illuminance simulations, extending from approximately 86.2 seconds to 1892.1 seconds. To balance computational efficiency with the recommended accuracy, the default settings are employed for Radiance parameters throughout the simulations. This compromise follows common practice in daylight simulation workflows, where accuracy must be weighed against iterative testing needs.

Table 3.1 Radiance parameters (Website of Radiance, 2020)

Radiance parameter	Sym.	Recommended Parameters			Radiance	Value used in simulations (-)	Value used to try calculation time
		Min.	Fast	Accurate	Max.		
Ambient Bounces	ab	0	0	2	8	2	5
Ambient Divisions	ad	0	32	512	4096	512	1024
Ambient Super-samples	as	0	32	256	1024	128	128
Ambient Accuracy	aa	0.5	0.2	0.15	0.0	0.25	0.1
Ambient Resolution	ar	8	32	128	0	16	256

According to the recommendations of the Illuminating Engineering Society (IES), the percentage of areas with an illuminance level exceeding 1000 lux for more than 250 hours annually (ASE 1000,250h) is calculated based on direct solar radiation. The North American Illuminating Engineering Society (IESNA) suggests that this percentage, a metric included in LEED v4, should remain below 10% (Pilechiha et al., 2020; Tabadkani et al., 2018; Futrell et al., 2015a, b; IESNA, 2012; L. Heschong et al., 2011).

For annual window solar radiation calculations, adjustments are made to minimize summer solar radiation while maximizing winter solar radiation throughout the year.

For PMV calculations, indoor temperature, air velocity, Mean Radiant Temperature and air humidity are determined instantly as a result of the Energyplus simulation and the values were transferred to the Ladybug PMV calculation section.

In the optimization processes, the Octopus plugin is configured to minimize the input parameter values. The aim of optimizations is that minimizing ASE value, while maximizing the sDA value and maximize beneficial solar radiation while minimizing detrimental solar radiation. There is need a single value for yearly solar radiation. To unify solar radiation results with indices such as ASE and sDA, a composite indicator is formulated, allowing the evaluation of solar radiation as a single optimization criterion.

3.5. Analysis and Evaluation of Simulation and Optimization Results

As a result of the multi-objective optimization process, a wide range of alternative solutions is generated through the combination of design and KPI. To evaluate the performance of this solution set and identify the most appropriate outcomes, the analysis followed a multi-stage process, structured under the same categories later used in the results section.

The first stage involved the use of the Octopus plugin and the Pareto scatter plot. The points located on the Pareto front of this graph represent the set of non-dominated solutions, meaning those that achieve better performance in at least one objective without deterioration in others. This step enabled the identification of potential optimal solutions and the overall distribution of the solution space. Each point corresponded to a design variation, evaluated in terms of summer and winter solar radiation (kWh/m²), Annual Sunlight Exposure (ASE, %), and Spatial Daylight Autonomy (sDA, %). Among these, winter solar radiation and sDA are treated as criteria to be maximized due to their contribution to thermal benefit and daylight sufficiency, respectively; while ASE and summer solar radiation are considered minimization criteria due to the risks associated with excessive glare, thermal load, and visual discomfort. Following the standards and literature thresholds referenced in this thesis (e.g., ASE < 10%, sDA ≥ 75%), performance criteria were classified as either maximization or minimization objectives.

Because the Octopus plugin is configured to minimize all KPI during the optimization process, inverse operations are applied within Grasshopper for maximization criteria such as winter solar radiation and sDA. As such, maximum values are effectively represented as minimum values in the Pareto scatter plot. In this way, the Pareto graph effectively visualized all performance targets in a comparable manner.

The most appropriate solutions were identified by selecting the points closest to the origin (ideal point) within the three-dimensional performance space. This selection strategy integrates both quantitative and visual assessment metrics, thereby contributing a holistic perspective to the multi-criteria decision-making process. Consequently, the Octopus Pareto scatter plot graph serves as a critical analytical tool in interpreting the outcomes of the parametric optimization process and in grounding the decision-making process on objective functions.

However, drawing a definitive conclusion about a single "best" outcome solely based on the Pareto scatter plot is not feasible. Rather, by evaluating the designs and corresponding

calculation results of the most favorable scenarios, users can select the most appropriate solution based on specific project requirements. In this study, optimal results are first identified through the Pareto graph, after which their numerical performance is compared and the differences in design parameters are examined. To limited the identification of optimal scenarios, process, dominated and redundant cases are removed, acceptability constraints are applied, and near-duplicate solutions are consolidated. The outcome is a reduced yet representative set of scenarios that captures the full spectrum of performance trade-offs, ensuring that extreme, compromise, and intermediate options remain available for decision-making.

In the fallowing stage of identification, Pareto-optimal solutions are further examined under the heading "**Evaluation of Optimization Results in terms of KPI."** At this stage, the selected scenarios are evaluated in terms of their calculated KPI values, while also considering extreme or worst-case conditions to establish a reference for comparison. This dual approach ensured that both favorable and unfavorable boundary conditions are systematically addressed.

It is evident that qualitative assessments alone are insufficient to select the most appropriate solution among the optimal outcomes identified through the Pareto scatter plot generated via the Octopus plugin. Therefore, additional analyses were required to determine the best-performing design. At this point, normalization-based analyses, which can be integrated into decision support systems, are known to support data-driven decision-making in architectural design (Attia et al., 2012). One of the Multi-Criteria Decision-Making (MCDM) methods, the Technique for Order Preference by Similarity to Ideal Solution (TOPSIS), enables the identification of the best alternative by evaluating the relative distances of a set of alternatives from the ideal and anti-ideal solutions (Hwang & Yoon, 1981). For this reason, in order to select among the optimal scenarios determined by the optimization process, the performance results are normalized and a TOPSIS analysis are conducted. This part of the analysis is described under the heading **"Application of TOPSIS Analysis."** In this step, the raw KPI data were normalized using vector normalization (scaling values between 0 and 1), after which a weighted normalized decision matrix is created. Equal weights (0.25) are assigned to each KPI, reflecting the balanced consideration of thermal and daylighting performance indicators.

To construct the normalized decision matrix for the analysis, the original data are scaled between 0 and 1 using vector normalization. The vector normalization formula is used as follows:

$$n_{ij} = \frac{x_{ij}}{\sqrt{\sum_{k=1}^{m} x_{kj}^2}} \tag{3.1}$$

nij, , i. represents the normalized value of the i- alternative with respect to the j- criterion, xij is the original value, and m is the number of alternatives.

For the weighted normalized decision matrix, the normalized values are multiplied by the respective weights of the criteria. In façade/shading optimization, equal-weight TOPSIS has been used to rank Pareto-optimal solutions that balance thermal control and daylighting (Chen & Tan, 2025); in this analysis procedure utilize the same neutral stance. In façade engineering MCDM workflows, assigning explicit criterion weights is standard practice (Bianchi et al., 2024); treating criteria equally at early stages helps avoid implicit bias, so each of the four KPIs receives 0.25. The weighted normalized value vij is calculated as:

$$v_{ij} = w_j \times n_{ij} \tag{3.2}$$

where wj denotes the weight of the j criterion.

Subsequently, the ideal solution (A*) and negative ideal solution (A−) are determined. The ideal solution comprises the best weighted normalized values for each criterion (maximum for benefit criteria, minimum for cost criteria), while the negative ideal solution comprises the worst values. Distances to these reference points (ideal (di+) and negative ideal (di−)) are calculated using the Euclidean distance formula, and finally, the relative closeness coefficient (Ci*) is obtained.

$$d_i^+ = \sqrt{\sum_{j=1}^{n} (v_{ij} - v_j^*)^2}$$
$$d_i^- = \sqrt{\sum_{j=1}^{n} (v_{ij} - v_j^-)^2} \tag{3.3}$$

where n is the number of criteria.

$$C_i^* = \frac{d_i^-}{d_i^+ + d_i^-} \tag{3.4}$$

The value of Ci∗ ∗ ranges between 0 and 1, where values closer to 1 indicate alternatives that are closer to the ideal solution.

This value, ranging between 0 and 1, is then used to rank alternatives according to their similarity to the ideal solution, providing a quantitative foundation for the final selection of optimal designs.

Finally, the design parameters of the optimal solutions are evaluated. Under the heading **"Evaluation of Optimization Results in terms of Design Parameters,"** geometric characteristics such as angle, dimensions, perforation ratio, and reflection coefficient are systematically compared across optimal scenarios. This step allowed the connection between performance outcomes and specific design configurations to be explicitly established, serving as a bridge between parametric simulation outputs and practical design guidelines.

Through this structured approach—**Pareto analysis, KPI-based evaluation, normalization and TOPSIS decision-making, and design parameter assessment—**the analysis framework ensures that the evaluation of results is transparent, replicable, and grounded in both quantitative and design-oriented criteria.

4
APPLICATION OF THE DEVELOPED METHOD

A method was developed to design of perforated solar screens (PSS) in terms of thermal and visual comfort. This method tested in terms of its applicability to real world. To achive this aim current three classroom were selected as study area considering their fetures and properties. Depending on method firstly data collection and analysis were done.

4.1. Data collection and analysis to test developed method

The dimensions of the classrooms were determined through architectural drawings and on-site measurements. Additionally, the optical and thermophysical properties of the building envelope were identified using data obtained from measurements and technical documentation.

4.1.1. Observations of classrooms

Within the scope of this study, a camera system was installed in the classrooms, and the recordings were analyzed to assess factors such as window and curtain opening frequencies, user locations, and related behaviors. Data including the academic calendar, classroom usage periods, observations, camera records, number of users, clothing insulation levels, and activity levels were collected.

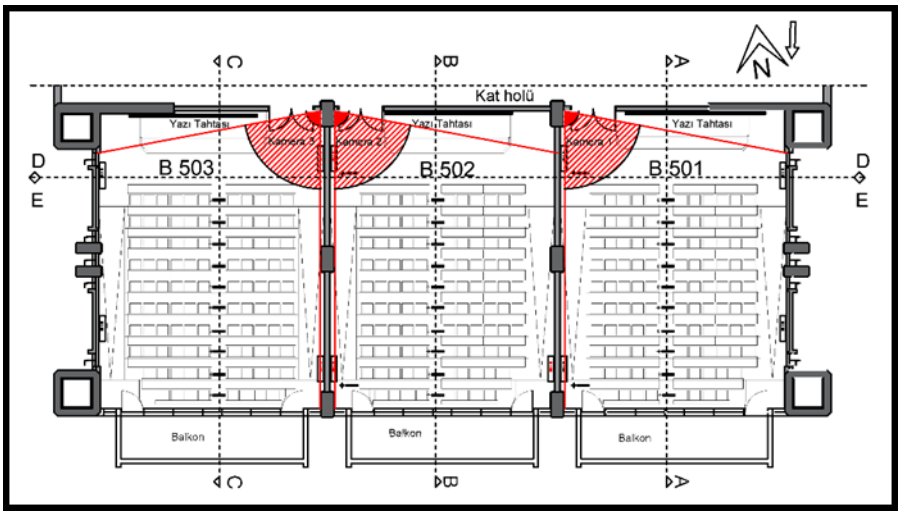

Figure 4.1 Camera Positions and Fields of View (Red-shaded areas indicate non-visible zones)

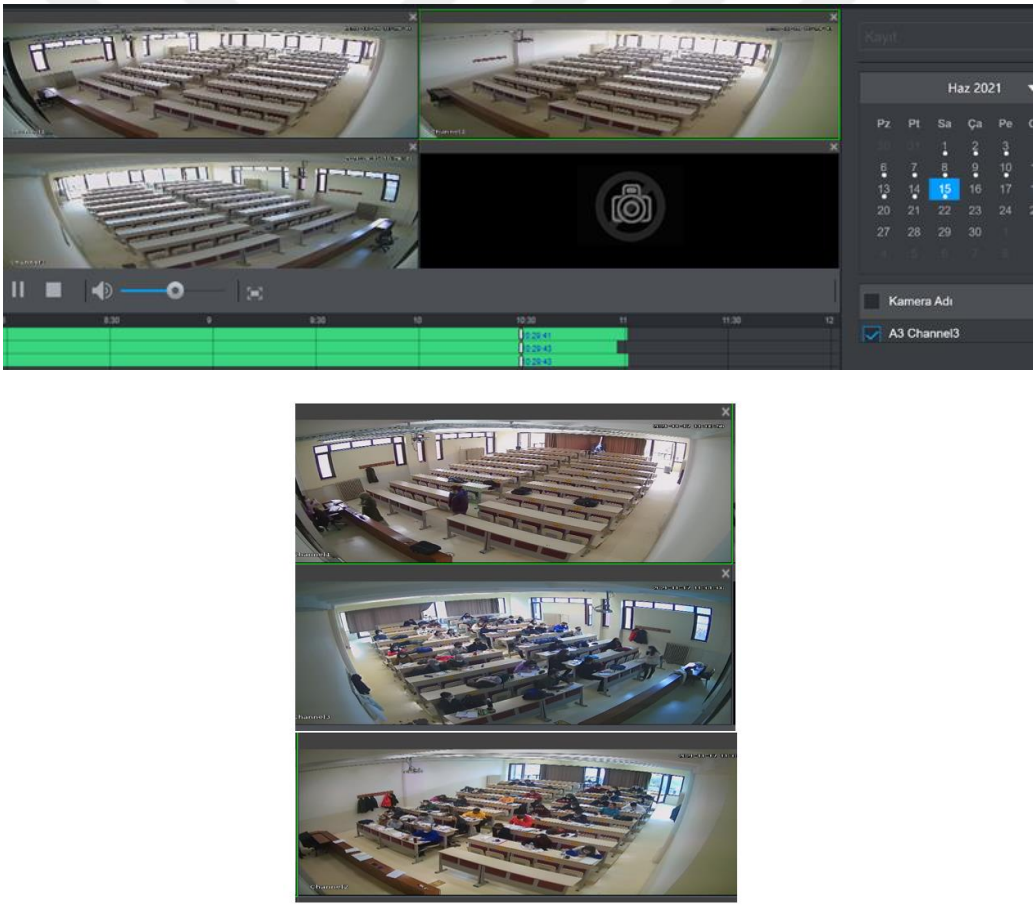

Figure 4.2 Photograph Captured from Classroom Cameras on 15.06.2021 at 10:00 AM

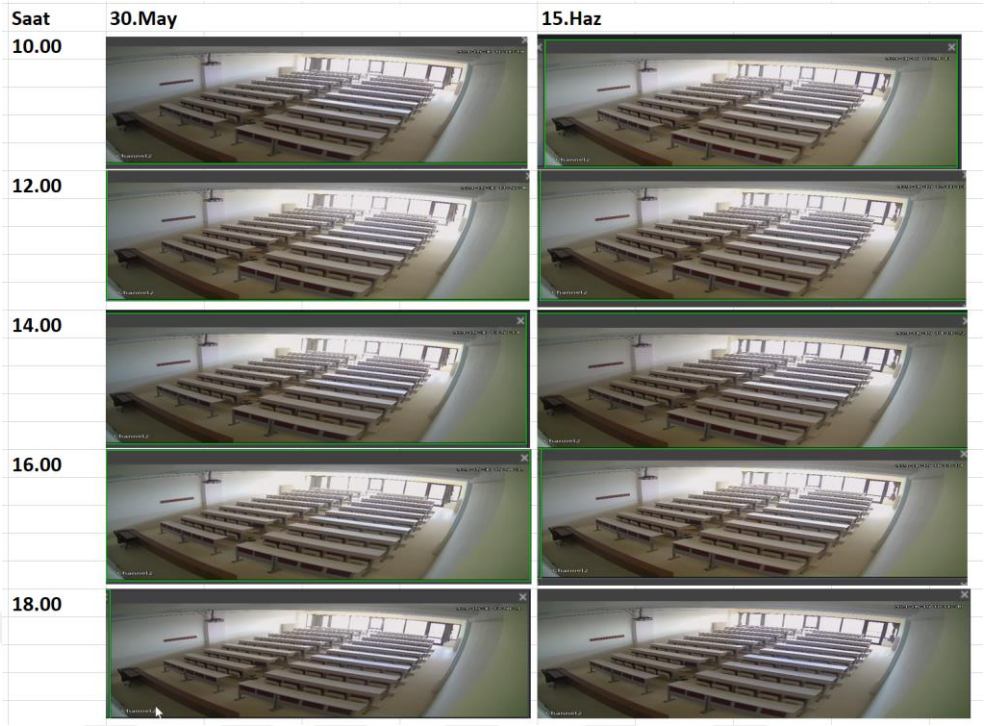

Figure 4.3 Photograph Captured from Classroom Cameras on 30.05.2021 and 15.06.2021 at 10:00, 12:00, 14:00, 16:00 and 18:00

4.1.2. Conducting of Field Studies on Current Classrooms

In educational spaces, which are actively utilized by approximately 22% of the national population, ensuring comprehensive comfort in physical environmental parameters such as light, sound, and heat is crucial (10. ATMK-November-Rengin). Turkey is home to 207 universities, and university students and academic staff constitute 9% of the population. Of this group, 26.3% are affiliated with the 61 universities located in Istanbul (Yüksek Öğretim Kurumu, 2020). Both students and academic staff spend significant amounts of time in university buildings, particularly classrooms.

The selected three classrooms have high transparency ratio on the south-facing facade and individual facades oriented towards the south, southeast, and southwest. Thermal and visual comfort measurements and surveys were conducted to assess the suitability of these classrooms for working environments. These classrooms feature an amphitheater-style seating arrangement, with the primary viewing direction oriented towards the north.

4.1.2.1. Application of Objective Method (Measurements)

Three classrooms with south, southeast, and southwest orientations were identified. These classrooms numbered B 501, B 502, and B 503 located at Yıldız Technical University's Beşiktaş Campus. The classroom B 501 is characterized by facades oriented towards the south and east, classroom B 502 features a south-facing facade, and classroom B 503 is defined by facades facing south and west. Thermal and visual comfort field studies were conducted to determine the suitability of these classrooms for the study.



Figure 4.4 Field study location



Figure 4.5 Exterior and interior visuals of classrooms

Furnished plans of classrooms B-501, B-502, and B-503 are provided in Figure 4.6 and sectional drawings of classroom B-501 are presented in Figure 4.7. For both

thermal and visual comfort evaluations, PMV (Predicted Mean Vote) and daylight illuminance level values were measured continuously and intermittently at the specified points.

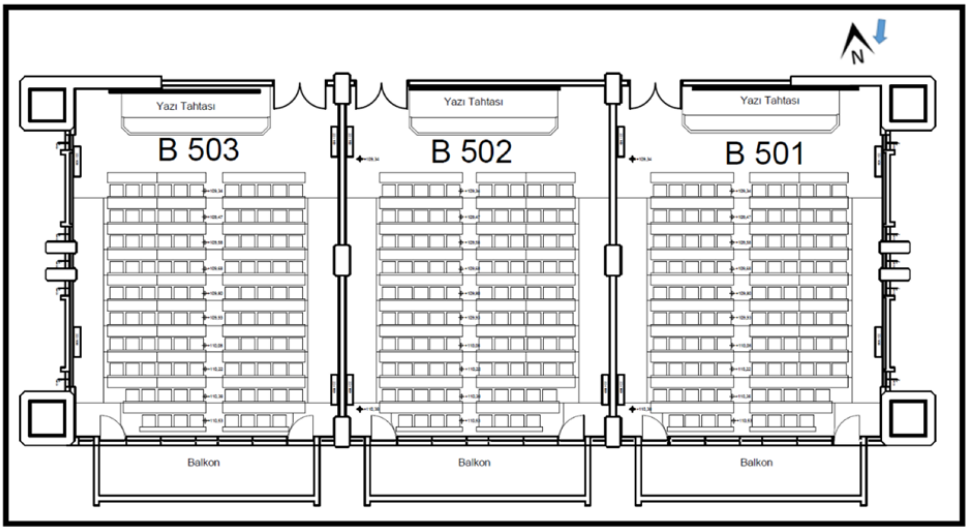

Figure 4.6 Furnished plan of classrooms B- 501- B-502 and B- 503

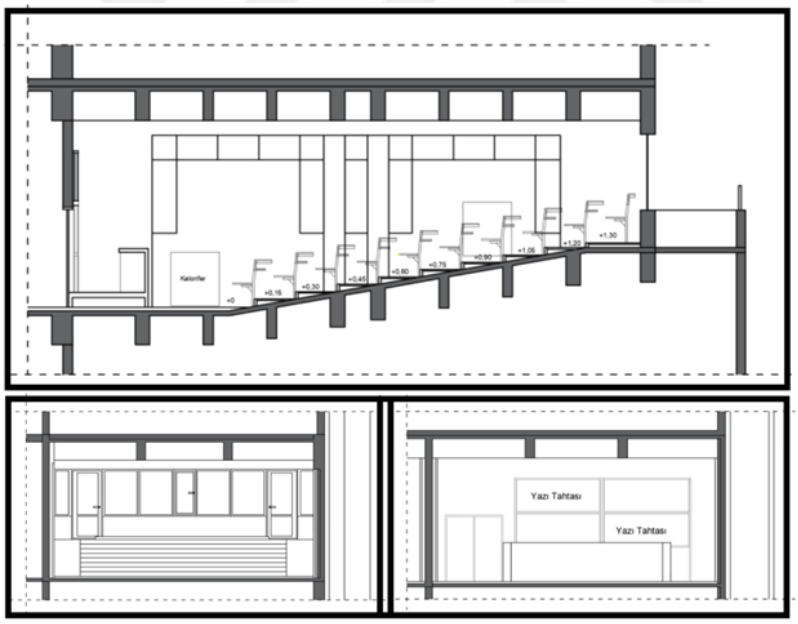

Figure 4.7 Sections of classroom B-501

There are variations in the transparent areas of the east and west facades—11.5% for B 501 and B 503, respectively—pose a challenge. The transparency ratio of the south facades of all classrooms are consistent. Given the significant influence of transparent areas on comfort conditions, it is proposed to replace the transparent

areas on the east and west facades of Classrooms B 501 and B 503 with opaque materials to ensure uniform conditions across the study.

This modification will be carried out using materials that comply with the limit values specified for Istanbul as a 2nd Region Degree Day Zone in TS 825-2013 (e.g., Ud: 0.57 W/m²K) or based on the current U-value of the building envelope. Following this adjustment, the newly added interior surfaces will be painted to match the reflection factor of the existing interior surfaces, ensuring consistency in visual and thermal performance.

The room characteristics of the classrooms are summarized in Table 4.1, and the current transparency ratio is detailed in Table 4.2.

Table 4.1 Physical characteristics of classrooms

Classrooms	**Direction of classroom**	**Dimensions**	**Heating system and number of Radiator**	**Capacity (person)**
B 501	South and East	11,76 × 9,08 × (2,7-3,80)	Gas central heating systems, Cast iron radiator- 4 radiators	109
B 502	South	11,76 × 8,90 × (2,7-3,80) Trapezoidal Prism	Gas central heating systems, Cast iron radiator- 3 radiators	109
B 503	South and West	11,76 × 9,08 × (2,7-3,80) Trapezoidal Prism	Gas central heating systems, Cast iron radiator- 4 radiators	109

Table 4.2 Current transparency ratios of rooms

Room	**Direction of Classroom**	**Capacity (person)**	**Dimension of Classroom**	**Direction of transparent component**	**Transparency Ratio (WWR – Window to Wall Ratio)**		
					East	**South**	**West**
B 501	South, East	109	11,76 × 9,08 × (2,7-3,80)	**South and East**	%11,5	%60	-
B502	South	109	11,76 × 8,90 × (2,7-3,80)	**South**	-	%60	-
B503	South, West	109	11,76 × 9,08 × (2,7-3,80)	**South and west**	-	%60	%11,5

The TESTO 635 Humidity and Temperature Measurement Device, along with the Pressure Measurement Device (Figure 4.8), was employed to measure the U-value of both opaque and transparent building envelope components. This device is capable of measuring the U-value (in $W/m^2 \cdot K$), surface temperature (Tw), and indoor temperature (Ti). The U-values obtained from these measurements are presented in Table 4.3.



Figure 4.8 TESTO 635 - Humidity and Temperature Measurement Device, capable of measuring pressure

Table 4.3 Building envelope section layers according to architectural drawings and U values from measurements

Building envelope Components	**Measurement U-Value (W/m^2K)**	**Section Layers (Project)**	
		Material	**Thickness (m)**
Exterior Wall	0,387	Plaster	0,02
		Heraklith	0,03
		Exposed Concrete	0,15
Internal Wall	0,732	Perforated Particleboard	0,025
		Exposed Concrete	0,05
		Bakelite Glass Wool	0,05
		Perforated Particleboard	0,025
Ceiling-Floor	-	Rubber Floor Covering	0,05
		Alum	0,025
		Leveling Concrete	0,04
		Reinforced Concrete Floor	0,1

Table 4.3 Building envelope section layers according to architectural drawings and U values from measurements (Continued…)

Building envelope Components	**Measurement U-Value (W/m^2K)**	**Section Layers (Project)**	
		Material	**Thickness (m)**
Terrace Roof	-	Tile Mosaic	0,025
		Mortar	0,025
		Ruberoid and Water Insulation(3 layers)	-
		Polyurethane heat insulation	0,05
		Vapor Insulation	-
		Slope concrete	0,03 – 0,24
		Reinforced Concrete Floor	0,1
Window	1,847	-	-
Door	1,5	-	-

The building envelope section layers for the rooms, as depicted in the architectural project drawings, are provided in Table 4.4.

The building envelope section layers and U-values, determined through both measurements and architectural project drawings, were compared with the values specified in TS825 2013. Approximate values for the section layers and U-values were derived, and suggested section layers were developed (Table 4.4). To ensure accurate data input into the simulation program, these two tables were utilized. By considering the values presented in Tables 4.3 and 4.4, determinations were made based on the building envelope requirements outlined in the ASHRAE 90.1-2010 standards. The building envelope characteristics were then used to input data into the simulation program, where the corresponding building envelopes were created.

Table 4.4 Building envelope section layers and U values determined in TS825 2013 according to architectural drawing section layers

Building envelope Components	**TS825 U-Value (W/m^2K)**	**Section Layers (TS825)**	
		Material	**Thickness (m)**

Table 4.4 Building envelope section layers and U values determined in TS825 2013 according to architectural drawing section layers (Continued…)

Building envelope Components	**TS825 U-Value (W/m^2K)**	**Section Layers (TS825)**	
		Material	**Thickness (m)**
Exterior Wall	0,689	Plaster made using only gypsum (without aggregate)	0,02
		Wood fiber thermal insulation boards	0,03
		Concretes made using porous lightweight aggregates and without quartz sand	0,15
Internal Wall	0,531	Flat particle boards	0,025
		Concretes made using porous lightweight aggregates and without quartz sand	0,05
		Glass Foam	0,05
		Flat chipboards	0,025
Ceiling-Floor	2,215	Linoleum	0,05
		Cement mortar screed	0,025
		Unreinforced Concrete	0,04
		Reinforced Concrete	0,1
Terrace Roof	0,381	Marble	0,025
		Lime mortar, lime-cement mortar	0,025
		Polyurethane rigid foam	0,05
		Concretes made using porous lightweight aggregates and without quartz sand	0,15
		Reinforced Concrete	0,1
Window	2,1	Double Glass Low-e, Plastic Joinery (two chambers) (9 cm space – 2.4 U 12 is -2.3)	16 cm space
Door	2	Interior door	-

The reflection coefficients of the classroom interior surfaces and furnishings were measured using the Minolta Spectrophotometer CM-2600d. The light transmission coefficient of the glass was determined through illuminance measurements and found to be 76%.

Table 4.5 Reflection coefficients of the classroom interior surfaces and furnishings

Surfaces	Standard Illuminant C		Standard Illuminant D65			
	Munsell		Yxy			
	SCI	SCE	SCI		SCE	
	2°	2°	2°	10°	2°	10°
Interior Wall	Hue;1,6 Y Value;8,9 Croma; 2,5	Hue;1,6 Y Value;8,9 Croma; 2,5	75,73 0,34 0,36	74,39 0,35 0,36	75,6 0,34 0,36	74,27 0,35 0,36
Floor	Hue;1,3 Y Value;8,4 Croma; 2,6	Hue;1,4 Y Value;8,3 Croma; 2,7	66,17 0,35 0,36	64,99 0,35 0,36	63,99 0,35 0,36	62,81 0,35 0,36
Green Chalkboard	Hue;7,2 G Y Value;4 Croma; 2,8	Hue;7,06 G Y Value;3,9 Croma; 2,9	12,12 0,28 0,36	12,06 0,29 0,36	11,72 0,28 0,36	11,6 0,29 0,36
White Chalkboard	Hue;6,5 Y Value;9 Croma; 0,3	Hue;6,1 Y Value;8,7 Croma; 0,3	77,64 0,31 0,33	77,47 0,31 0,33	72,98 0,31 0,33	72,8 0,31 0,33
Desk and Chair	Hue;2,3 Y Value;7,6 Croma; 1,9	Hue;2,5 Y Value;7,4 Croma; 2	52,23 0,34 0,35	51,64 0,34 0,36	48,57 0,34 0,36	47,99 0,34 0,36
alcony Floor	Hue;0,8 Y Value;7,7 Croma; 1,1	Hue;0,7 Y Value;7,6 Croma; 1,1	53,41 0,33 0,34	53 0,33 0,34	52,32 0,33 0,34	51,91 0,33 0,34
Ceiling	-	-	-	-	-	-

Table 4.6 Classroom Device Specifications, Visual Representations, and Spatial Configurations (The luminaire is equipped with two fluorescent lamps)

Device Features	Photograph	Device Layout Plan
PHILIPS MASTER TL5 HE 28W/840 1SL/40 ***Fluorescent*** ***Luminous flux: 2900 lm*** ***Efficacy: 96 lm/W*** ***Color Temperature: 4000K*** ***Color Rendering index: 82*** ***24×2=48 pieces*** ***Dimensions: 1.163 x 0.3 x 0.1 m***		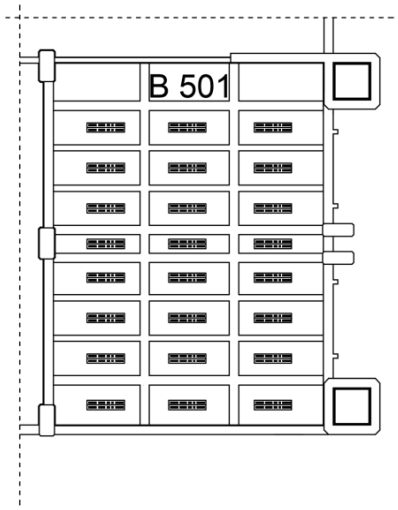

-Thermal Comfort Measurements

Thermal comfort assessments were done based on objective parameters, which can be categorized into personal and environmental factors. To understand thermal comfort conditions of these classrooms personal factors determined depending on survey results and standardized values and environmental factors were determined with measurements. As a personal factor clothing insulation values and activity level used as input parameter in measurements. To evaluate thermal comfort conditions, measurements were made as long term and short term.

Since the study involves continuous measurements over one year, clothing insulation values will be recalculated using survey results and will be updated in the measurement device at four-month intervals (June, September, December, May). In classrooms, where activities generally involve sitting, listening, reading, and writing, the most appropriate activity level is categorized as "sedentary activity" in ISO 7730 and ASHRAE standards. For this activity, activity level of 1.2 met (70 W/m^2) is specified.

Prior to fixing the measurement devices in classrooms, initial measurements were conducted to determine the measurement protocol. For each measurement point, the device was set to record data every 30 seconds for a duration of 5 minutes. To ensure accurate results, devices were allowed to adapt to the environment by being stationed for 15 minutes before measurements began. Subsequently, a waiting period of 5 minutes was observed at each point prior to recording data. Once the devices are fixed, measurements will be conducted continuously.

Thermal Comfort Measurement Standards and Setup;

The ASHRAE 55 standard specifies the following guidelines for measurement for a seated occupant:

- Air temperature and average air speed shall be measured at heights of 0.1 m, 0.6 m, and 1.1 m above the ground for a seated person.
- Radiant temperature asymmetry and humidity shall be measured at a height of 0.6 m above the ground.
- Operative temperature or PMV shall also be measured at a height of 0.6 m above the ground.

Accordingly, thermal comfort measurement devices will be positioned at a height of 0.6 m during the study.

The measurement points were determined based on classroom layouts and the research objectives. To evaluate the transparency ratio and the influence of the PSS, measurements are planned at two locations within each classroom: one point near the transparent area and another farther away from it. This approach ensures a comprehensive analysis of the shading device's impact on thermal comfort across different zones within the classroom.

Table 4.7 Field study measurement Parameters

Measurement points	**Measurement Height**	**Measurement type-time and interval**	**Activity Level**	**Clothing insulation level**
4 points for each classroom	0.6 meters	According to Time - 5 min - 30 sec Short-term and long-term measurements	1,2 met	Be determine depending on periods (0,5 clo and 0,8 clo)

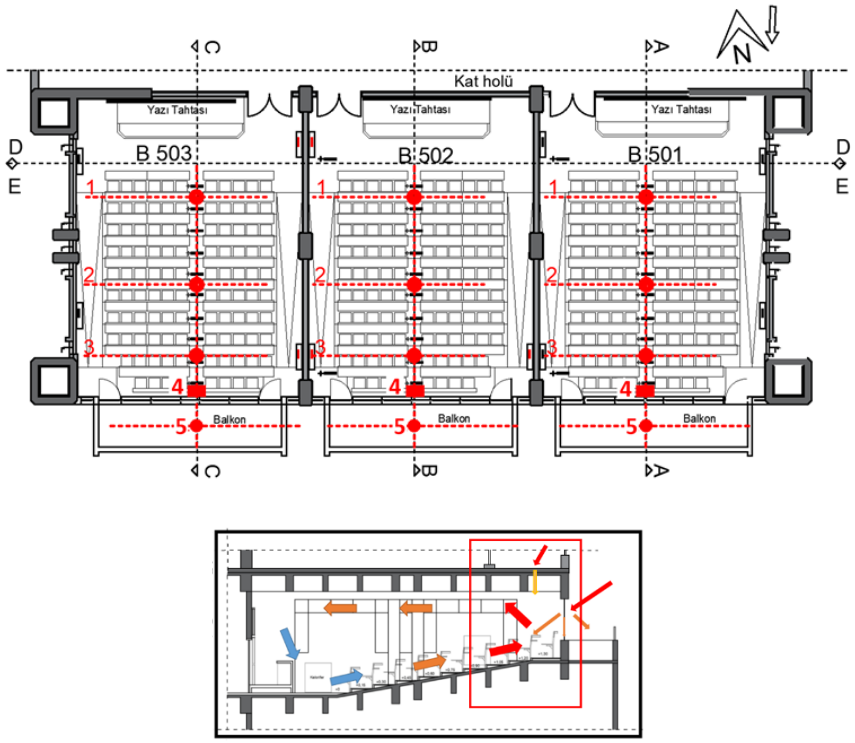

Figure 4.9 Thermal Comfort Measurement Points in Classrooms (Points 1, 2, and 3 for short-term measurements, and Point 4 for fixed measurements, Point 5 for outdoor weather conditions measurement)

For the thermal comfort measurements, four sets of devices were acquired from the equipment set provided below, with three sets to be used for long-term measurements and one set for variable measurements. The measurements have been conducted within the specified range. The Delta Ohm HD 32.3A (Figure 4.10) Microclimate Analysis Device and Testo 480 Digital Temperature and Humidity Meter were used to measure indoor air temperature, air velocity, humidity, Mean Radiant Temperature. Additionally, by inputting personal factors (e.g., clothing insulation level and activity level) into the device, the PMV (Predicted Mean Vote) and PPD (Predicted Percentage of Dissatisfied) values for the measurement points are calculated.

Three sets of Delta Ohm HD 32.3A were permanently installed in front of windows for long-term measurements. The devices are designed to perform calculations in accordance with the standards ISO 7730, ISO 7726, and ISO 7243. The technical specifications of the probes used for PMV-PPD measurements with the device are provided in Table 4.8. Each channel (3 inputs) has a memory capacity of 67,600 records and can operate for up to 200 hours (approximately 8 days). Ahlborn ALMEMO® 5690-1 Data Logger was connected to the microclimate analyzer to store measurement data continuously.

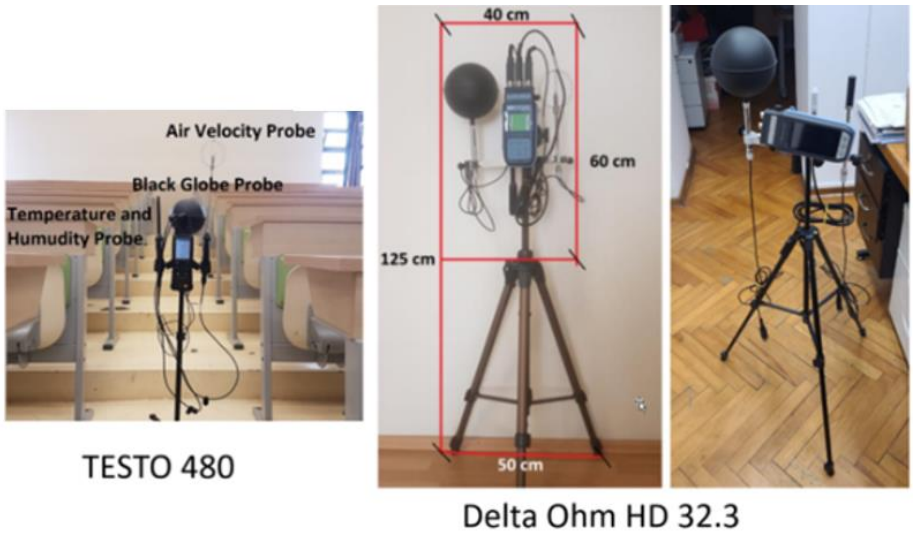

Figure 4.10 TESTO 480 and Delta Ohm HD 32.3A PMV-PPD measurement devices

This comprehensive approach to device selection and deployment ensures accurate, reliable, and continuous data collection for evaluating thermal comfort conditions in the study area.

Table 4.8 Delta Ohm thermal comfort measurement device probes

Probes			
Measurements	Radiant Temperature sıcaklık (Tn)	Relative Humidity and Air Temperature (Rh-T)	Air Velocity (Va)
PMV/PPD	✓	✓	✓
Accuracy	Class 1/3 DIN	T = 1/3 DIN RH = ±2% (90 to 100% RH) @ T=15 to 35°C (±1.5 + 1.5% of the measurement) % @ T=remaining range	±(0.05 + 0.5% of the measurement) m/s
Measurement range	-30 °C to 120 °C	T= -40°C to 100 °C UR= 0 to 100%	0.05 m/s ile 5 m/s From 0 °C to 80 °C
Solution	0.1 °C	0.1 RH	0.01 m/s
Temperature accuracy @20 °C	0.003% / °C	0.02% RH/°C	0.06% /°C
Accuracy after 1 year	0.1 °C / Year	0.1% RH/ Year	0.12 °C / Year
Response Time	15 minutes	15 minutes	

The measurement devices to be permanently installed in the classrooms were compared under identical conditions in a laboratory setting to ensure consistency and reliability. The evaluation of these comparative results is crucial for interpreting the measurement data collected after the fixed installations. The first device was placed in Classroom B-501, the second in Classroom B-502, and the third in Classroom B-503.

To prevent damage to the thermal comfort measurement devices from undesired environmental factors during long-term measurements, protective enclosures were designed. These enclosures were constructed to be disassemblable, allowing easy access to the devices when needed. However, as the protective enclosures could

potentially influence environmental conditions such as indoor air temperature, radiant temperature, air currents, and relative humidity, their impact on measurement results was considered.

The design of the protective enclosures ensured that the dimensions of the perforations would not affect the measurement results while preventing external access to the probes. Furthermore, the frame dimensions of the enclosures were calibrated to maintain adequate distance from the measurement devices, minimizing the influence of environmental factors on the measurements. After the production of the enclosures, the variation in measurement results with and without the enclosures will be analyzed.

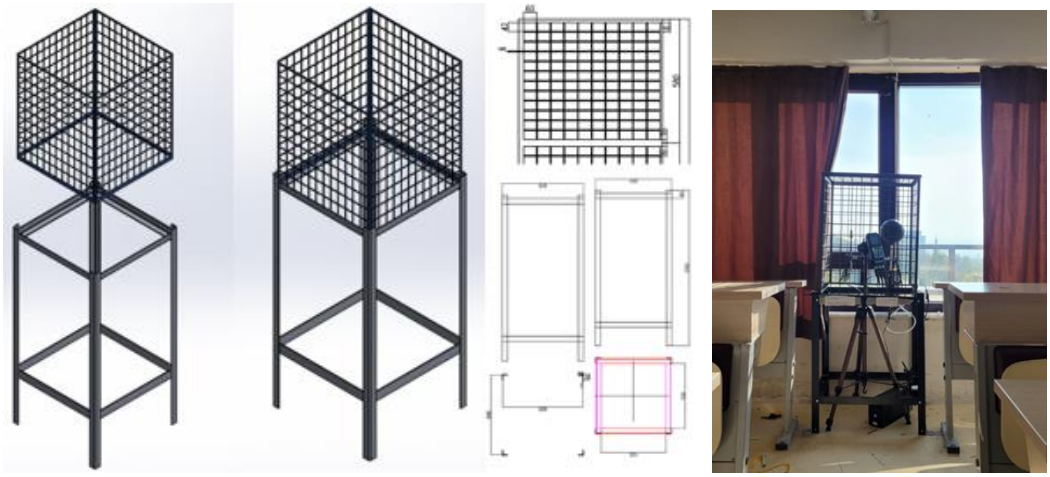

Figure 4.11 Protective enclosures for thermal comfort measurement devices

Additionally, to minimize potential damage caused by electrical system issues during long-term measurements, separate uninterruptible power supply (UPS) devices were procured for each measurement device.

The long-term thermal comfort measurements in the classrooms were conducted at Point 4, as indicated in Figure 4.9. This location was determined based on a joint assessment with an occupational health and safety specialist, considering identified risk factors. To evaluate whether the protective enclosures influenced the measurement results, devices were tested both with and without the enclosures at the designated measurement point.

-Visual Comfort Measurements;

Visual comfort assessments are conducted by determining illuminance levels and verifying them against ranges specified in the standards.

Measurements are planned to be conducted on work planes, with horizontal illuminance measured on desks and vertical illuminance on chalkboard. The grid points for measurements were determined depending on formula given in TS EN 17037:2023 standard and measurement time interval.

The calculations and results for the work plane and the chalkboard plane in the selected rooms are presented below. The grid points derived from these calculations are represented as red dots in the plan view (work plane) and section view (blackboard plane) presented in Figure 4.12.

For the working plane; $p = 0.5 \times 5\log10(8.45)$ p =2.22 (distance according to the number of points is 2.11 and 2.18)

For the chalkboard plane; $p = 0.5 \times 5\log10(5.20)$ p =1.58 (distance according to the number of points is 1.73)

To accurate evaluation is possible with decreasing time interval between measuremnts. So the number of grid points decreased to optimize the measurement process. The Konica Minolta Illuminance Meter was employed to measure illuminance level at each point.

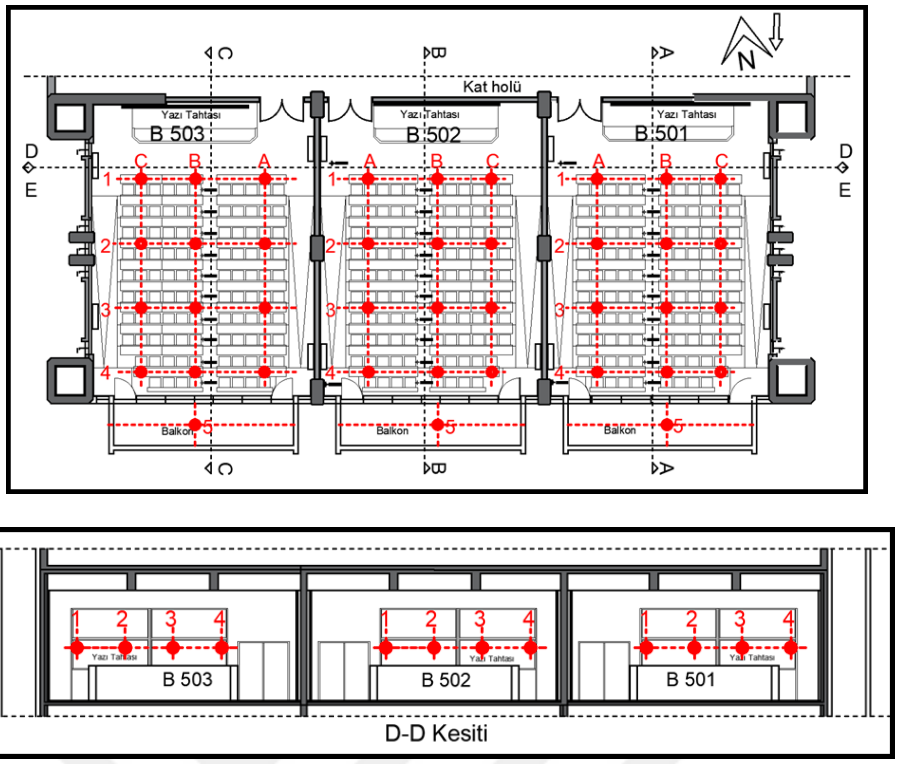

Figure 4.12 Measurement Points for Illuminance Levels in Classrooms and on chalkboard

The Konica Minolta CM 2600d Spectrophotometer was utilized to determine critical factors affecting illuminance, including reflection factor of interior surfaces, light transmission factor of glass.

This comprehensive methodology ensures a robust assessment of visual comfort in classrooms, addressing all critical parameters and aligning with relevant standards to enhance the learning environment.

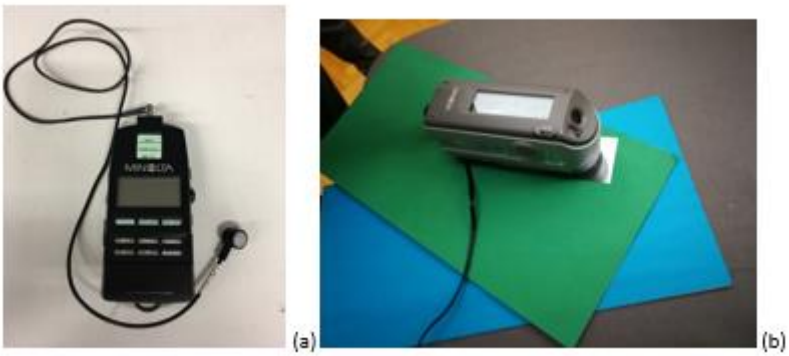

Figure 4.13 (a) Konica Minolta illuminance meter and (b) Konica Minolta Cm 2600d Spectrophotometer

4.1.2.2. Application of Subjective Method (Survey)

Thermal comfort surveys were done in two phases: "before the lesson" and "after the lesson."

The visual comfort survey was administered in a single stage, post-lesson, to ensure accurate evaluation of the environment. The survey forms and questions are provided in the appendix 6, 7 and 8.

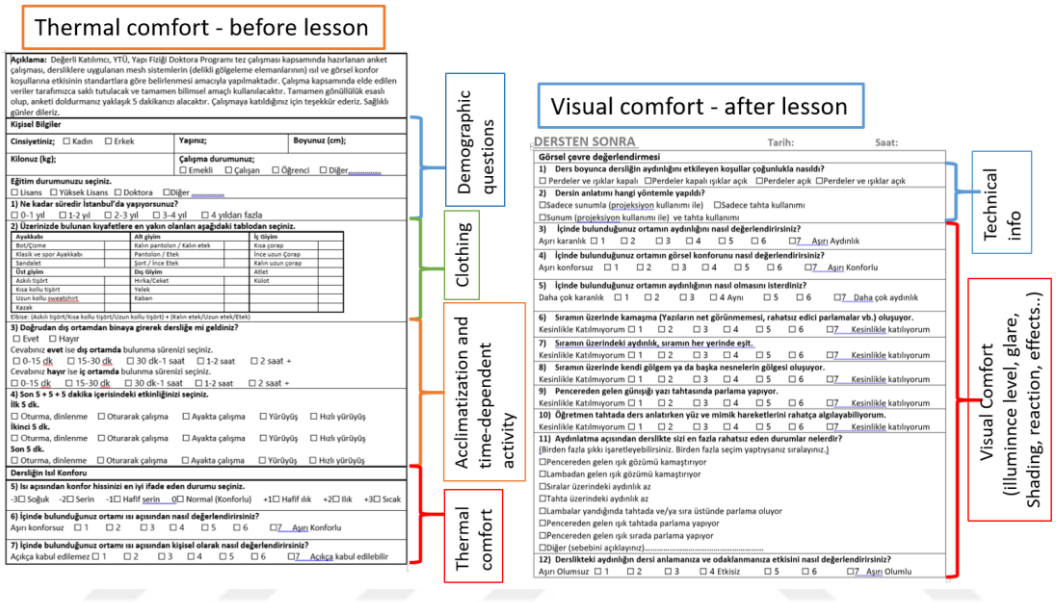

Figure 4.14 Thermal and visual comfort surveys

4.1.3. Conducting Verifications for Measurements and Simulations

Verifications were made for both measurement studies and simulations. The verification for thermal comfort evaluations was examined with a comparison of measurement devices with each other, evaluation of the status of measurement devices within protective enclosures, and comparison of thermal conditions across classrooms. The simulations were verified with thermal and visual comfort measurement results.

4.2. Field Study and Verification Results

4.2.1. Verifications for Measurements

Inıtially, verifications were done for calibration and interrelation of measurement devices, the impact of protective enclosures of measurement devices on thermal

conditions, and the comparison of thermal comfort across classrooms. Measurements were conducted under controlled laboratory and real-world conditions, with statistical analyses focusing on Mean Bias Error (MBE) and R^2 metrics. The results demonstrated high consistency among the measurement devices, confirmed the non-influence of protective enclosures on device performance, and supported reliable inter-classroom comparisons, adhering to ASHRAE Standard 14 guidelines. These findings underscore the reliability and accuracy of the methodologies employed for assessing thermal conditions and device performance.

Calibration and determination of the relationship between devices;

Measurements were conducted at 15-second intervals for a one-hour period in a controlled laboratory environment on September 9, 2021. Device 1 was positioned in classroom B-501, Device 2 in classroom B-502, and Device 3 in classroom B-503.

The measurement outcomes for devices 1 and 2, devices 1 and 3, and devices 2 and 3 were compared. Mean Bias Error (MBE) was calculated for air temperature (Ta), globe thermometer temperature (Tg), and Predicted Mean Vote (PMV) values.

The temperature and PMV measurements obtained from all three devices demonstrated a high degree of similarity. Regarding Tg values, the smallest discrepancy was observed between devices 2 and 3, followed by devices 1 and 2, and finally devices 1 and 3.

The MBE analysis for PMV revealed that the discrepancy between devices 1 and 2 equaled the difference between devices 2 and 3, both of which were smaller than the difference between devices 1 and 3. From the MBE analysis for air temperature, it was evident that there was negligible variation between devices 1 and 2, while the discrepancies between devices 1 and 3, and devices 2 and 3, were relatively similar.

Table 4.9 The mean values and standard deviations of the measurement results obtained under both protected and unprotected conditions for the devices

			Tg (C°)	Ta (C°)	RH (%)	Va (m/s)	PMV	PPD (%)
Protected	**1. device**	**Mean**	**34,20**	**33,41**	**46,50**	**0,009**	**2,83**	**97,99**
		Std. deviation	0,34	0,15	0,52	0,01	0,08	0,80
	2. device	**Mean**	33,88	32,67	47,31	0,023	2,72	96,84
		Std. deviation	0,35	0,11	0,62	0,015	0,08	1,07
Unprotected	**1. device**	**Mean**	**34,74**	**33,76**	**45,93**	**0,018**	**2,96**	**98,90**
		Std. deviation	0,31	0,21	0,39	0,015	0,08	0,36
	2. device	**Mean**	34,56	32,88	46,78	0,025	2,88	98,44
		Std. deviation	0,25	0,11	0,26	0,017	0,06	0,40

Tg: Mean Radiant Temperature, Ta: Air Temperature, RH: Relative Humidity, Va: Air Velocity

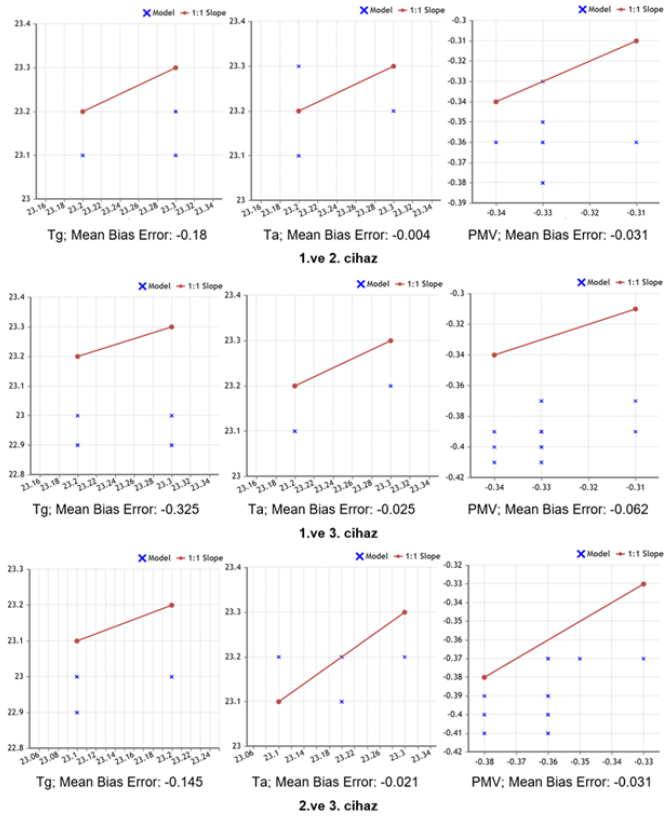

Figure 4.15 Verification of measurement devices (MBE results for PMV, air temperature and globe temperature)

Evaluation of Protective enclosures's Effect;

The impact of protective enclosures measures on thermal conditions was evaluated by calculating MBE for temperature and PMV values using data obtained from measurements conducted on August 19, 2021, under both protected and unprotected conditions.

For Device 1, the standard deviation of temperature measurements was 0.15 under protected conditions and 0.21 under unprotected conditions. The calculated MBE values were 0.158 for temperature and 0.123 for PMV.

For Device 2, the standard deviation for both protected and unprotected conditions was 0.11. The corresponding MBE values were 0.041 for temperature and 0.15 for PMV.

Comparison of thermal conditions across classrooms;

Thermal conditions across classrooms were compared by statistically analyzing PMV values recorded over the week of March 1–7, employing MBE and R^2 as evaluation metrics. According to ASHRAE Standard 14, an MBE value within ±10% is considered acceptable. The proximity of MBE values to ±10% or 0 enhances the reliability of inter-classroom comparisons. Additionally, R^2 values approaching 1 indicate a robust correlation, reflecting a high degree of consistency in the measured values.

The comparative analysis of PMV results yielded the following ranking of classroom relationships, from the strongest to the weakest:

B-502 and B-503 > B-501 and B-503 > B-501 and B-502.

Classroom B-501 exhibited the weakest correlation with the other classrooms, though its relationship with B-503 was stronger than with B-502. Nevertheless, as all MBE values remained within the acceptable limits defined by ASHRAE Standard 14, the comparisons among classrooms were deemed valid and reliable.

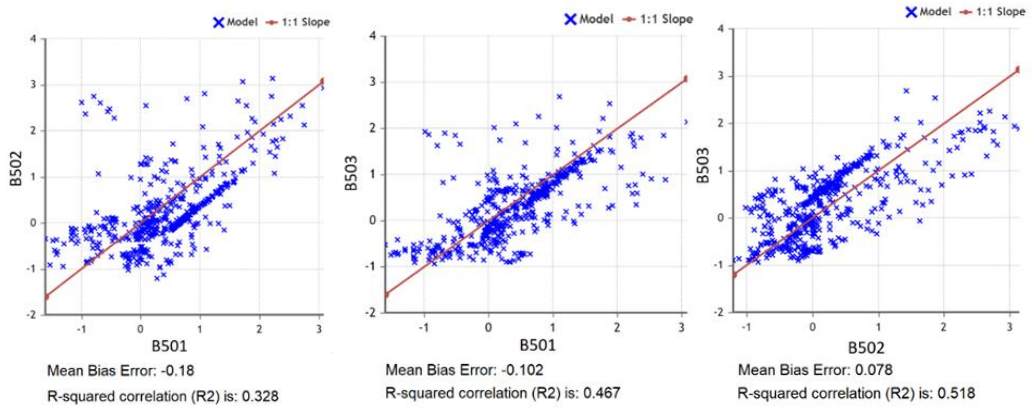

Figure 4.16 Comparison of classrooms

4.2.2. Thermal comfort Measurement and Survey Results

The current conditions of the selected rooms were identified and analyzed through objective (measurements) and subjective (survey) studies to evaluate thermal comfort. Measurements were conducted as long-term and short-term. Long-term measurements commenced on September 16, 2021, while short-term measurements have been regularly conducted since July 12, 2021. The measurement schedule is provided in Figure 4.17. Long-term measurements were conducted exclusively to assess thermal comfort.

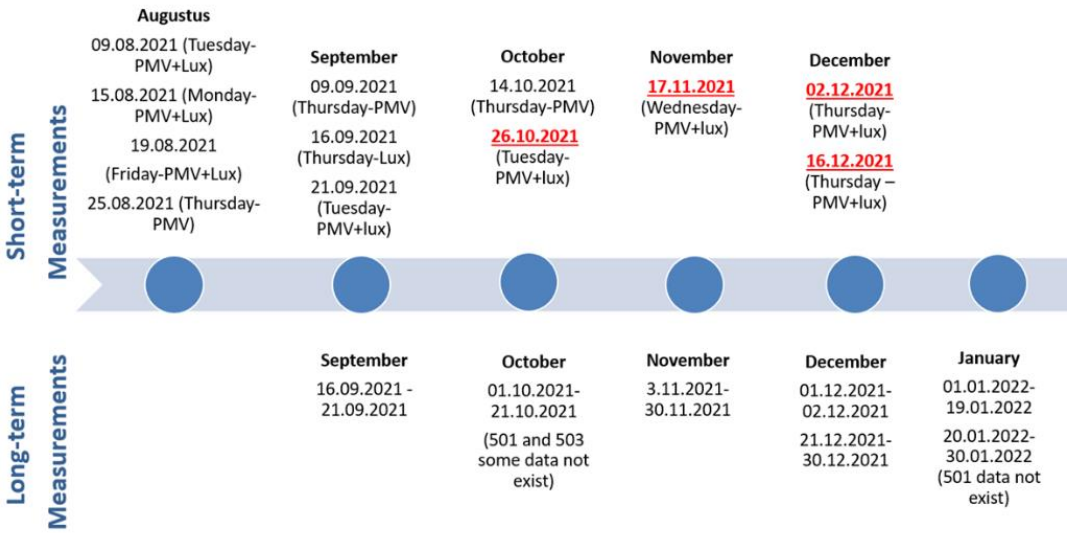

Figure 4.17 Measurement Schedule

4.2.2.1. Thermal comfort measurement results

Both long-term and short-term (instantaneous) thermal comfort measurements were conducted on selected days. Initial short-term measurements in the classrooms were made using the Testo-480 device, until the acquisition of Delta Ohm measurement device. The education period commenced during the week of October 4, 2021. Short-term measurements were conducted on September 21, 2021; October 14, 2021; October 26, 2021; and November 17, 2021. For long-term measurements, weekly data were collected from October 11–15, 2021, and November 15–19, 2021, while monthly measurement results were derived from data spanning November 3–19, 2021. The activity level was standardized at 1.2 met, with clothing insulation levels set to 0.5 clo in September, 0.7 clo in October, and 0.8 clo in November and December.

On October 26, 2021, under clear sky conditions during class hours, short-term measurements were conducted using the Delta Ohm 32.3 device. Results are presented in Figure 4.18. Measurements revealed significant differences in PMV values between Points 1 and 3. Discomfort was observed at Point 3, located near the south-facing window, as indicated by elevated PMV values, whereas Points 1 and 2 remained within the comfort zone.

University classrooms are predominantly designed as lecture halls, including the selected classrooms, which feature a lecture hall seating arrangement with a north-facing viewing direction (Figure 4.5, 4.6 and 4.7). Thermal comfort measurements revealed discomfort in areas near the windows, attributable to the high transparency ratio of the south-facing façades. Due to the volumetric shape of the classrooms and thermophysical principles—where heated air rises and is replaced by cooler air—hot air accumulated near the windows. This phenomenon exacerbated discomfort in these areas, especially during occupancy.



Figure 4.18 Short-term Measurement Results on October 26, 2021 (Mean Radiant Temperature, Air Temperature, Relative Humidity, Air velocity, and PMV)

On November 17, 2021, short-term measurements were conducted during class hours under overcast sky conditions using the Delta Ohm 32.3 device. Figure 4.19 presents the results for that day, while Figure 4.20 shows the long-term measurement results for Classroom B-503. Figure 4.21 illustrates the occupancy of Classroom B-503 between 8:00 AM and 5:00 PM, and Figure 5.22 shows the occupancy of all three classrooms during the same time period.

Classroom usage was assessed based on the percentage of curtain openness, the extent of south-facing window openings relative to balcony door openings, and the number of occupants. Curtain openness was recorded as 0% when fully closed and 100% when fully open. Window openness was noted as 30% for fully open balcony doors and 15% for one open door. The number of people/occupant represents the number of current users in the classroom at the moment.

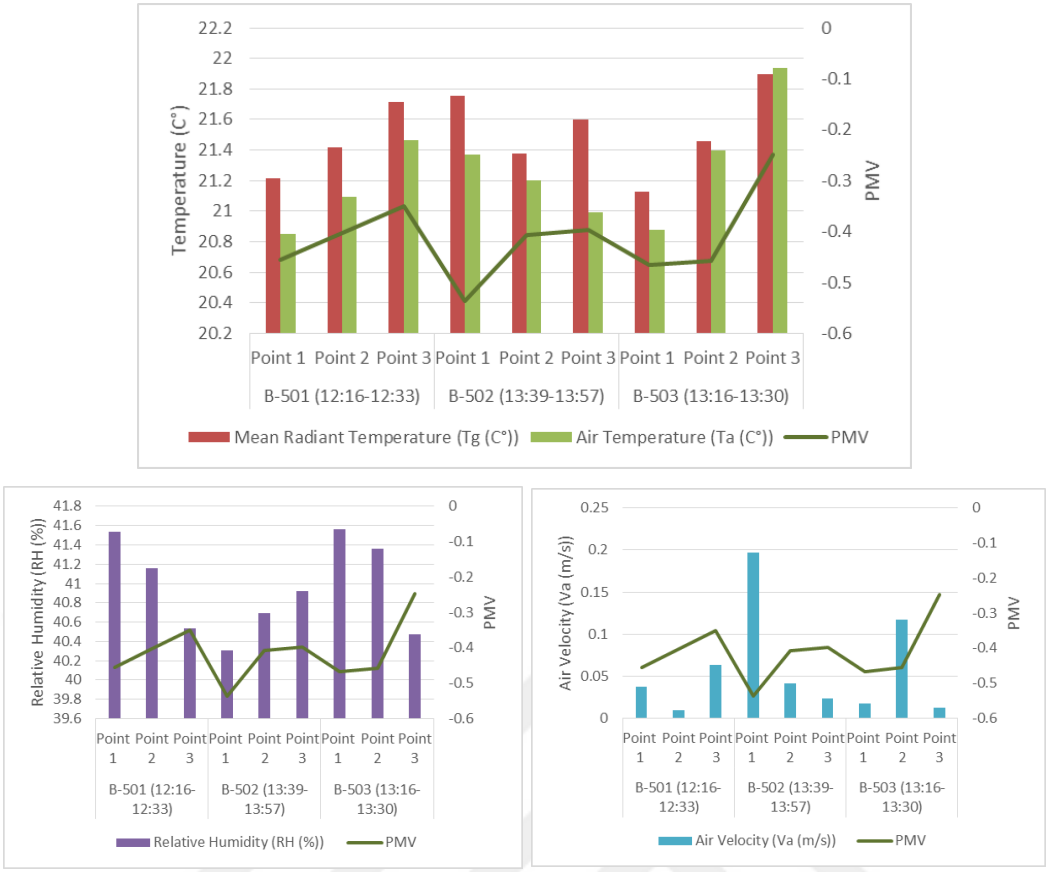

Figure 4.19 Short-term Measurement Results on November 17, 2021 (Mean Radiant Temperature, Air Temperature, Relative Humidity, Air velocity, and PMV)

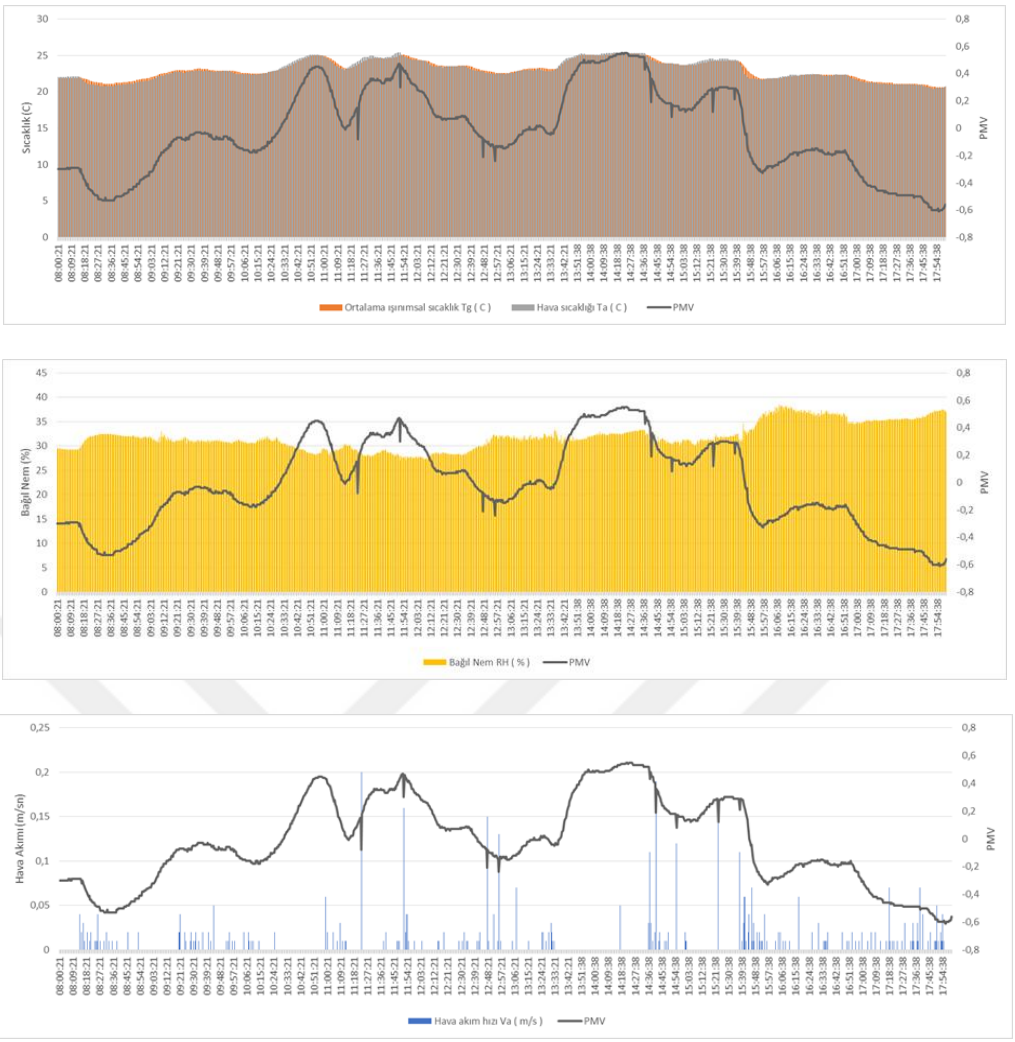

Figure 4.20 Long-term Measurement Results for Classroom B-503 on November 17, 2021 (Mean Radiant Temperature, Air Temperature, Relative Humidity, Air velocity, and PMV)

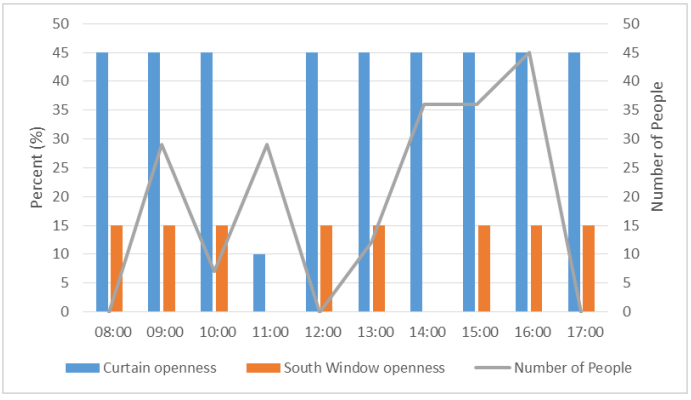

Figure 4.21 Occupancy of Classroom B-503 from 8:00 AM to 5:00 PM on November 17, 2021

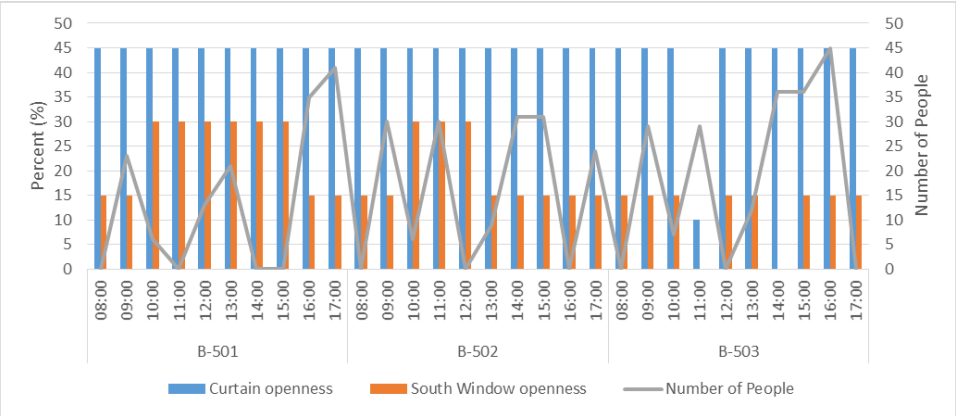

Figure 4.22 Occupancy of All Classrooms from 8:00 AM to 5:00 PM on November 17, 2021

As weekly examples of long-term measurement data, results for November 15–19, 2021 (Figure 4.23) are provided. Data were collected at 9:00 AM, 11:00 AM, 1:00 PM, 3:00 PM, and 5:00 PM for Classrooms B-502 and B-503.

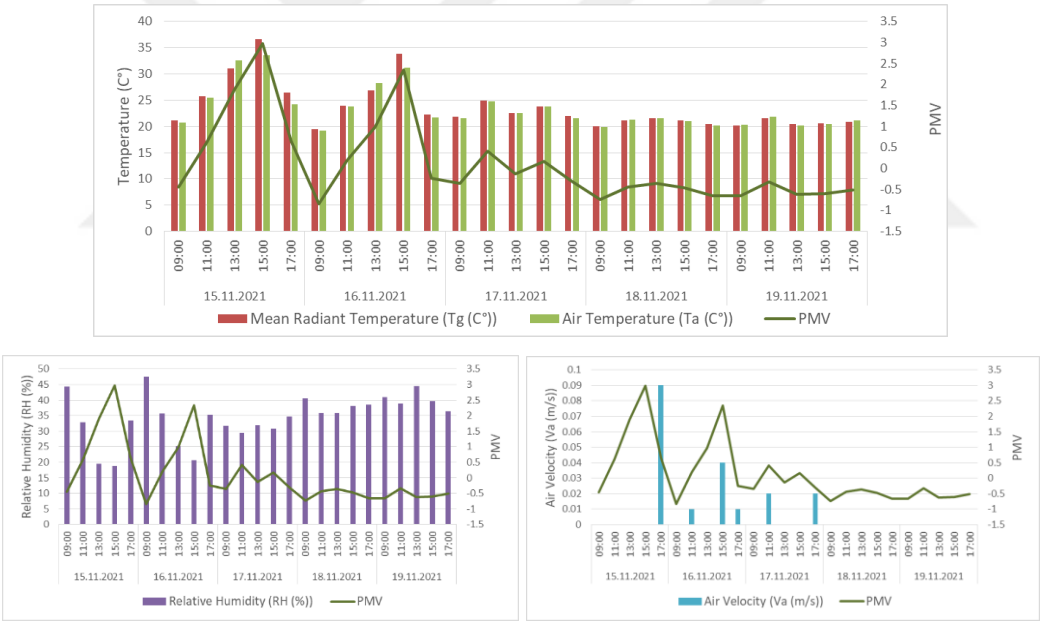

Figure 4.23 Long-term Measurement Results for Classroom B-503 from November 15–19, 2021 (Mean Radiant Temperature, Air Temperature, Relative Humidity, Air velocity, and PMV)

For monthly data, results for November 3–19, 2021 (Figures 4.24, 4.26, 4.28) are presented. These data were collected from three classrooms at 9:00 AM, 11:00 AM, 1:00 PM, 3:00 PM, and 5:00 PM. Additionally, the occupancy of the classrooms on these dates is provided in Figures 4.25 (B-501), 4.27 (B-502), and 4.29 (B-503). As

the classrooms were not in use during weekends, no usage data is available for those period.

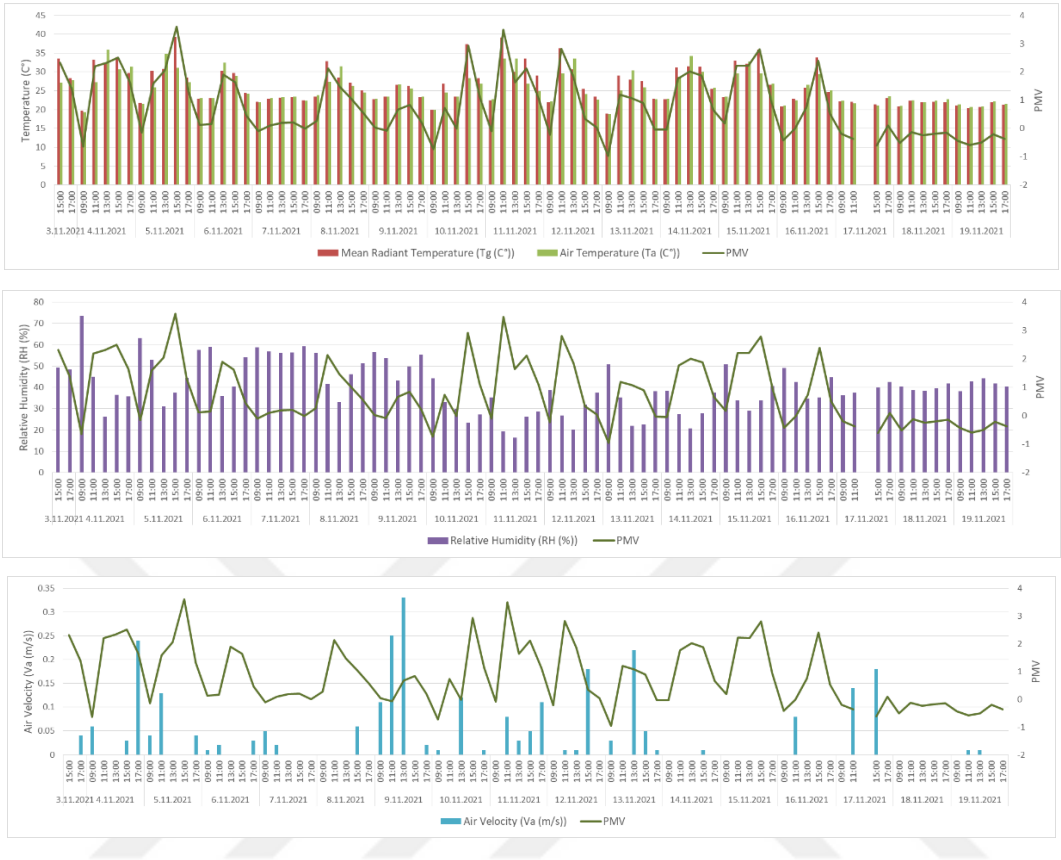

Figure 4.24 Long-term Measurement Results for Classroom B-501 from November 3–19, 2021 (Mean Radiant Temperature, Air Temperature, Relative Humidity, Air velocity, and PMV)

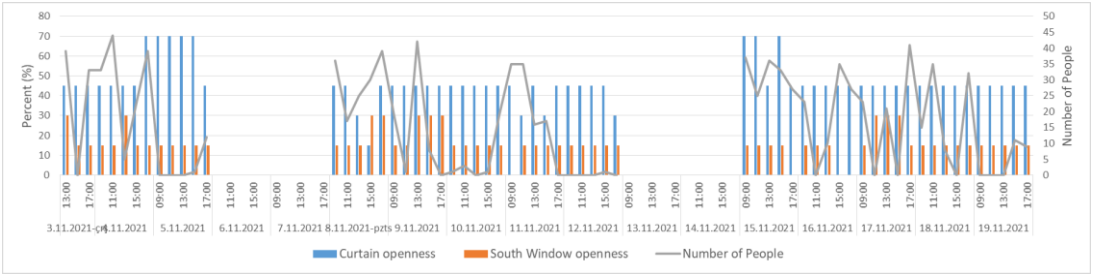

Figure 4.25 Occupancy of Classroom B-501 from 8:00 AM to 5:00 PM between November 3–19, 2021

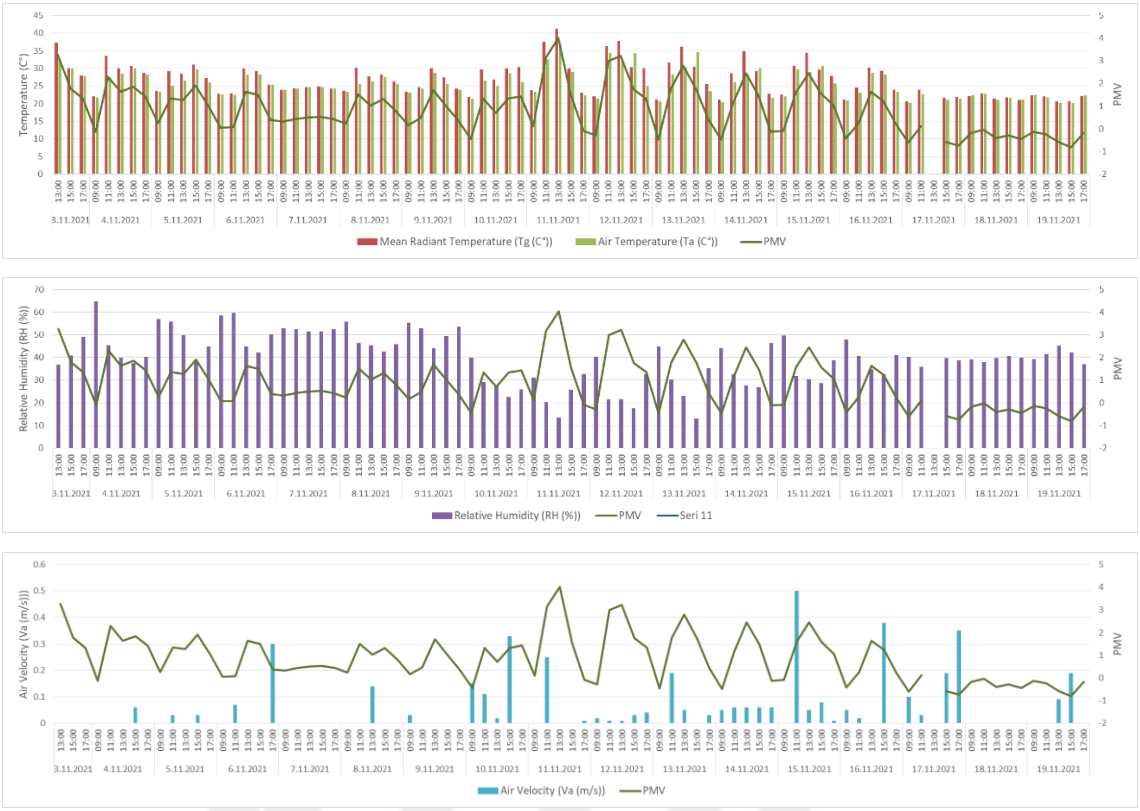

Figure 4.26 Long-term Measurement Results for Classroom B-502 from November 3–19, 2021 (Mean Radiant Temperature, Air Temperature, Relative Humidity, Air velocity, and PMV)

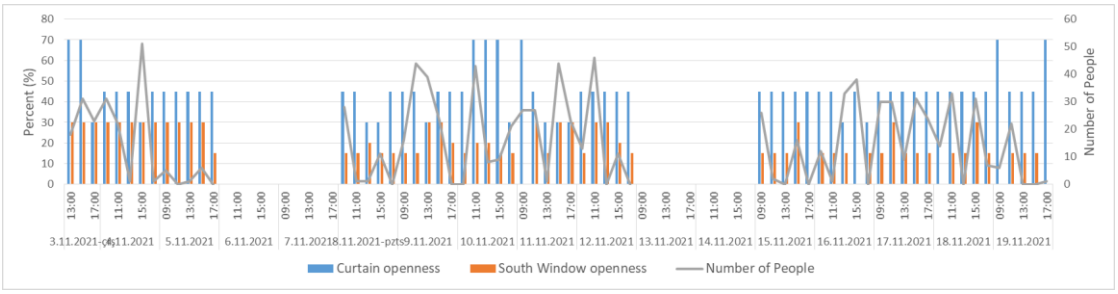

Figure 4.27 Occupancy of Classroom B-502 from 8:00 AM to 5:00 PM between November 3–19, 2021

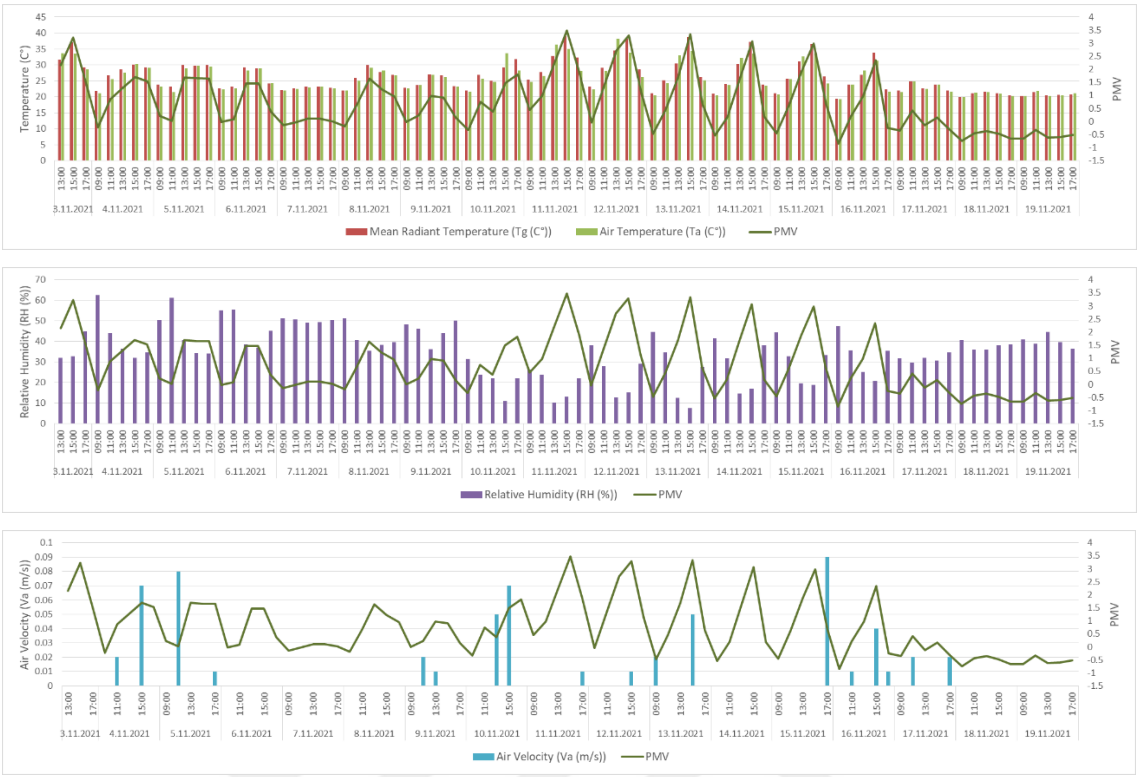

Figure 4.28 Long-term Measurement Results for Classroom B-503 from November 3–19, 2021 (Mean Radiant Temperature, Air Temperature, Relative Humidity, Air velocity, and PMV)

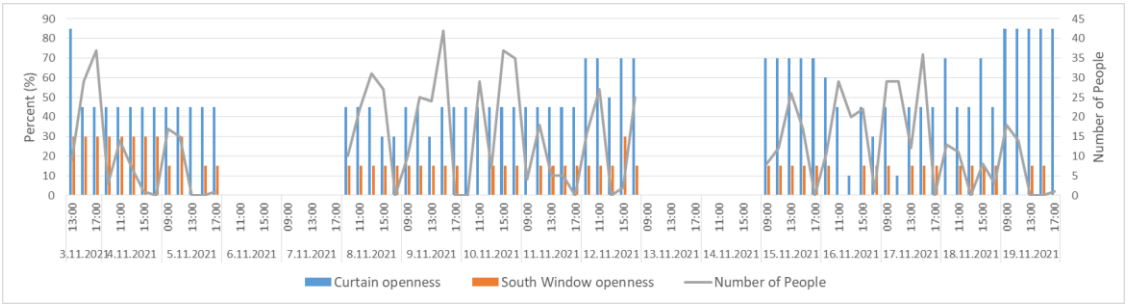

Figure 4.29 Occupancy of Classroom B-503 from 8:00 AM to 5:00 PM between November 3–19, 2021

4.2.2.2. Thermal comfort survey results

Surveys conducted as part of the field study were administered on October 26, 2021; November 17, 2021; December 1, 2021; and December 16, 2021. For analysis purposes, the results from the survey conducted on November 17, 2021, were utilized. Since the surveys were administered concurrently with the measurements, they were distributed to students before class and collected immediately after the lesson.

Survey responses were analyzed using frequency analysis to determine the percentage distribution of answers for each question (Table 4.10). Additionally, linear regression analysis was performed to identify relationships between survey questions and to explore potential correlations.

Table 4.10 Results of the Thermal Comfort Survey Conducted in Classrooms on November 17, 2021 (Results are presented as percentage values (%))

Before Lesson							
Question 5 (Thermal Sensation)	**Hot (+3)**	**Warm (+2)**	**Slightly Warm (+1)**	**Neutral (± 0)**	**Slightly Cool (-1)**	**Cool (-2)**	**Cold (-3)**
	4,2		16,7	50	25	4,2	
Question 6	**Extremely Uncomfortable-1**	**2**	**3**	**4**	**5**	**6**	**Extremely Comfortable-7**
			16,7	29,2	25	20,8	8,3
Question 7	**Clearly Unacceptable-1**	**2**	**3**	**4**	**5**	**6**	**Clearly Acceptable-7**
			12,5	16,7	16,7	33,3	20,8
After Lesson							
Question 6 (Thermal Sensation)	**Hot (+3)**	**Warm (+2)**	**Slightly Warm (+1)**	**Neutral (± 0)**	**Slightly Cool (-1)**	**Cool (-2)**	**Cold (-3)**
		4,2	16,7	45,8	25	8,3	
Question 7	**Extremely Uncomfortable-1**	**2**	**3**	**4**	**5**	**6**	**Extremely Comfortable-7**
			16,7	25	33,3	25	
Question 8	**Clearly Unacceptable-1**	**2**	**3**	**4**	**5**	**6**	**Clearly Acceptable-7**
		4,3	13	13	30,4	30,4	8,7

Table 4.10 Results of the Thermal Comfort Survey Conducted in Classrooms on November 17, 2021 (Results are presented as percentage values (%))

(Continued…)

After Lesson							
Question 9 (Solar Radiation from Window)	**Strongly Disagree -1**	**2**	**3**	**4**	**5**	**6**	**Strongly Agree-7**
	25	29,2	8,3	25	4,2		8,3
Question 10	**Much Cooler-1**	**2**	**3**	**4**	**5**	**6**	**Much Warmer-7**
		4,2	12,5	45,8	29,2	4,2	4,2
Question 13 (Understanding of Lesson)	**Extremely Negative -1**	**2**	**3**	**4**	**5**	**6**	**Extremely Positive-7**
			29,2	20,8	29,2	16,7	4,2

An analysis of the relationship between students' thermal sensations and their seating location revealed that individuals seated closer to the south-facing window reported feeling warmer compared to those seated farther away (Figure 4.30).

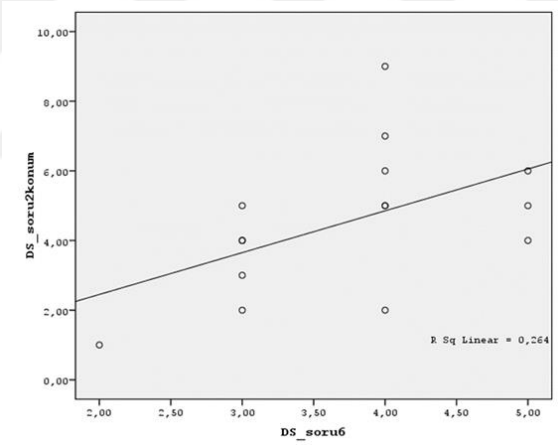

Figure 4.30 Linear Regression Graph of Thermal Sensation Based on Location

Furthermore, responses to Question 9, which assessed whether sunlight entering through the window caused discomfort, revealed that students who reported experiencing discomfort were predominantly seated near the south-facing window. This relationship is depicted in Figure 4.31.

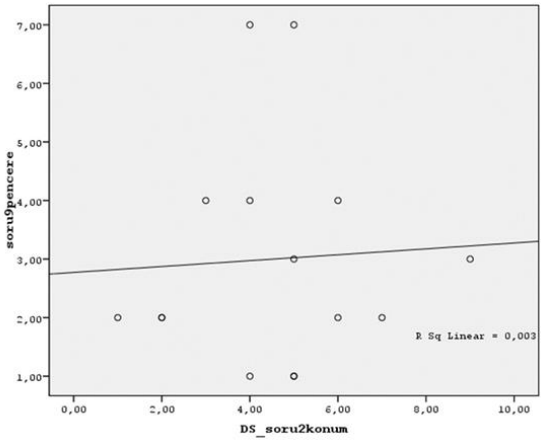

Figure 4.31 Linear Regression Graph Assessing the Impact of Solar Radiation from the Window Based on Location

4.2.3. Visual comfort Measurement and Survey Results

4.2.3.1. Visual Comfort Measurement Results

Illuminance level measurements were conducted to evaluate the visual comfort conditions. On August 3, 2021, the illuminance levels in the classrooms were measured under varying conditions, including whether the curtains were open or closed and whether the classrooms were occupied (Figure 4.32).

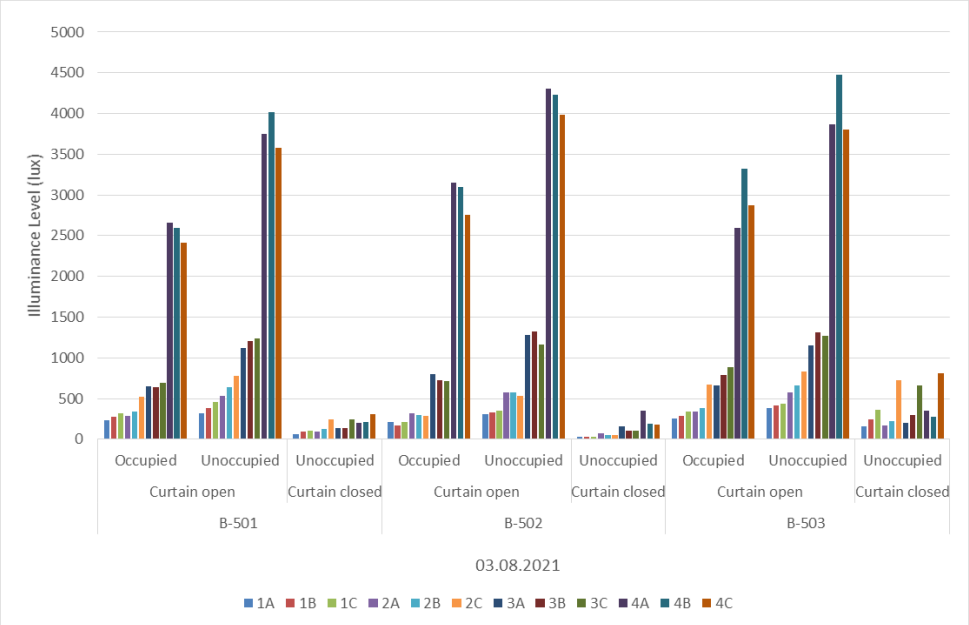

Figure 4.32 Results of the illuminance level measurement conducted on August 3, 2021 (external horizontal illuminance: 94,500 lux).

Simultaneous illuminance measurements were taken on the same days as thermal comfort measurements. The results from measurements conducted on September 21, 2021, October 26, 2021, and November 17, 2021, are presented in Figures 4.33, 4.34, and 4.35, respectively. These measurements were conducted in unoccupied classrooms.

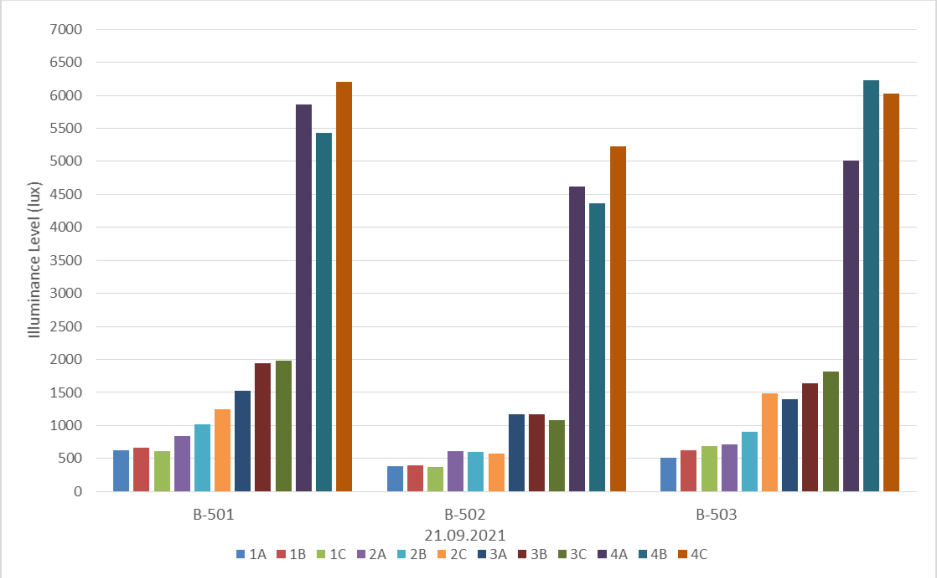

Figure 4.33 Results of the illuminance level measurement conducted on September 21, 2021 (external horizontal illuminance: 60,000 lux)

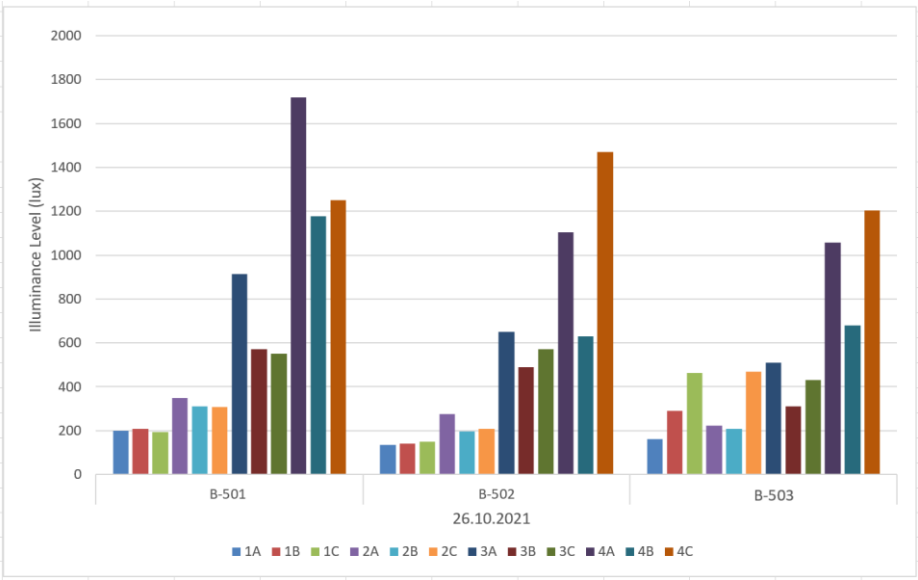

Figure 4.34. Results of the illuminance level measurement conducted on October 26, 2021 (external horizontal illuminance: 26,000 lux)

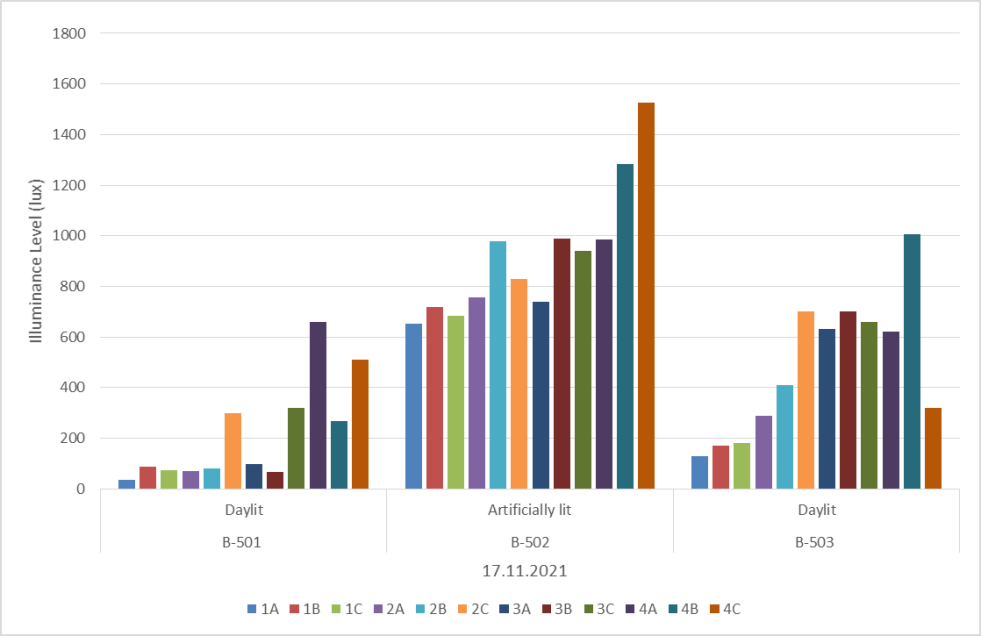

Figure 4.35 Results of the illuminance level measurement conducted on November 17, 2021 (external horizontal illuminance: 15,000 lux)

Periodic illuminance measurements were carried out on specific dates since August, and the results are provided in Figures 4.36 and 437. The external horizontal illuminance levels at the time of the measurements were recorded as 94500 lux on 03.08.2021, more than 100000 lux on 09.08.2021, 98000 lux on 13.08.2021, 88000 on 16.09.2021, 60000 lux on 21.09.2021, 26000 lux on 26.10.2021 and 15000 lux on 17.11.2021. The results of the illuminance measurements with the curtains open are shown in Figure 4.36, while the measurements with the curtains closed are displayed in Figure 4.37.

Similarly, visual comfort measurements indicated excessive illumination on the working planes near the windows, reaching levels that could cause discomfort. These findings demonstrated that the selected classrooms were suitable for the implementation of PSSs to improve thermal and visual comfort conditions.



Figure 4.36 Illuminance level measurements in classrooms with curtains open on the specified dates.

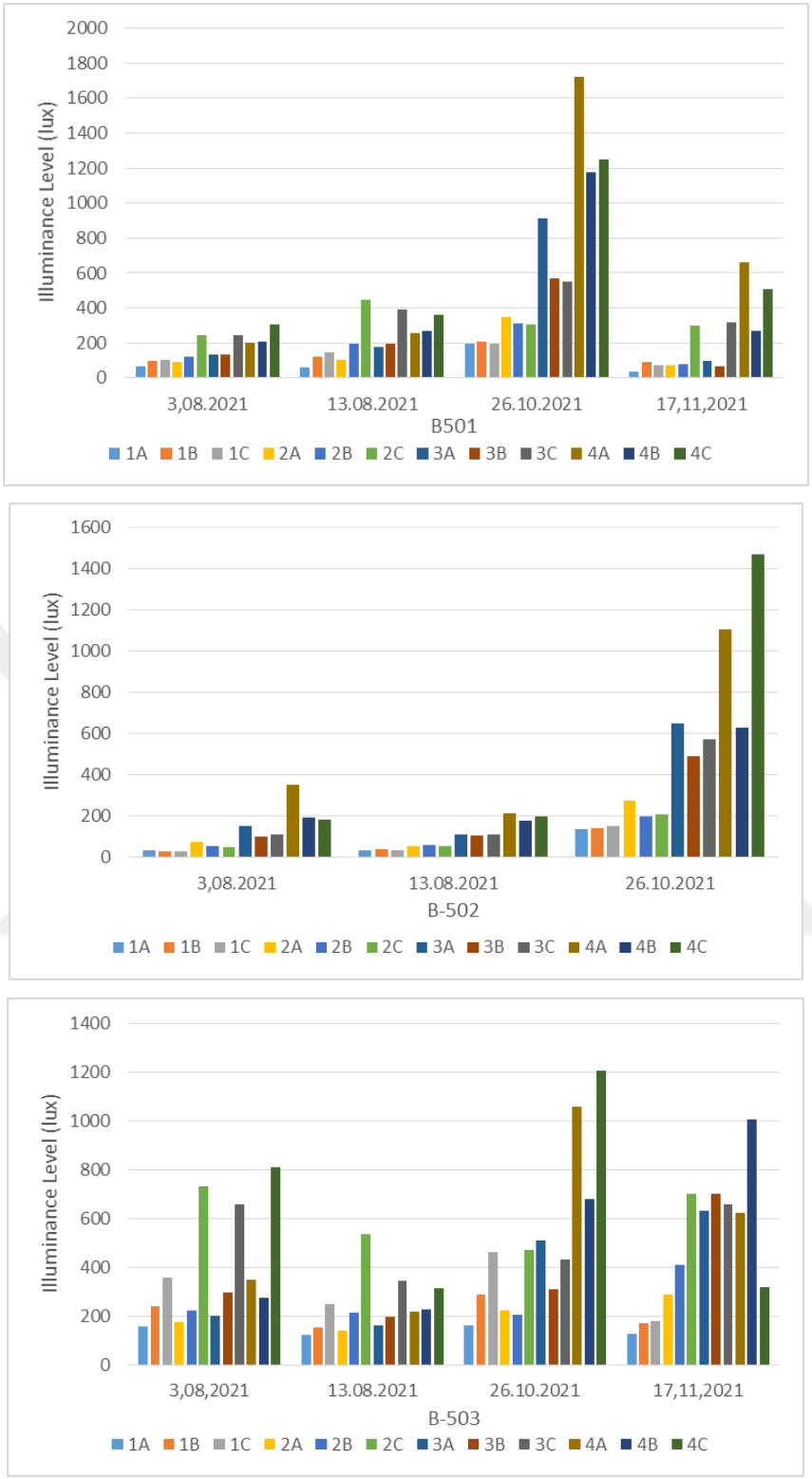

Figure 4.37 Illuminance level measurements in classrooms with curtains closed on the specified dates.

4.2.3.2. Visual Comfort Survey Results

The survey results related to visual comfort were analyzed using frequency analysis, determining the percentage of responses for each question (Table 4.11). Additionally, linear regression analysis was performed to examine the relationships between survey questions and explore potential correlations.

Table 4.11 Visual comfort survey results conducted on November 17, 2021 (expressed as percentages (%))

Question number	**Extremely Dark – Uncomfortable – Strongly Disagree -1**	**2**	**3**	**4**	**5**	**6**	**Extremely Bright – Comfortable – Strongly Agree -7**
3			8,7	8,7	47,8	34,8	
4		8,7	21,7	17,4	34,8	13	4,3
5		4,3	17,4	52,2	4,3	21,7	
6	9,1	27,3	18,2	13,6	18,2	9,1	4,5
7	4,3	4,3	26,1	8,7	21,7	13	21,7
8	17,4	13	34,8	4,3	13	13	4,3
9	17,4	13	4,3	13	17,4	13	21,7
10	4,3	17,4	4,3		8,7	13	52,2
12		13,6	22,7	13,6	31,8	9,1	9,1

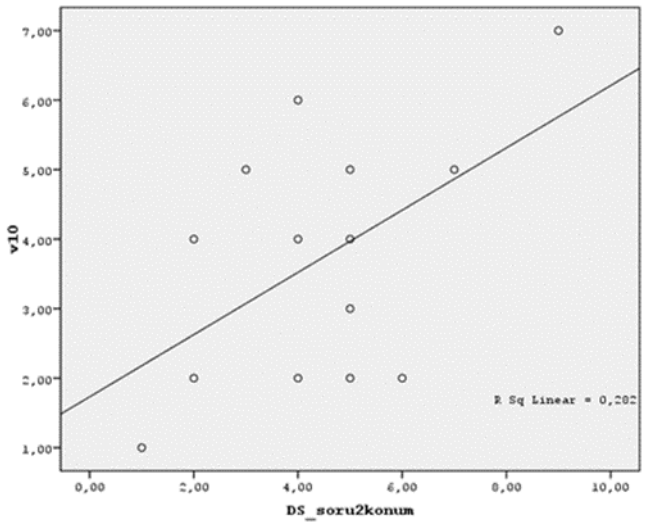

Figure 4.38 Linear regression graph illustrating the relationship between glare on the desks and student location.

To examine the relationship between responses to the question regarding glare on the desks and student location, linear regression analysis was performed for the location question and the sixth question from the visual comfort survey. The

analysis revealed that students who reported experiencing glare were seated near the south-facing window (Figure 4.38).

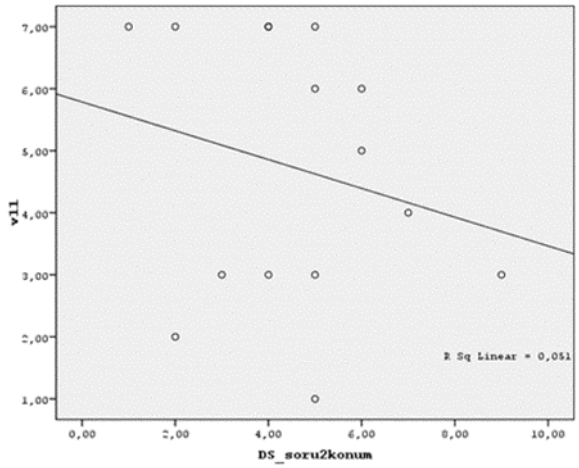

Figure 4.39 Linear regression graph of illuminance distribution uniformity on desks based on student location.

To explore the relationship between responses to the question regarding the uniformity of illuminance distribution on desks and student location, linear regression analysis was conducted for the location question and Question 7 from the visual comfort survey. The results indicated that students who perceived the illuminance distribution on their desks as even were those seated closer to the board (Figure 4.39).

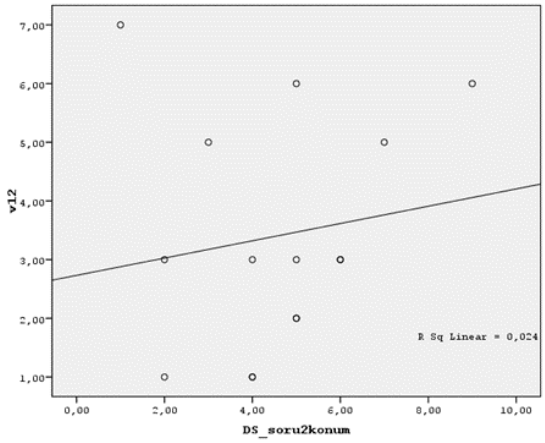

Figure 4.40 Linear regression graph illustrating shadow formation on desks based on student location

To investigate the relationship between responses regarding shadow formation on desks and student location, linear regression analysis was performed for the location question and Question 8 from the visual comfort survey. The findings indicated that students who reported experiencing shadow formation on their desks were seated near the south-facing windows (Figure 4.40).

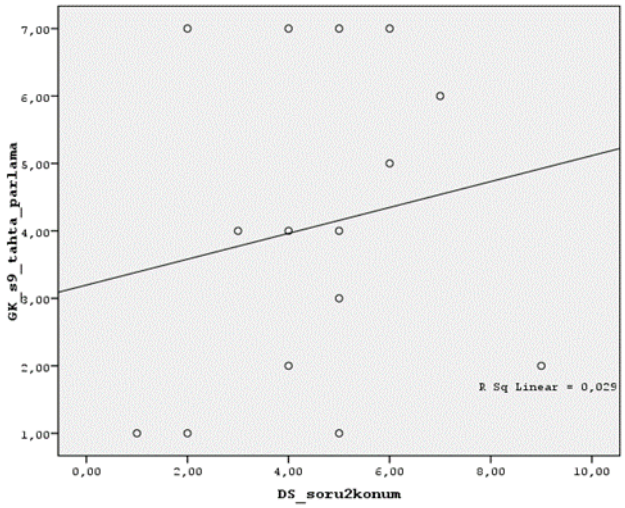

Figure 4.41 Linear regression graph of the effect of sunlight on glare on the board based on student location

Finally, to examine the relationship between responses regarding the effect of sunlight on glare on the board and student location, linear regression analysis was conducted for the Question 8 and the location question. The analysis revealed that students who reported that sunlight entering through the window caused glare on the board were seated near the south-facing windows (Figure 4.41).

4.2.4. Verification Results for Simulations

To optimize PSSs designed for existing classrooms in accordance with thermal and visual comfort requirements, initially simulations were verified against on-site measurements. The measurement results were compared with the simulation outcomes to verify the reliability of the simulation framework prior to optimization. The regression analyses demonstrate a high degree of agreement between measured and simulated values. For air temperature, the correlation reached an R^2 of 0.97, confirming the accuracy of thermal predictions. Similarly, PMV results yielded an

R^2 of 0.92, indicating that the model successfully replicated thermal comfort trends observed on-site. The illuminance level comparison showed an even stronger agreement, with an R^2 of 0.97, verifying the accuracy of daylight simulations.

These results (Figure 4.42–4.45) confirm that the simulation program provides consistent outputs aligned with field measurements across both thermal and visual parameters. These verification steps ensure that the optimization of PSSs is based on robust, context-specific input data, and that subsequent design evaluations can be regarded as reliable.

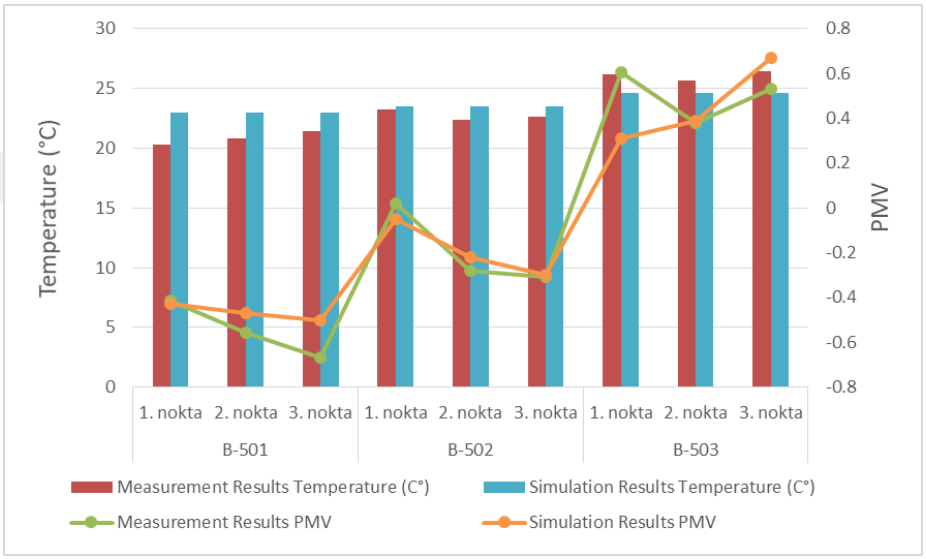

Figure 4.42 Measurements and Simulation results for air temperature and PMV

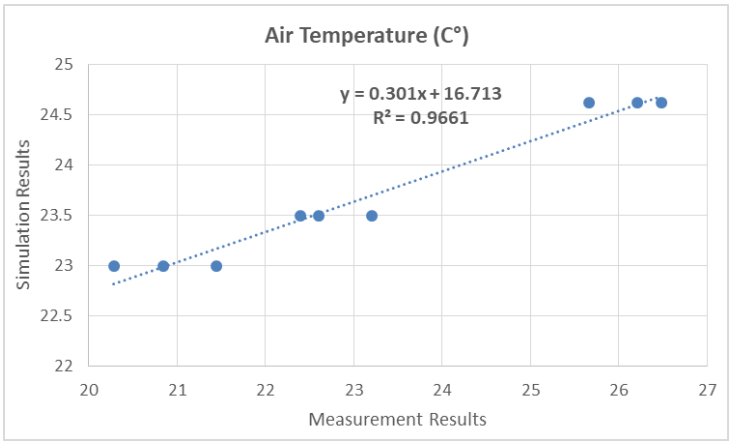

Figure 4.43 Regression for air temperature (Date/Period: 24.02.2021 / 14.30-17.00 - (for each classroom for three points (total 9 points))

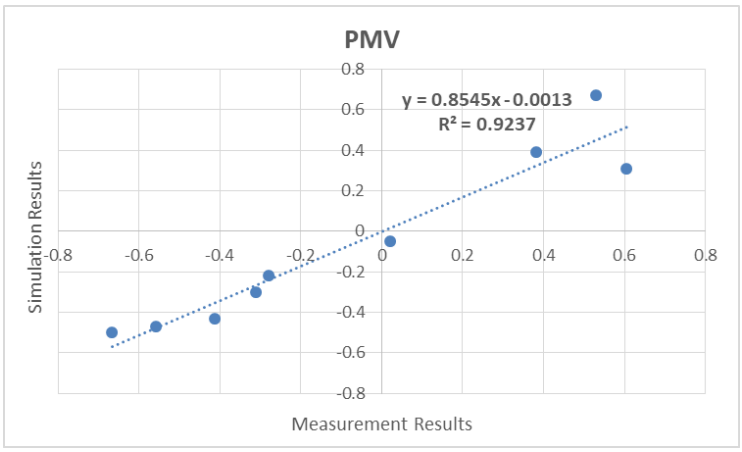

Figure 4.44 Regression for PMV (Date/Period: 24.02.2021 / 14.30-17.00 - (for each classroom each three points (total 9 points))

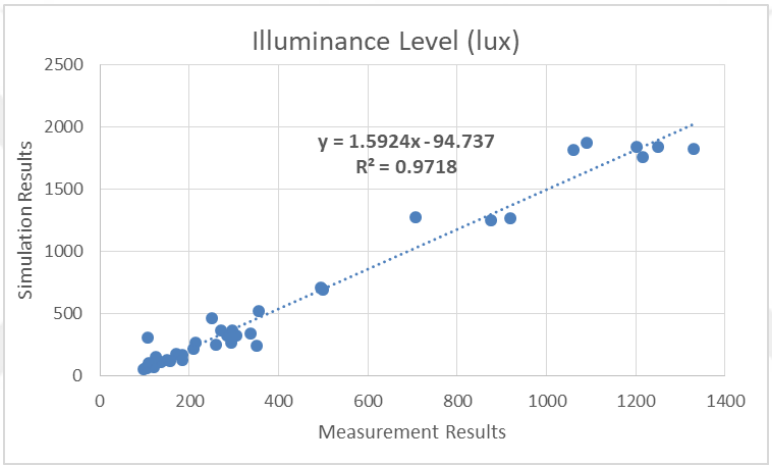

Figure 4.45 Regression for illuminance level (Date/Period: 24.02.2021 / 12.20-15.40 - (for each classroom for 12 points (total 36 points))

4.3. Designing of Perforated Solar Screens (PSS) for classrooms

In this study, the PSSs were designed with an angled configuration, differing from previous designs and those proposed in the literature. Given that the design is angled, the determination of design parameters is constrained by existing studies and catalogs. It is essential to consider the manufacturability of these design parameters based on the angle and establish feasible limits for the angle parameter within the scope of production capabilities. The optimization process, conducted in two stages, results in changes to the value ranges of the design parameters.

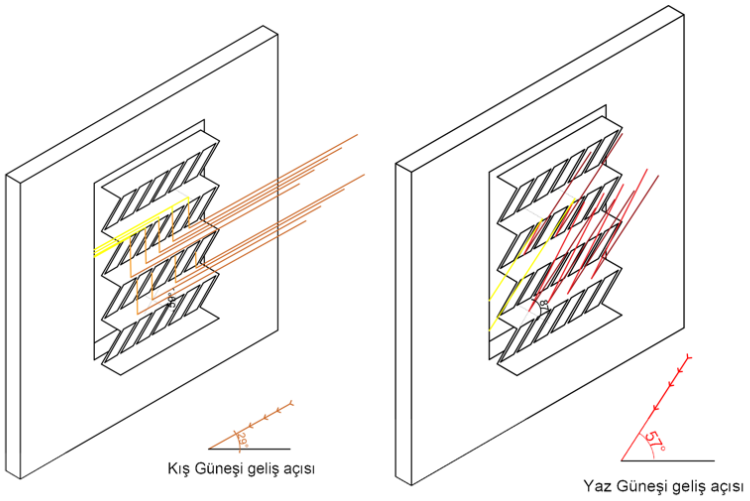

Figure 4.46 Example of the designed PSS based on solar angles

The designed PSS is illustrated in Figure 4.46, 4.47 and 4.48, based on the solar radiation angles reaching the southern side according to latitude for the Northern Hemisphere, as provided in Table 4.12.

Table 4.12 Solar radiation angles reaching the southern side according to latitude for the Northern Hemisphere (N. Lechner, 2001)

L°	24	25	26	27	28	29	30	31	32	33	34	35	36	37	38	39	40	41	42	43	44	45
X°	74	73	72	71	70	69	68	67	65.5	64.5	63.5	62.5	60.5	59.5	59	58.5	58	57	56	55	54	53
Y°	46	45	44	43	42	41	40	39	37.5	37.5	35.5	34.5	32.5	31.5	31	30.5	30	29	28	27	26	25

Where, L° represents the Earth's latitude on the Northern Hemisphere, X° the summer angle measured from the window sill to the sun's altitude and Y° the winter angle measured from the window head to the sun's altitude [40,41].

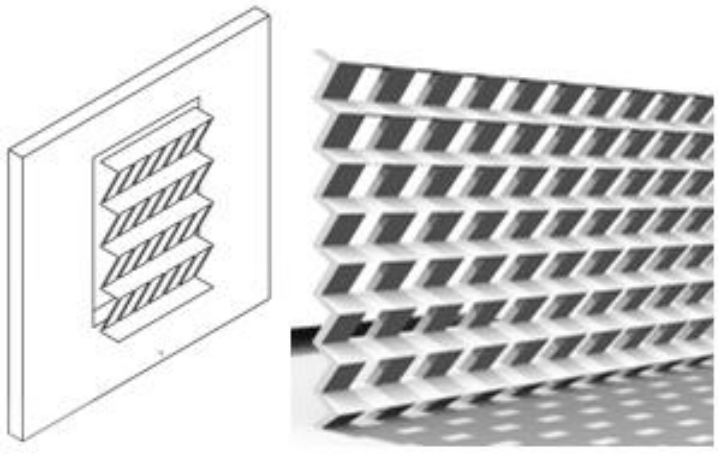

Figure 4.47 3D model of the designed PSS and its variable design parameters

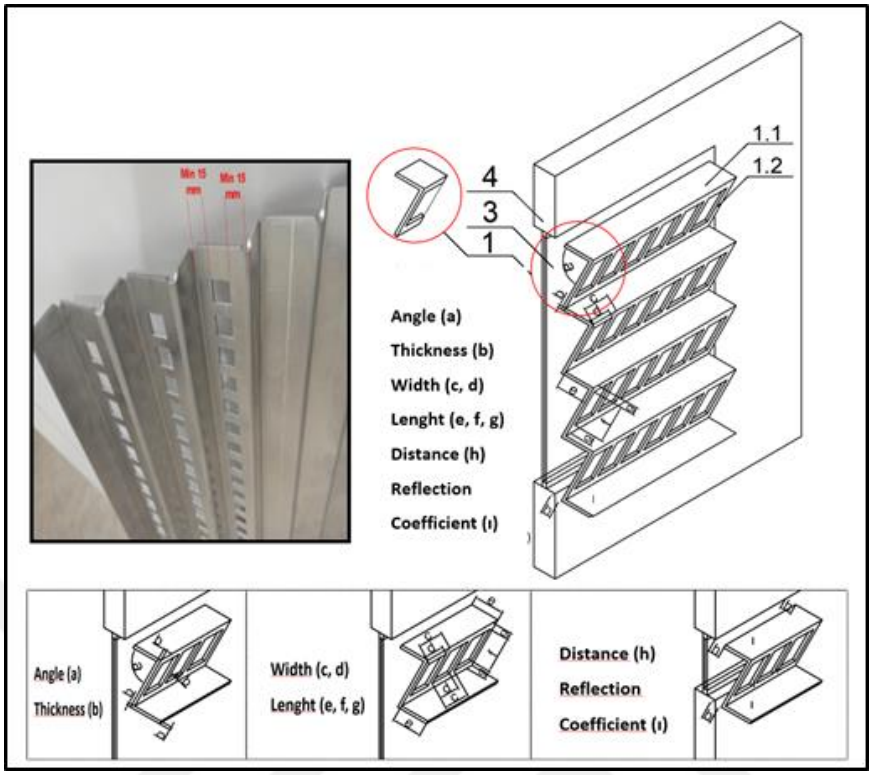

Figure 4.48 Representation of the basic design principle of the designed PSS according to solar radiation (a) and design parameters (b)

To assess the manufacturability of the optimized PSS, these design parameters were reviewed in collaboration with experts at Çuhadaroğlu Aluminum Industry and Trade Inc. Based on these discussions and prior research, the appropriate ranges for the design parameters were established. Samples were sourced from the company, and the reflection factors of these samples were measured. The reflection coefficient values used for optimization were selected based on these measurements.

The color schemes and reflection coefficient ranges of the samples were examined. As shown in Appendix 6, the reflectance factors were not organized in a specific order. For optimization, an evaluation was conducted considering both the color characteristics and the reflection coefficient values. It was determined that materials with yellow (Y) in the Munsell color system exhibited a consistent reflection coefficient order. The reflectance factors of these samples, highlighted in red in

Appendix 6, are approximately 0.47, 0.67, and 0.77. These values were selected as design parameters for the optimization process.

Table 4.13 The colorimetric measurements and reflection coefficient of the samples

Colorimetric measurements		**Yxy**		**Munsell**	
Standard illuminant		**C**		**C**	
View angle		**2°**		**2°**	
Sample picture	**Sample code**	**SCI**	**SCE**	**SCI**	**SCE**
	ALU-SAN 9010 C2 İBA 03.12.2019	81.4	78.78	2.3 Y	2.3 Y
		0.32	0.32	9.1	9
		0.33	0.33	1.1	1.1
	7044 PULLER Kalınlık=103nm parlaklık=40gloss	48.17	45.59	6.4 Y	6.4 Y
		0.32	0.32	7.3	7.2
		0.32	0.33	0.7	0.7
	Yellow 5478 PE70 gloss 1084016/1 Lab Up-1070-05478-T	68.95	64.99	4.9 Y	5.0 Y
		0.32	0.33	8.5	8.3
		0.34	0.34	1.4	1.5

Following the first optimization, the value ranges of the design parameters were adjusted for the second optimization, as presented in Table 4.14. The maximum and minimum values of the design parameters from the first optimization were used to revise the ranges for the second optimization. The design parameters for thickness (b) and additional area (g) were excluded from the optimizations. Including the thickness (b) would significantly increase the calculation time for daylight analysis, from approximately 80 seconds to 12,000 seconds. Consequently, calculations involving thickness variations were only considered for the most optimal solutions identified during the optimization process. The additional area (g) was determined based on manufacturability, as assessed in collaboration with the production team, and it was finalized after evaluating the sample for production feasibility.

Table 4.14 Perforated solar screen (PSS) design variables

Variables	1.Optimization Possible Values	2.Optimization Possible Values	Units
Angle (a)	0- 180 (5° interval)	20-35 (5° interval)	**Degree (°)**
Full + empty area width (c)	0,02 - 0,10	0,06 – 0,1	**Meter (m)**
Empty area width (d)	0,01 - 0,09	0,04 – 0,09	**Meter (m)**
Full area width (e)	0,02-0,10	0,07 – 0,1	**Meter (m)**
Empty area length (f)	0,02-0,10	0,07 – 0,1	**Meter (m)**
Distance from facade (h)	0,02 - 0,15	0,04 – 0,1	**Meter (m)**
Reflection coefficient (ı)	0.47, 0.67,0.77	0.47, 0.67,0.77	**coefficient**
Variables	**Calculation Values**		**Units**
Thickness (b)	0,001-0,003	0,001-0,003	**Meter (m)**
Additional space (g)	0,015		**Meter (m)**

The design parameter value ranges were adjusted in the second optimization based on the results obtained from the first optimization. In the results of the first optimization, the maximum and minimum values for the design parameter ranges of PSSs, recommended as optimal, were determined. Subsequently, these value ranges were modified for the second optimization.

The thickness (b) was excluded from the optimization process. Although we narrowed the range of variables, computational efficiency remained significantly high. Therefore, after the first stage optimization, simulations were done to calculate the PMV values of optimal solutions.

One of the primary objectives of the design is to enhance thermal and visual comfort conditions by reducing direct solar radiation and increasing indirect solar radiation during the cooling period. Therefore, the variables defined in the design must be re-optimized for each room where the design will be applied, in order to achieve the best possible indoor thermal and visual comfort conditions. Design variations can be created by altering the length, angle, and factor values of any, some, or all of the variables.

Table 4.15 3D Model examples of the designed PSSs

Date	Time	Position of the Sun	Perforation Ratio	Thickness	Model
21.12.2020	16.00	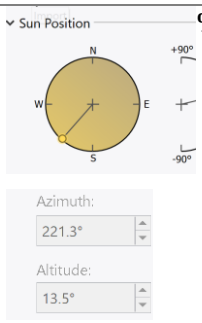	%50	0,2	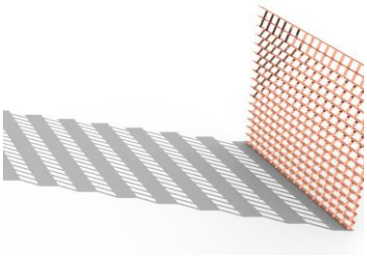
21.06.2020	16.00	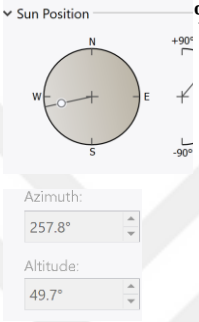	%50	0,2	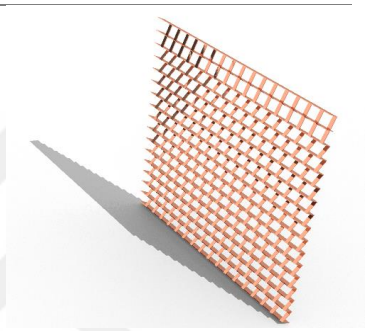
21.03.2020	16.00	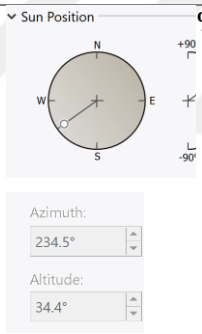	%50	0,2	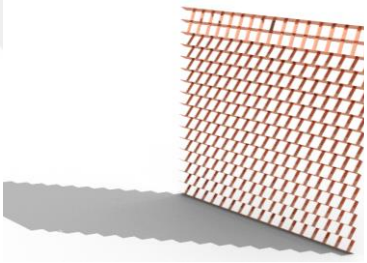

Table 4.16 Examples of design versions dependent on the angle variable (with other variables held constant)

Angle	20°	60°	100°	140°	180°
3D Model from outside	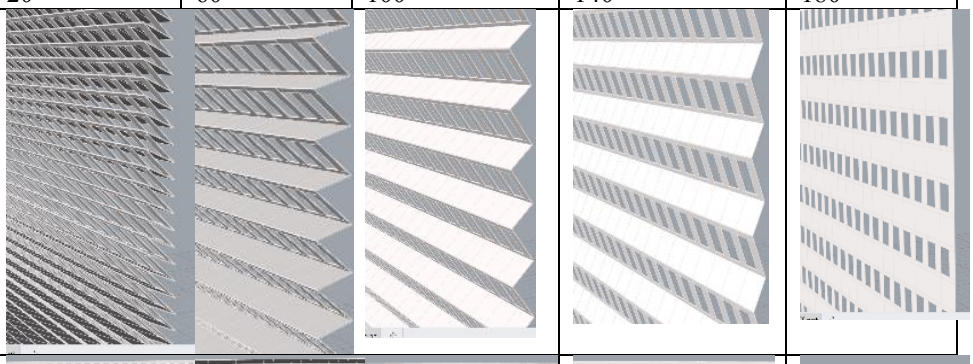				
3D Model form inside	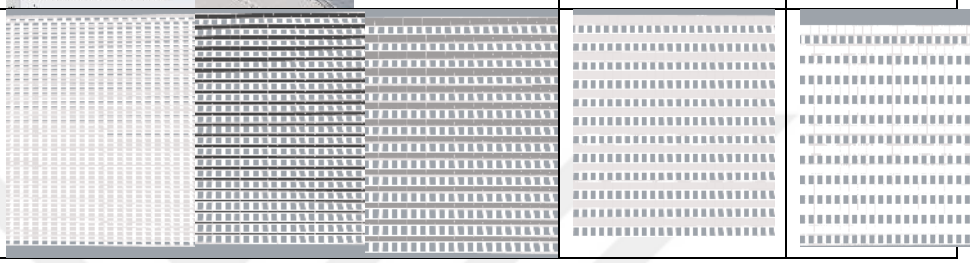				

4.4. Conducting Simulations and Optimizations for Designed Perforated Solar Screens (PSS)

The study outlines a systematic approach to the parametric modeling, simulation, and multi-objective optimization to design PSSs, emphasizing their influence on thermal and visual comfort.

For the simulation process, the model was initially constructed to closely represent real-world conditions. In line with simulation method, the modeling framework incorporated detailed boundary conditions, material properties, and occupancy-related parameters to enhance representativeness. The optical and thermophysical properties of the rooms are documented in Table 4.3 and 4.4 .

The rooms modeled within the simulation program, along with the parametric model of the designed PSS, are depicted in Figure 4.49. Furthermore, proximate environmental influences—such as potential shading devices or surrounding structures—were systematically reviewed to confirm the absence of external factors that could compromise the validity of the results. This verification step ensured that the obtained simulation outcomes could be attributed solely to the designed PSS

configurations without unintended interference. The tested rooms were not influenced by adjacent environmental obstructions capable of generating shading effects in their immediate surroundings.

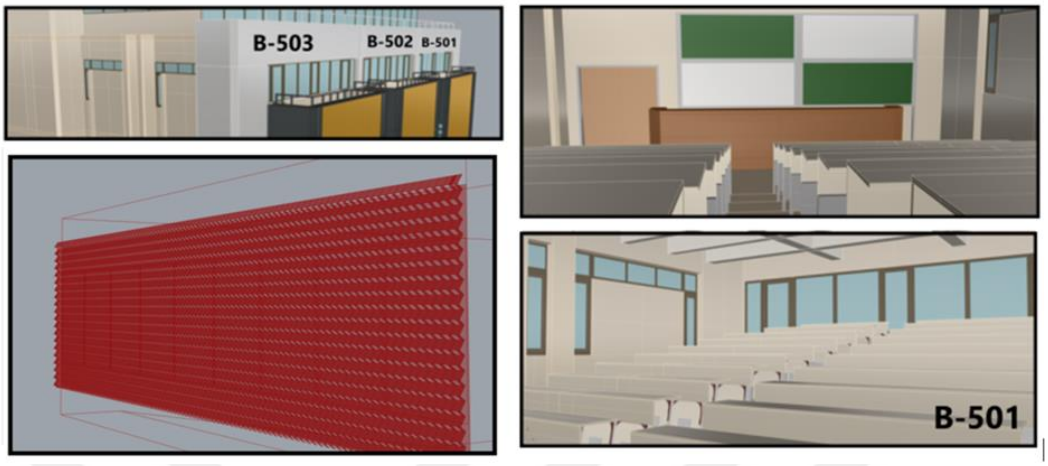

Figure 4.49 3D Model of rooms and parametric PSS

The optimization was carried out and, subsequently, simulations were done to provide more detailed evaluations while also reducing calculation times.

First stage optimization was performed for;

- Spatial Daylight Autonomy (sDA),
- Summer and winter solar radiation on windows
- Annual Sun Exposure (ASE)

Second stage simulations were performed for;

- Predicted Mean Vote (PMV)

Computation times were considered a critical factor during optimization. Table 4.17 provides details related to the calculation times for the parameters, with specific examples drawn from the B502 middle classroom and various PSSs. In the first stage, shorter computation times allowed for broader value ranges for design parameters. The total number of PSS combinations generated from design parameters in this stage reached 9,920,232. In the first stage of optimization, the number of variables for the design parameters was as follows: Angle (a): 36, c: 9, c-d: 9, e: 9, f: 9, h: 14, and ı: 3. During the second stage, these numbers were reduced to: Angle (a): 4, c: 5, c-d: 2, e: 4, f: 4, h: 7, and ı: 3. By narrowing the range of variables, the number of combinations for PSSs generated from the design parameters decreased from 9,920,232 to 13,440, significantly improving computational efficiency.

In the second stage, the inclusion of PMV calculations significantly increased computation times. For example, PMV calculations without shading devices required approximately 9 seconds, while those with shading devices exceeded 14,400 seconds (Figure 50). To manage these computational demands, the range of design parameter values was reduced during the second stage.

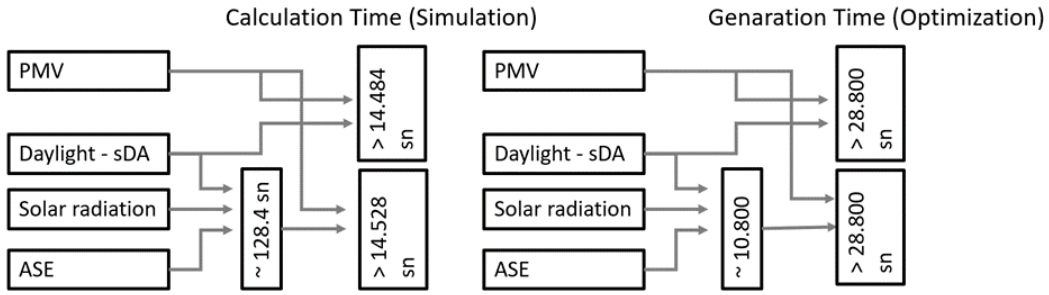

Figure 4.50 Calculation and generation time of KPIs (sDA,ASE,Solar Radiation and PMV)

Table 4.17 Influence of geometrical resolution on simulation time

Design parameters	Calculation parameters	Calculation time(s)	Calculation time for defined parameters (s)
No shading	**Daylight - sDA-DA-UDI**	~ 44.2	~ 77.8
	Solar radiation -summer	~ 3	
	Solar radiation - winter	~ 3	
	ASE	~ 12.8	
	View out	~ 3	
	PMV	~ 9	
1 **a: 5*5=25, c:0.1, c-d: 0.01, e:0.1, f:0.1, h:0.05, ı: 0.77**	**Daylight - sDA-DA-UDI**	~ 84.4	~ 143.1
	Solar radiation -summer	~ 7.2	
	Solar radiation - winter	~ 6.8	
	ASE	~ 18.6	
	View out	~ 11.7	
	PMV	> 14.400	
2 **a: 5*5=25, c:0.1, c-d: 0.01, e:0.1, f:0.1, h:0.09, ı: 0.77**	**Daylight - sDA-DA-UDI**	~ 87.0	~ 157.3
	Solar radiation -summer	~ 9.6	
	Solar radiation - winter	~ 9.4	
	ASE	~ 25.5	
	View out	~ 17.1	
	PMV	> 14.400	
3 **a:5*5=25, c:0.1, c-d: 0.01, e:0.09, f:0.1, h:0.09, ı: 0.77**	**Daylight - sDA-DA-UDI**	~ 75.7	~136.5
	Solar radiation -summer	~ 7.3	
	Solar radiation - winter	~ 6.7	
	ASE	~ 18.7	
	View out	~ 9.6	
	PMV	> 14.400	

Table 4.17 Influence of geometrical resolution on simulation time (Continued…)

Design parameters	Calculation parameters	Calculation time(s)	Calculation time for defined parameters (s)
4 **a:6*5=30, c:0.1, c-d: 0.01, e:0.09, f:0.1, h:0.1, ɪ: 0.77**	Daylight - sDA-DA-UDI	~ 74.2	~ 135.0
	Solar radiation -summer	~ 8.1	
	Solar radiation - winter	~ 7.9	
	ASE	~ 20.6	
	View out	~ 17.1	
	PMV	> 14.400	
5 **a:7*5=35, c:0.1, c-d: 0.01, e:0.07, f:0.1, h:0.07, ɪ: 0.77**	Daylight - sDA-DA-UDI	~ 66.6	~ 119.4
	Solar radiation -summer	~ 6.8	
	Solar radiation - winter	~ 6.3	
	ASE	~ 17.6	
	View out	~ 4.8	
	PMV	> 14.400	
6 **a:5*5=25, c:0.09, c-d: 0.01, e:0.1, f:0.1, h:0.04, ɪ: 0.77**	Daylight - sDA-DA-UDI	~ 86.2	~ 163.4
	Solar radiation -summer	~ 10.4	
	Solar radiation - winter	~ 11.8	
	ASE	~ 30.3	
	View out	~ 33.8	
	PMV	> 14.400	

In summary;

Simulations were done leveraging advanced software tools, the workflow integrates design, analysis, and multi-objective optimization to achieve energy-efficient and comfortable environments.

- **Software Utilized:** Rhinoceros & Grasshopper, EnergyPlus, Ladybug & Honeybee, Radiance & DAYSIM and Octopus.
- **Optimization Process:** Stage 1: Spatial Daylight Autonomy (sDA), Annual Sun Exposure (ASE), and solar radiation.

  Stage 2: Predicted Mean Vote (PMV)

- **Computational Strategy:** The optimization process employs iterative refinement to balance computational efficiency and analytical depth and in Stage 2 simulations for PMV enable detailed evaluations.
- **Technical Specifications of the Computer:**

  Processor (CPU): Intel Core i7-10750H, 2.6 GHz, 6 cores/12 threads, 10TH GEN-24 cores

Memory (RAM): 32 GB DDR4, 3200 MHz

Storage: 1.5 TB NVMe SSD, Read/Write Speed: 3500/3000 MB/s

Graphics Processing Unit (GPU): NVIDIA GeForce GTX 1660 Ti, 6 GB GDDR6

Operating System: Windows 10 Pro, Version 22H2

The system utilized a 512 GB SSD in C and 1 TB Samsung SSD 870 EVO in D for data storage.

4.4.1. Simulation settings for KPI

Detailed information regarding the simulation settings is presented in Table 4.18, which outlines the KPI utilized during the optimization process. Additional details about KPI and simulation settings for non-optimization calculations are provided in Appendix 5.

Table 4.18 Definitions of KPI and simulation settings used in optimization

	KPI	Definition and Limitations	Methods	Calculation area	Calculation settings
1. Optimization	Annual sunlight exposure (ASE)	In simulations, annual sunlight exposure (ASE) exceeding 1000 lux for more than 250 hours per year (ASE 1000,250h) has been calculated based on direct sunlight. According to the recommendation of the Illuminating Engineering Society (IES), the percentage of the area calculated for ASE 1000,250h, which is one of the LEED v4 metrics, should be kept below 10%.	Calculation / Optimization	Working plane, h: 0,85m, Grid: 0,5 m,	All year-All day
	Solar radiation	In simulations, the amount of solar radiation that needs to be utilized and protected on the exterior surface of windows is calculated. It is desired to maximize the amount of solar radiation to be utilized while minimizing the amount that needs to be protected.	Calculation / Optimization	Window Outside surface, Grid: 0,1 m	Summer period (Months 6-7-8), Winter period (Months 12-1-2) – All day

Table 4.18 Definitions of KPI and simulation settings used in optimization

Continued…)

	KPI	Definition and Limitations	Methods	Calculation area	Calculation settings
1. Optimization	Spatial Daylight autonomy (sDA)	In simulations, Spatial daylight autonomy (sDA) calculations have been performed based on usage hours throughout the year. Spatial Daylight autonomy is a metric that provides the percentage of the area where the target illuminance level is met by daylight during usage hours throughout the year. Keeping these values at their maximum has been entered as a command.	Calculation / Optimization	Calculation area: from wall 0,5 m working plane: 0.85, Grid: 0,5 m	All year-8,00-17,00
2. Simulation	PMV (Predicted Mean Vote)	PMV (Predicted Mean Vote), a measure used in determining thermal comfort in climate-controlled environments, is accepted as comfortable within the range of -0.5<PMV<+0.5 according to ISO 7730 and ASHRAE 55 standards. The closer the PMV value is to zero, the more comfortable the indoor environment is considered to be.	Measurement / Calculation / Optimization	Working plane, h:1,1m, Grid: 0,5m	Duration and time: 8.00-17.00

In the calculation of daylight illuminance levels for Istanbul, the Perez clearness index method was employed, utilizing a sky condition classification system. For the simulations, the sunny clear sky type was selected to represent clear sky conditions, while the partly sunny sky type was used to reflect average conditions. To balance computational efficiency with the recommended accuracy, the default settings were employed for Radiance parameters throughout the simulations.

Daylight illuminance levels were evaluated using target illuminance levels specified in the TS EN 17037:2023 standard. Adjustments were made to align the simulations with the calculation surfaces described in the standard. In accordance with TS EN 17037:2023, the calculation height was set at 0.85 m above ground level, and grid intervals for the calculation surface were determined to be 0.5 m.

ASE (Annual Sun Exposure) were calculated and evaluated depending on values given in IESNA and LEED v4. For annual window solar radiation calculations, adjustments are made to minimize summer solar radiation while maximizing winter solar radiation throughout the year. The grid intervals on the working plane are uniformly set to 0.5 m for all calculations. However, for solar radiation calculations, the surface is assigned specifically to the window front face, differing from other calculation surfaces. A finer grid

interval of 0.1 m is applied to this surface due to the critical importance of grid precision for accurate assessments.

For PMV calculation, indoor temperature, air velocity, Mean Radiant Temperature and air humidity were determined instantly as a result of the Energyplus simulation and the values were transferred to the Ladybug PMV calculation section. In order to calculate PMV values according to the results calculated via Energyplus, activity level and clothing insulation level values were entered. In addition, calculation period determinations were made.

The thermal comfort calculations were conducted for June and December during the time period of 11:00 to 15:00. Clothing insulations are determined as 0.5 clo for summer months and 0.8 clo for winter months. According to the ASHRAE 55 standard, an activity level of 1.1 met is adopted for tasks such as sitting, reading, and writing. The calculation surface is positioned at a height of 1.1 meters above ground level, with grid intervals set to 0.5 meters. During thermal comfort calculations, the HVAC system is disabled.

As mentioned section 2.2.1 thermal comfort the BS EN 15251:2007 specifies the temperature values required to achieve the range of -0.5 < PMV < +0.5, depending on function, activity level (met), and clothing insulation level (clo). Considering the values given in the standard, for the calculations, the minimum value entered for opening windows in summer months as a natural ventilation setting is 26.0 °C. For heating, 22 °C was entered as the minimum temperature value.

Additional details regarding simulation settings are provided in Figure 4.51.

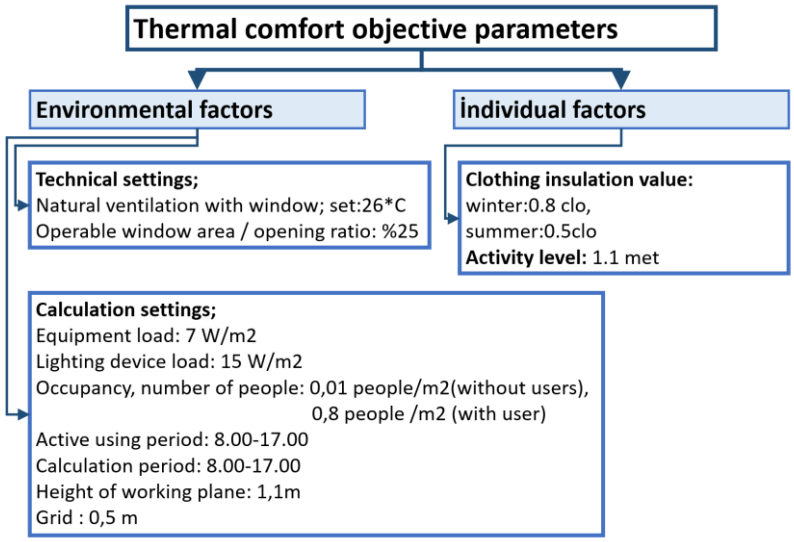

Figure 4.51 Thermal Comfort calculation adjustments

In the optimization processes, the Octopus plugin is configured to minimize the input KPI values. In the first optimization phase, the goal was to minimize the ASE value, in alignment with Octopus's calculation logic, while maximizing the sDA value. For solar radiation calculations, the objective was to maximize beneficial solar radiation while minimizing detrimental solar radiation on the window surface.

Unlike other parameters, solar radiation was addressed distinctly during optimization, with separate parameters defined for summer and winter solar radiation. As Octopus is programmed to minimize values, equations were formulated to ensure that the sDA and beneficial solar radiation parameters, though calculated as minimum values, achieved maximum results.

Optimization processes were halted manually. The first optimization was terminated at the 24th generation for each room, during which approximately 2,700 design options were evaluated. To facilitate the interpretation of optimal results, value ranges were refined and narrowed within the Octopus result reading interface.

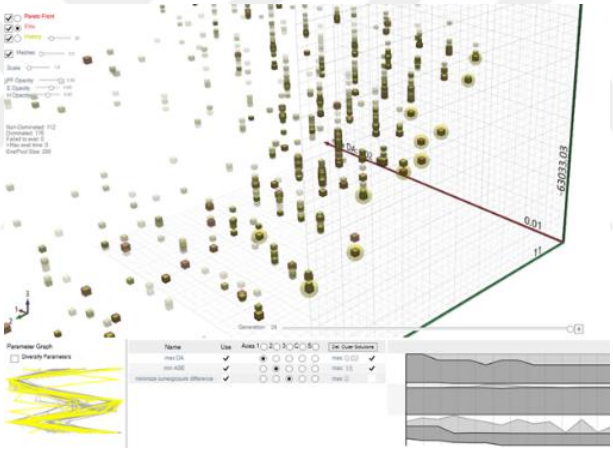

Figure 4.52 Example graph of optimization results performed with the Octopus plugin

5
RESULTS

5.1. Analysis of Simulation and Optimization Results to Determine Optimum Perforated Solar Screens (PSS)

5.1.1. Evaluation of Optimization Results in terms of KPI

To find the best design options of PSSs the limitations for each calculation has been applied. The limitations were determined depending on results and limits given in standards and litrature. Optimization was performed for;

- Summer and winter solar radiation on windows
- Annual Sun Exposure (ASE) to evaluate visual and thermal comfort
- Spatial Daylight Autonomy (sDA)

As a result of the optimization, the best scenarios were determined. Firstly, optimization results in Octopus pareto scatter plot were interpreted in order to identify the optimal solutions of PSSs.

In this study, the final set of 11 optimal scenarios for each classroom was not arbitrarily determined by the Octopus algorithm alone but was established through a systematic selection process based on key performance indicators (KPI). During the evolutionary search, dominated and redundant solutions were eliminated, and after applying study-specific acceptability constraints (e.g., ASE thresholds, daylight autonomy targets, geometric feasibility) and merging near-duplicate cases within simulation tolerances, the solution set stabilized at 11 distinct designs. These 11 scenarios represent the minimal yet sufficient collection of “decision-meaningful” points on the trade-off surface, including extreme solutions,

compromise solutions “knee points,” and mid-range alternatives, thereby ensuring that all significant performance trade-off relationships are captured for subsequent evaluation and selection.

After that, these scenarios were evaluated in terms of KPI. To make comparisons, the calculation results of the worst-case conditions were also considered. Subsequently, normalization and TOPSIS analyses were carried out, and numerical data were utilized to see if it was possible to say which one was the best. Finally, the optimal solutions were evaluated in terms of their design parameters. Classrooms with southeast (B-501), south (B-502), and southwest (B-503) orientations were evaluated separately, and common inferences were drawn.

- **Solar radiation incident on the window plane** is the most significant passive energy source affecting the building envelope. In this study, the values expressed under the headings “summer and winter solar radiation” represent the amount of total solar energy (kWh/m2) incident on the window surface, calculated separately for summer and winter periods. This parameter is of critical importance for assessing the effectiveness of the PSS, as it affects thermal heat gain potential, cooling loads, and daylight performance. The performance of the PSSs is evaluated based on the extent to which it limits or optimizes the solar energy reaching the window.
- **Annual Sunlight Exposure (ASE)** refers to the percentage of a space that receives more than 1000 lux of direct sunlight for over 250 hours per year. This value is used in the evaluation of sunlight availability, glare-related visual comfort issues, and thermal comfort. The threshold recommended by CIBSE LG10, IESNA (2012) (IES LM-83), and LEED v4 is ASE < 10%. A high ASE value causes visual discomfort, glare, uncontrolled and ineffective use of daylight, increased cooling loads, and decreased user satisfaction. Reinhart & Wienold (2011) state that exceeding the 10% ASE threshold impairs comfort and increases the frequency of blind usage. Mardaljevic (2012) emphasizes that high ASE values lead to discomfort and user dissatisfaction due to glare.
- **Spatial Daylight Autonomy (sDA)** expresses the percentage of a space that receives at least 300 lux of natural daylight for a specific number of hours

annually. It is typically evaluated in the form of sDA (300lx, 50%), meaning that 300 lux of daylight is achieved for at least 50% of the working hours (8 hours per day, 5 days per week). If at least 75% of the space meets this criterion for at least 50% of the year (i.e., sDA ≥ 75%), the space is considered to receive good natural lighting (Reinhart & Wienold (2011) and IESNA (2012)).

5.1.1.1. Determination of the Optimum Perforated Solar Screen for Classroom B-501 (Southeast-Oriented)

As a result of the optimizations, 11 scenarios were identified as the best-performing scenarios for classroom B-501.

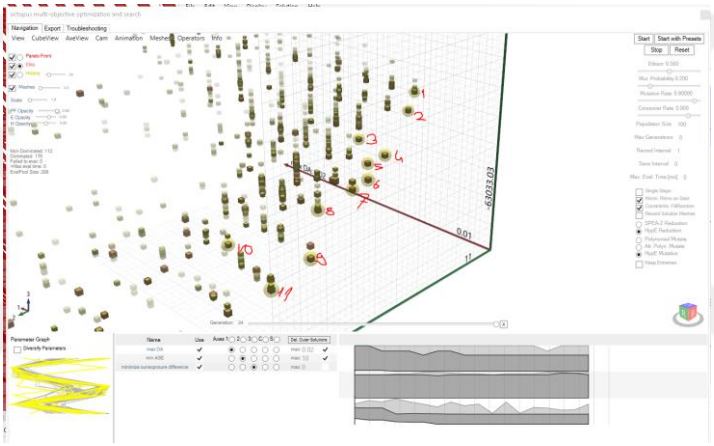

Figure 5.1 The best scenarios determined for classroom B-501 is shown in the Octopus Pareto scatter plot coordinate graph

When evaluating the optimum results for classroom B-501, it is observed that in the best scenarios, summer solar radiation ranges between 22.348–57.341 kWh/m², while winter solar radiation ranges between 25.675–85.846 kWh/m². The highest summer solar radiation was obtained in the Opt-10 scenario (57.341 kWh/m²), whereas the highest winter solar radiation was observed in the Opt-9 scenario (85.846 kWh/m²). The scenarios that maximize the benefits of natural lighting vary between summer and winter periods. While high solar radiation during winter may contribute to thermal gain and reduce heating loads in the space, excessive solar energy during summer may increase cooling loads and adversely affect indoor comfort and energy efficiency. Thus, a more integrated seasonal strategy is more effective than approaches focusing solely on a single period. In the Opt-1 scenario

(summer: 25.233 kWh/m², winter: 25.675 kWh/m²), equal and low solar radiation values were obtained for both summer and winter, resulting in lower solar energy gains. Although this situation is favorable for preventing overheating in summer, it may lead to increased heating demand due to insufficient thermal gain in the interior during winter. Additionally, this scenario is less effective compared to others in terms of achieving the daylight illuminance levels required for benefiting from natural lighting.

In the worst-case scenarios, the lowest summer solar radiation is 23.588 kWh/m², while the highest reaches 226.982 kWh/m², indicating inadequate solar control and the potential for excessive thermal gain. In these worst-case scenarios, conditions such as increased cooling loads due to excessive thermal gain and obstruction of natural lighting through over-shading emerge. In the second worst-case scenario, the amount of winter solar radiation incident on the window is 2.947 kWh/m², which could lead to low indoor temperatures and high heating demand during the winter months. The highest winter solar radiation gain in the worst-case scenarios was calculated as 162.958 kWh/m².

When examining the scenarios in terms of both summer and winter solar radiation, the scenarios providing the lowest solar radiation in summer and the highest in winter can be interpreted based on the proportional difference in the amount of solar radiation incident on the window. Consequently, it is observed that scenarios Opt-2, Opt-8, and Opt-9 (with proportional differences of 52.86%, 52.55%, and 67.70%, respectively) offer a more equilibrated distribution of solar radiation compared to the others. Scenarios Opt-8 and Opt-9 stand out with relatively low solar radiation in summer and high values in winter. This indicates that façade strategies prioritizing proportional seasonal equilibrium can significantly enhance both thermal and visual comfort. These values are favorable for optimizing energy gains, ensuring sufficient daylight illuminance, and controlling glare, and are considered suitable designs in terms of both visual and thermal comfort. Particularly in cases where the proportional difference is high (e.g., above 30%), the contribution of solar energy gained in winter is significantly greater than that in summer, which can be interpreted as ideal for energy efficiency. This reinforces the importance of designs that do not merely minimize summer gains but also strategically maximize

winter benefits. In addition to these values, it is also necessary to ensure that, along with sufficient daylight illuminance in the interior through natural lighting, problems such as uneven daylight distribution and glare due to excessive brightness are also prevented.

Table 5.1 Calculation results of the best scenarios for classroom B-501

Scenario	Summer Solar Radiation (kWh/m²)	Winter Solar Radiation (kWh/m²)	ASE (%)	sDA (%)
opt-1	25.233	25.675	12	78.43
opt-2	22.348	34.162	13	73.04
opt-3	30.123	34.543	14	89.21
opt-4	33.556	44.293	14	83.82
opt-5	34.273	40.625	15	94.6
opt-6	37.356	50.434	15	89.21
opt-7	38.109	53.279	16	89.21
opt-8	41.321	63.34	17	100
opt-9	51.158	85.846	17	73.04
opt-10	57.341	83.755	18	100
opt-11	40.535	40.901	16	94.6

When the amount of annual solar radiation (kWh/m²) incident on the window plane is converted into heat gain (MJ/m²), it is observed that in some cases, summer heat gain is greater than or nearly equal to winter heat gain. This condition may lead to overheating during the summer months, especially when cooling is needed, thereby increasing energy consumption. In scenarios where the proportional difference is low and/or negative, it is evident that the PSS used in the scenario is insufficient to prevent excessive heat gain in summer and may even result in unfavorable outcomes.

Scenarios Opt-9 and Opt-10 are those in which the highest heat gains are achieved during both summer and winter periods. In this case, high heat gain in winter may reduce the heating load of the space, but the heat gain obtained in summer may increase the cooling load. On the other hand, scenario Opt-2 is the one with the lowest summer heat gain. However, in this scenario, the winter heat gain is also lower than in the others. This may lead to insufficient heat gain during the winter period and consequently increase heating loads.

Scenarios in which the amount of winter solar radiation is greater than that of summer, and in which the proportional difference is significantly positive (evaluated as above 30% based on the data), can be considered more favorable scenarios with well-equilibrated seasonal conditions. These scenarios provide heat gain in winter while ensuring solar radiation control in summer, thereby contributing to reduced cooling loads.

Table 5.2 Values of annual solar radiation incident on the window plane for classroom B-501 expressed in terms of heat gain

Scenario	Summer Heat Gain (MJ/m²)	Winter Heat Gain (MJ/m²)
opt-1	90.8388	92.43
opt-2	80.4528	122.9832
opt-3	108.4428	124.3548
opt-4	120.8016	159.4548
opt-5	123.3828	146.25
opt-6	134.4816	181.5624
opt-7	137.1924	191.8044
opt-8	148.7556	228.024
opt-9	184.1688	309.0456
opt-10	206.4276	301.518
opt-11	145.926	147.2436

In the worst-case scenarios, the minimum ASE value was observed as 11%, while the maximum reached 41%. In these worst scenarios, when a PSS completely obstructs the south façade, the ASE value was calculated as 11%. Due to the solar radiation entering through the windows located on the east façade of the classroom, the ASE value exceeded the standard limit. This condition should be considered in the evaluation of the best scenarios for the design of PSSs. In the best scenarios, ASE values were observed in the range of 11%–18%. These values can be considered to provide comfortable and optimized daylight performance.

Moreover, the literature states that an ASE value between 10% and 20% is considered acceptable (Reinhart & Wienold, 2011). Therefore, ASE values for all good scenarios in the results of classroom B-501 are within acceptable limits.

Among the best scenarios, those that enable a comfortable space in terms of both ASE values and natural lighting should be selected.

In the best scenarios, sDA values range between 73.04% and 100%. In nine of these scenarios, the sDA value exceeds 75%, indicating that comfortable daylight illuminance can be provided in nearly the entire space. Among these, selecting the ones with lower ASE values would help prevent glare and excessive sunlight exposure. In this way, both energy efficiency and user comfort can be achieved.

In the worst-case scenario, even though the windows on the south façade are entirely obstructed by shading, the classroom receives sunlight through the windows on the eastern section, resulting in an sDA value of 32.34%. Additionally, in this case, solar radiation enters through the east-facing window during both summer and winter. In this scenario, the solar radiation incident on the window is 23.588 kWh in summer and 2.947 kWh in winter, and the ASE value is 11%. The low sDA value in this worst-case scenario indicates that sufficient daylight cannot be provided in the interior and is thus considered unacceptable.

In the third worst-case scenario, an sDA value of 100% indicates that natural lighting is continuously provided throughout the entire interior space. Although this might initially seem favorable, the ASE value in this scenario is also 41%, meaning that the design results in excessive sun exposure that disrupts visual comfort and increases heat gain, thereby negatively impacting thermal comfort. A high ASE value can lead to visual discomfort and increased energy consumption. As observed in this scenario, when the daylight level exceeds the optimum threshold, issues such as glare, extreme contrast, and thermal discomfort may arise (Reinhart & Wienold, 2011). This underlines the fact that maximizing daylight availability without adequate solar control can be as problematic as insufficient daylight provision.

In the best scenarios, the sDA values range between 73.04% and 100%, with four scenarios achieving a value of 89.21%. In scenarios Opt-8 and Opt-10, an sDA of 100% was achieved. Since PSSs were employed in these scenarios, the ASE values were calculated as 17% and 18%, respectively. Therefore, it can be concluded that the design may yield favorable outcomes in terms of both visual and thermal comfort. Nevertheless, high ASE values indicate a potential risk of glare. In other

scenarios (e.g., the first four), while ASE values are below 15%, sDA values vary between 73.04% and 89.21%. This demonstrates that while providing sufficient daylight illuminance, it is also possible to prevent conditions that may negatively affect visual comfort. Even if solar radiation gain is lower, a more controlled and adequate level of natural lighting can still be achieved (as in Opt-1 and Opt-3). The same applies to scenarios with ASE values of 15% and above. For instance, in Opt-5, although the ASE value is relatively low, the sDA value is higher compared to other scenarios.

High sDA values increase user satisfaction, while low ASE values minimize glare and excessive solar gain. In scenarios Opt-4 (83.82% sDA, 14% ASE) and Opt-5 (94.6% sDA, 15% ASE), ASE and sDA values demonstrate a coherent integration, and solar radiation and heat gains are provided at optimal levels. In these scenarios, although the amount of solar radiation incident on the window is high, ASE remains under control. Thus, efficient and comfortable lighting is possible. This coherence confirms that PSS optimization should focus on harmonizing sDA and ASE rather than treating them as independent parameters. This indicates that effective solar control is achieved while still providing natural daylighting. These scenarios can be considered optimal in the design optimization of PSSs.

5.1.1.2. Determination of the Optimum Perforated Solar Screen for Classroom B-502 (South-Oriented)

As a result of the optimizations, 11 scenarios were identified as the best-performing ones for classroom B-502.

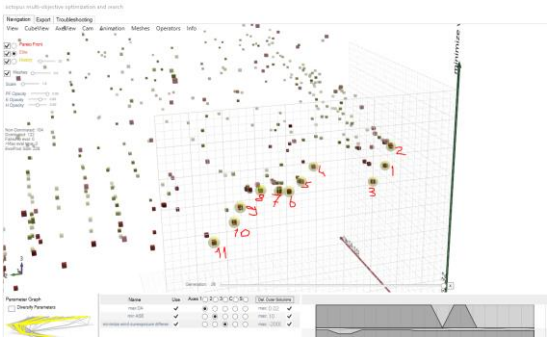

Figure 5.2 The best scenarios determined for classroom B-502 is shown in the Octopus Pareto scatter plot coordinate graph

When evaluating the optimum results for classroom B-502, it is observed that in the best scenarios, summer solar radiation ranges between 51.770–76.825 kWh/m², while winter solar radiation ranges between 72.735–107.727 kWh/m². The highest summer solar radiation was obtained in the Opt-11 scenario (76.825 kWh/m²), and the highest winter solar radiation was also obtained in the Opt-11 scenario (107.727 kWh/m²). The scenarios that maximize the benefits of solar radiation vary between the summer and winter periods. In these best-performing scenarios, the levels of solar radiation during summer are relatively high. Therefore, selecting scenarios in which the window surface receives lower solar radiation during summer may help ensure sufficient heat gain in winter while also preventing increased cooling loads in summer.

In the worst-case scenarios, the lowest summer solar radiation was calculated as 14.334 kWh/m², while the highest reached 260.038 kWh/m². These worst-case scenarios reveal negative outcomes such as increased cooling loads due to excessive heat gain and impeded natural lighting caused by over-shading. The lowest winter solar radiation incident on the window was calculated as 1.778 kWh/m², while the highest winter solar radiation gain was 173.736 kWh/m². Such extreme variations confirm the risks of both under- and over-shading, reinforcing the need for optimized shading devices.

When the scenarios are examined in terms of both summer and winter solar radiation, the scenario that provides the lowest solar radiation in summer and the highest in winter should be identified. In making this determination, when considering the proportional difference in solar radiation incident on the window, it is observed that scenarios Opt-1 and Opt-3 (with proportional differences of 45% and 46.23%, respectively) offer a more more favorable distribution of solar radiation of solar radiation compared to the others. In all of the best scenarios, the proportional difference exceeds 30%, meaning that the contribution of solar energy in winter is greater than in summer, which can be interpreted as advantageous for energy efficiency.

Table 5.3 Calculation results of the best scenarios for classroom B-502

Scenario	Summer Solar Radiation (kWh/m²)	Winter Solar Radiation (kWh/m²)	ASE (%)	sDA (%)
opt-1	58463	84783	0	61.11
opt-2	51770	72735	0	61.11
opt-3	59652	87230	1	61.11
opt-4	59109	84732	3	55.56
opt-5	60834	86575	4	61.11
opt-6	68269	92461	5	66.67
opt-7	62755	89428	5	61.11
opt-8	70907	94663	6	61.11
opt-9	69359	94013	7	66.67
opt-10	75507	105623	7	61.11
opt-11	76825	107727	8	66.67

When the amount of annual solar radiation (kWh/m²) incident on the window plane is converted into heat gain (MJ/m²), it is observed that in some cases, summer heat gain is greater than or close to winter heat gain. This condition may lead to overheating during the summer months—when cooling is required—and consequently result in increased energy consumption. In cases where the proportional difference is low and/or negative, it is evident that the shading devices used in the scenario is insufficient to prevent excessive summer heat gain and may even lead to unfavorable outcomes.

Scenarios Opt-10 and Opt-11 are those in which the highest heat gain was obtained during both summer and winter periods. In such cases, high heat gain in winter may help reduce the heating load of the space, yet the heat gain in summer may increase the cooling demand. On the other hand, scenario Opt-2 provides the lowest summer heat gain. However, in this scenario, the winter heat gain is also lower compared to the others. As a result, it may lead to insufficient heat gain in winter and thereby increase heating loads. This suggests that minimizing summer gains without sufficient winter compensation may compromise overall energy performance.

Table 5.4 Annual solar radiation incident on the window plane for classroom B-502 expressed in terms of heat gain

Scenario	Summer Heat Gain (MJ/m²)	Winter Heat Gain (MJ/m²)
opt-1	210,466	305,619
opt-2	186,372	261,846
opt-3	214,747	314,028
opt-4	212,792	305,435
opt-5	219,002	311,670
opt-6	245,768	332,859
opt-7	225,918	321,941
opt-8	255,265	340,787
opt-9	249,692	338,447
opt-10	271,825	380,243
opt-11	276,570	387,817

In the worst-case scenarios, the minimum ASE value was observed as 0%, while the maximum reached 22%. The fact that ASE values remain within this range indicates that there is no excessive discomfort in the space in terms of annual sun exposure and that it can be easily controlled. In the best scenarios, ASE values are below 10%, making them suitable in terms of visual comfort. The lowest ASE values, which are 0%, were obtained in Opt-1 and Opt-2 scenarios. However, while the shading devices used generates minimal ASE, it should also enable daylight illuminance to support the natural lighting of the space. For this reason, sDA values gain importance.

In the best scenarios, sDA values range between 55.56% and 66.67%. In these scenarios, the sDA value is predominantly 61.11% (in seven scenarios). Since sDA values are below 75%, it indicates that sufficient daylight illuminance is not fully achieved in the space. Nevertheless, the sDA values are at a good level, showing that the lighting requirement can still be met. Under extreme conditions—i.e., when no shading device is used—the sDA value is calculated as 77.78%, and the ASE value as 28%. In this case, the designed PSSs significantly reduce ASE values in the space while preventing excessive decreases in sDA values. With their angled

configuration, these devices enhance the entry of indirect daylight into the interior and thus contribute to natural lighting.

The scenarios in which the sDA value reaches its maximum of 66.67% are Opt-6, Opt-9, and Opt-11. Since ASE values in all scenarios remain within acceptable limits, selecting designs with the highest sDA values will provide the most favorable conditions for both thermal and visual comfort. In the scenarios with the highest sDA values, ASE remains low, and the scenarios with the lowest summer solar radiation are Opt-6 and Opt-9. In these scenarios with high sDA values, the proportional difference between summer and winter solar radiation incident on the window is 35%, indicating that the solar radiation levels are very close to each other.

5.1.1.3. Determination of the Optimum Perforated Solar Screen for Classroom B-503 (South-Oriented)

As a result of the optimizations, 11 scenarios were identified as the best-performing ones for classroom B-503.

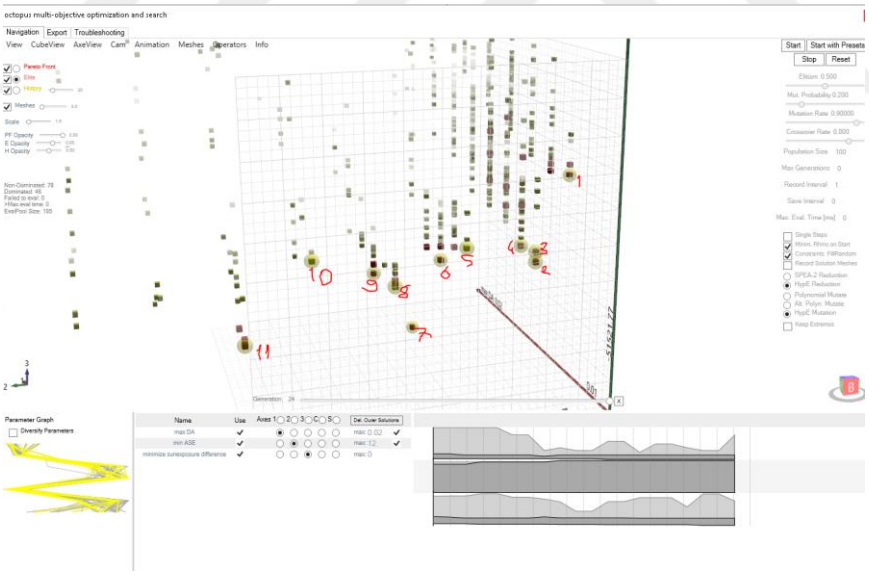

Figure 5.3 The best scenarios determined for classroom B-503 is shown in the Octopus Pareto scatter plot coordinate graph

When the optimum results for classroom B-503 are evaluated, it is observed that, in the best scenarios, summer solar radiation ranges between 36.048–68.951 kWh/m², while winter solar radiation ranges between 56.299–116.433 kWh/m².

When the scenarios are analyzed in terms of both summer and winter solar radiation within these specified ranges, scenarios such as Opt-6, Opt-9, and Opt-11 can be considered advantageous. These scenarios are favorable in terms of optimizing energy gain while maintaining glare control.

In the Opt-7 scenario, the highest winter solar radiation—116.433 kWh/m²—was obtained. In this case, passive heat gain was achieved. High levels of solar radiation during the winter season can reduce heating loads in the interior space; however, excessive solar energy gain during the summer can increase cooling loads, thereby negatively affecting indoor comfort and energy efficiency. Therefore, it is important to select scenarios in which the amount of solar radiation incident on the window is lower in summer than in winter, to ensure a optimal performance. Moreover, to benefit from natural lighting, the amount of solar radiation must be sufficient to provide the required daylight illuminance.

An evaluation was conducted based on the proportional differences between summer and winter solar radiation. In the best-performing scenarios for classroom B-503, the solar radiation levels were sufficient to ensure an adequate level of daylight illuminance. In all scenarios, the proportion of solar radiation incident on the window surface is lower in summer than in winter, with this proportional difference ranging from 41% (Opt-5) to 68% (Opt-7, Opt-9, and Opt-11). Such high proportional differences confirm that the optimization strategy effectively favors winter gains, which is ideal for overall energy efficiency. Since the scenario results are proportionate and effective in terms of both summer and winter solar radiation, ASE and sDA values must also be considered when evaluating thermal and visual comfort suitability. In this way, while ensuring sufficient daylight levels in the interior through natural lighting, uniform distribution of daylight can be achieved, and issues such as glare caused by excessive illumination can be prevented.

In the worst-case scenarios, for example in Scenario 1, the amount of winter solar radiation incident on the window was 2.939 kWh/m², a value that may lead to low indoor temperatures and high heating demand during the winter months. Among the worst scenarios, the lowest summer solar radiation was 26.692 kWh/m², while the highest reached 238.496 kWh/m², indicating that solar control was not adequately achieved and that there is a high potential for excessive thermal gain.

During winter, the minimum and maximum solar radiation levels were 2.939 kWh/m² and 161.807 kWh/m², respectively. When compared to the values obtained in the best scenarios, it becomes evident that effective solar protection was achieved during summer, while solar radiation utilization in winter was also achieved at a high level.

Table 5.5 Calculation results of the best scenarios for classroom B-503

Scenario	Summer Solar Radiation (kWh/m²)	Winter Solar Radiation (kWh/m²)	ASE (%)	sDA (%)
opt-1	36.048	56.299	7	83.33
opt-2	50.917	80.118	8	94.44
opt-3	51.183	78.94	8	94.44
opt-4	50.094	78.551	8	88.89
opt-5	63.878	90.099	9	94.44
opt-6	47.411	78.843	9	83.33
opt-7	68.951	116.433	9	72.22
opt-8	64.074	94.654	10	94.44
opt-9	47.288	79.676	10	83.33
opt-10	59.082	86.727	11	88.89
opt-11	53.165	89.571	12	94.44

When the annual solar radiation incident on the window plane (kWh/m²) is converted into heat gain (MJ/m²), the Opt-7 scenario stands out as the scenario providing the highest heat gain in both summer and winter periods. In this case, the resulting heat gain may lead to overheating during the summer season. On the other hand, the Opt-1 scenario yields the lowest summer heat gain. However, in this scenario, winter heat gain is also lower compared to the others. This may result in insufficient heat gain during the winter period and, consequently, increased heating loads. Thus, minimizing summer heat gain alone does not necessarily result in optimal energy outcomes if winter benefits are compromised. This highlights the importance of not only maximizing energy gains but also moderating them to maintain seasonal comfort.

In this respect, scenarios such as Opt-2 and Opt-6 are more favorable than others in terms of winter energy gain through radiation and solar radiation control during

summer. When examining the proportional difference between summer and winter heat gain in the scenarios, it is observed that this ratio exceeds 40%. This indicates the necessity of evaluating other KPI—such as ASE and sDA—when selecting the most appropriate scenario.

Table 5.6 Annual solar radiation incident on the window plane for classroom B-503 expressed in terms of heat gain

Scenario	Summer Heat Gain (MJ/m²)	Winter Heat Gain (MJ/m²)
opt-1	129.77	202.68
opt-2	183.30	288.42
opt-3	184.26	284.18
opt-4	180.34	282.78
opt-5	229.56	324.36
opt-6	170.68	283.83
opt-7	248.22	419.16
opt-8	230.67	340.75
opt-9	170.24	286.83
opt-10	212.70	312.22
opt-11	191.39	322.45

In the best-performing scenarios, ASE values were observed to range between 7% and 12%. These values indicate that a comfortable and well-controlled sun exposure performance was achieved. The lowest ASE value was recorded in the Opt-1 scenario at 7%, suggesting that direct sunlight exposure was effectively limited, thereby enhancing visual comfort. However, sDA in this scenario was lower compared to the others. In the worst scenarios, ASE values were found to be as high as 33%. This shows that low ASE values must be accompanied by sufficiently high sDA values to guarantee both glare control and daylight autonomy.

In the worst-case scenarios, even when the south façade was entirely shaded, the ASE value was calculated as 7%. This is due to solar radiation entering through the west-facing windows. This situation should be considered when evaluating the best scenarios for PSS design. ASE values between 7% and 12% in the best scenarios suggest that optimal control was achieved while still ensuring a comfortable and opmized daylighting performance.

When ASE values are high, sDA values may still be satisfactory; however, visual discomfort may arise. Conversely, low ASE values can sometimes be accompanied by low sDA values. Therefore, ASE and sDA should be evaluated together. All good-performing scenarios exhibited acceptable ASE levels, and those that support both low ASE and sufficient natural lighting should be prioritized in terms of providing comfortable indoor conditions. For instance, when examining Table 5.5, scenarios such as Opt-2 and Opt-3 represent optimal performance with high sDA values (94.44%) and low ASE values (8%). These scenarios also offer well-proportioned gains in summer and winter solar radiation.

In the best scenarios, sDA values ranged from 72.22% to 94.44%. Except for Opt-7, all other scenarios achieved sDA values above 75%, indicating that comfortable daylight illuminance was achieved across most of the interior space, while ASE values were kept under control to prevent glare and excessive sunlight exposure. In this way, both energy efficiency and user comfort were simultaneously achieved.

In the worst scenario, sDA was calculated as 27.78%, representing the minimum level. Although the south façade was entirely shaded, low sDA was obtained due to solar radiation entering from the west-facing windows. This indicates that adequate daylighting was not achieved in the interior space, and such a scenario is considered unacceptable.

In one of the worst-case scenarios (Scenario 4), sDA reached 100%, meaning that daylight was continuously present throughout the entire interior space. While this may initially appear favorable, the ASE value in this scenario was 33%, which indicates excessive sun exposure that negatively affects visual comfort and increases heat gains, thereby compromising thermal comfort. When illuminance exceeds optimal levels, problems such as glare, visual contrast, and thermal discomfort may arise (Reinhart & Wienold, 2011). This example demonstrates that maximizing daylight alone does not equate to optimal comfort, as uncontrolled gains undermine both visual and thermal quality.

Poor-performing scenarios generally fail to provide visually, thermally, and psychologically comfortable environments. In contrast, the best-performing

scenarios demonstrated optimal performance by maintaining an appropriate relationship between sDA and ASE values.

Among the best scenarios, five achieved an sDA value of 94.44%. The PSSs used in these scenarios also maintained ASE values within comfort thresholds. However, scenarios with the lowest ASE value of 8%—namely Opt-2 and Opt-3—were more advantageous than the others. These scenarios are expected to yield more favorable results in terms of both visual and thermal comfort. In particular, Opt-2 is a more suitable option due to the higher proportional difference between summer and winter solar radiation, resulting in lower solar gains during summer. On the other hand, Opt-3 can also be considered a viable option, as its values are relatively close.

High sDA values enhance user satisfaction, while low ASE values help minimize glare and excessive solar heat gain. However, as previously noted, the amount of solar energy gain should also be included in the evaluation. The Opt-9 scenario achieves a well-proportioned distribution of summer and winter solar radiation, exhibits ASE values within acceptable limits, and ensures daylight access (sDA) in the interior space.

Within this framework, Opt-2 and Opt-3 scenarios can be considered the most optimal among those tested for the design optimization of PSSs on the south-facing façade of classroom B-503. These scenarios effectively brings daylight into the interior while achieving maximum daylight autonomy. An ASE value of 8% indicates that uncontrolled light entry was limited. While solar radiation incident on the window surface is relatively high, ASE remains under control, allowing for efficient and comfortable illumination. This reflects both effective solar control and a high level of natural lighting (sDA = 94.44%).

5.1.1.4. Evaluation of results of optimum perforated solar scrrens for B-501, B-502, and B-503

Optimization results, considering both KPI and design parameters, proposed the best designs for each classroom: B-501, B-502, and B-503. The KPI included summer solar radiation, winter solar radiation, annual sun exposure (ASE, %), and spatial daylight autonomy (sDA, %). Unlike conventional uniform perforated solar

screens, the perforated solar screens in this study were designed with angled slats, which provided more adaptive modulation of daylight availability and solar control.

- In rooms without shading devices, ASE values in the B-501 classroom (southeast-oriented) were higher compared to the other two rooms. Consequently, controlling ASE in B-501 was more challenging, which affected the values of other calculation parameters as well. Given that the ASE value was 11% when the south façade was completely shaded in B-501, the best scenario values for this classroom were evaluated accordingly. While the ASE threshold was considered 10% for B-502 and B-503 classrooms, a higher threshold of 20% was accepted for B-501. This condition reflects the stronger solar exposure in B-501, where angled screen configurations were particularly necessary to achieve acceptable visual and thermal comfort.
- As a result, in the optimal design, the algorithm allowed a higher amount of solar radiation on the south façade windows of the B-503 classroom (southwest-oriented), which also resulted in higher sDA values compared to the other two classrooms.
- In the south-oriented B-502 classroom, ASE values were lower, so the optimization aimed to maximize sDA values. However, since sDA was 77.78% without shading in this room (compared to 100% in the other classrooms), the best scenarios in the optimization showed sDA values below 70%. This finding indicates that in B-502, the proposed angled perforated solar screen design reduced excessive ASE effectively, but the compromise was a partial reduction in daylight autonomy.
- Examining the average solar radiation incident on the windows in the best results, the ranking from highest to lowest was B-502, B-501, and B-503 respectively. This indicates that in B-501, the algorithm minimized ASE values but this also caused a reduction in solar radiation levels. The angled PSSs contributed to this outcome by selectively blocking direct solar penetration during peak hours, thus reducing overall gains.
- Among the classrooms, the most consistent performance outcomes were observed in B-503. Here, solar radiation levels were between those of the

other two classrooms, ASE values were on average below the acceptable threshold, and the highest sDA values were achieved.

Table 5.7 Mean and standard deviation values of the best scenario calculation results for the classrooms

Class rooms		Summer Solar Radiation (kWh/m²)	Winter Solar Radiation (kWh/m²)	ASE (%)	sDA (%)
B-501	Mean	37.40	50.62	15.18	87.74
	Std.dev.	10.32	19.73	1.83	9.67
B-502	Mean	64.86	90.91	4.18	62.12
	Std.dev.	7.86	9.83	2.86	3.35
B-503	Mean	53.83	84.54	9.18	88.38
	Std.dev.	9.45	14.56	1.47	7.22

- The average sDA values in the best results are 87.74% (std. dev.: 9.6) for B-501, 62.12% (std. dev.: 3.3) for B-502, and 88.38% (std. dev.: 7.2) for B-503. The optimization algorithm for B-501 produced more extreme design options compared to the others. Despite the lower solar radiation levels in B-501, the ASE value is higher. This indicates that while solar control can be effectively managed in this room, there is a higher likelihood of unfavorable visual comfort conditions and more difficulty in controlling them. The angled design in B-501 mitigated part of this challenge, but because of the orientation, ASE is harder to manage than in B-502 and B-503.
- In B-503, the the equilibrium between ASE and sDA values is better compared to the other rooms, resulting in improved visual comfort conditions. However, in this room, scenarios that ensure an integrated control of summer and winter solar radiation levels must be identified to achieve optimal thermal comfort conditions. Here, the designed angled PSSs proved advantageous, as they provided proportional seasonal regulation of solar gain and reduced excessive sun exposure without sacrificing daylight autonomy.

- Overall, a proportional equilibrium between summer and winter solar radiation gains has been achieved. However, due to the higher solar radiation levels during both seasons in B-502 and B-503 classrooms, these rooms are more exposed to overheating risks. Therefore, especially the design of the shading device is critical for effective shading during summer months. At this point, the angled design differentiates itself from flat or uniform perforations by enabling dynamic modulation of solar entry, which reduces overheating risk without eliminating winter solar gains.

Although control is primarily aimed at the south façade, the thermal and visual comfort conditions inside the rooms are influenced by the transparency ratios of other façades. As a result, the best performing perforated soalr screens designs vary accordingly. This confirms that proposed perforated solar screens (PSS) designed with angle, by redirecting and diffusing daylight making them more adaptable than conventional designs.

Based on the results obtained from the method applied in this thesis, it has become clear that the design parameters of the PSS require specific optimization for each room. The study highlights that even if the physical properties of the rooms are identical, orientation plays a significant role. In the B-501 and B-503 classrooms (southeast and southwest oriented), the design characteristics of the PSSs on the south façade are affected by the presence of east and west façades and their transparent areas.

The angled PSS design distinguishes itself from conventional uniform systems by enabling proportional seasonal regulation—reducing excessive summer gains while still allowing sufficient winter benefits. This adaptive modulation directly contributes to improved visual and thermal comfort. The angled perforated PSS designs introduced in this study represents a novel approach compared to earlier uniform or flat designs, as it enable more effective control of excessive sun exposure, seasonal equilibrium of solar gains, and more adaptive daylight distribution across rooms.

5.1.2. Application of TOPSIS Analysis and Evaluation of Optimization Results in terms of KPI

The best scenarios obtained from the optimization were further analyzed through normalization and TOPSIS methods. The TOPSIS method is widely used in multi-criteria decision-making to identify significant differences and determine optimal solutions.

In normalization, each performance value was scaled between 0 (worst) and 1 (best), making them comparable within the same parameter (Zanakis et al., 1998). Calculations were conducted to minimize summer solar radiation, maximize winter solar radiation, minimize ASE, and maximize sDA values.

In the TOPSIS method, a weighted normalized decision matrix was created by multiplying normalized values with the weights of the KPI. Equal weighting was assigned to each KPI, with a weight of 25% each. Ideal solutions were identified, and distances to the ideal condition (Si+, Si-) were calculated. The relative closeness to the ideal solution (Ci), i.e., the TOPSIS score, was then computed. Below are the results of the equally weighted normalization analysis and TOPSIS scores.

Table 5.8 TOPSIS results for classroom B-501 (southeast orientation)

Scenario	Weighted Normalized Values				Si+	Si-	Ci*	Rank
	Solar Radiation		ASE	sDA				
	Summer	Winter						
opt-1	0.049	0.036	0.059	0.067	0.086	0.069	0.446	8
opt-2	0.044	0.048	0.064	0.062	0.076	0.073	0.492	4
opt-3	0.059	0.048	0.069	0.076	0.074	0.060	0.445	9
opt-4	0.065	0.062	0.069	0.072	0.064	0.057	0.472	7
opt-5	0.067	0.057	0.074	0.081	0.069	0.055	0.443	10
opt-6	0.073	0.070	0.074	0.076	0.060	0.056	0.482	6
opt-7	0.074	0.074	0.079	0.076	0.059	0.056	0.489	5
opt-8	0.081	0.088	0.084	0.085	0.054	0.066	0.546	2
opt-9	0.100	0.120	0.084	0.062	0.066	0.085	0.565	1
opt-10	0.112	0.117	0.089	0.085	0.074	0.084	0.531	3
opt-11	0.079	0.057	0.079	0.081	0.075	0.044	0.372	11

According to the TOPSIS analysis results, the best scenario for classroom B-501 was identified as Opt-9. However, Opt-9 has a relatively higher ASE value compared to others, and its sDA value is below 75%.

Table 5.9 TOPSIS results for classroom B-502 (south orientation)

Scenario	Weighted Normalized Values				Si+	Si-	Ci*	Rank
	Solar Radiation		ASE	sDA				
	Summer	Winter						
opt-1	0.067	0.070	0.000	0.074	0.022	0.123	0.851	1
opt-2	0.060	0.060	0.000	0.074	0.030	0.124	0.808	3
opt-3	0.069	0.072	0.015	0.074	0.025	0.108	0.811	2
opt-4	0.068	0.070	0.045	0.067	0.052	0.079	0.604	4
opt-5	0.070	0.071	0.060	0.074	0.064	0.065	0.502	5
opt-6	0.079	0.076	0.076	0.081	0.079	0.051	0.392	6
opt-7	0.072	0.074	0.076	0.074	0.078	0.051	0.392	7
opt-8	0.082	0.078	0.091	0.074	0.094	0.036	0.279	8
opt-9	0.080	0.078	0.106	0.081	0.108	0.028	0.206	10
opt-10	0.087	0.087	0.106	0.074	0.109	0.032	0.225	9
opt-11	0.089	0.089	0.121	0.081	0.124	0.032	0.204	11

For classroom B-502, the TOPSIS results indicated Opt-1 as the best scenario. The results showed that the daylighting potential of B502 is limited compared to B-501 and B-503. Therefore, given the low sDA values for this space, priority should be given to scenarios with higher sDA values.

Table 5.10 TOPSIS results for classroom B-503 (southwest orientation)

Scenario	Weighted Normalized Values				Si+	Si-	Ci*	Rank
	Solar Radiation		ASE	sDA				
	Summer	Winter						
opt-1	0.050	0.050	0.057	0.071	0.054	0.062	0.534	4
opt-2	0.070	0.070	0.065	0.080	0.039	0.050	0.561	1
opt-3	0.071	0.069	0.065	0.080	0.040	0.049	0.552	2

Table 5.10 TOPSIS results for classroom B-503 (southwest orientation) (Continued…)

Scenario	Weighted Normalized Values				Si+	Si-	Ci*	Rank
	Solar Radiation		ASE	sDA				
	Summer	Winter						
opt-4	0.069	0.069	0.065	0.076	0.040	0.048	0.548	3
opt-5	0.088	0.079	0.073	0.080	0.048	0.043	0.476	8
opt-6	0.065	0.069	0.073	0.071	0.041	0.044	0.518	6
opt-7	0.095	0.102	0.073	0.061	0.052	0.058	0.529	5
opt-8	0.088	0.083	0.081	0.080	0.050	0.042	0.461	9
opt-9	0.065	0.070	0.081	0.071	0.044	0.041	0.480	7
opt-10	0.082	0.076	0.089	0.076	0.053	0.034	0.394	11
opt-11	0.073	0.079	0.097	0.080	0.053	0.041	0.439	10

In classroom B-503, Opt-2 was ranked highest in the TOPSIS analysis, followed by Opt-3. Lower solar radiation values in B-501 and higher values in B-502 influenced the TOPSIS results due to the equal weighting applied in the calculations. In terms of summer solar gains, B-501 shows lower values compared to B-503. While western façades face a higher risk of overheating during summer, eastern façades are exposed to less thermal load in the morning. Thermal control requirements are higher on western façades during summer. Regarding winter solar gains, all three classrooms achieved high values, with B-503 reaching maximum levels, indicating a higher potential for energy efficiency during winter compared to B-502 and B-501.

Although B-503 receives more summer solar radiation than B-501, its ASE values are lower, and sDA values are higher, indicating more controlled natural daylighting. This confirms that PSSs designed at an angle can reduce direct solar penetration without compromising daylight autonomy, distinguishing them from conventional uniform and/or flat PSSs.

The average sDA values in B-503 are higher with lower standard deviation compared to B-501. This suggests that achieving a coherent integration between solar control and daylight access is more challenging in B-501 than in B-503.

The relationship between ASE and sDA concerning visual comfort is complex. Although an increase in ASE often accompanies an increase in sDA, this typically leads to more areas with excessive illumination that cause discomfort (IES LM-83-12). The optimization results for B-503 demonstrate that ASE can be controlled while maintaining high sDA levels. This outcome underscores the advantage of angled PSSs, which allow daylight distribution to be fine-tuned in ways that flat or uniform devices cannot achieve.

5.1.3. Evaluation of Optimization Results in terms of Design Parameters

When examining the dimensions of the optimal scenarios for the B-501 classroom, it is observed that the design dimensions—and consequently the perforation ratios—are quite similar. The reflection coefficient was predominantly set at 0.77. Although the results indicate similar designs in this regard, significant variations were found in the slat angles. The angles ranged from 15° to 60°, with a mean value of 32.27° and a standard deviation of 15.71.

Optimization results indicate that narrower angles in these configurations contributed to better visual comfort, better thermal comfort and more efficient daylight distribution. The results of optimum PSS designs showed that narrower angled configurations improved daylight uniformity, regulated solar radiation, and controlled sun exposure, confirming the role of angle modulation as a decisive design parameter.

Table 5.11 Design feature of the optimal scenarios for classroom B-501 (Southeast orientation)

Scenario	Angle (a)	Width (c)	Width (d)	Length (e)	Length (f)	Distance from facade (h)	Reflection coefficient (ı)	Perforation ratio
Opt-1	25	0.07	0.06	0.1	0.08	0.04	0.77	37
Opt-2	60	0.09	0.07	0.1	0.08	0.04	0.77	35
Opt-3	15	0.09	0.07	0.1	0.08	0.04	0.77	35
Opt-4	35	0.09	0.07	0.1	0.09	0.04	0.77	38
Opt-5	15	0.09	0.08	0.1	0.08	0.05	0.77	38
Opt-6	30	0.09	0.07	0.09	0.08	0.04	0.77	37
Opt-7	40	0.09	0.07	0.1	0.1	0.04	0.67	40

Table 5.21 Design feature of the optimal scenarios for classroom B-501 (Southeast orientation)(Continued…)

Scenario	Angle (a)	Width (c)	Width (d)	Length (e)	Length (f)	Distance from facade (h)	Reflection coefficient (ı)	Perforation ratio
Opt-8	20	0.07	0.05	0.1	0.09	0.04	0.77	36
Opt-9	60	0.07	0.04	0.07	0.09	0.04	0.77	38
Opt-10	30	0.08	0.07	0.1	0.1	0.04	0.77	43
Opt-11	25	0.09	0.07	0.1	0.09	0.04	0.67	38
Mean	32.27	0.08	0.07	0.10	0.09	0.04	0.75	37.80
Std dev.	15.71	0.01	0.01	0.01	0.01	0.00	0.04	2.34

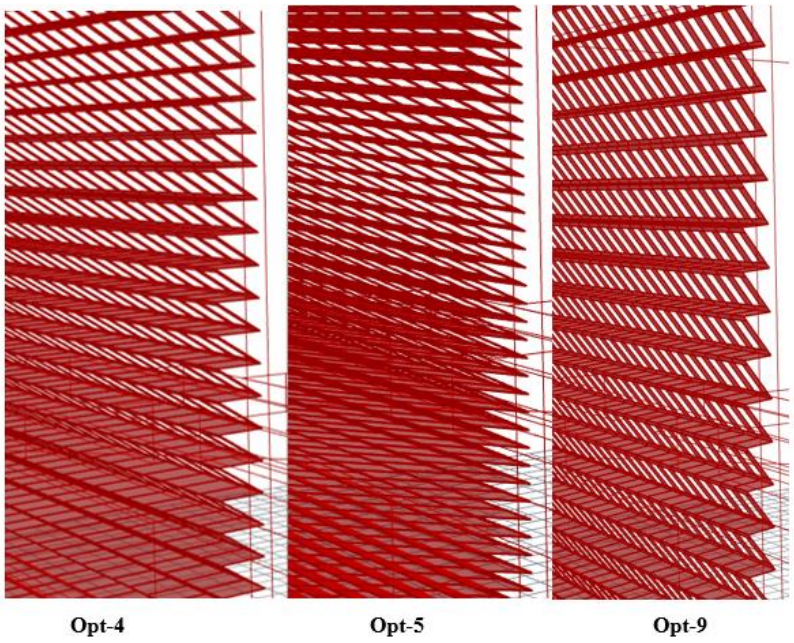

Figure 5.4 Designs of Opt-4, Opt-5, and Opt-9 Scenarios for the B-501 Classroom

Table 5.13 Design feature of the optimal scenarios for classroom B-502 (South orientation)

Scenario	Angle (a)	Width (c)	Width (d)	Length (e)	Length (f)	Distance from facade (h)	Reflection coefficient (ı)	Perforation ratio
Opt-1	40	0.1	0.09	0.09	0.1	0.06	0.67	46
Opt-2	35	0.1	0.09	0.09	0.09	0.06	0.77	44
Opt-3	40	0.1	0.09	0.08	0.09	0.04	0.77	46

Table 5.14 Design feature of the optimal scenarios for classroom B-502 (South orientation)(Continued…)

Scenario	Angle (a)	Width (c)	Width (d)	Length (e)	Length (f)	Distance from facade (h)	Reflection coefficient (ı)	Perforation ratio
Opt-4	40	0.08	0.07	0.08	0.09	0.05	0.67	45
Opt-5	40	0.08	0.07	0.08	0.09	0.07	0.77	45
Opt-6	35	0.09	0.08	0.09	0.1	0.07	0.77	46
Opt-7	40	0.1	0.09	0.08	0.09	0.07	0.77	46
Opt-8	35	0.1	0.09	0.09	0.1	0.06	0.67	46
Opt-9	35	0.1	0.09	0.09	0.1	0.07	0.77	46
Opt-10	35	0.09	0.08	0.09	0.1	0.05	0.67	46
Opt-11	35	0.1	0.09	0.09	0.1	0.05	0.77	46
Mean	37.27	0.09	0.08	0.09	0.10	0.06	0.73	45.69
Std dev.	2.61	0.01	0.01	0.01	0.01	0.01	0.05	0.77

When the dimensions of the optimal scenarios for the B-502 classroom are examined, it is observed that the design dimensions—and consequently the perforation ratios—are quite similar. The reflection coefficient was predominantly set at 0.77. In the best-performing scenarios identified for the B-502 classroom, the slat angles are also closely aligned, with an average of 37.27° and a standard deviation of 2.61. This indicates that there are no significant differences among the designs of optimal scenarios proposed for the B-502 classroom. The relative homogeneity of angles in B-502 illustrates that, for south-facing façades, performance is less sensitive to angle variability, yet the angled approach still provides subtle advantages by moderating seasonal solar radiation. The results indicate that the angle became a more critical factor in B-501 and B-503 than in B-502.

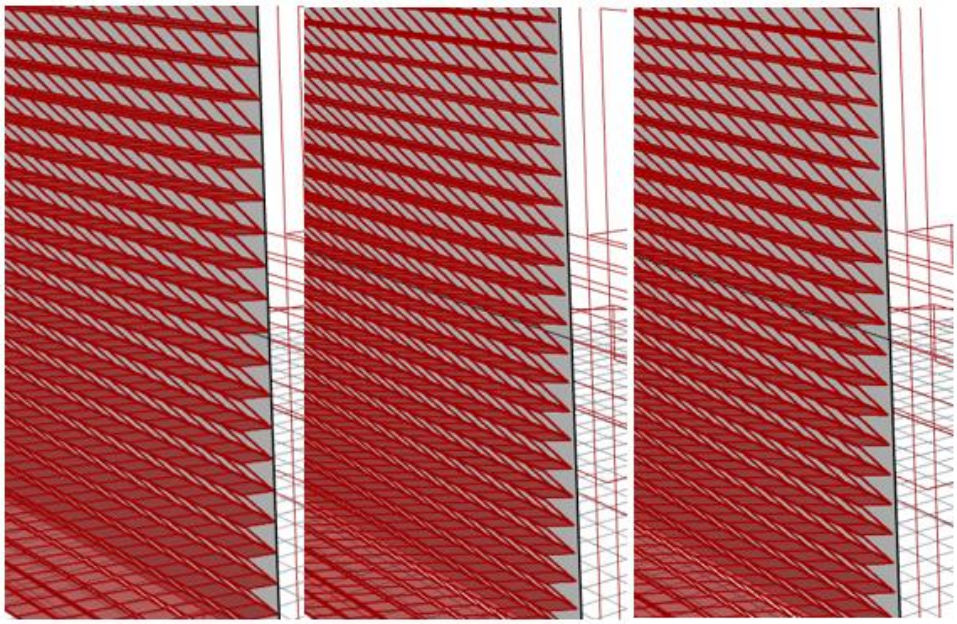

Figure 5.5 Designs of Opt-2, Opt-6, and Opt-9 Scenarios for the B-502 Classroom

Table 5.15 Design feature of the optimal scenarios for classroom B-503 (Southwest orientation)

Scenario	Angle (a)	Width (c)	Width (d)	Length (e)	Length (f)	Distance from facade (h)	Reflection coefficient (ı)	Perforation ratio
Opt-1	30	0.09	0.07	0.08	0.07	0.07	0.77	36
Opt-2	20	0.1	0.09	0.1	0.09	0.05	0.77	41
Opt-3	20	0.09	0.08	0.1	0.09	0.04	0.77	41
Opt-4	20	0.09	0.08	0.1	0.09	0.05	0.77	41
Opt-5	30	0.1	0.09	0.09	0.09	0.08	0.77	44
Opt-6	20	0.09	0.07	0.08	0.07	0.05	0.77	36
Opt-7	60	0.09	0.07	0.07	0.09	0.04	0.47	45
Opt-8	35	0.1	0.09	0.07	0.07	0.04	0.77	43
Opt-9	20	0.1	0.08	0.08	0.07	0.04	0.77	37
Opt-10	40	0.07	0.06	0.08	0.09	0.04	0.67	45
Opt-11	20	0.1	0.09	0.08	0.07	0.04	0.77	40
Mean	28.64	0.09	0.08	0.08	0.08	0.05	0.73	40.84
Std dev.	12.67	0.01	0.01	0.01	0.01	0.01	0.09	3.15

When the dimensions of the optimal scenarios for the B-503 classroom are examined, it is observed that the design dimensions—and consequently the perforation ratios—are quite similar. The reflection coefficient was predominantly defined as 0.77. Although the results appear to reflect similar design characteristics, there are significant differences in the slat angles. The angles range from 20° to 60°, with an average of 28.64° and a standard deviation of 12.67.

The 20° angle represents the most frequently selected angle. The optimization results also demonstrate that 20° angled PSS is effective in controlling solar radiation and maximizing daylight autonomy while keeping ASE within acceptable limits.

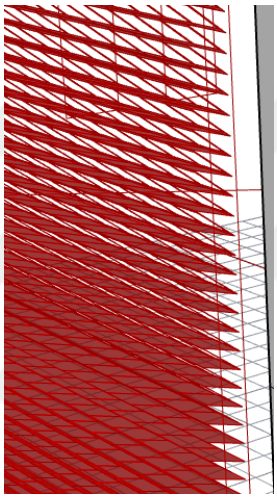

Figure 5.6 Designs of Opt-2 Scenarios for the B-503 Classroom

In general, the angles determined in the scenarios ranged between 15° and 60°. These values correspond to configurations where the solid portion of the PSS is nearly parallel to the horizontal plane, enabling increased penetration of indirect solar radiation into the interior space. This design approach is fundamentally different from previous uniform or/and flat PSSs, since the angled design allows daylight redirection and selective control of solar penetration depending on seasonal needs.

In the B-502 classroom, the perforation ratio is higher compared to B-501 and B-503, and the angles are closer to being parallel with the horizontal (y) plane. This is attributed to the fact that even without a shading device, the sDA values in B-502 were relatively low. Therefore, when a PSS is added, the design aims to maximize

the perforation ratio to allow maximum daylight penetration while still mitigating unwanted thermal heat gains. This again confirms that in classrooms, especially with lower baseline daylight autonomy without shading, the shading design should be prioritized, and still angle is important, whereas in rooms more exposed to solar asymmetry (like B-501 and B-503), angle adjustments play a larger role.

The formation of an angle nearly parallel to the horizontal plane allows for the penetration of indirect solar radiation into the interior, while undesirable direct solar gains during the summer are effectively blocked. This feature underscores the distinctive advantage of angled PSS, which simultaneously enables daylight enhancement and solar protection—functions not equally achievable with conventional uniform PSS designs.

5.1.4. Evaluation of Optimization Results in terms of PMV

The Predicted Mean Vote (PMV) index was employed to evaluate thermal comfort conditions across the three classrooms (B-501, B-502, and B-503). According to ASHRAE 55 (2020) and ISO 7730 (2005), indoor environments are considered thermally comfortable when PMV values remain within the range of –0.5 to +0.5, corresponding to a Predicted Percentage Dissatisfied (PPD) below 10%. Values outside this band indicate deviations from optimal comfort, with higher PMV scores reflecting warm discomfort due to increased heat gain. The PMV results of optimal scenarios is presented in Table 5.14.

Table 5.14 PMV results of the optimal scenarios for three classrooms

Scenario	B-501	B-502	B-503
Unshaded window	1.42	1.84	1.447
Fully shaded window	1.12	1.46	1.15
Opt-1	1.15	1.449	1.16
Opt-2	1.145	1.451	1.147
Opt-3	1.149	1.46	1.147
Opt-4	1.129	1.454	1.148
Opt-5	1.146	1.449	1.153
Opt-6	1.1297	1.45	1.147
Opt-7	1.144	1.453	1.18
Opt-8	1.149	1.45	1.16

Table 5.14 PMV results of the optimal scenarios for three classrooms (Continued…)

Scenario	B-501	B-502	B-503
Opt-9	1.133	1.452	1.14
Opt-10	1.151	1.455	1.17
Opt-11	1.136	1.456	1.145

In the table 5.14, the unshaded window represents the base case for maximum solar heat gain and daylight penetration, and the fully shaded window represents using an opaque exterior device.

In the unshaded window scenarios, PMV values were found to be well above the recommended range, reaching 1.42 in B-501, 1.84 in B-502, and 1.447 in B-503. These values confirm that unshaded façades are exposed to excessive solar heat gain, resulting in significant thermal discomfort and a high likelihood of user dissatisfaction. Conversely, the fully shaded window consistently produced lower PMV values (1.12 in B-501, 1.46 in B-502, and 1.15 in B-503), representing the maximum reduction in thermal load achievable through complete shading. This indicates that full coverage minimizes solar radiation and reduces overheating risk. However, such configurations simultaneously block daylight penetration, compromising visual comfort and daylight autonomy.

The optimized perforated shading scenarios yielded PMV values that consistently fell between the fully shaded and unshaded cases. Across all classrooms, optimized designs demonstrated incremental improvements in thermal comfort, lowering PMV values relative to the unshaded window case.

The optimized cases show relatively small variation across different configurations, with PMV values generally within narrow bands (approximately 1.129–1.151 in B-501, 1.449–1.456 in B-502, and 1.14–1.18 in B-503). This suggests that once shading is introduced, incremental adjustments in geometry lead to marginal but consistent improvements rather than radical shifts in thermal comfort. Importantly, even though the reductions do not bring PMV into the ASHRAE/ISO comfort range, they represent a measurable improvement over the unshaded case, highlighting the potential of perforated angled screens to reduce solar heat gain.

In B-501 and B-503, the reductions in PMV were more noticeable, indicating that angled perforated devices effectively moderated solar gains on southeast- and southwest-oriented classrooms. B-502 exhibited higher PMV values across all optimized cases (around 1.45), suggesting that the strictly south-facing orientation remained more susceptible to thermal loading even with optimized designs.

While none of the optimized scenarios achieved PMV values within the strict comfort band (–0.5 to +0.5), the observed reductions compared to the unshaded case underscore the effectiveness of perforated shading devices in attenuating solar heat gain and shifting indoor conditions toward improved comfort. Importantly, the consistent reduction across multiple classrooms demonstrates the adaptability of angled perforated geometries in responding to different orientations.

Overall, the PMV results confirm that shading plays a critical role in reducing excessive solar gains and limiting thermal discomfort in Istanbul's mixed climate. Although indoor conditions remained slightly warm relative to the ASHRAE 55 and ISO 7730 thresholds, the perforated shading devices represent a substantial improvement over unshaded conditions and contribute meaningfully to energy-efficient façade performance.

6
DISCUSSION

The optimization of PSSs has been widely studied for their role in improving daylight quality and reducing thermal loads. While prior research largely focused on uniform/flat or static perforation designs (Reinhart & Wienold, 2011; Heidari & Sharples, 2020), this study introduces angled perforations as a novel strategy. By evaluating classrooms with different orientations through multi-criteria methods, the findings show that angled geometries significantly enhance visual and thermal performance, offering passive adaptability that conventional designs cannot achieve.

The findings of this study highlight the significance of orientation of rooms, geometric configuration of PSS, and multi-criteria evaluation methods in determining the performance of PSS. Across the three classrooms examined (B-501, B-502, and B-503), the optimization results revealed that while reflection coefficients and perforation ratios remained relatively consistent, the angle of the perforated shadings emerged as the most decisive factor in reconciling visual and thermal comfort. This outcome confirms earlier findings that emphasized the need for solar control in classroom design (Reinhart & Wienold, 2011; Heidari & Sharples, 2020), yet it extends the discussion by demonstrating that angled perforations, unlike conventional flat or uniform perforated designs, enable more adaptive modulation of solar gains. The range of optimal angles observed (15–60°) shows that angle adjustments are not only critical for reducing excessive daylight can result glare and managing illuminance levels but also for providing seasonal flexibility by enhancing winter solar gains while preventing excessive summer overheating.

A consistent pattern across the results was the complex relationship between annual sun exposure (ASE) and spatial daylight autonomy (sDA). While literature indicates that increases in sDA often coincide with higher ASE, which can lead to discomfort (IES LM-83-12), this study demonstrated that angled perforations can decouple this relationship by redirecting daylight deeper into the space. For example, scenarios in B-503 achieved both high sDA values (>94%) and controlled ASE (~8%), illustrating that angled designs provide opportunities for glare control without reducing daylight availability. These results echo recent work on dynamic and adaptive shading (Abdelhamid et al., 2024), although in contrast to mechanically adjustable systems, the angled perforated screens examined here achieve comparable outcomes through passive geometric modulation (fixed). In this regard, the study demonstrates a practical advancement by offering a non-mechanical, static solution that nonetheless exhibits adaptive behavior.

In parallel, the PMV analysis confirmed that while unshaded cases exhibited values far above the ASHRAE 55 and ISO 7730 comfort thresholds (e.g., 1.42 in B-501, 1.84 in B-502), optimized perforated designs consistently reduced PMV values toward more tolerable levels (e.g., ~1.13–1.15 in B-501 and B-503). This outcome highlights a critical performance trade-off also discussed in the literature: opaque shading systems may achieve the lowest PMV values by eliminating solar heat gain (Cho et al., 2014), but they simultaneously suppress daylight, thereby reducing sDA and negatively impacting visual comfort. By contrast, optimized angled PSS designs in this study limited radiant heat gains while preserving daylight access—confirming arguments by Tzempelikos (2010) and Huang & Zhai (2020) that shading strategies must integrate thermal and daylighting criteria rather than prioritizing one at the expense of the other.

Orientation was another determining factor in shaping optimization outcomes. In B-501 (southeast-oriented), reducing ASE proved more challenging due to strong morning exposure, whereas in B-503 (southwest-oriented), the angled perforations provided an effective reconciliation between high winter gains and controlled afternoon overheating. By contrast, B-502 (south-oriented) was characterized by relatively low baseline daylight autonomy, and thus the optimization favored higher perforation ratios to maximize daylight penetration. These results align with prior

studies that identified orientation as a primary variable in determining façade performance (Blanco et al., 2019; Chi et al., 2021), yet the present research shows that angled perforations offer the adaptability required to address orientation-specific challenges in ways that uniform designs cannot achieve.

The PMV patterns supported this interpretation: reductions were more substantial in B-501 and B-503, while B-502 remained thermally stressed at ~1.45 even under optimized conditions. This finding reflects prior work noting that south-facing façades are particularly vulnerable to direct solar load in Mediterranean climates (Marino et al., 2017), yet also shows that angled perforated solar screen (PSS) designed in this thesis can still moderate discomfort while ensuring daylight autonomy.

The use of the TOPSIS method further enriched the evaluation of results by providing a quantitative decision-making framework. However, some discrepancies emerged between subjective evaluations and TOPSIS rankings, especially in B-501, where scenarios preferred for their harmonized ASE and sDA performance ranked lower due to the weighting of solar radiation gains. This reflects earlier concerns regarding the sensitivity of multi-criteria methods to weighting assumptions (Gaber et al., 2025). Nevertheless, the application of TOPSIS in this study confirmed that angled perforations performed consistently well across conflicting indicators, reinforcing their robustness as a design strategy. Moreover, it underscores the necessity of complementing simulation-based qualitative assessments with structured decision-making methods to capture interrelations across thermal and visual domains.

Overall, this study contributes to the literature on perforated systems by demonstrating that angled PSS designs, as a novel configuration, offer advantages over conventional uniform/flat perforated or double-skin systems (Huang et al., 2024; El-Bahrawy et al., 2025). Unlike previous studies that addressed thermal and visual comfort separately (Srisamranrungruang & Hiyama, 2020, 2021; Chi et al., 2021), the results here showed that angled PSS can achieve both within a single optimization framework. Even though strict thermal comfort thresholds (PMV –0.5 to +0.5) were not reached, the optimized designs shifted conditions significantly closer to acceptable levels while simultaneously improving daylight metrics.

Furthermore, by explicitly linking design parameters such as angle and perforation ratio to performance indicators, the study provides new evidence that optimization of PSSs must move beyond static design assumptions and incorporate orientation, seasonal variation, and geometric modulation into a holistic approach. In this respect, the angled PSS design proposed here represents both a methodological and practical advancement, bridging gaps in existing literature while offering a viable strategy for improving visual and thermal comfort.

7
CONCLUSION

Previous studies have confirmed that parametric optimization, considering façade orientation and daylighting effects in shading device design, is effective in enhancing both visual and thermal comfort (Reinhart & Andersen, 2006). The orientation-specific optimization and design of shading devices are critical for building energy performance and indoor comfort (Reinhart & Walkenhorst, 2001; Tzempelikos & Athienitis, 2007). However, the interrelationship between orientations has not been thoroughly examined—for instance, how the design of a shading device on the south façade of a southwest-oriented space might be influenced by the adjacent west façade. Additionally, previous studies have not specifically addressed perforated shading devices with angled geometries, which this study positions as a novel design strategy.

The primary aim of this study is to present a systematic method that integrates environmental performance metrics with parametric design flexibility, with the objective of ensuring thermal and visual comfort conditions in indoor environments. Unlike conventional studies focusing on static or uniform perforations, this research emphasizes angled PSSs as an innovative solution capable of providing adaptive daylight modulation and seasonal solar control. In this context, the method enables parametric variation of angle, perforation ratio, and reflection coefficient, thereby capturing the adaptive potential of angled geometries. The applicability of the proposed method was tested in existing indoor spaces, and the most appropriate PSS designs for these spaces were identified.

Thermal and visual comfort-based optimization was conducted for PSS intended for the south façade of spaces with different orientations, incorporating design parameters. Multi-objective optimization was conducted by evaluating KPI including summer and winter solar radiation, Annual Sun Exposure (ASE), and Spatial Daylight Autonomy (sDA). Both simulation-based performance assessments and a TOPSIS-based multi-criteria decision analysis were applied to identify the best-performing scenarios and subsequent simulation-based performance assessments were applied to determine PMV. The workflow integrates parametric simulation with decision-support analysis, allowing systematic comparison of angled shading alternatives under varying orientation and seasonal conditions. This dual approach not only validated the optimization results but also highlighted the robustness of angled geometries in consistently achieving proportional seasonal equilibrium.

As an application of the method developed in this thesis, this study aimed to determine the optimal design parameters of PSS for three classrooms with different orientations—B-501 (southeast-oriented), B-502 (south-oriented), and B-503 (southwest-oriented)—based on thermal and visual comfort metrics. The southeast (B-501) and southwest (B-503) oriented classrooms share identical physical properties, except for orientation. These two cases have additional façades with transparent surfaces—east for the southeast-oriented space and west for the southwest-oriented one. The third classroom (B502), oriented strictly south, has transparency only on the south façade.

- A key contribution distinguishing this study from previous works is the optimization of PSS designs exclusively for south façades in southeast-, southwest-, and south-oriented spaces, enabling the identification of orientation-specific variations. The transparency ratio is 60% on the south façade, whereas it is only 11.5% on the east and west façades. Despite uniform physical conditions and the relatively low transparency ratio on the east and west façades, both orientation and façade transparency significantly influenced the design optimized for the south façade. Even when designing a PSS for a façade with the same orientation and transparency ratio, the spatial orientation and the presence of transparent surfaces on adjacent

façades influenced the indoor thermal and visual comfort, and thus the PSS design.

The results reveal that although the design targets the south façade, the presence of east and west façades in the space significantly alters the optimal shading solution and performance outcomes. A single optimal scenario could not be identified for both orientations; instead, the adoption of different strategies based on specific design priorities (e.g., thermal comfort versus daylight access) is necessary. Hence, integrated optimization approaches that evaluate visual and thermal comfort simultaneously are recommended for a holistic assessment.

This study demonstrated that the optimization of PSSs requires explicit integration of angled geometries with orientation and seasonal solar gain analysis. Across the three classrooms analyzed (B-501, B-502, and B-503), results indicated that while perforation ratio and reflection coefficient remained relatively stable, slat angle was the most decisive parameter in determining both thermal and visual performance. Narrower angles supported higher daylight autonomy and improved solar control, whereas wider angles increased solar radiation levels but often resulted in higher ASE values.

- The results revealed that orientation plays a critical role in determining the effectiveness of shading strategies. In B-501, although the received solar radiation was lower compared to the other classrooms, ASE values were higher, making glare control more challenging. Consequently, this space exhibited a more complex relationship between solar gain control and visual comfort, and the optimization algorithm produced more extreme design solutions. The average sDA in B-501 was 87.74%, but the standard deviation was relatively high (9.6), indicating greater variability in performance outcomes. In contrast, B-503 achieved better consistency, with an average sDA of 88.38% and a lower standard deviation (7.2), and with ASE values kept well within acceptable limits, reflecting coherent integration in daylighting quality and thermal performance.
- In B-502, due to the relatively low base sDA values observed even without shading, the design optimization tended to favor higher transparency ratios and shading angles closer to horizontal to maximize daylight penetration.

Here, the optimization scenarios showed less variation in angle and geometry, with shading angles averaging around 37.27°, and standard deviation of only 2.61, indicating more uniform design outcomes. The PSSs aimed to allow maximum useful daylight while mitigating overheating risks in summer. This further demonstrates that angled geometries can be flexibly tuned to address deficiencies in baseline daylight conditions.

- Across all classrooms, the angle of the perforated shadings varied between 15° and 60°, with many optimal designs forming shallow angles parallel to the horizontal plane. This configuration allowed for effective control of direct solar radiation while enhancing diffuse daylight entry, thereby contributing to improved visual comfort and reduced cooling loads. Such angled configurations distinguish the proposed design from previous flat perforation systems, functioning as passive modulation devices that provide seasonal adaptability.
- TOPSIS analysis was used to provide an objective ranking of optimal scenarios based on equally weighted performance criteria. While results in B-503 aligned with the simulation-based evaluation, differences emerged in B-501 and B-502. The differences between evaluation and TOPSIS highlight the sensitivity of decision-making outcomes to the weighting of KPI, and suggest the need to customize weighting schemes depending on design priorities. Nevertheless, across all weighting configurations, angled perforated designs consistently demonstrated proportional seasonal equilibrium, reinforcing their robustness.

The comparative evaluation of optimization and TOPSIS analysis further revealed that angled PSS consistently achieved a coherent seasonal performance—maximizing winter heat gains while minimizing summer overheating. This advancement distinguishes angled PSS from conventional uniform or flat perforated shading systems, positioning them as an effective passive strategy for mitigation of excessive solar radiation, daylight redirection, and seasonal visual and thermal comfort.

- Thermal analysis showed that in all classrooms, achieving a proportional distribution between summer and winter solar gains was essential. While

higher winter solar radiation supports passive heating, excessive summer radiation can lead to overheating. B-503 exhibited the most well-moderated solar gain profile, while B-502 showed the highest winter solar gain, and B-501 the lowest. In all three cases, optimal scenarios presented significant seasonal variation, but efforts to control ASE often led to reductions in total solar gain.

Finally, the PMV analysis—conducted through simulations after optimization—confirmed the thermal comfort implications of shading. In unshaded cases, PMV values were significantly above the recommended range, reflecting severe warm discomfort. Fully shaded windows lowered PMV values but simultaneously blocked daylight, reducing visual comfort. Optimized perforated designs consistently achieved intermediate values, demonstrating measurable reductions in solar heat gain while preserving daylight access. Although none of the scenarios reached the strict thermal comfort band (–0.5 to +0.5), the optimized cases shifted indoor conditions closer to tolerable levels. This highlights that angled PSSs act as effective dual-performance devices, reducing thermal discomfort compared to unshaded façades while maintaining daylight autonomy.

Moreover, orientation-specific optimization emphasized the decisive role of angled geometries: in southeast- and southwest-oriented classrooms, angle variability was critical to managing asymmetric solar exposure, while in the south-oriented classroom, higher perforation ratios were prioritized to compensate for lower baseline daylight autonomy. This underscores that current solutions are insufficient, and angled geometries like those proposed in this thesis provide the adaptability necessary for orientation-specific shading design.

- Overall, the findings suggest that orientation, façade transparency, and environmental context must be considered simultaneously in the shading design process. Even with similar spatial configurations, each classroom required different strategies to achieve thermal and visual comfort. While B-503 exhibited the most coherent and favorable performance, B-501 and

B-502 required more nuanced optimization due to their respective solar exposure characteristics.

- This research demonstrates the value of combining parametric modeling with multi-criteria decision-making in developing high-performance, climate-responsive, and user-centered shading solutions. It also underscores the importance of integrating architectural intent with simulation-based evidence in order to arrive at designs that are both environmentally efficient and conducive to occupant well-being.

Overall, this study contributes to the literature by providing empirical evidence that angled PSSs can simultaneously reconcile thermal and visual comfort within a single optimization and simulation framework, offering a practical, passive, and adaptable approach to façade design. Through this framework, the best-performing PSSs were identified, ensuring sufficient daylight illuminance indoors, improving visual comfort, and moderating seasonal solar heat gains to support thermal comfort.

Nevertheless, certain limitations should be acknowledged. The evaluation relied on a selected set of key performance indicators (KPIs) derived from international standards and literature (e.g., ASE, sDA, solar radiation, and simulated PMV), while additional criteria such as view out and glare were not explicitly considered. Moreover, the simulations were applied to classrooms within a specific climatic and geographic context, which limits the generalizability of the findings.

By implementing the proposed method, this study also makes a further contribution by conducting separate optimizations for three classrooms with similar physical characteristics but different orientations (south, southwest, and southeast), thereby highlighting how orientation-specific differences affect performance outcomes. The methodological framework developed in this thesis is therefore broadly applicable not only to façades with varying orientation and transparency but also to diverse building types and climatic conditions, extending its relevance beyond PSSs to the design and optimization of shading devices of multiple forms.

For future studies, several directions can be suggested. Future research should build on these findings by validating the proposed methodology in real-world case studies

and by testing its applicability across different building functions, orientations, latitudes, and façade configurations. Future studies can also expand the set of KPIs by incorporating additional indicators from standards, such as view out and glare, and even extending the framework to include acoustic comfort, to provide a more comprehensive evaluation of comfort conditions. Furthermore, hybrid strategies that combine angled PSSs with dynamic control mechanisms may be explored to enhance adaptability under variable climatic conditions. In addition, the angled design provides opportunities for integration with photovoltaic (PV) systems, and future research could examine PSS–PV hybrid solutions by coupling comfort-related performance with energy consumption analysis. Finally, the effectiveness of the proposed design can be further assessed by implementing the PSS in real building environments to determine performance under actual operating conditions.

REFERENCES

Abdelhamid, F. M., Serag, E. M., Abou Eleinen, O., & Noaman, A. (2024). The effect of parametric patterned façade variations on daylight quality, visual comfort and daylight performance in architecture studio-based tutoring. Journal of Daylighting, 11(3), 173–186.

Acuner, E. (2013). Binalarda Enerji Verimliliği. Erişim tarihi: 2019. http://eski.emhk.itu.edu.tr/%5Cimg%5Cemhk%5Cdatafiles/Ebru%20ACUNER%20-%20Binalarda%20Enerji%20Verimlili%C4%9Fi.pdf

Alawadhi, E. M. (2018). Double solar screens for window to control sunlight in Kuwait. Building and Environment, 144, 392–401. https://doi.org/10.1016/j.buildenv.2018.08.010

Allab, Y., Pellegrino, M., Guo, X., Nefzaoui, E., & Kindinis, A. (2016). Energy and comfort assessment in educational building: Case study in a French university campus. Energy and Buildings. https://doi.org/10.1016/j.enbuild.2016.11.028

ANSI/ASHRAE Standard 62.1 (2007). Ventilation for Acceptable Indoor Air Quality. https://www.mintie.com/assets/pdf/education/ASHRAE%2062.1-2007.pdf

ANSI/IES LM-83-12 (2012). Approved Method: IES Spatial Daylight Autonomy (sDA) and Annual Sunlight Exposure (ASE). https://webstore.ansi.org/preview-pages/IESNA/preview_IES%2BLM-83-12.pdf

ASHRAE 55, (2020). ANSI/ASHRAE Standard 55-2020. Thermal environmental conditions for human occupancy. American Society of Heating, Refrigerating and Air-Conditioning Engineers (ASHRAE).

ASHRAE 14, (2014). ANSI/ASHRAE Standard 14-2014. Measurement of energy, demand, and water savings. American Society of Heating, Refrigerating and Air-Conditioning Engineers (ASHRAE).

Arens, E., Hoyt, T., Zhou, X., Huang, L., Zhang, H., & Schiavon, S. (2015). Modeling the comfort effects of short-wave solar radiation indoors. Building and Environment, 88, 3–9. https://doi.org/10.1016/j.buildenv.2014.09.004

Atzeri, A., Cappelletti, F., Gasparella, A., Shen, H., & Tzempelikos, A. (2014). Assessment of long-term visual and thermal comfort and energy performance in open-space offices with different shading devices. In 3rd International High Performance Buildings Conference at Purdue.

Attia, S., Hensen, J. L. M., Beltrán, L., & De Herde, A. (2012). Selection criteria for building performance simulation tools: contrasting architects' and engineers' needs. Journal of Building Performance Simulation, 5(3), 155–169. https://doi.org/10.1080/19401493.2010.531751

A. J., & Arastech, D. (2006). Window-related Energy Consumption in the US Residential and Commercial Building Stock. Lawrence Berkeley National Laboratory (LBNL), Berkeley, CA.

Bakó-Biró, Z., Clements-Croome, D. J., Kochhar, N., Awbi, H. B., & Williams, M. J. (2012).

Ventilation rates in schools and pupils' performance. Building and Environment, 48, 215–223. https://doi.org/10.1016/j.buildenv.2011.08.018

Bakmohammadi, P., & Noorzai, E. (2020). Optimization of the design of the primary school classrooms in terms of energy and daylight performance considering occupants' thermal and visual comfort. Energy Reports, 6, 1590–1607. https://doi.org/10.1016/j.egyr.2020.09.011

Balanlı, A., & Taygun, G. T. (2005). Yapı Biyolojisi ve Asbest. Mimar.İst, 16, 107–110.

Barbhuiya, S., & Barbhuiya, S. (2013). Thermal comfort and energy consumption in a UK educational building. Building and Environment, 68, 1–11. https://doi.org/10.1016/j.buildenv.2013.06.002

Bellia, L., Marino, C., Minichiello, F., & Pedace, A. (2014). An overview on solar shading systems for buildings. Energy Procedia, 62, 309–317. https://doi.org/10.1016/j.egypro.2014.12.392

Bianchi, S., Andriotis, C., Klein, T., & Overend, M. (2024). Multi-criteria design methods in façade engineering: State-of-the-art and future trends. Building and Environment, 250, 111184. https://doi.org/10.1016/j.buildenv.2024.111184

Bingür, S., & Çakır Kıasif, G. (2018). Çevresel, Sosyal ve Ekonomik Bağlamda Akıllı Cephe Sistemlerinin Sürdürülebilir Kalkınmaya Etkileri. Haliç Üniversitesi Fen Bilimleri Dergisi, 1, 63–98.

Boyce, P., Hunter, C., & Howlett, O. (2003). The Benefits of Daylight through Windows. Lighting Research Center - Rensselaer Polytechnic Institute, Troy, New York.

Brembilla, E., Chi, D. A., Hopfe, C. J., & Mardaljevic, J. (2019). Evaluation of climate-based daylighting techniques for complex fenestration and shading systems. Energy and Buildings, 109454. https://doi.org/10.1016/j.enbuild.2019.109454

Bulgurcu, H. (2018). Havalandırma ve İç Hava Kalitesi. Bölüm 1. http://deneysan.com/Content/images/documents/havalandirma-1_46167331.pdf

CEN (2021). European Committee for Standardization. (2021). EN 17037:2018+A1:2021 Daylight in buildings (EN 17037:2018+A1:2021). Brussels: CEN.

CEN Standard EN15251 (2007). Indoor environmental input parameters for design and assessment of energy performance of buildings addressing indoor air quality, thermal environment, lighting and acoustics. Brussels, Belgium.

Chandra, M. (2003). Computation of solar radiation and heat transmission properties of glass for use in buildings. Architectural Science Review, 46(2), 175–186.

Chen, T., & Tan, L. (2025). Multiobjective optimization of external shading for west-facing university dormitories in Kunming considering solar radiation and daylighting. Scientific Reports, 15, 21876. https://doi.org/10.1038/s41598-025-04465-8

ÇED kurum görüşü hazırlama (2013). T.C. Orman ve Su Bakanlığı Meteoroloji Genel Müdürlüğü. http://www.mgm.gov.tr/FILES/arastirma/cevre/ced-kurumgorusu.pdf

Chi, D. A., Moreno-Rangel, D., & Navarro, J. (2017). Design optimisation of perforated solar façades in order to balance daylighting with thermal performance. Building and Environment, 125, 383–400. https://doi.org/10.1016/j.buildenv.2017.09.007

Chi, D. A., Moreno-Rangel, D., & Navarro, J. (2019). A comprehensive evaluation of perforated façades for daylighting and solar shading performance: Effects of matrix, thickness and separation distance. Journal of Daylighting, 6(2), 97–111. https://doi.org/10.15627/jd.2019.10

Chi, D. A., Moreno-Rangel, D., & Navarro, J. (2021). Impact of perforated solar screens on daylight availability and low energy use in offices. Advances in Building Energy Research, 15(1), 117–141. https://doi.org/10.1080/17512549.2018.1550439

Chi, D. A., Moreno-Rangel, D., Esquivias, P. M., & Navarro, J. (2016). Optimization method for

perforated solar screen design to improve daylighting using orthogonal arrays and climate-based daylight modelling. Journal of Building Performance Simulation, 10(2), 144–160. https://doi.org/10.1080/19401493.2016.1197969

Chi Pool, D. A. (2019). A comprehensive evaluation of perforated façades for daylighting and solar shading performance: Effects of matrix, thickness and separation distance. Journal of Daylighting, 6, 97–111. http://dx.doi.org/10.15627/jd.2019.10

Cho, J., Yoo, C., & Kim, Y. (2014). Viability of exterior shading devices for high-rise residential buildings: Case study for cooling energy saving and economic feasibility analysis. Energy and Buildings, 82, 771–785. https://doi.org/10.1016/j.enbuild.2014.07.092

Chlela, F., Husaunndee, A., Inard, C., & Riederer, P. (2009). A new methodology for the design of low energy buildings. Energy and Buildings, 41(9), 982–990. https://doi.org/10.1016/j.enbuild.2009.05.001

Daisey, J. M., Angell, W. J., & Apte, M. G. (2003). Indoor air quality, ventilation and health symptoms in schools: An analysis of existing information. Indoor Air, 13, 53–64. https://doi.org/10.1034/j.1600-0668.2003.00153.x

Daneshi, H., et al. (2022). Development of a hybrid machine-learning and optimization tool for performance-based solar shading design. arXiv. https://doi.org/10.48550/arXiv.2201.03028

David, M., Donn, M., Garde, F., & Lenoir, A. (2011). Assessment of the thermal and visual efficiency of solar shades. Building and Environment, 46(7), 1489–1496. https://doi.org/10.1016/j.buildenv.2011.01.022

Directive 2010/31/EU of the European Parliament and of the Council of 19 May 2010 on the Energy Performance of Buildings (Recast). Official Journal of the European Union.

El-Bahrawy, A. M. F., Elsayed, M. S., & Abdou, A. I. (2025). Balancing the parameters of perforated solar screens to optimize daylight and glare performance in office buildings. Journal of Daylighting, 12, 167.

Elsiana, F., Yuliani, N., Khotimah, N. H., et al. (2024). Daylighting evaluation of perforated screen façade with light shelf in the tropics. Dimensi: Journal of Architecture and Built Environment, 51(1), 39–48.

Enerji Verimliliği Kanunu. (2011). http://www.eie.gov.tr/verimlilik/document/EnVerKanunu_Mayis2011.pdf

Es, K. C., & Girgin, Z. C. (2018). Atmosferik korozyona dayanıklı çelik cephe panellerinin çevresel koşullar açısından değerlendirilmesi. 9. Ulusal Çatı & Cephe Konferansı, 12–13 Nisan 2018.

Eşsiz Ö.,Ekinci S., (2004), Metal Cephe kaplamalarının Dünden Bugüne Gelişimi, 1.Ulusal Çatı&Cephe Kaplamalarında Çağdaş Malzeme ve Teknolojileri Sempozyumu.

EU Directive on the energy performance of buildings (2002/91/EC). Energy Saving Trust, briefing note, 2006.

Freewan, A. A. Y. (2014). Impact of external shading devices on thermal and daylighting performance of offices in hot climate regions. Solar Energy, 102, 14–30.

Franek, L., & Jiang, X. (2013). Orthogonal design of experiments for parameter learning in image segmentation. Signal Processing, 93(6), 1694–1704. https://doi.org/10.1016/j.sigpro.2012.08.016

Futrell, B. J., Ozelkan, E. C., & Brentrup, D. (2015a). Bi-objective optimization of building enclosure design for thermal and lighting performance. Building and Environment, 92, 591–602.

Futrell, B. J., Ozelkan, E. C., & Brentrup, D. (2015b). Optimizing complex building design for annual daylighting performance and evaluation of optimization algorithms. Energy and

Buildings, 92, 234–245.

Gadelhak, M. (2013). Integrating computational and building performance simulation techniques for optimized facade designs. In International eCAADe Conference, 2, 261–270.

Gaber, B., Zhan, C., Han, X., Omar, M., & Li, G. (2025). Enhancing daylight and energy efficiency in hot climate regions with a perforated shading system using a hybrid approach considering different case studies. Buildings, 15(6), 988.

Geetha, N. B., & Velraj, R. (2012). Passive cooling methods for energy efficient buildings with and without thermal energy storage – A review. Energy Education Science and Technology Part A: Energy Science and Research, 29(2), 913–946.

Gong, X., Akashi, Y., & Sumiyoshi, D. (2012). Optimization of passive design measures for residential buildings in different Chinese areas. Building and Environment, 58, 46–57.

Grondzik, W. T., & Kwok, A. G. (2010). Mechanical and electrical equipment for buildings. John Wiley & Sons.

Harris, C. M. (2006). Dictionary of Architecture and Construction (4th ed.). McGraw-Hill.

Heidari, A., Taghipour, M., & Yarmahmoodi, Z. (2021). The effect of fixed external shading devices on daylighting and thermal comfort in residential building. Journal of Daylighting, 8(2), 165–180. https://doi.org/10.15627/jd.2021.15

Heschong, L. (2011). Daylight Metrics PIER Daylighting Plus Research Program Technical Report. California Energy Commission.

Hong, T., Koo, C., & Jeong, K. (2012). A decision support model for reducing electric energy consumption in elementary school facilities. Applied Energy, 95, 253–266. https://doi.org/10.1016/j.apenergy.2012.02.052

Huang, L., & Wu, J. (2014). Effects of the splayed window type on daylighting and solar shading. Building and Environment, 81, 436–447. https://doi.org/10.1016/j.buildenv.2014.07.026

Huang, L., & Zhai, Z. (2020). Critical review and quantitative evaluation of indoor thermal comfort indices and models incorporating solar radiation effects. Energy and Buildings, 224, 110204. https://doi.org/10.1016/j.enbuild.2020.110204

Huang, L., Zou, K., & Zhang, X. (2024). Effects of non-uniform perforated solar screen on daylighting and visual comfort performance. Journal of Building Engineering, 97, 110684. https://doi.org/10.1016/j.jobe.2024.110684

IES (2012). LM-83-12: Approved Method: IES Spatial Daylight Autonomy (sDA) and Annual Sunlight Exposure (ASE). New York: IES.

ISO 15099 (2003). Thermal performance of windows, doors and shading devices — Detailed calculations. International Organization for Standardization.

ISO 7730:2005 (2005). International Organization for Standardization, Ergonomics of the thermal environment — Analytical determination and interpretation of thermal comfort using calculation of the PMV and PPD indices and local thermal comfort criteria. International Organization for Standardization (ISO).

IESNA (2012). LM-83-12 IES Spatial Daylight Autonomy (sDA) and Annual Sunlight Exposure (ASE). New York, USA.

Jayaweera, T., et al. (2021). Enhancing the daylight and energy performance of external shading devices in high-rise residential buildings in dense urban tropics. Journal of Green Building, 87–108. https://doi.org/10.3992/jgb.16.3.87

Jinia, M. A., Trisha, S. H., & Mahmood, T. (2015). Performance of fixed shading devices on daylight penetration in the tropical city like Dhaka. American Journal of Energy Science, 2(3), 21–27.

Ji, W., Luo, M., Cao, B., Zhu, Y., Geng, Y., & Lin, B. (2018). A new method to study human metabolic rate changes and thermal comfort in physical exercise by CO_2 measurement in an airtight chamber. Energy and Buildings, 177, 402–412.

Kirimtat, A., & Koyunbaba, B. K., Chatzikonstantinou, I., & Sariyildiz, S. (2016). Review of simulation modeling for shading devices in buildings. Renewable and Sustainable Energy Reviews, 53, 23–49.

Kirimtat, A., & Manioğlu, G. (2024). A simulation-based performance evaluation of new generation dynamic shading devices with multi-objective optimization. Journal of Building Engineering, 90, 109322. https://doi.org/10.1016/j.jobe.2024.109322

Koebel, M., Lucon, O., Croiset, E., & Baudouin, L. (2013). Renewable energy sources and climate change mitigation: Special report of the Intergovernmental Panel on Climate Change. Cambridge University Press.

Koç, M., & Kalfa, S. (2021). The effects of shading devices on office building energy performance in Mediterranean climate regions. Journal of Building Engineering, 44, 102653. https://doi.org/10.1016/j.jobe.2021.102653

Konis, K. (2013). Evaluating daylight effectiveness and occupant visual comfort in a side-lit open-plan office building in San Francisco. Building and Environment, 59, 662–677. https://doi.org/10.1016/j.buildenv.2012.09.017

Lavin, C., & Fiorito, F. (2017). Optimization of an external perforated screen for improved daylighting and thermal performance of an office space. Procedia Engineering, 180, 571–581. https://doi.org/10.1016/j.proeng.2017.04.216

Lechner, N. (2001). Heating, Cooling, Lighting: Design Methods for Architects. Wiley.

Lu, Y., Lin, W.-E., Hsieh, P.-J., & Yen, T.-J. (2019). Nonuniform woven solar shading screens: Shading, daylighting and mechanical performance. Sustainability, 11(20), 5652. https://doi.org/10.3390/su11205652

Mahdavinejad, M., & Mohammadi, S. (2016). Parametric optimization of daylight and thermal performance through louvers in hot and dry climate of Tehran. Journal of Fundamental and Applied Sciences, 8(3), 1221–1236.

Marino, C., Nucara, A., & Pietrafesa, M. (2017). Thermal comfort in indoor environment: Effect of the solar radiation on the radiant temperature asymmetry. Solar Energy, 144, 295–309. https://doi.org/10.1016/j.solener.2017.01.014

Mardaljevic, J. (2015). Climate-based daylight modelling and its discontents. CIBSE Technical Symposium, 1–12.

Naik, N. S., & Kachhwaha, S. S. (2023). Significance of dynamic over static solar screens on façade performance of buildings: A review. Building and Environment, 242, 110674.

Naik, N. S., & Su, Y. (2022). Dynamic solar screens for high-performance buildings: A review of design and optimisation methods. Architectural Science Review, 65(6), 551–566. https://doi.org/10.1080/00038628.2022.2063248

Ohki, C., Okamoto, T., Tadaki, J., Ohga, H., & Yoshizawa, N. (2019). Façade design optimization based on energy usage, glare, and view using Radiance and Newhasp. Proceedings, 1486–1496. https://doi.org/10.25039/x46.2019.po145

Oral, G. K. (t.y.). Sağlıklı Binalar için Enerji Verimliliği ve Isı Yalıtımı. VIII. Ulusal Tesisat Mühendisliği Kongresi, İzmir.

Özçuhadar, T. (2007). Sürdürülebilir çevre için enerji etkin tasarımın yaşam döngüsü sürecinde incelenmesi. Yüksek Lisans Tezi, İstanbul Teknik Üniversitesi.

Park, G. (2007). Analytic Methods for Design Practice. Springer.

Pereira, L. D., Riamondo, D., Corgnati, S. P., & Silva, M. G. (2014). Energy consumption in schools – A review paper. Renewable and Sustainable Energy Reviews, 40, 911–922. https://doi.org/10.1016/j.rser.2014.08.010

Pilechiha, P., Mahdavinejad, M., Rahimian, F. P., Carnemolla, P., & Seyedzadeh, S. (2020). Multi-objective optimisation framework for designing office windows: Quality of view, daylight and energy efficiency. Applied Energy, 114356. https://doi.org/10.1016/j.apenergy.2019.114356

Radiance (2020). Recommended Radiance rendering options. https://floyd.lbl.gov/radiance/refer/Notes/rpict_options.html

Reinhart, C. F. (2001). Daylight availability and manual lighting control in office buildings: Simulation studies and analysis of measurement. Ph.D. Thesis, University of Karlsruhe, Germany.

Reinhart, C. F., & Andersen, M. (2006). Development and validation of a radiance model for a translucent panel. Energy and Buildings, 38(7), 890–904. https://doi.org/10.1016/j.enbuild.2006.03.006

Reinhart, C. F., & Wienold, J. (2011). The daylighting dashboard – A simulation-based design analysis for daylit spaces. Building and Environment, 46(2), 386–396. https://doi.org/10.1016/j.buildenv.2010.08.001

Sabry, H., Sherif, A., Gadelhak, M., & Aly, M. (2014). Balancing the daylighting and energy performance of solar screens in residential desert buildings: Examination of screen axial rotation and opening aspect ratio. Solar Energy, 103, 364–377.

Sekki, T., Airaksinen, M., & Saari, A. (2015). Measured energy consumption of educational buildings in a Finnish city. Energy and Buildings, 87, 105–115.

Shahbazi, Y., Heidari, M., & Haghparast, F. (2019). An early-stage design optimization for office buildings' facade providing high-energy performance and daylight. Indoor and Built Environment, 28(10), 1350–1367.

Shahdan, D., et al. (2018). External shading devices for energy-efficient building. IOP Conference Series: Earth and Environmental Science, 117, 012034. https://doi.org/10.1088/1755-1315/117/1/012034

Shen, H., & Tzempelikos, A. (2013). Sensitivity analysis on daylighting and energy performance of perimeter offices with automated shading. Building and Environment, 59, 303–314.

Sherif, A., Sabry, H., & Rakha, T. (2012). External perforated solar screens for daylighting in residential desert buildings: Identification of minimum perforation percentages. Solar Energy, 86(7), 1929–1940. https://doi.org/10.1016/j.solener.2012.02.029

Sherif, A., El-Zafarany, A., & Arafa, R. (2012). External perforated window solar screens: The effect of screen depth and perforation ratio on energy performance in extreme desert environments. Energy and Buildings, 52, 1–10.

Sönmez, B., & Çakır Kıasif, G. (2018). Çevresel, Sosyal ve Ekonomik Bağlamda Akıllı Cephe Sistemleri. Haliç Üniversitesi Fen Bilimleri Dergisi, 1, 63–98.

Spain GBC (2014). LEEDv4 Diseño y Construcción de Edificios.

Srisamranrungruang, T., & Hiyama, K. (2020). Balancing of natural ventilation, daylight, thermal effect for a building with double-skin perforated facade (DSPF). Energy and Buildings, 210, 109765.

Srisamranrungruang, T., & Hiyama, K. (2021). Correlations between building performances and design parameters of double-skin facade utilizing perforated screen. Japan Architectural Review, 4(3), 533–544.

Tabadkani, A., Banihashemi, S., & Hosseini, M. R. (2018). Daylighting and visual comfort of

oriental sun responsive skins: A parametric analysis. Building Simulation, 11(4), 663–676.

Taguchi, G., & Yokoyama, T. (1993). Taguchi Methods: Design of Experiments. ASI Press.

Touloupaki, E., & Theodosiou, T. (2017). Optimization of building form to minimize energy consumption through parametric modelling. Procedia Environmental Science, 38, 509–514.

TS EN 12464-1 (2021).Turkish Standards Institution, TS EN 12464-1:2021. Light and lighting — Lighting of work places — Part 1: Indoor work places. Turkish Standards Institution (TSE), International Organization for Standardization.

TS EN 17037:2019+A1:2023. (2023). Daylight in buildings. Turkish Standards Institution. Daylighting for Building Standard. International Organization for Standardization.

Tzempelikos, A., & Athienitis, A. K. (2007). The impact of shading design and control on building cooling and lighting demand. Solar Energy, 81(3), 369–382.

Tzempelikos, A., Bessoudo, M., Athienitis, A. K., & Zmeureanu, R. (2010). Indoor thermal environmental conditions near glazed façades with shading devices—Part II: Thermal comfort simulation and impact of glazing and shading properties. Building and Environment, 45(10), 2517–2525.

Ünver, R. (2015). Eğitim yapılarında konfor ne demek? Led & Lighting Dergisi, 16, 114–121.

US Department of Energy (2012). Building Energy Data Book. http://uildingsdatabook.eren.doe.gov/TableView.aspx?table=1.1.13

USGBC (2013). LEED v4 for Building Design and Construction. Washington, DC.

USGBC (2017). LEED Interpretation, ID#100002149. https://www.usgbc.org/leedaddenda/100002149

Utlu, Z., & Hepbaşlı, A. (2005). Analysis of energy and exergy use of the Turkish residential–commercial sector. Building and Environment, 40, 654.

Valladares-Rendón, L. G., Schmid, G., & Lo, S.-L. (2017). Review on energy savings by solar control techniques and optimal building orientation for the strategic placement of facade shading systems. Energy and Buildings, 140, 458–479.

Velds, M. (1999). Assessment of lighting quality in office rooms with daylighting systems. Doctoral dissertation, Technical University of Delft, The Netherlands.

Website of Radiance (2020). Recommended Radiance rendering options. https://floyd.lbl.gov/radiance/refer/Notes/rpict_options.html

Wenjie, J., Luo, M., Cao, B., Zhu, Y., Geng, Y., & Lin, B. (2018). A new method to study human metabolic rate changes and thermal comfort in physical exercise by CO_2 measurement in an airtight chamber. Energy and Buildings, 177, 402–412.

Working Group For Sustainable Construction (2004). Final Report on Methods and Techniques. Brussels, Belgium.

Xue, P., Mak, C., & Cheung, H. (2014). The effects of daylighting and human behaviour on luminous comfort in residential buildings: A questionnaire survey. Building and Environment, 81, 51–59.

Yılmaz, F. Ş., & Yener, A. K. (t.y.). Aydınlatma tasarımında görsel konfor, enerji performansı ve çevresel etki değerlendirmesi. http://www.emo.org.tr/ekler/7c828bf2dd8d7e4_ek.pdf

Yi, H., Srinivasan, R., & Braham, W. (2015). An integrated energy–emergy approach to building form optimization: Use of EnergyPlus, Emergy Analysis and Taguchi-Regression Method. Building and Environment, 84, 89–104.

YÖK (2020). 2018–2019 Öğretim yılı yükseköğretim istatistikleri [2018–2019 Academic Year

Higher Education Statistics]. https://istatistik.yok.gov.tr/

Zhang, A., Bokel, R., Dobbelsteen, A. V. D., Sun, Y., Huang, Q., & Zhang, Q. (2017). Optimization of thermal and daylight performance of school buildings based on a multi-objective genetic algorithm in the cold climate of China. Energy and Buildings, 139, 371–384.

Zhang, Y., Zhou, X., Zheng, Z., Oladokun, M. O., & Fang, Z. (2020). Experimental investigation into the effects of different metabolic rates of body movement on thermal comfort. Building and Environment, 168, 106489. https://doi.org/10.1016/j.buildenv.2019.106489

Zanakis, S. H., Solomon, A., Wishart, N., & Dublish, S. (1998). Multi-attribute decision making: A simulation comparison of select methods. European Journal of Operational Research, 107(3), 507–529.

Zani, A., Di Milano, P., Giovanni, A., Blanco, J. D., et al. (2018). A new modeling approach for the assessment of the effect of solar radiation on indoor thermal comfort. ResearchGate. https://www.researchgate.net/publication/333844121

Zomorodian, Z. S., Tahsildoost, M., & Hafezi, M. (2016). Thermal comfort in educational buildings: A review article. Renewable and Sustainable Energy Reviews, 59, 895–906.

Zorer Gedik, G. (2002). An approach to designing an optimal shading device. Architectural Science Review, 45(4), 285–293. https://doi.org/10.1080/00038628.2002.9696942

Zoroğlu, F. (2017). Alışveriş merkezlerinin ısıl konfor ve enerji tüketimi açısından değerlendirilmesi. Yüksek Lisans Tezi, Yıldız Teknik Üniversitesi.

A
APPENDIX

Appendıx 1. The outdoor air temperature on measurement days

Date	Time	Mean Radiant Temprature (C°)	Air Temperature (C°)	Relative Humidity, RH (%)	Air Velocity, Va (m/s)
03.08.2021	14:58	43,4	38,7	37,6	0,54
09.08.2021	13:55	52,2	40,2	24,1	0,44
13.08.2021	14:20	47,9	34,4	36,3	0,78
19.08.2021	15:12	31,63333	30,00778	62,35556	0,492389
9.09.2021					
21.09.2021	13:46	32,23333	30,38571	37,79524	0,185714
14.10.2021					
26.10.2021	16:11	17,89048	15,38095	57,5619	0,647619
17.11.2021	14:17	20,73571	18,75714	45,20714	0,525

Appendıx 2. Illuminance level of classrooms and blackboards at measurement points in daylight illumination (lx)

Tarih: 20.12.2019														
Saat		**Masa üzeri**										Yazı Tahtası (Beyaz)		
		1		**2**		**3**		**4**	**5**	**6**	**7**	1	2	3
	Derslik	**Gölgesiz**	**Gölgede**	**Gölgesiz**	**Gölgede**	**Gölgesiz**	**Gölgede**							
13,47	**502**	**11830**	**4470**	**10800**	**2680**	**11130**	**4440**	**410**	**280**	**290**	**740**	810	803	760
13,25	**503**	**12168**	**5050**	**12130**	**2800**	**12950**	**5240**	**470**	**548**	**470**	**1078**	1180	1220	1320
12,04	**401**	**4300**	**740**		**270**		**520**	**120**	**130**	**140**	**238**	316	178	168
12,33	**402**	**6800**	**814**		**220**		**480**	**102**	**124**	**102**	**220**	216	198	213
12,49	**403**	**6460**	**1092**		**330**		**619**	**143**	**149**	**130**	**230**	**175**	180	205

Appendıx 3. Illuminance level of classrooms and blackboards at measurement points in integrated lighting (lx)

Tarih: 20.12.2019														
Saat	**Masa üzeri**											Yazı Tahtası (Beyaz)		
	Derslik	**1**		**2**		**3**		**4**	**5**	**6**	**7**	1	2	3
		Gölgesiz	**Gölgede**	**Gölgesiz**	**Gölgede**	**Gölgesiz**	**Gölgede**							
13,57	**502**	**7100**	**5160**	**6290**	**2520**	**8200**	**5180**	**630**	**680**	**735**	**1240**	850	880	850
13,35	**503**	**13240**	**5900**	**13420**	**3080**	**18100**	**6470**	**820**	**890**	**680**	**1800**	1080	1154	1218
12,2	**401**	**4600**	**1440**		**1400**		**1180**	**750**	**1100**	**860**	**1570**	590	500	520
12,45	**402**	**8550**	**1770**		**1328**		**1460**	**672**	**910**	**638**	**1520**	410	390	395
13,05	**403**	**4580**	**1760**		**1340**		**1202**	**840**	**1145**	**720**	**1630**	405	425	420

Appendıx 4. The colorimetric properties and reflectance factors of production materials (samples-patterns)

Colorimetric measurements		Yxy		Yxy		Yxy		Yxy		Munsell		Lab	
Standard illuminant		D65		D65		C		C		C		D65	
View angle		10°		2°		10°		2°		2°		10°	
Sample picture	Sample code	SCI	SCE	SCI	SCE	SCI	SCE	SCI	SCE	SCI	SCE	SCI	SCE
	7037 Ax	23.28	21.45	23.27	21.45	23.27	21.45	23.26	21.44	3.8BG	5.4 BG	55.36	53.44
		0.31	0.31	0.31	0.31	0.3	0.3	0.3	0.3	5.4	5.2	-0.78	-0.85
		0.33	0.33	0.32	0.32	0.31	0.31	0.31	0.31	0.1	0.1	-0.2	-0.16
	9006 D	78.84	74.92	78.98	75.06	78.81	74.89	78.96	75.05	5.3 GY	4.9 GY	91.16	89.35
		0.31	0.31	0.31	0.31	0.31	0.31	0.31	0.31	9	8.8	-1.52	-1.5
		0.33	0.33	0.33	0.33	0.32	0.32	0.32	0.32	0.4	0.4	3.12	3.32
	130.80.10	55.53	47.82	55.86	48.16	55.49	47.79	55.84	48.84	6.7 GY	6.4 GY	79.34	74.71
		0.32	0.32	0.31	0.31	0.31	0.31	0.31	0.31	7.8	7.3	-3.68	-3.97
		0.34	0.35	0.34	0.34	0.33	0.33	0.33	0.33	1	1.1	6.66	7.38
	ALU-SAN	80.77	78.16	81.36	78.74	80.77	78.16	81.4	78.78	2.3 Y	2.3 Y	92.03	90.85

	9010 C2 İBA 03.12.2019	0.33	0.33	0.32	0.32	0.32	0.32	0.32	0.32	9.1	9	0.57	0.59
		0.34	0.34	0.34	0.34	0.33	0.33	0.33	0.33	1.1	1.1	8.66	8.76
	7044 PULLER Kalınlık=103nm parlaklık=40gloss	47.86	45.28	48.16	45.58	47.86	45.27	48.17	45.59	6.4 Y	6.4 Y	74.74	73.08
		0.32	0.32	0.32	0.32	0.32	0.32	0.32	0.32	7.3	7.2	-0.24	-0.24
		0.34	0.34	0.34	0.34	0.33	0.33	0.32	0.33	0.7	0.7	5.49	5.64
	Yellow 5478 PE70 gloss 1084016/1 Lab Up-1070-05478-T	68.16	64.2	68.93	64.98	68.13	64.17	68.95	64.99	4.9 Y	5.0 Y	86.09	84.07
		0.33	0.33	0.33	0.33	0.33	0.33	0.32	0.33	8.5	8.3	-0.04	-0.02
		0.35	0.35	0.35	0.35	0.34	0.34	0.34	0.34	1.4	1.5	10.92	11.51
	White B554 PE PRMD-5gloss-2015057/1-Lab/UD 10680B554-T	78.46	74.48	78.62	74.64	78.43	74.45	78.6	74.62	5.2 GY	4.7 GY	90.99	89.15
		0.31	0.31	0.31	0.31	0.31	0.31	0.31	0.31	9	8.8	-1.69	-1.67
		0.33	0.33	0.33	0.33	0.32	0.32	0.32	0.32	0.4	0.4	3.54	3.78

Appendıx 5. Calculation parameters and simulation settings

	Parameters	Defination and Limitations	Methods	Methods	Calculation area	Calculation settings
Visual Comfort	View out	The calculation area, based on the percentage of the calculation area where there is a total viewing angle of 60 degrees, with 30 degrees above and below the horizon line at eye level in simulations.	Simulation	Calculation / Optimization	Working plane, h:1,2 m, Grid : 0,5 m	
	Daylight illuminance	An equation has been formulated to ensure that areas exceeding 1000 lux and falling below 300 lux are minimized based on the calculation surface in simulations. Luminance measurements have been conducted on both horizontal and vertical working planes in the area study.	Simulation / Field Study	Measurement / Calculation / Optimization	Working plane, h:0,85m, Grid : 0,5m	July 15 - Clear sky 10,00-12,00-14,00-16,00
	Useful daylight illuminance (UDI)	In simulations, useful daylight illuminance (UDI) and daylight autonomy (DA) calculations have been performed based on usage hours throughout the year. The UDI value indicates the percentage of usage hours during which the illuminance level meets the specified threshold values. In optimization, the UDI value is taken between 300 lux and 3000 lux (UDI autonomous). Daylight autonomy is a metric that provides the percentage of the area where the target illuminance level is met by daylight during usage hours throughout the year. Keeping these values at their maximum has been entered as a command.	Simulation	Calculation / Optimization	Calculation area: from wall 0,5 m working plane: 0.85, Grid: 0,5 m	All year- 8,00-17,00
	Daylight autonomy (DA)		Simulation	Calculation / Optimization		
	Annual sunlight exposure (ASE)	In simulations, annual sunlight exposure (ASE) exceeding 1000 lux for more than 250 hours per year (ASE 1000,250h) has been calculated based on direct sunlight. According to the recommendation of the Illuminating Engineering Society (IES), the percentage of the area calculated for ASE 1000,250h, which is one of the LEED v4 metrics, should be kept below 10%.	Simulation	Calculation / Optimization	Working plane, h: 0,85m, Grid: 0,5 m,	All year- All day
	Daylight Glare Probability (DGP)	Glare is discomfort, inconvenience, or visual performance and visibility losses caused by areas being significantly brighter than the eyes are adapted to. High luminance differences between direct sunlight and bright and dark areas in the field of view can lead to glare. In simulations, the calculation of Daylight Glare Probability (DGP) is conducted at eye level, and DGP calculations are made by determining vertical illuminance levels with measurements. It is recommended that the DGP value does not exceed 0.45 for more than 5% of the usage time (BS EN 17037). The closer the DGP value is to 0, the less glare is present.	Simulation / Field Study	Measurement / Calculation / Optimization	Position of speaker , h:1,7	1July 15 - Clear sky- 10,00-12,00-14,00-16,00
Thermal and Visual Comfort	Solar radiation	In simulations, the amount of solar radiation that needs to be utilized and protected on the exterior surface of windows is calculated. It is desired to maximize the amount of solar radiation to be utilized while minimizing the amount that needs to be protected.	Simulation	Calculation / Optimization	Window Outside surface, Grid: 0,1 m	Summer period (Months 6-7-8), Winter period (Months 12-1-2) – All day

	Parameters	Defination and Limitations	Methods	Methods	Calculation area	Calculation settings
Thermal Comfort	PMV (Predicted Mean Vote)	PMV (Predicted Mean Vote), a measure used in determining thermal comfort in climate-controlled environments, is accepted as comfortable within the range of -0.5<PMV<+0.5 according to ISO 7730 and ASHRAE 55 standards. The closer the PMV value is to zero, the more comfortable the indoor environment is considered to be.	Simulation / Field Study	Measurement / Calculation / Optimization	Working plane, h:1,1m, Grid: 0,5m	Duration and time: 8.00-17.00
	Adaptive Comfort	The Adaptive Comfort Model is used to determine the thermal comfort of naturally ventilated indoor spaces. In calculations, along with determining the adaptive comfort state, attention is paid to the percentage of time spent in adaptive comfort and warm conditions. It is expected that the adaptive comfort state is maximized, the percentage of time spent in comfortable conditions is maximized, and the percentage of time spent in warm conditions is minimized.	Simulation	Calculation / Optimization	Working plane, h:1,1m, Grid: 0,5m	Duration and time: 8.00-17.00
	Window interior surface temperature	During the summer months, it is desired that the temperature of the window interior surface is minimized, while during the winter months, it is desired that it is maximized.	Simulation / Field Study	Measurement / Calculation / Optimization	Working plane, h:1,1m, Grid: 0,5m	Duration and time: 8.00-17.00
	Heat gains	During the summer months, it is desired to minimize heat gain, while during the winter months, it is desired to maximize it.	Simulation	Calculation / Optimization	Working plane, h:1,1m, Grid: 0,5m	Duration and time 8.00-17.00
	Adj MRT (Adjusted Mean Radiant Temperature)	MRT (Mean Radiant Temperature), used to determine the heat exchange between users and their surroundings through longwave radiation, includes shortwave radiation in its calculation, and when re-calculated, it is referred to as Adj MRT (corrected MRT) or ΔMRT. When Adj MRT is included in the PMV model, PMV is also similarly named.	Simulation	Calculation / Optimization	Working plane, h:1,1m, Grid: 0,5m	Duration and time: 8.00-17.00

Appendıx 6. Thermal comfort survey conducted before the lesson

THERMAL COMFORT QUESTİONNAIRE

– BEFORE THE LESSON – Date:

Explanation: This survey has been prepared within the scope of a doctoral dissertation in the Building Physics Program at Yıldız Technical University. The aim is to evaluate the effects of perforated shading devices applied to classrooms on thermal comfort conditions and to assess occupants' satisfaction with the indoor environment according to international standards (ASHRAE 55, 2017; ISO 7730, 2005).

Personal Information

Gender: ☐ Female ☐ Male	Age:	Height (cm):
Weight (kg):	Employment status: ☐ Retired ☐ Employee ☐ Student ☐ Other…	

Please indicate your education level:

☐ Graduate ☐ Undergraduate

1) How long have you been living in Istanbul?

☐ 0-1 year ☐ 1-2 year ☐ 2-3 year ☐ 3-4 year ☐ More 4 year

2) Please select the clothing items you are currently wearing (closest options).

Footwear		**Lower Garments**		**Underclothing**	
Boots		Heavy trousers / Heavy skirt		Short socks	
Shoes		Trousers / Skirt		Thin long socks	
Sandals		Shorts / Light skirt		Thick long socks	
Upper Garments		**Outer Garments**		**Undershirt (Vest)**	
Sleeveless shirt		Cardigan / Jacket		Briefs	
Short-sleeved shirt		Waistcoat			
Long-sleeved sweatshirt		Overcoat			
Sweater					

Dress: (Sleeveless T-shirt/Short-sleeved T-shirt/ Long-sleeved T-shirt) + (Skirt)

3) Did you come directly from outdoors into the classroom?

☐ Yes ☐ No

If yes, please indicate the duration of your outdoor exposure:

☐ 0-15 min. ☐ 15-30 min. ☐ 30 min.-1 h. ☐ 1-2 h. ☐ 2 h +

If no, please indicate the duration of your indoor exposure:

☐ 0-15 min. ☐ 15-30 min. ☐ 30 min.-1 h. ☐ 1-2 h. ☐ 2 h +

4) Please specify your activity level during the last 15 minutes (divided into three 5-minute intervals):

First 5 min.

☐ Sitting, resting ☐ Light activity (office, school, laboratory) ☐ Walking ☐ Brisk walking

Second 5 min.

☐ Sitting, resting ☐ Light activity (office, school, laboratory) ☐ Walking ☐ Brisk walking

Last 5 min.

☐ Sitting, resting ☐ Light activity (office, school, laboratory) ☐ Walking ☐ Brisk walking

Thermal Comfort in the Classroom

5) Please indicate your thermal sensation (7-point ASHRAE/ISO thermal sensation scale).

-3☐ Cold (-3) -2☐ Cool (-2) -1☐ Slightly cool (-1) 0☐ Neutral (0) – Comfortable

+1☐ Slightly warm (+1) +2☐ Warm (+2) +3☐ Hot (+3)

6) How do you evaluate the current thermal environment?

☐ Very comfortable ☐ Comfortable ☐ Uncomfortable but acceptable

☐ Uncomfortable and unacceptable ☐ Very uncomfortable ☐ Extremely uncomfortable

7) How would you personally evaluate the acceptability of the current thermal environment?

☐ Clearly acceptable ☐ Acceptable ☐ Unacceptable ☐ Clearly unacceptable

8) How would you prefer the thermal environment to be?

☐ Much hotter ☐ Warmer ☐ A little hotter ☐ Neither hot nor cold (same, no change)

☐ A little colder ☐ Colder ☐ A lot colder

Appendıx 7. Thermal comfort survey conducted after the lesson

THERMAL COMFORT QUESTİONNAIRE

– AFTER THE LESSON – Date:

Personal Information

1) Please select the clothing items you are currently wearing (closest options).

Footwear		Lower Garments		Underclothing	
Boots		Heavy trousers / Heavy skirt		Short socks	
Shoes		Trousers / Skirt		Thin long socks	
Sandals		Shorts / Light skirt		Thick long socks	
Upper Garments		**Outer Garments**		**Undershirt (Vest)**	
Sleeveless shirt		Cardigan / Jacket		Briefs	
Short-sleeved shirt		Waistcoat			
Long-sleeved sweatshirt		Overcoat			
Sweater					

Dress: (Sleeveless T-shirt/Short-sleeved T-shirt/ Long-sleeved T-shirt) + (Skirt)

2) Please mark the location closest to your current seat in the classroom:

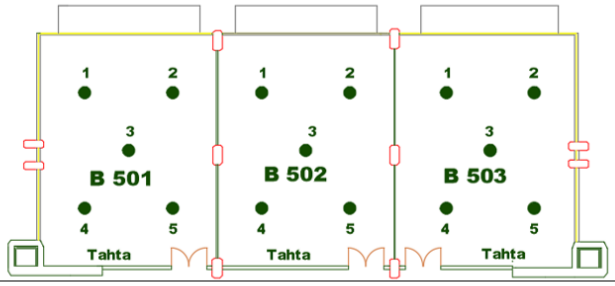

3) How long have you been in the classroom?

☐ 0-15 min. ☐ 15-30 min. ☐ 30 min.-1 h. ☐ 1-2 h. ☐ 2 h +

4) Please indicate your activity during the last 15 minutes:

☐ Sitting, resting ☐ Light activity (office, school, laboratory) ☐ Walking ☐ Brisk walking

Thermal Comfort in the Classroom

5) Did you choose your seat based on thermal conditions?

☐ Yes ☐ No

6) Please indicate your thermal sensation (7-point ASHRAE/ISO thermal sensation scale).

-3☐ Cold (-3) -2☐ Cool (-2) -1☐ Slightly cool (-1) 0☐ Neutral (0) – Comfortable

+1☐ Slightly warm (+1) +2☐ Warm (+2) +3☐ Hot (+3)

7) How do you evaluate the current thermal environment?

☐ Very comfortable ☐ Comfortable ☐ Uncomfortable but acceptable

☐ Uncomfortable and unacceptable ☐ Very uncomfortable ☐Extremely uncomfortable

8) How would you personally evaluate the acceptability of the current thermal environment?

☐ Clearly acceptable ☐ Acceptable ☐ Unacceptable ☐ Clearly unacceptable

9) How would you prefer the thermal environment to be?

☐ Much hotter ☐ Warmer ☐ A little hotter ☐ Neither hot nor cold (same, no change)

☐ A little colder ☐ Colder ☐ A lot colder

10) If you feel thermally uncomfortable, what actions do you usually take?

☐Change my seat ☐Leave the classroom ☐Adapt to the environment (by adding/removing clothing) ☐Close the blinds

☐Use natural ventilation ☐Adjust the heating/ventilation system

11) If you experience local thermal discomfort, please indicate which apply:

☐ Cold (-3) Wall ☐ Hot (+3) Wall ☐ Cold (-3) Window ☐ Hot (+3) Window

☐ Cold (-3) Ceiling ☐ Hot (+3) Ceiling ☐ Cold (-3) Floor ☐ Hot (+3) Floor

12) If you are not satisfied with the thermal environment, what might be the cause of your discomfort?

☐ Transparency ratio and the heating effect of solar radiation ☐ Insufficient space

☐ Other ☐ Insufficient HVAC/ventilation ☐ High occupancy density

13) How does the classroom's thermal environment affect your comprehension and concentration?

☐ Very positive ☐ Positive ☐ Neutral ☐ Negative ☐ Very negative

Appendıx 8. Visual comfort survey conducted after the lesson

VİSUAL COMFORT QUESTİONNAİRE

- AFTER LESSON - -DATE-

Visual Environment Assessment
1) How would you describe the illuminance of the current environment? (TS EN 17037 scale) ☐ Extremely dark ☐ Very dark ☐ Dark ☐ Neutral ☐ Bright ☐ Very Bright ☐ Extremely Bright
2) How do you find the current environment in terms of daylight illuminance? ☐ Very comfortable ☐ Comfortable ☐ Uncomfortable but acceptable ☐ Uncomfortable and unacceptable ☐ Very uncomfortable ☐ Extremely uncomfortable
3) How would you personally evaluate the acceptability of the daylight conditions? ☐ Clearly acceptable ☐ Acceptable ☐ Unacceptable ☐ Clearly unacceptable
4) How would you prefer the daylight conditions to be? ☐ Much darker ☐ Darker ☐ Slightly darker ☐ No change ☐ Slightly brighter ☐ Brighter ☐ Much brighter
5) Please evaluate the illuminance at the working plane according to the following aspects: **Does it cause glare (e.g., difficulty in clearly perceiving text)?** ☐ Yes ☐ No **It causes luminance contrast (a substantial difference in luminance levels)** ☐ Yes ☐ No
6) How does the daylighting in the classroom affect your comprehension and concentration? ☐ Very positive ☐ Positive ☐ Neutral ☐ Negative ☐ Very negative

Appendıx 9. Short-term Measurement Results on September 21, 2021 (Mean Radiant Temperature, Air Temperature, Relative Humidity, Air velocity, and PMV).

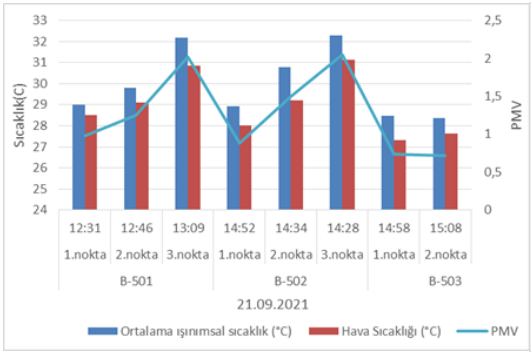

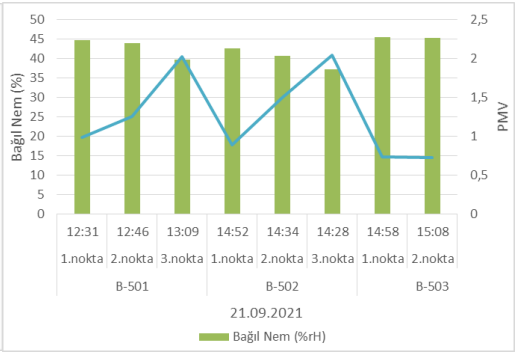

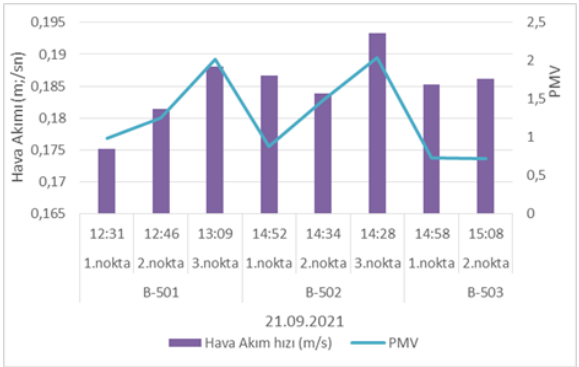

Appendıx 10. Long-term Measurement Results for Classroom B-503 on September 19, 2021 (Mean Radiant Temperature, Air Temperature, Relative Humidity, Air velocity, and PMV)

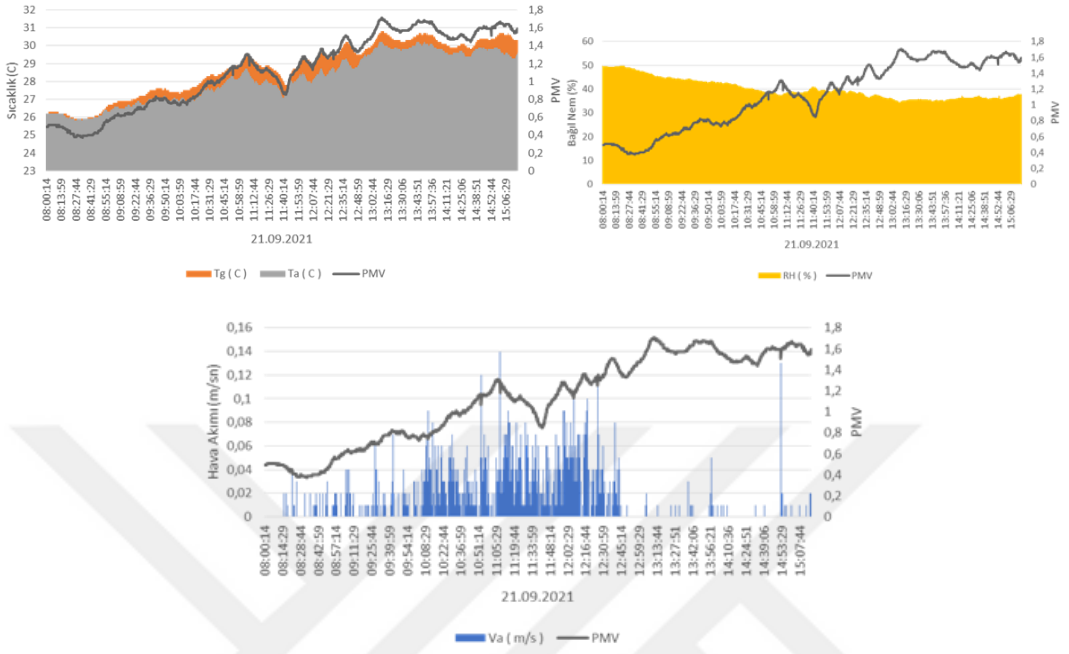

Appendıx 11. Short-term Measurement Results on October 14, 2021 (Mean Radiant Temperature, Air Temperature, Relative Humidity, Air velocity, and PMV with 0.5 clo)

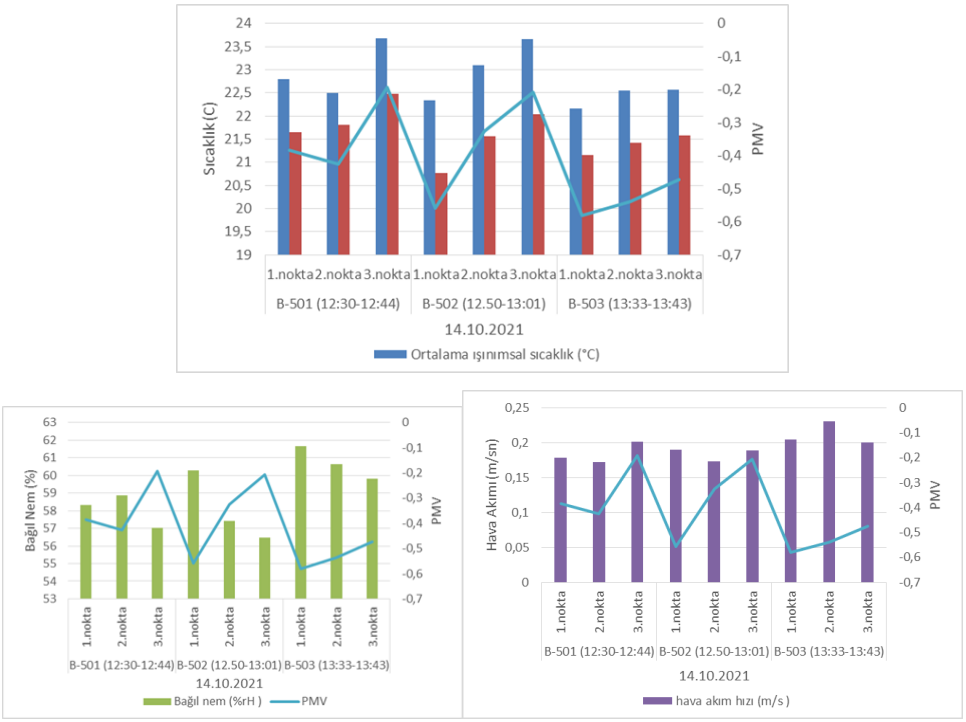

Appendıx 12. Long-term Measurement Results for Classroom B-502 on October 14, 2021 (Mean Radiant Temperature, Air Temperature, Relative Humidity, Air velocity, and PMV with 0.7 clo)

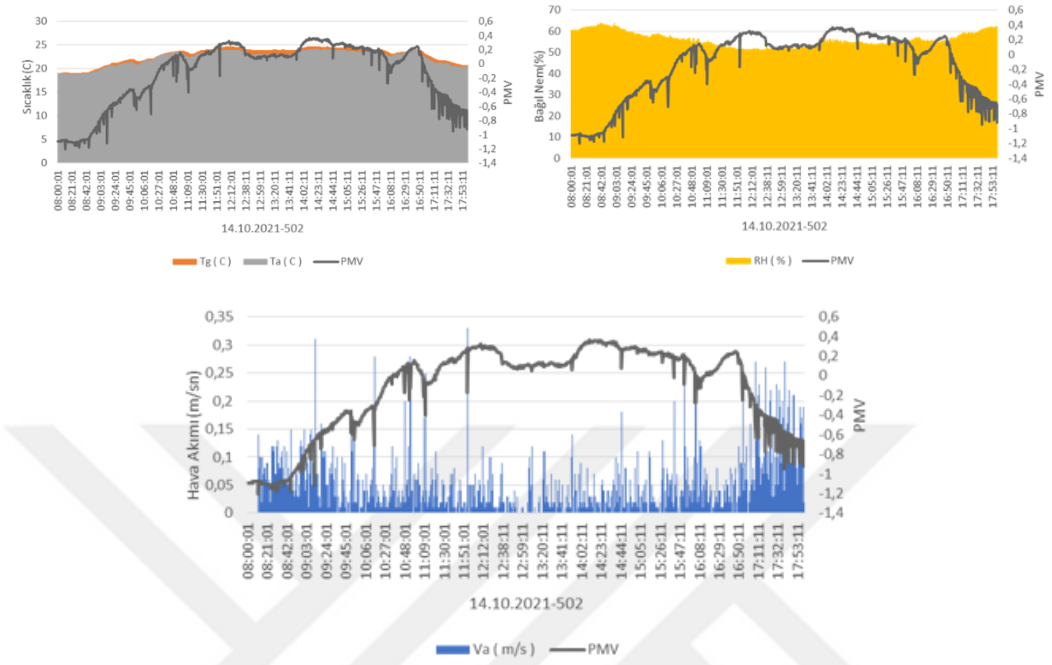

Appendıx 13. Long-term Measurement Results for Classroom B-502 from October 11–15, 2021 (Mean Radiant Temperature, Air Temperature, Relative Humidity, Air velocity, and PMV)

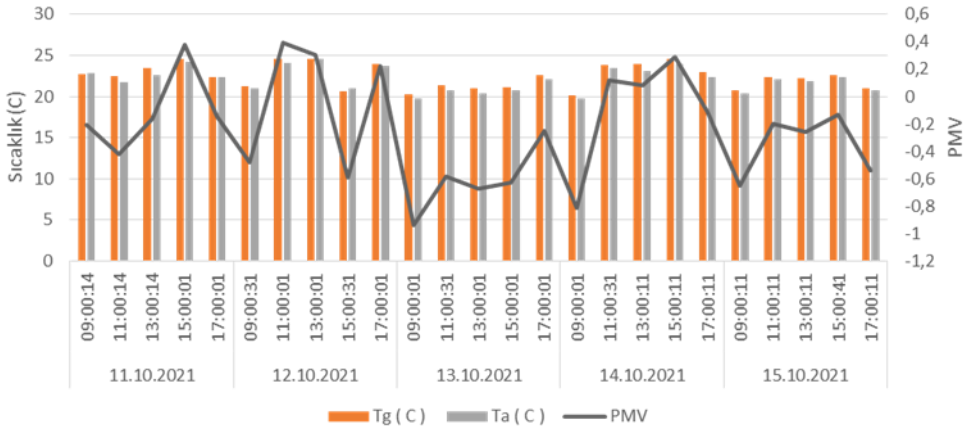

Appendıx 14. Ethical Committee Approval for surveys

YILDIZ TEKNİK ÜNİVERSİTESİ
Sosyal ve Beşeri Bilimler Araştırmaları Etik Kurulu

Toplantı Tarihi: 30.11.2021 **Toplantı No: 2021.11**

SOSYAL VE BEŞERİ BİLİMLER ARAŞTIRMALARI ETİK KURULU TOPLANTI KARARI

Yürütücülüğünü Üniversitemiz FEN BİLİMLERİ ENSTİTÜSÜ öğretim üyelerinden Prof. Dr. Gülay Zorer Gedik danışmanlığında lisansüstü öğrencisi Fatma ZOROĞLU ÇAĞLAR tarafından yapılacak olan "Güneş Denetim Elemanı Olarak Mesh Sistemlerin Isıl Konfor Ve Enerji Tüketimi Açısından Tasarımına Yönelik Deneysel Bir Yöntem" adlı çalışma ve bu çalışmada kullanılacak veri toplama araçları ve yöntemlerine ilişkin bilgilerde etiğe aykırı herhangi bir bulguya rastlanmamıştır.

Etik Kurul Üyeleri

Evrak No : 21100[illegible]
Tarih : 07.10.20[illegible]

İş Sağlığı ve Güvenliği Tehlike ve Risk Tespit Formu

Uygunsuzluk Tespit Edilen Bölümün/Birimin Mevcut Durumu

NO	BÖLÜM	TEHLİKE KAYNAKLARI / TEHLİKELER	RİSK	ETKİLENENLER	ÖNLEM ALINMADAN ÖNCE RİSK PUANI			
					OLASILIK (1-5)	ŞİDDET (1-5)	RİSK SKORU (O X Ş)	ÖNEM DERECESİ
1	Makine Fakültesi B Blok 501-502-503 derslik	Acil durumlarda takılma ve düşmeleri engellemek için merdiven alanlarının boş bırakılması / Takılma düşme ,tahliye zorluğu	Acil Durumlarda Tahliye Zorluğu	Öğrenciler	3	5	15	YÜKSEK

Kaynak Resim - Doküman





Önem Matrisi

RİSK SKORU = OLASILIK X ŞİDDET	ŞİDDET				
OLASILIK	1- Çok hafif	2-Hafif	3- Orta	4-Ciddi	5- Çok ciddi
1 - Çok küçük	Önemsiz 1	Düşük 2	Düşük 3	Düşük 4	Düşük 5
2- Küçük	Düşük 2	Düşük 4	Düşük 6	Orta 8	Orta 10
3- Orta	Düşük 3	Düşük 6	Orta 9	Orta 12	Yüksek 15
4- Yüksek	Düşük 4	Orta 8	Orta 12	Yüksek 16	Yüksek 20
5- Çok yüksek	Düşük 5	Orta 10	Yüksek 15	Yüksek 20	Kabul Edilemez 25

Riskin Tespit Şekli				Riskin Giderilmesi İçin Gereken Süre			
	İç Tetkik/Denetim	X	Paydaş Bildirimi	X	Risk Acilen Giderilmelidir.		Risk .... Gün İçinde Giderilmelidir.

Riskin Giderilmesi İçin Yapılması Önerilen İşlemler

Derslik alanında olası bir tehlike anında tüm paydaşların bulundukları yerleri derhal ve güvenli bir şekilde terk etmeleri gerekmektedir. Koridor üzerinde bulunan cihaz tahliyeyi geciktirmekte ve öğrenciler için takılma düşme tehlikesi yaratmaktadır. Cihazın takılma ve düşmeye sebep olmayacak , koridorda kaçışı engellemeyecek şekilde uygun bir alana taşınmasını önermekteyiz. Ayrıca cihazın,

kabin alanı daraltılarak daha küçük ebatlarda bir kabin içine alınmasını da önermekteyiz. Ek olarak, sınıf içindeki tüm malzemelerin devrilmeye karşı sabitlenmesi , açıkta bulunan kablolarında öğrencilerin erişmesini engelleyecek şekilde kanal içinden taşınması ve sınıf içindeki koridorun boş olması da gerekmektedir.

Tehlikeyi Bildiren Kişinin Bilgileri		E-İmzalıdır	Önerileri Yapan Kişinin Bilgileri		E-İmzalıdır	Onaylayan Kişinin Bilgileri		E-İmzalıdır
Adı/Soyad	Y.EMRE AKSU		Adı/Soyad	Y.EMRE AKSU		Adı/Soyad		
Birim/Ünvan	İSG Koordinatörlüğü/ İSG Uzmanı		Birim/Ünvan	İSG Koordinatörlüğü/ İSG Uzmanı		Birim/Ünvan		
Telefon	3979		Telefon	3979		Telefon		
Mail	yeaksu@yildiz.edu.tr		Mail	yeaksu@yildiz.edu.tr		Mail		

Tespit edilen riskin belirlenen süre içerisinde giderilerek tarafımıza bilgi verilmesi hususunu bilgilerinize arz/rica ederim
İş Sağlığı ve Güvenliği Koordinatörü

Form No: FR-1155- İş Sağlığı ve Güvenliği Tehlike ve Risk Tespit Formu; Revizyon Tarihi: 27.10.2016; Revizyon No: 00

PUBLICATIONS FROM THE THESIS

Conference Papers

1. F. Zoroğlu, M. Plenikowski and M. Ahmadi , "The Assessment of External Vertical Perforated Shading System in Terms of Visual Comfort ," BUILDSIM-NORDIC 2022, Kobenhavn, Denmark, pp.1, 2022

2. F. Zoroğlu, A.B. Atmaca and G. Zorer Gedik, "The Impact of Transparency Ratio on Visual Comfort: The Case Study of an Educational Building in Istanbul," 3rd International Conference of Contemporary Affairs in Architecture and Urbanism (ICCAUA-2020) , Antalya, Turkey, pp.5, 2020

3. F. Zoroğlu, G. Zorer Gedik and H. Gökdemir, "The Impact of Transparency Ratio on Thermal Comfort: The Case Study of an Educational Building in Istanbul," 3rd International Conference of Contemporary Affairs in Architecture and Urbanism (ICCAUA-2020) , no.316379, Antalya, Turkey, pp.6, 2020

Papers

1. F. Zoroğlu and G. Zorer Gedik, "A new design proposal for perforated solar screens and optimization in terms of solar control," Civil Engineering and Architecture, vol.9, no.7, pp.2416-2426, 2021

2. F. Zoroğlu, G. Zorer Gedik and H. Gökdemir, "The impact of transparency ratio on thermal comfort: A field study on educational building," Civil Engineering and Architecture, vol.8, pp.890-897, 2020

Books

1. F. Zoroğlu, A.B. Atmaca and G. Zorer Gedik, "The Impact of Transparency Ratio on Visual Comfort: A Field Study on Educational Building," In New Approaches in Contemporary Architecture and Urbanism, İstanbul: Cinius Yayınları, 2020, pp.53-60.

Projects

1. G. Zorer Gedik and F. Zoroğlu, "Güneş Denetim Elemanı Olarak Mesh Sistemlerin Isıl Konfor ve Enerji Tüketimi Açısından Tasarımına Yönelik Deneysel Bir Yöntem", 4165 - FDK-2021-4165, YTU Coordinatorship of Scientific Research Projects, 2021-2025.

Scholarships

1. TUBITAK – 2214-A International Research Fellowship Programme for PhD Students – Technical University of Denmark (DTU) - February / October 2022

Awards

1. Best Presentation Award, 4 Th International Conference Of Contemporary Affairs İn Architecture And Urbanism Iccaua, 2021

2. Best Paper Award, 3 Th International Conference Of Contemporary Affairs İn Architecture And Urbanism Iccaua, 2020, publicated from thesis (conference papers 3)

Patent

1. F. Zoroğlu and G. Zorer Gedik, "Bir Perdeleme Elemanı", 022/012179, Utility Model, Turkish Patent and Trademark Office, the process continues.